ISSN 0918-4597

NRIM

Research Activities

1994

National Research Institute for Metals

Japan

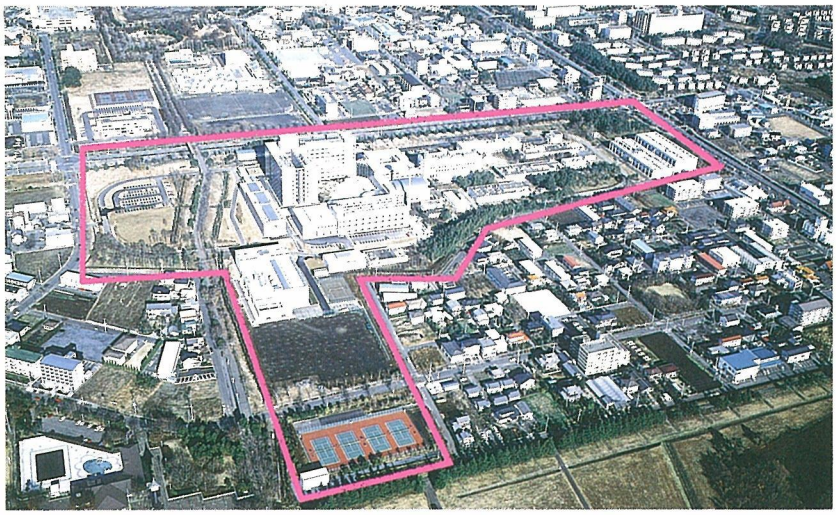

Sengen Site

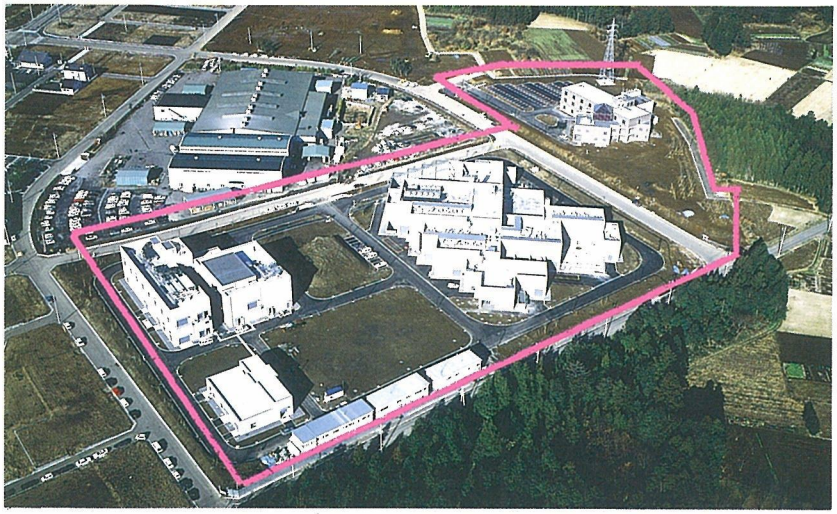

Shibasaki Site

Meguro Site

Preface

The National Research Institute for Metals (NRIM) was founded in 1956 as a research institution attached to the Science and Technology Agency of the Government of Japan. NRIM has since then played an essential role in research and development of metals and alloys in Japan. The number of its staff members is now beyond 300, while the size of its budget is reaching ¥10 billion for fiscal year 1994.

NRIM's research activities are dedicated to fundamental and applied research in advanced materials, such as metallic and oxide superconductors, heat-resisting alloys, structural intermetallic compounds, etc. Special efforts are devoted also to research in reliability of materials to ensure safety of structural components and facilities. These include production of standard creep and fatigue data on the Japanese commercial alloys, and studies on failure mechanisms and materials life prediction methods.

During the past 38 years, NRIM has made a number of contributions to the progress in materials science and technology. In the field of superconducting materials, for example, the bronze method for fabricating metallic superconducting wires was developed in late 60's, and a new oxide superconductor of Bi-Sr-Ca-Cu was discovered in 1988 which showed a superconducting critical temperature, T_c, above 100 K. A computer-aided alloy design method for superalloys was established, based on which several heat resisting alloys of excellent properties were in fact developed. Very long term research programs have been carried out on creep and fatigue properties, including creep rupture tests over 100,000 hours. As a result of this type of research, a series of "NRIM Creep and Fatigue Data Sheets" have been published which we believe are one of the most reliable creep and fatigue data sets for commercial alloys in the world. These data sheet programs will be continued in the NRIM Meguro Site along with their original research plans. NRIM is thus contributing to the progress in materials life time prediction as well as advanced materials assessment technology.

NRIM is currently moving from Tokyo to Tsukuba and the integration of personnels and research facilities will be completed in 1995. We take this opportunity to extend our materials research frontiers, and have initiated various challenging activities with respect to the studies using high magnetic fields, ultra-high vacuum and high-energy beam assisted excited states, and computer-aided materials science. We strongly hope that with all these new activities and excellent research circumstances NRIM will accomplish an innovative reform of its materials research.

Kazuyoshi Nii

Dr. Kazuyoshi NII
Director-General

NRIM Research Activities 1994

Contents

Research Topics

❒ Magnetic Study of Ce at High Pressure

T. Matsumoto, Materials Physics Division

Keywords: magnetic state, cerium, α-γ transition, Kondo effect

The phase transition and the valence instability of cerium metal have been the subject of many investigations in recent decades[1, 2]. It is generally believed that 4*f* electrons in most of the rare-earth metals are located far inside the 6*s* and 5*d* electrons and behave as localized electron. However, Ce and many Ce based metallic compounds exhibit intermediate valence which is derived from both delocalized and localized *f* electron nature. In the Temperature-Pressure (*TP*) plane of solid Ce metal, the α, β and γ-phases, which have fcc, dhcp and fcc structures, respectively, are separated by lines of first order phase transitions[1, 2]. An isostructural change with large **volume collapse** (–17%) and **demagnetization** occur at the transition from γ- to α-Ce[1, 2]. Recently, the volume collapse had been theoretically explained by a Kondo model[3]. In this context, we focus on the decrement of the magnetic susceptibility with decreasing volume in α- and γ-Ce. Here, the present results of the susceptibility under pressure is tried to analyze as a function of volume by using the single impurity Kondo model.

Figure 1 shows the magnetic susceptibility of Ce as a function of temperature and pressure at H = 1.2 T. As shown in this figure, the susceptibility in the γ-phase obeys the Curie-Weiss law, while the susceptibility shows thermal hysteresis associated with the α-γ transition. It is interesting to notice the decrease of the susceptibility with increasing pressure in γ-Ce. We try to fit the susceptibility data in γ-Ce to $\chi(T) = \chi_0 + C/(T + \theta_p)$ where χ_0, C and θ_p are the constant susceptibility, the Curie constant and the Weiss temperature, respectively. For example, at P = 0.4 GPa, χ_0, C and θ_p are obtained 1.18×10^{-4} emu/mol, 0.749 Kemu/mol and 57 K, respectively. Figure 2 shows the results of C and θ_p. The measured effective magnetic moment μ_{eff} is close to the value of free Ce^{3+}, 2.54, and is independent of pressure. On the other hand, the Weiss temperature θ_p varies strongly with pressure.

In γ-Ce, the decrement of the susceptibility with pressure seems to result from the increment of θ_p. The susceptibility is numerically given for a S = 1/2 single-impurity Kondo model above T_K:

$$\chi_{imp} = \frac{C}{T + 2T_K} \tag{1}$$

where T_K is the Kondo temperature well represented by the form

$$T_K = 0.364\varepsilon_f J^{1/2} \exp(-1/J) \tag{2}$$

where J is the effective Kondo coupling constant and ε_f is the energy difference between the 4f level

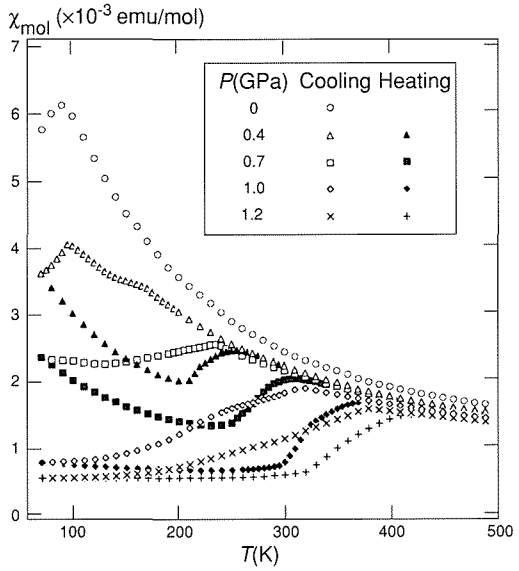

Fig. 1 Magnetic susceptibility of Ce as a function of temperature and pressure.

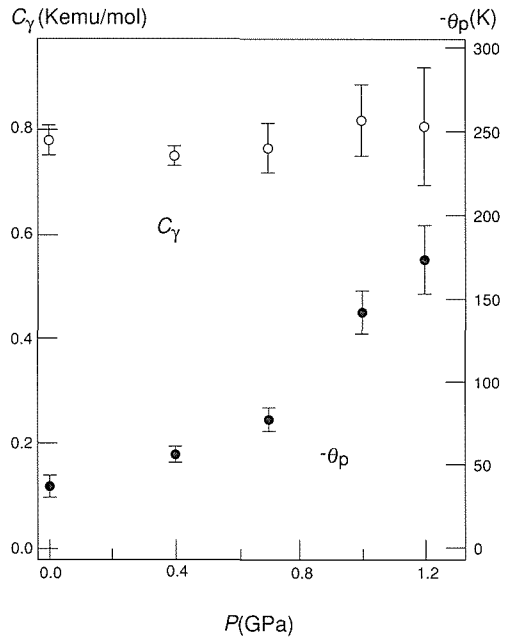

Fig. 2 The Curie constant and Weiss temperature as a function of pressure. Open (close) markers represent the data on cooling (heating) cycle.

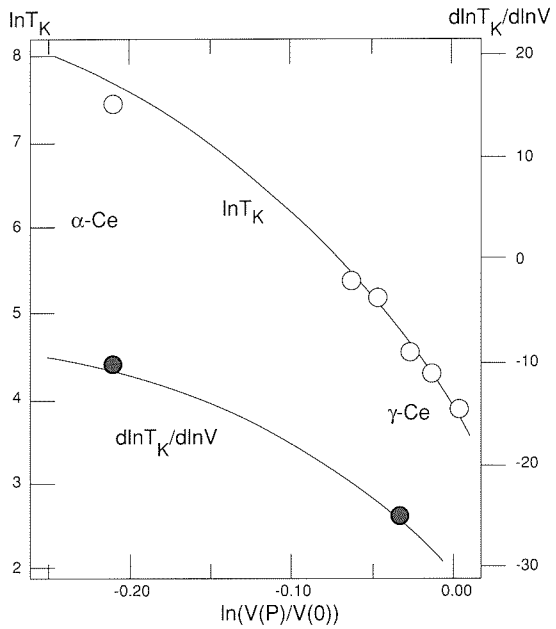

Fig. 3 The Kondo (spin fluctuation) temperature and its Grüneisen constant of Ce as a function of reduced volume. See text for solid lines.

and Fermi level[4]. In the viewpoint of the Kondo model, the origin of the decrement of the susceptibility with pressure in γ-Ce can be regarded as the increment of T_K. Although the relation of $\theta_p = 2T_K$ can not be directly applied to the temperature-dependent term of the susceptibility in γ-Ce with a total moment of $j = 5/2$, it is plausible to use a relation θ_p/T_K = const. This gives the Grüneisen constant of the Kondo temperature, $\Gamma_K = d\ln T_K/d\ln V = \Gamma_p = d\ln\theta_p/d\ln V$. Here, Γ_p is obtained to be –25 at around $V(P)/V(0) = 0.968$ in the γ-phase from the present result of θ_p vs. P. In this estimation, the pressure was converted to the volume by using a previous report of P-V isotherms of Ce[5]. This large value of Γ_p, which means that T_K increases rapidly with decreasing volume, is comparable to that of dilute Ce in La or Y metal[6]. By the way, we obtain $\Gamma_K = \Gamma_f + (1/2 + 1/J)\Gamma_J$ from the volume differential of equation 2 where Γ_f and Γ_J are the Grüneisen constant of ε_f and J, respectively. On the assumption of $\Gamma_f << (\Gamma_J$ or $\Gamma_K)$[7], J is estimated to be 0.270 at V(P)/V(0) = 0.968 by using the empirical value $\Gamma_J = 6$ for dilute Ce in La or Y[6] and $\Gamma_K = -25$. These derive $J = 0.222(V(P)/V(0))^{-6}$. Using $\varepsilon_f = 2$ eV[8], T_K can be, therefore, calculated as a function of volume from equation 2.

On the other hand, in the case of low temperature limit $T << T_K$, a theoretical impurity susceptibility is shown to become a constant value, $\chi(0) = C/T_{sf}$, where T_{sf} is the spin fluctuation temperature[4]. If this aspect can be applied to the susceptibility of α-Ce measured at $P = 1.2$ GPa, which shows nearly temperature independent, T_{sf} is estimated to be 1550 K. Also, the Grüneisen constant of T_{sf}, $d\ln T_{sf}/d\ln V = -(1/k_T)d\ln\chi(0)/dP$, can be estimated to be –10 by using the results of the pressure dependence of susceptibility at room temperature and the compressibility k_T in the α-phase reported previously[5, 9]. Figure 3 shows the dependence of T_K (T_{sf}) and $d\ln T_K/d\ln V$ ($d\ln T_{sf}/d\ln V$) on the reduced volume $V(P)/V(0)$. The solid lines in Fig. 3 are the values of T_K and $d\ln T_K/d\ln V$ calculated by using equation 2 and $J = 0.222(V(P))/V(0))^{-6}$ as a function of $V(P)/V(0)$. It is very interesting to notice that the values of T_{sf} and $d\ln T_{sf}/d\ln V$ in the α-phase lie on the extrapolation of the theoretical value for the γ-phase, respectively. That is, the single impurity Kondo model well explains the pressure dependence of the susceptibility in α- and γ-Ce.

References

1. *Valence Fluctuation Phenomena*, J.M. Lawrence et al., Rep. Prog. Phys., 44 (1981): 1–122.
2. *Cerium*, D.C. Koskenmaki and K.A. Gschneider, Jr., Vol. 1, Chap. 4, *Handbook on the Physics and Chemistry of Rare Earths*, edited by K.A. Gschneider and L. Eyring, (North-Holland, Amsterdam, 1978).
3. *Kondo Volume Collapse and the γ–α Transition in Cerium*, J.W. Allen and R.M. Martin, Phys. Rev. Lett., 49 (1982): 1106–10. *The γ–α Transition in Cerium Compounds*, M. Lavagna et al., J. Phys., F 13 (1983): 1007–15.
4. *Renormalization-Group Approach to the Anderson Model of Dilute Magnetic Alloys*, H.R. Krishnamurthy et al., Phys. Rev., B 21 (1980): 1044–47.
5. *On the Existence of a Critical Point for the Phase Transition in Cerium*, R.I. Beecroft and C.A. Swenson, J. Phys. Chem. Solid, 15 (1960): 234–39.
6. *Pressure as a Parameter in the Study of Dilute Magnetic Alloys*, J.S. Schilling, Adv. Phys., 28 (1979): 657–715.
7. This condition is speculated from the fact that the difference of the binding energy of 4*f* electron between α- and γ-Ce obtained by photoemission is very small; *Photoemission Studies of the γ–α Phase Transition in Ce: Change in 4f Character*, D. Wieliczka et al., Phys. Rev., B 26 (1982): 7056–59.
8. *Resonant Photoemission Studies of Mixed-Valence, Reduced-Moment, and Antiferromagnetic Cerium Compounds*, J.W. Allen et al., Phys. Rev. Lett., 46 (1981): 1100–03; *$CeRu_2$ and $CeCo_2$: Superconductors with 4f Electrons*, J.W. Allen et al., Phys. Rev., B 26 (1982): 445–48.
9. *Magnetic Susceptibility of Cerium Metal under Pressure*, M.R. MacPherson et al., Phys. Rev. Lett., 26 (1971): 20–23.

❒ High Resolution Electron Microscope Study of Deformation Structures in Fe-based Shape Memory Alloys

S. Kajiwara and K. Ogawa, Physical Properties Division*

Keywords: shape memory effect, martensitic transformation, lattice image, nanometric substructure, high resolution electron microscopy

Recently, studies of shape memory effects have begun to concentrate in Fe-based shape memory alloys to find an alloy comparable to the famous NiTi alloy, because the latter alloy is very expensive and a much cheaper shape memory alloy is being sought. The most promising alloy will be among Fe-Mn-Si alloys[1] and their modification, i.e., Fe-Mn-Si-Cr-Ni alloys[2, 3] which have a property of corrosion-resistance. The martensitic transformation involved in the shape memory effect of these alloys is from face-centered cubic structure (f.c.c.) to hexagonal close-packed structure (h.c.p.) by deformation and its reverse transformation on heating to recover the original shape.

In the present work[4], in order to understand the mechanism of the shape recovery of these alloys, transformation structures induced by extension after different heat treatments which give rise to different degrees of shape recoveries have been studied with high resolution electron microscope in view of nanometric scales.

The alloy used is an Fe-14Mn-6Si-9Cr-5Ni (mass%) alloy. One kind of the specimens has been subjected to such a thermomechanical treatment that a specimen which had been solution-heat treated at 1320 K for 30 min was first cold rolled by 10% at room temperature and then heated to 970 K for 10 min. This heat treatment produces a better shape memory effect than that of specimens which were merely subjected to the solution-treatment; that is, the shape recovery of the former is about 80%, while that of the latter is about 50% when the amount of shape change is 4% elongation. The Ms temperatures of the thermomechanically treated and the non-thermomechanically treated specimens are 250 K and 300 K, respectively. The specimens of 4 mm in width, 40 mm in gauge length and 0.4 mm in thickness were extended by 4% at room temperature after both types of the heat-treatments.

For convenience sake, we denote hereafter in this paper the specimens thermomechanically treated as specimen A and those solution-treated only as specimen B.

Figures 1 and 2 show high resolution electron micrographs taken from specimens A and B, respectively. In these micrographs we can see lattice images of (00.1) and (10.0) of h.c.p. martensite and that of (111) of f.c.c. parent phase, of which spacings are 0.42 nm, 0.22 nm and 0.21 nm, respectively. (In these figures suffixes, h and f, denote h.c.p. and f.c.c. structures, respectively.) Upwards arrows indicate regions of f.c.c. phase which reveal $(111)_h$ lattice images. As seen in Fig. 1, the f.c.c. phase with the thickness of down to 3–5 layers of the (111) lattice spacing are mixed with the h.c.p. phase in specimen A, but no such mixture is seen in the case of specimen B (Fig. 2). Lattice images with the spacing of 0.63 nm are seen besides those of the $(00.1)_{h.c.p.}$ in Fig. 2 and these are considered to correspond to stacking faults with a stacking order similar to 9R structure, namely, ABC/BCA/CAB, because the spacing of the lattice image is about 1.5 times larger than that of $(00.1)_{h.c.p.}$ lattice image.

In order to know more quantitatively the distribution of the mixture of f.c.c. phase and h.c.p. phase, lattice images of each phase have been examined along a given line perpendicular to the $(00.1)_{h.c.p.}$ lattice image. The width of the observed deformation bands was in the range of 100–200 nm. More than ten of such bands in each specimen were examined in detail. The results indicate that there is a clear difference in the distribution between specimens A and B; that is, for specimen A, the band usually consists of a mixture of f.c.c and h.c.p. phase with the thickness of 1–10 nm, while for specimen B, there are very few cases where the f.c.c. phase is mixed with h.c.p. phase in the band. This fact may be related to the difference in shape recovery between specimens A and B. That is, it is quite conceivable that the reverse transformation to the parent phase is much easier for specimen A than for specimen B, because it is not necessary to nucleate the f.c.c. phase in specimen A. But in specimen B it will be necessary to nucleate the f.c.c. phase in the band in order to initiate the reverse transformation in nanometric scales. To minimize the shape deformation of each martensite plate for the shape recovery, it will be important to make the reverse transformation proceed in a scale as small as possible. If the reverse transformation occurs in a large scale in the sense that the h.c.p. band transforms as a whole, then the resistance accompanying the shape deformation may be greater because the accommodation deformation must be large in that case.

A mixture of f.c.c. and h.c.p. phases in nanometric scales in specimen A is considered to have resulted from the existence of stacking faults in

*Materials Characterization Division

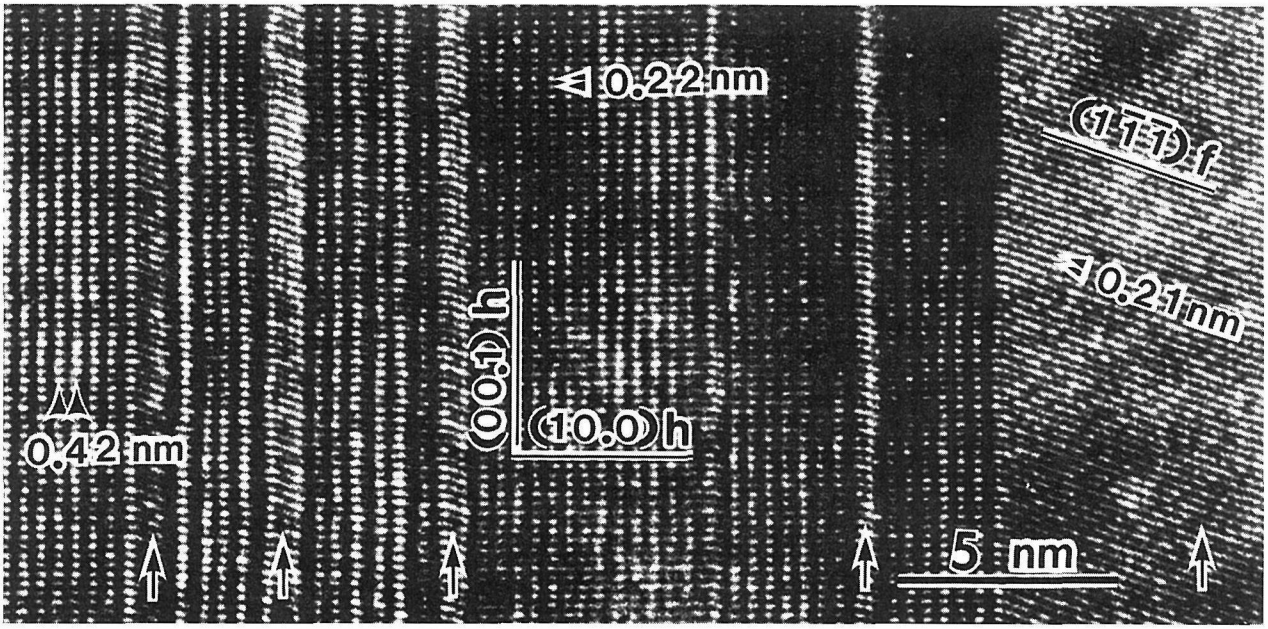

Fig. 1 High resolution electron micrograph showing lattice images of $(10.0)_{h.c.p.}$ as well as $(00.1)_{h.c.p.}$ and $(111)_{f.c.c.}$ for specimen A.

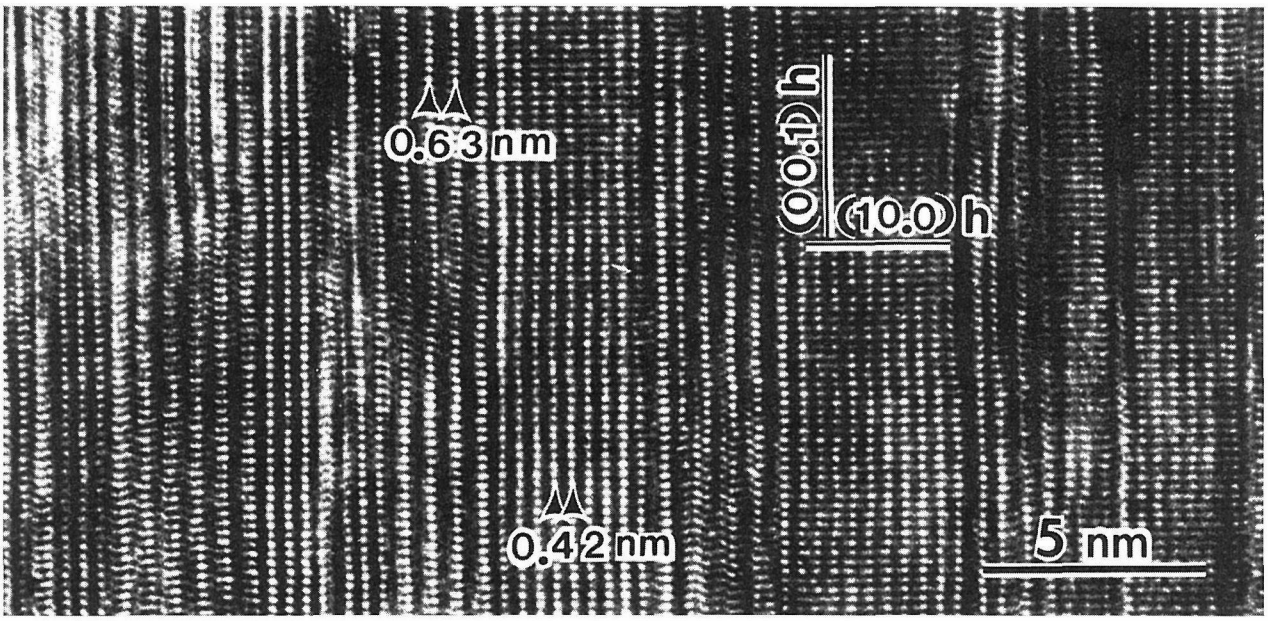

Fig. 2 High resolution electron micrograph showing lattice images of $(00.1)_{h.c.p.}$ and $(10.0)_{h.c.p.}$ for specimen B. In this figure we also notice lattice images of 0.63 nm spacing which may correspond to stacking faults with a stacking order of ABC/BCA/CAB.

austenite before the extension. That is, these stacking faults provide nucleation sites for the f.c.c. to h.c.p. transformation. In specimen B, since there is no such stacking faults, the transformation by extension will proceed by thicking a band once the h.c.p. phase has nucleated at a certain place. Therefore, it is necessary that, to obtain good shape memory effect, many stacking faults in austenite are scattered as uniformly as possible so that the resulting deformation band consists of a uniform mixture of f.c.c. and h.c.p. phase in nanometric scales.

References

1. *Development of a Shape Memory Alloy Fe-Mn-Si*, A. Sato and T. Mori, Mater. Sci. Eng., A 146 (1991): 194–204.
2. *Shape Memory Effect in Fe-Mn-Si-Cr-Ni Polycrystalline Alloys*, H. Otsuka, H. Yamada, H. Tanahashi, and T. Maruyama, Proc. Int. Conf. Martensitic Transformation, Sydney, 1989 Materials Science Forum, 9 (1989): 655–60.
3. *Effect of Alloying Elements on Shape Memory Effect of Fe-Cr-Ni-Mn-Si (-Co) Alloys*, Y. Moriya, H. Suzuki, S. Hashizume, T. Sampei, and I. Kosasu, Proc. Int. Conf. on Stainless Steels, Chiba, ISIJ, (1991): 527–32.
4. *HREM Study of Stress-Induced Transformation Structures in an Fe-Mn-Si-Cr-Ni Shape Memory Alloy*, K. Ogawa and S. Kajiwara, Met. Trans. JIM, 34 (1993): 1169–76.

❒ Analysis of Preferential Substitution Site of the Third Element in TiAl($L1_0$) Compound by the Cluster Variation Method

H. Onodera, T. Abe and T. Yokokawa, Materials Design Division

Keywords: $L1_0$ TiAl compound, substitution site, cluster variation method (CVM), antiphase boundary (APB) energy

Introduction

Intermetallic titanium aluminide, TiAl($L1_0$) is of current interest for applications in the aerospace industry owing to its low density, high specific strength and good oxidation resistance. However, the poor ductility at room temperature has prevented its practical use. Recently it has been shown that the addition of the third element (e.g. V, Nb, Mn and Cr) into TiAl results in the improvement of the ductility. For the understanding of the mechanism of the improvement, it seems to be very important to reveal the substitution site of the third element and long range order parameter in the TiAl-X alloy.

The cluster variation method (CVM) developed by Kikuchi[1] has been used widely and successfully for the analysis of order-disorder phenomena in cubic structures such as fcc and bcc. Recently, we applied the CVM to the calculation of hcp-DO_{19} phase equilibrium in the Ti-Al system and revealed the effect of tetragonality on the phase equilibrium[2]. The CVM can calculate the probabilities of atom configurations affected by the interactions between atoms in the same and different sublattices in a most reliable manner. Thus, in the present study[3], the preferential substitution site of the third element in the $L1_0$ TiAl structure has been investigated by CVM with Lennard-Jones pair potential. At the same time, antiphase boundary (APB) energies were calculated in the TiAl and TiAl-X alloys.

Calculation of Free Energy

The equiatomic TiAl compound has $L1_0$ type superlattice where aluminum and titanium layers are piled up in <001> direction, alternatively, as shown in Fig. 1. Configurational entropy for $L1_0$ type superlattice was introduced by the CVM using the tetrahedron cluster shown in Fig. 1. Distance of Ti-Al pair in tetrahedron cluster is longer than those of Ti-Ti and Al-Al pairs because c axis is longer than a axis. The average configurational entropy per a lattice point, S, is written as

$$S=-k_B\begin{bmatrix}2\sum_{ijkl} L\left(Z^{TTAA}_{ijkl}\right)\\ -\sum_{ij}\left\{L\left({}^sY^{TT}_{ij}\right)+L\left({}^sY^{AA}_{ij}\right)+4L\left({}^lY^{TA}_{ij}\right)\right\}\\ +(5/2)\sum_{i}\left\{L\left(X^T_i\right)+L\left(X^A_i\right)\right\}\end{bmatrix}, \quad (1)$$

where the superscripts T, A, l, and s show the Ti and Al sublattices, the second and first nearest neighbor atomic distances, respectively. Z, Y, X and k_B are tetrahedron cluster, pair, and point probabilities and Boltzmann constant, respectively, and L(X) = Xln(X) − X. In the present approximation, the enthalpy, H, is given by the sum of the energies of first and second nearest neighbor pairs as

$$H=\sum_{ij}\left\{e_{ij}(rs)\left({}^sY^{TT}_{ij}+{}^sY^{AA}_{ij}\right)+4e_{ij}(rl)\left({}^lY^{TA}_{ij}\right)\right\}, \quad (2)$$

where the pair energy, $e_{ij}(r)$ is dependent upon the interatomic distance, r. In order to obtain the most probable atom configuration at equilibrium, the grand potential, Ω, of the system defined as

$$\Omega=H-TS+PV-\sum_i \mu_i X_i, \quad (3)$$

is minimized with respect to both tetrahedron cluster probability and the atomic volume, V, at a constant temperature, T, pressure, P, and the chemical potential of the i atom μ_i under the normalization condition, $\Sigma Z_{ijkl} = 1$.

The pair interactions are expressed by the Lennard-Jones (L-J) pair potential of the form,

$$e_{ij}(r)={}^oe_{ij}\left\{\left(r_{ij}/r\right)^8-2\left(r_{ij}/r\right)^4\right\}. \quad (4)$$

The L-J potential parameters ${}^oe_{ij}$ and r_{ij}, were evaluated from cohesive energies and lattice parameters of pure elements and from the energies of formation and lattice parameters of compounds.

Preferential Substitution Site of the Third Element

The calculated concentration at 1573 K of the third element, X, in the Al sublattice forTiAl-1at%X alloys are shown in Fig. 2 as a function of

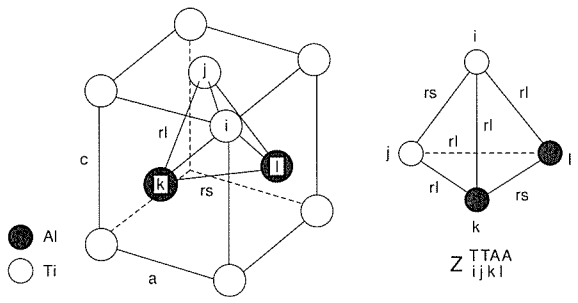

Fig. 1 Tetrahedron cluster for $L1_0$ structure used in the CVM calculation.

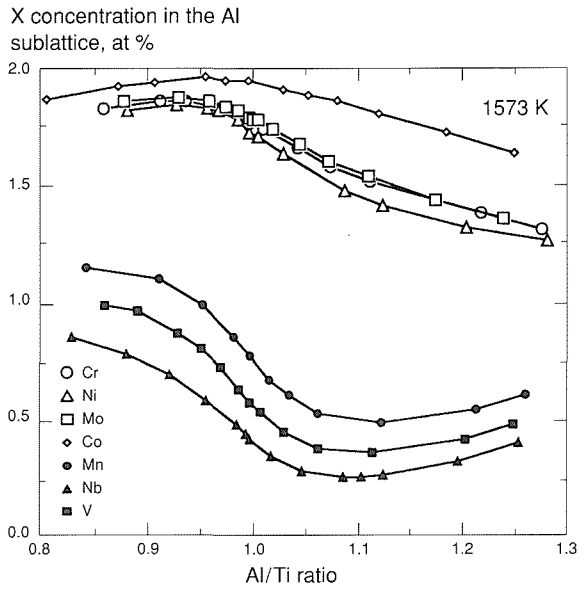

Fig. 2 Variation of alloy element concentration in the Al sublattice with Al/Ti ratio. The bulk alloy element concentration is 1at%.

the ratio of Ti and Al contents (Al/Ti ratio). The preferential substitution site of the third element in TiAl-1at%X alloys varied depending on Al/Ti ratio. Especially, for Mn, Nb, and V, the preferential substitution site is remarkably changed on both sides of stoichiometry. In the Ti-rich region, Co, Cr, Ni and Mo mainly occupy the Al sublattice, and Mn, Nb and V occupy both sublattices. In the Al-rich region, Mn, Nb and V mainly occupy the Ti sublattice, and Co, Mo, Ni and Cr occupy both sublattices. Thus, the substitution behavior is classified into two groups; (1) Cr, Co, Mo, and Ni which are preferentially substituted for Al, and (2) Nb, Mn and V which are preferentially substituted for Ti.

These calculated results are in good agreement with the experimentally determined substitution characteristics of Ni, Nb, V, Mn and Cr in literatures, which were measured by means of electron channeling (ALCHEMI) or X-ray diffraction method. The observed difference of substitution behavior can be interpreted from the interaction parameters, $\phi_{A\text{-}B}$, which is defined by equation (5)

$$\phi_{A-B} = e_{AB} - (e_{AA} + e_{BB})/2, \qquad (5)$$

where e_{AB}, e_{AA} and e_{BB} are potential energies of A-B, A-A and B-B pairs, respectively. The $\phi_{Ti\text{-}X}$ is larger than $\phi_{Al\text{-}X}$ for Co, Cr, Mo and Ni which are preferentially substituted for Al. This suggests that these elements have stronger bond with Ti atom than with Al atom. On the contrary, the opposite tendency is observed for Mn, Nb and V, which are preferentially substituted for Ti.

Antiphase Boundary (APB) Energy

The APB, intrinsic stacking fault (ISF) and complex stacking fault (CSF) play important role in deformation of intermetallic compound.

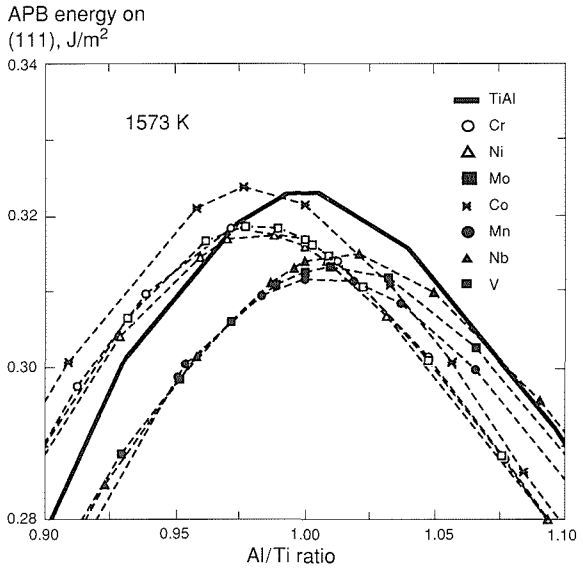

Fig. 3 Variations of APB energy on (111) plane with alloy element additions as a function of Al/Ti ratio.

The calculated APB energy on the (111) plane is shown in Fig. 3 as a function of Al/Ti ratio. For the TiAl alloy (solid line), the APB energy has the maximum value at stoichiometry and decreases with increasing deviations from it. By the additions of V, Nb and Mn, which are preferentially substituted for Ti, the peak position deviates from stoichiometry to the Al-rich region, and the peak hight is decreased. By the additions of Mo and Ni, which are preferentially substituted for Al, the peak position deviates to the Ti-rich region. Thus, the effect of third element additions on APB energy seems to be correlated with the substitution behavior of the element. For the calculated APB energies on the (001) and (101) planes, the same tendencies were observed.

References

1. *A Theory of Cooperative Phenomena*, R. Kikuchi, Phys. Rev., 81 (1951): 998–1003.
2. *Modeling of α/α_2 Phase Equilibrium in the Ti-Al System by the Cluster Variation Method*, H. Onodera, T. Abe, and T. Yokokawa, Acta Metall. Mater., 42 (1994): 887–92.
3. *Analysis of Preferential Substitution Site of the Third Element in TiAl ($L1_0$) Compound by the Cluster Variation Method*, T. Abe, T. Yokokawa, and H. Onodera, Proc. of COMMP '93, ISIJ, Tokyo, Japan, (1993): 308–13.

❒ Processing and Characterization of Nanostructured Materials

Y. Sakka, Chemical Processing Division

Keywords: nanocomposite, colloidal processing, reaction sintering, ultrafine particle, catalysis

Nanostructured materials can be classified into two general categories. One category consists of materials of only nanometer-sized particles. The other consists of materials where nanosized particles are distributed within the intra- and/or intergrain regions of micron-sized grains. These nanostructured materials have been receiving increasing attention due to their unique chemical and physical properties which cannot be obtained from the conventional materials. In the present topics, processing and characterization of the nanostructured materials of both categories are introduced.

Nanostructured Materials Using Ultrafine Particles

Metal ultrafine particles (UFPs) can be made by a variety of methods, from the vapor phase and liquid phase. Studies on the utilization of metal UFPs have been conducted as powders, films and bulk materials. In the case of bulk materials, fabrication of dense nanophase materials by consolidating UFPs has been conducted successfully, but attempts of fabrication of porous materials are limited. Initial sintering characteristics of UFPs are important factors which control the structure of the porous materials with large specific surface areas. We use the metal UFPs stabilized with an appropriate amount of surface oxide.

Figure 1 shows variation of crystallite sizes of three kinds of Fe UFPs, which have been stabilized with oxygen and exposed to air, after heating at fixed temperatures for 1 h in vacuum. The sintering diagrams in vacuum can be divided into three regions[1, 2]. In the first region, large amounts of H_2O and CO_2 are evolved. In the second region, sintering of the surface oxide is observed and in the third region, a significant shrinkage and grain growth occur due to sintering of both oxide and metal phases. In preparing the porous bodies, sintering UFPs in the second region in vacuum or an inert gas atmosphere followed by reduction of the surface oxide is suitable.

To obtain the porous bodies with sufficient high specific surface areas and strength, sintering under a pressure might be desirable. In electro-discharge sintering (EDS), the powders are heated by instantaneous high electric pulsed power application under a uniaxial pressure which also results in an *in situ* cleaning ability of UFPs from the adsorbed gases[3]. Figure 2 shows a typical EDS shrinkage features of Ni UFPs heated by electric pulsed power (1 kA for 80 ms) in a graphite die (diameter of 1 cm) under 50 MPa. Maximum shrinkage rate is seen around 600 K after 20 s. The specific surface areas of the samples at points A and B are 44.8 and 17.9 m^2/g, respectively, and no significant grain growth of both samples is observed. These results indicate that the EDS process is suitable for the fabrication of porous materials consisting of UFPs.

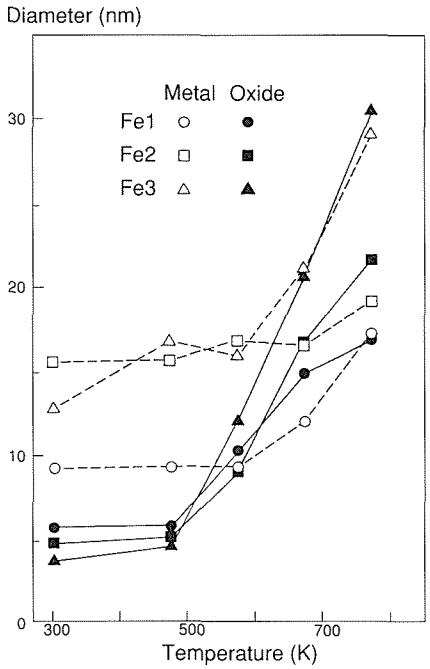

Fig. 1 Variation of crystallite sizes of three kinds of Fe UFPs after sintering for 1 h in vacuum.

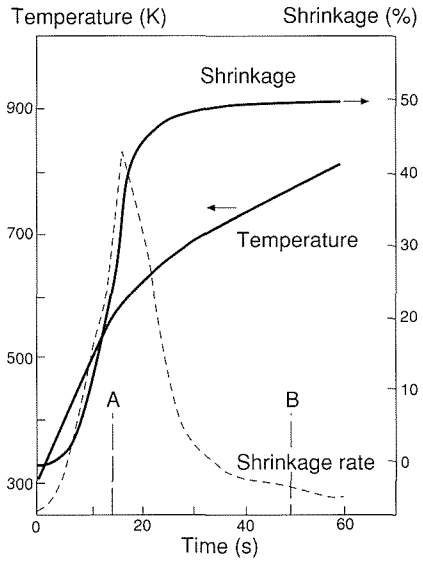

Fig. 2 EDS sintering diagram of Ni UFPs.

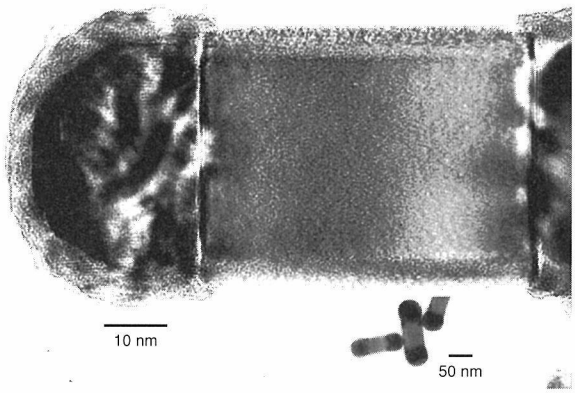

Fig. 3 TEM micrograph of Fe-TiN composite UFP.

Characterization of Nanocomposite Particles

Fe, Ni and Co are among the most active catalysts for the reactions of hydrogenation of carbon monoxide to hydrocarbons. Their UFPs are expected to be advanced catalysts, but cannot be used as they are of low thermal stability. Therefore, the UFPs must be stabilized with stable materials. Ceramic-supported metal catalysts are one of the best solution of the above problem. Recently, Ohno et al. (at NRIM) have developed a new technique preparing metal, ceramics and their bonded UFPs by vaporization-consolidation of metals or alloys in N_2 and/or H_2 atmosphere using a DC arc plasma[4]. The UFPs prepared by this method are well-dispersed and free of anion contamination compared to those by the wet process. Figure 3 shows a typical TEM micrograph of Fe-TiN composite UFPs. Dumbbell-like morphology is seen, where spherical parts are metal. To examine the catalytic property, temperature-programmed desorption experiments are performed for the (Fe, Ni, Co)-TiN composite UFPs after exposure to hydrogen at fixed temperatures. Thermal desorption peaks of hydrogen from Fe, Ni and Co above room temperature have been detected in the temperature range of 300–450 K. However, hydrogen desorption peaks above 450 K are observed for all the (Fe, Ni, Co)-TiN composite UFPs[5]. This implies that new adsorption states of hydrogen exist on the composite UFPs. Spillover hydrogen desorbed from TiN surface may be a feasible explanation.

Processing of Nanocomposite by Reaction Sintering

For the powder processing of fine powders, colloidal dispersion and consolidation techniques have high potential in controlling pore volume and pore size distribution of compacts. Desired structures, such as hierarchically structured and nanocomposite materials, can be achieved by the colloidal processing.

SiC-mullite-Al_2O_3 nanocomposites are processed through a novel colloidal consolidation and reaction sintering[6]. Our procedure consists of three steps shown in Fig. 4. Firstly, micron-sized SiC and

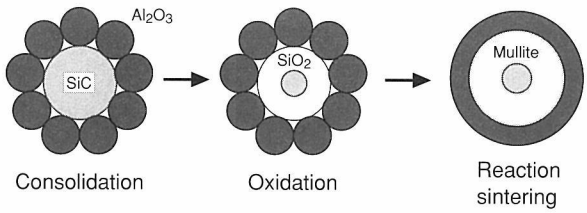

Fig. 4 Schematic illustration of the process steps used to produce nanocomposite by reaction sintering.

Al_2O_3 particles are colloidally dispersed and consolidated to form uniformly mixed compacts. Secondly, SiC particles are partially oxidized until the SiC particle is reduced to a nanometer-sized core and finally, these nanometer-sized core particles are trapped within a mullite matrix as the silica oxidation product reacted within the alumina to form the mullite matrix. This process offers several advantages and thereby warrants further research: (1) it eliminates the need to reduce the particle size of the inclusion phase to the nanometer range by milling and thus provides better control in minimizing impurities; (2) due to volume increase during reaction sintering, sintering shrinkage is lower, and (3) the presence of amorphous silica as a transient phase results in enhanced densification by viscous deformation and thus provides an opportunity to process these composites without pressure.

References

1. *Surface Chemistry and Sintering Characteristics of Ni Ultrafine Powders*, Y. Sakka and T. Uchikoshi, Powder Metall., 36 (1993): 179–85.
2. *Sintering Characteristics of Fe and FeCo Alloy Ultrafine Powders*, Y. Sakka, T. Uchikoshi, and E. Ozawa, J. Mater. Sci., 28 (1993): 203–17.
3. *Fabrication of Porous Materials by Consolidating Ultrafine Metal Powders*, Y. Sakka, T. Uchikoshi, S. Ohno, and H. Okuyama, Proc. Powder Metallurgy World Congress, (1993): 792–95.
4. *Synthesizes of the Composite Ultrafine Particles of Fe-TiN, Ni-TiN and Co-TiN Systems by "Reactive Plasma-Metal" Reaction*, S. Ohno, K. Honma, H. Okuyama, and M. Ozawa, J. Jpn. Inst. Met., 53 (1989): 936–45 (in Japanese).
5. *Characterization of (Fe, Ni, Co)-TiN Nanocomposite Particles Synthesized by "Reactive Plasma-Metal Reaction" Method*, Y. Sakka, S. Ohno, T. Uchikoshi, H. Okuyama, and M. Ozawa, Advanced Materials '93, IA, (1994): 57–60.
6. *Processing of SiC-Mullite-Alumina Nanocomposites*, Y. Sakka, D.D. Bidinger, and I.A. Aksay, J. Am. Ceram. Soc., 78-2 (1995): in press.

❒ *In Situ* Strain Measurement by a Laser during Local Heating

Y. Muramatsu and S. Kuroda, Advanced Materials Processing Division

Keywords: strain measurement, laser speckle method, dynamic strain, spot diameter, cross correlation, image sensor, thermal stress, local distortion

Introduction

It has been very difficult to measure strains at high temperature such as these caused by a welding arc. These strains have been only estimated by numerical analysis using unreliable temperature dependence of physical properties. From the standpoint of production reliability, however, we often need to measure these strains *in situ* during production.

A possibility to measure these dynamic strains exists in a laser speckle method developed by Yamaguchi et al[1]. Laser speckles are random bright and dark patterns caused by interference of the scattered light from an object surface illuminated by a laser. Since the speckle pattern changes in a specific relation with the movement and deformation of the object surface, strains can be calculated from the change in the speckle pattern. It has been often used for measurement of the mechanical properties of materials where it is difficult to use strain gauges, such as polymer films.

If it can be applied to dynamic strain measurement at high temperature over 1273 K such as in the welded zone, we can better understand the deformation behavior of materials crucial to defect generation at high temperature such as hot cracking in welds.

Principle of the Strain Measurement

Figure 1 shows (a) the scheme of the laser speckle method and (b) the principle to calculate strains. An argon ion laser illuminates the bottom surface of a specimen plate, over which a gas tungsten arc (GTA) travels to weld. A stainless steel plate with 4 mm thickness was mostly used as the specimen. The light intensity distribution of the speckle formed on a pair of linear image sensors ①, ② is continuously recorded by a data logger during welding.

By comparing two speckle patterns at the time t_0 and $t_0 + \Delta t$ on each sensor, we can find out how the pattern shifted on each sensor in the x-direction $Ax(-\theta_o)$ and $Ax(\theta_o)$. Mathematically this is done by finding the maximum in the cross correlation functions between the two speckle patterns.

Then $Ax(-\theta_o) + Ax(\theta_o)$ gives the degree of shrinkage of the speckle pattern, which can be related to the strain ε_x at the illuminated spot by repeating this operation, a continuous strain curve can be obtained.

For comparison, grids were scratched on the surface of some specimens and photographed continuously during welding.

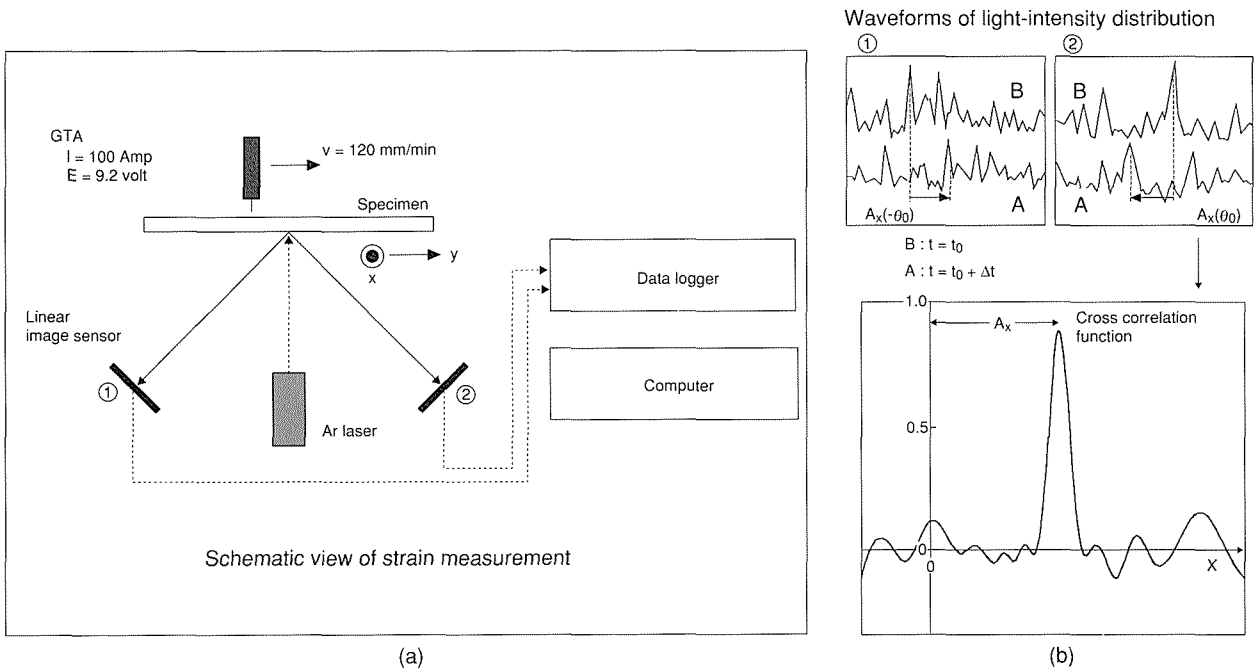

Fig. 1 Profile of the laser speckle strain measurement.

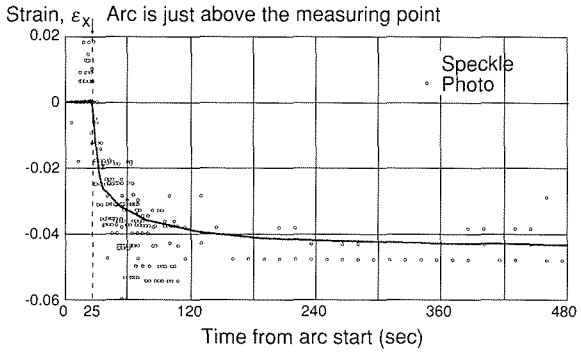

Fig. 2 Comparison of the measuring results between the laser speckle method and the sequential photographs in the direction (x) perpendicular to the heating line.

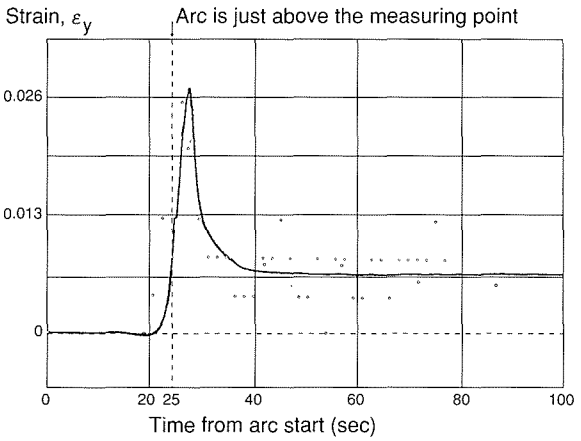

Fig. 3 Comparison of the measuring results between the laser speckle method and the sequential photographs in the direction (y) of the heating line.

Results of Measurement[2, 3]

Sampling interval Δt of 8 ms was sufficient to follow the change of the speckle pattern with our experimental conditions. Figures 2 and 3 compare the results of the laser speckle method (solid curve) with the strains measured on the photographs (circles) Both curves show a generally good agreement with the small circles. Moreover, we can measure the strain sufficiently at about 1273 K by this method.

There was a discrepancy in the x-direction, however, between the speckle and the photography; the former was too small when the heat source passes over the measuring point. This is probably caused by the local expansion in the thickness direction created by the heat source, which will be studied further.

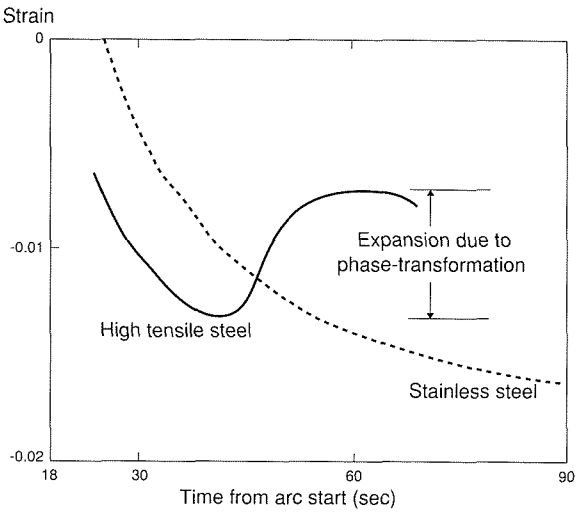

Fig. 4 Phase-transformation appeared in the strain curve of a high tensile steel after welding.

Formation of oxidized films, did not give strong effects on the measuring accuracy.

Another interesting result is shown in Fig. 4, in which the the expansion by phase-transformation of steels during cooling after welding is captured. The effects of cooling time on the behavior of phase-transformation, which seem to differ from those in CCT diagram, were also found out by this method. Therefore, we are expecting to obtain more information on the phase-transformation in actual welding.

References

1. *Advances in the Laser Speckle Strain Gauge*, I. Yamaguchi, Opt. Eng., 27 (1988): 214–18.
2. *Application of the Laser Speckle Method to Strain Measurement in the Welding Process*, Y. Muramatsu and S. Kuroda, Quarterly J. of the Japan Welding Soc., 10 (1992): 125–31 (in Japanese).
3. *Application of Laser Speckle Strain Measurement to Weld Monitoring*, Y. Muramatsu and S. Kuroda, Welding J., 73 (1994): 101s–09s.

❒ *In Situ* Observation of Ion Radiation Damage of Materials with the Transmission Electron Microscope (TEM)

K. Furuya, Materials Characterization Division

Keywords: radiation damage, *in situ* analysis, dual-beam ion irradiation, SUBNANOTRON, 1 MV TEM, 200 keV ion implanter, 30 keV ion sputter source

Introduction

Radiation damage of metallic materials is characterized by atomic displacements resulting from the interaction between atoms in the crystalline structure and energetic particles such as neutrons and ions. This atomic process produces many types of defects and defect clusters which are supposed to have a wide range of relaxation time varying from pico seconds to several hours. Therefore, the resultant microstructure generally becomes complicated with the formation of dislocation loops, voids, precipitates and so on. The difficulty of the basic understanding of radiation damage mainly comes from thermally unstable changes in lattice structure both during and after the irradiation experiments.

In situ irradiation of materials by means of transmission electron microscope (TEM) incorporated with ion accelerators is one of the fascinating methods to investigate the structural evolution induced by particles bombardments and implantation. Several technical problems, however, arise *in situ* facilities related to the decrease in the resolution because of the modification of TEM and to the continuous image drifts under the irradiations. The purpose of this research is to develop a new facility for *in situ* analysis of the microstructural aspects of materials under ion irradiation.

Development of *In Situ* TEM "SUBNANOTRON"

The facility so-called "SUBNANOTRON" consists of 1 MeV TEM with dual ion accelerators. The photograph of SUBNANOTRON is shown in figure 1. The voltage of 1 MeV for electron was chosen for the acceleration of electron to secure the resolution better than 0.15 nm, the penetration large enough for the observation of thick foils and the space at the specimen position large enough for the stressing, heating and cooling. The attached analytical tools such as SAD, EDS and i-EELS are essential to characterize the micro compositional changes of irradiated materials.

The construction of the SUBNANOTRON is now in the final stage for installing ion beams interface. Dual ion accelerator systems consist of 200 keV and 30 keV implanters with a hollow cathode heavy ion source and a RF discharge light ion source, respectively. The high energy beam is selected through a 1.5 T analyzing magnet at an angle of 45 degrees, and then deflected vertically

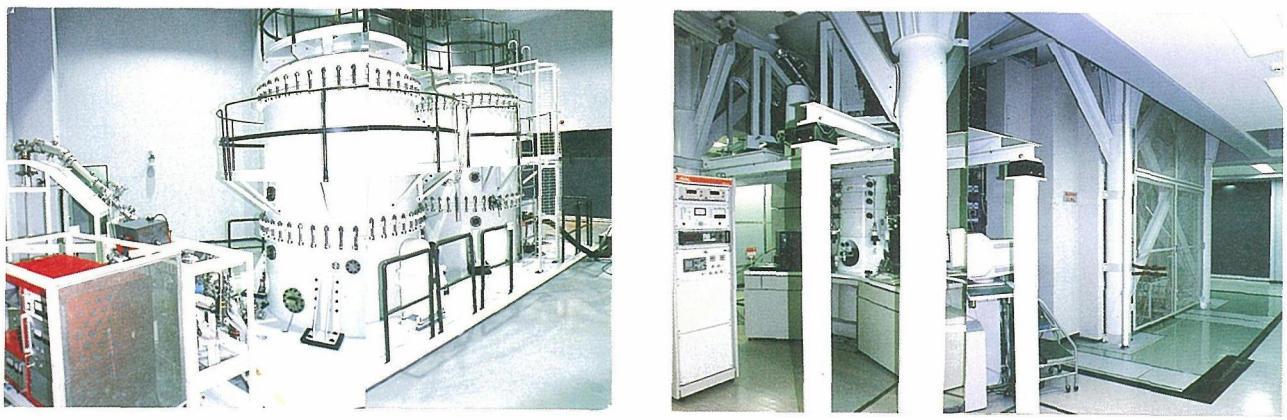

Fig. 1 Photograph of the in situ irradiation TEM named "SUBNANOTRON."

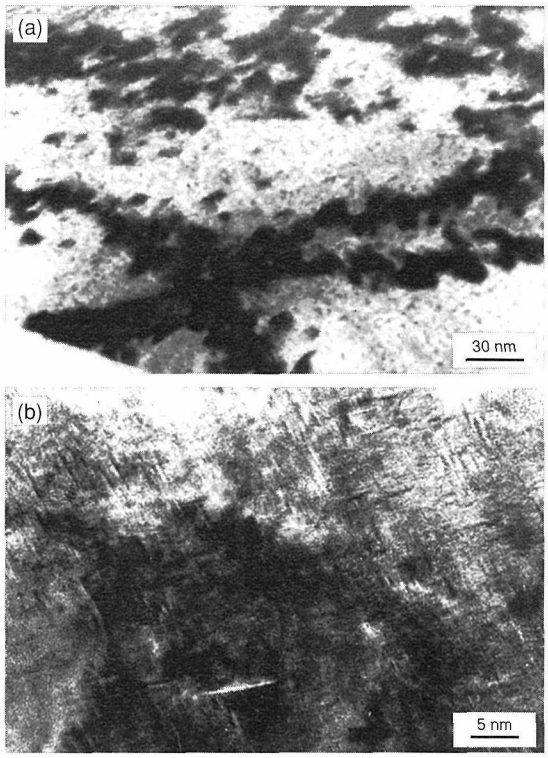

Fig. 2 Nanoscopic structure of secondary defects in Ni induced by 70 keV Ar^+ irradiation to a dose of 3.2 × 10^{19} ions/m^2 at room temperature. (a) a magnified bright image and (b) a lattice image at low magnification.

with an angle of 44 degrees for introducing into the TEM. The low energy beam is vertically analyzed before entering the port of the TEM. The beam lines were carefully controlled by electrostatic lens and evacuated by ion pumps and magnetically suspended turbo pumps for keeping the resolution of the TEM. TEM images are collected and magnified directly in a fiber optically coupled TV camera, and recorded with a VTR through a real time image processor.

High Resolution Observation of Ion Irradiated Defects in Ni

In situ irradiation of Ni was performed with the 200 keV TEM interfaced with an ion accelerator of 100 keV, which was designed as a prototype of SUBNANOTRON. Irradiation were carried out at room temperature with 70 keV Ar^+ of 3.5 × 10^{17} ions/m^2/s. After the *in situ* experiments, high resolution TEM (HRTEM) observations were performed with a 400 keV TEM.

The formation processes of secondary defects in Ni were clarified as follows: small dots nucleate at first, then they grow into loops and in some cases form dislocation networks. However, it is to be noted that close observations with HRTEM revealed that the details of defect's characteristics were dependent on the species of irradiation ion.

Figure 2 is the magnified photographs of defects induced by 70 keV Ar^+ irradiation. The bright field image, figure 2(a), displays a complicated network defects, whose appearance is quite different from

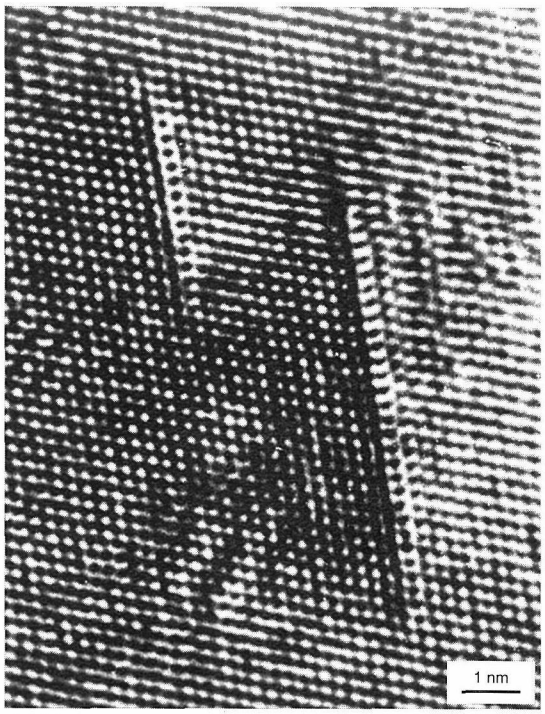

Fig. 3 High resolution image of the distorted line defects in Ni induced by 70 keV Ar^+ irradiation to a dose of 1.3 × 10^{19} ions/m^2 at room temperature. The defects are located on one of (111) planes with a size less than 10 nm length.

that of usually observed dislocation networks in irradiated metals. The morphology of defects comes from the aggregate of high dense dots which look dark due to a small shift of diffraction condition for transmitting electron beam. Figure 2(b) shows a low magnification lattice image of such dots, demonstrating a combination of amount of small line defects embedded in the distorted matrix.

Figure 3 shows a highly magnified lattice image of line defects in the Ni film tilted along [110] zone axis. These defects by Ar^+ irradiation have accompanied large distortion of lattice fringes in one of two series of apparent (111) planes, while no alteration in the number of lattice planes happens on both sides of lattice distortion. These facets imply that the strain on the preferential (111) planes is due to those particular defects or implanted Ar atoms which are directly resulting from the irradiation and do not have so high mobility as to rearrange the damaged lattice.

The present results surely demonstrate the usefulness of the *in situ* irradiation of materials in TEM followed by HRTEM observation for disclosing the mechanism of radiation damage in subnanometer scales. There remains, however, a different problem which is generally inherent in the observation on thin films where most of point defects, especially high mobility interstitials, annihilate easily on the surface during the irradiation. So that, further contrivance for solving the problem has to be made in the scheme of the *in situ* high resolution TEM observation with "SUBNANOTRON."

❒ *In Situ* Observation of MMC under Tensile Loading by Synchrotron X-ray CT

C. Masuda, Y. Tanaka, S. Nishijima, T. Hirano and K. Usami*, Failure Physics Division*

Keywords: X-ray CT, *in situ* observation, tensil test, metal matrix composite debonding

The Synchrotron Radiation CT (SR-CT) technique was applied successfully for the observation of SiC fiber in metal matrix composite (MMC). SiC fibers could be clearly discriminated from aluminum alloy matrix, as its coefficient of X-ray absorption differs by 8% from that of the fiber. The core carbon fiber of 3 μm in diameter and the debonding between the fiber and matrix could be also clearly observed[1, 2]. *In situ* observation was attempted to study the fracture process of MMC under static loading using SR-CT. Reconstruction of 3-dimensional images provided an excellent means to look at what was going in the MMC: fiber orientation, defects and voids formation were analyzed during loading.

Billets of SiC_f/A2024 composites were fabricated by powder metallurgy. The billets were then extruded to round bars of 6.5 mm in diameter and heat-treated under T6 condition. SiC fibers were rearranged almost parallel to the extrusion direction. Tensile test specimen was cut from the extruded bar. Specimens were machined to have a reduced section of 2 mm in diameter and 12 mm in length. Central part of the specimen was machined to an hourglass type of 1 mm in diameter for the SiC_f/A2024 composite in order to delimit fracture positions.

Figure 1 shows a block diagram of the SR-CT system for *in situ* observation of inner damage. A precision tensile testing machine is installed on the beam line 8C in the Photon Factory of the National Laboratory for High Energy Physics in Tsukuba. Monochromatic X-ray beam is used to irradiate the specimen on a small tensile testing machine. The X-ray passed through the specimen is detected by a 2-dimensional pickup tube. The specimen is under static loading rotated from 0 to 180 degrees in steps of 1 degree. The cross sectional image of the specimen is reconstructed by the back projection method. *In situ* observation of internal change under loading is thus tried under zero stress, 0.2% proof stress and stress near the fracture. The measurement time of one projection image is about 30 seconds.

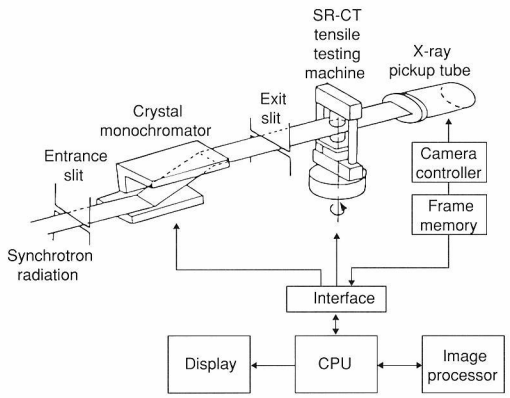

Fig. 1 Block digram of X-ray CT and in situ tensile machine

The output signal from the pickup tube is sent through the camera controller and stored in a 2 M bytes frame memory consisting of 1024 × 960 elements. Maximum of 40 CT images can be taken at once, which are condensed in 2-dimensional projection images of 960 scanning lines. The slicing position of the specimen to make a CT image can be selected with any small intervals, but in larger than X-ray line. Each line is imposed for several times to improve the S/N ratio of the transmitted X-rays.

Figure 2 shows monochromatic SR-CT images of SiC_f/A2024 composite at 0.2% proof stress and at near fracture stress. The SR-CT images are taken at 23 keV at ten neighboring slice planes, with cutting breadth of 31 μm and at the slice plane spacing of 162 μm. Black spots, gray circles and white background correspond respectively to the core carbon fibers, SiC fibers and A2024 aluminum alloy ma-

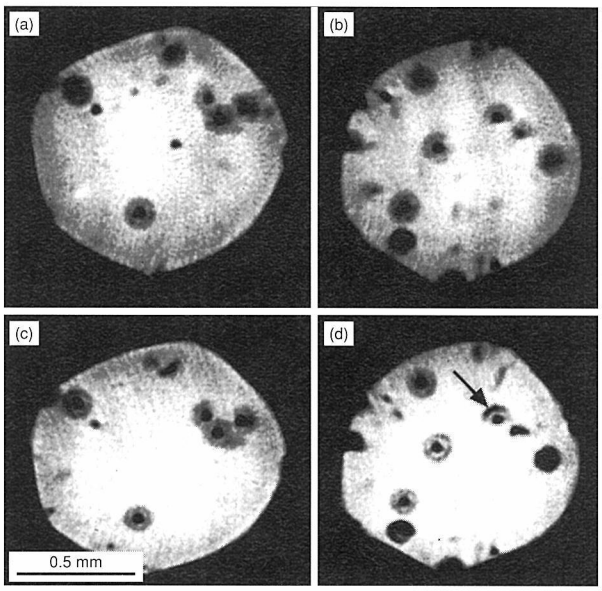

Fig. 2 Monochromatic SR-CT images

*Hitachi Research Laboratory, Hitachi Ltd.

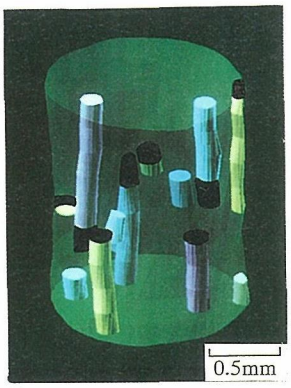

Fig. 3 3-dimensional image reconstructed from SR-CT cross sectional images

trix. Matrix and fibers are clearly discriminated, as the difference of the X-ray linear absorption coefficient is about 8% between aluminum and SiC. The carbon core fiber of 30 μm in diameter is neatly observed.

In situ observation position in Z direction can be slightly different between the 2 pairs, Fig. 2(a) and (c), (b) and (d), each corresponding to 2 stress levels at different sections of the specimen which is elongated during the test. Debonding is found at the interface between fiber and matrix in Fig. 2(d) as indicated by an arrows. Voids of about 140 μm are observed in Fig. 2(d). The number of voids observed under zero stress, 0.2% proof stress and near the fracture stress are 4 and 23, respectively, for the present experiment. It is clear that the voids are gradually increasing with increase of the plastic strain. Direct observation of the internal damage process is thus extremely significant to understand the failure mechanisms of the metal matrix composites.

Figure 3 shows 3-dimensional image reconstructed from 10 SR-CT images taken under a stress near the fracture. SiC short fibers are arranged almost parallel to the extruded direction corresponding well to the microstructural observation. The length of fibers is 1 mm at the maximum, while there are many shorter ones, which suggests that some fibers are broken during extrusion. Pull-outs at the end of fibers are observed.

In this composite, the critical length, l_c, of fibers for pull-out is estimated by:

$$lc = \sigma_f \, d/2\tau \qquad (1)$$

where σ_f is the tensile strength of fiber, d the diameter of fiber and τ the shear strength of matrix. With values of σ_f = 4 GPa, τ = 195 MPa (= 1/2 proof strength of matrix), and d = 140 μm, the value obtained for l_c is 1.43 mm, and far longer than the fibers in Fig. 3. It is therefore obvious that the pull-out is generally produced in the composite during the tensile test in the present experiment. It is concluded that 3-dimensional analysis by SR-CT images would be useful in verifying the arrangement of fibers in composites, and examining the locus and size of internal damages in function of the plastic strain or loading conditions as applied to the composite.

In an *in situ* observation carried out in another work by the authors, on SiC particle (average size is about 65 μm) reinforced aluminum matrix composite, the void size was controlled by Weibull statistics of 0.2 proof stress, maximum stress and near final failure stress. It was found the voids size increased with increasing true plastic strain on the basis of cross sectional CT images void size distribution.

Conclusions

In situ observation of inner damage was attempted for two types of metal matrix composite SiC_f/A2024 and SiCp/Al under tensile loading condition by Synchrotron radiation X-ray CT at the Photon Factory of the National Laboratory for High Energy Physics in Tsukuba. The results obtained in this study can be summarized as follows:

1. Internal SiC discontinuous fibers could be successfully observed at X-ray energies of 23 keV under static loading condition. The debonding between the SiC fibers and matrix and many voids could be clearly detected under the stress near the fracture.
2. The core carbon fiber of 3 μm in diameter in SiC_f/A2024 composite could be clearly observed under loading condition with a resolution of 10 μm.
3. The inner distribution of SiC fibers and many pull-outs at the end of the fibers could be studied by 3-dimensional image technique.
4. The fracture process of SiCp/Al composite could be analyzed by investigating the variation in the number of voids and average size of voids due to plastic strain.

Acknowledgment

This work was performed under the approval of the Photon Factory Program Advisory Committee (Proposal No. 89–179). We thank Messrs A. Yamakawa and M. Yamamoto at the Shounan Technocenter of Tokai Carbon Co. Ltd. to have supplied SiC_f/A2024 composite material for this study.

References

1. *Observation on Fibers in Long Fiber Reinforced MMC by X-ray CT using SR*, C. Masuda, Y. Tanaka, K. Usami, T. Hirano, Y. Imai, I. Shiota, E. Furubayashi, and H. Iwasaki, Nondestr. Test. Eval., 8–9 (1992): 779–89.
2. *Observation on Fibers in Long Fiber Reinforced MMC by X-ray CT using SR*, Y. Tanaka, C. Masuda, K. Usami, T. Hirano, Y. Imai, I. Shiota, E. Furubayashi, and H. Iwasaki, Trans I.S.I.J. in Japan, 78 (1992): 500–08.

❒ Evaluation of Fatigue Crack Growth in Welded Joints

A. Ohta, Environmental Performance Division

Keywords: fatigue crack, crack closure, welded joint, stress ratio, steel, random loading, synthetic sea water

The fatigue fracture usually occurs in a weld part of structures. Prior to the fracture, the fatigue crack grows from weld toe, lack of penetration and weld defect. The fatigue crack growth properties are evaluated by drawing the relationship between the fatigue crack growth rate and the stress intensity factor range. When the relationship between the stress intensity factor range and the fatigue crack growth rate is investigated on base metal, the relationship varies with the stress ratio, $R(= \sigma_{min}/\sigma_{max})$, as shown in Fig. 1.

However, the relationship for welded joints does not vary with R and is inferior to that for base metal at R = 0 as shown in Fig. 2. The properties for welded joints are similar to that for base metal at high R condition. On the analogy of this similarity, it can be deduced that the inferior fatigue crack growth properties of welded joints occur from high stress ratio condition around the crack tip due to the tensile welding residual stress.

The measured welding residual stress is shown in Fig. 3. It is clear that the tensile residual stress always induced around the middle part of specimen even after the extension of cracks. The relief of the tensile welding residual stress revealed that the fatigue crack growth properties of welded joints can be improved as that for base metal.

The properties were also investigated for five kind of steel welded joints. These properties coincide with each other for different steels. The relationship between the stress intensity factor and the fatigue crack growth rate for welded steels is evaluated by a statistical procedure on about five thousand plots. The 99.5 percent confidential limit

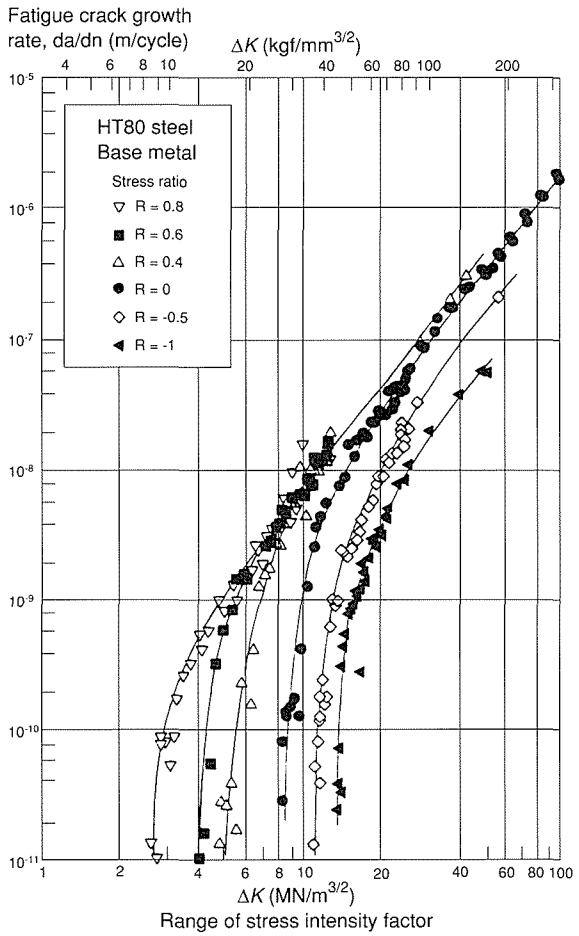

Fig. 1 Relationship between fatigue crack growth rate and range of stress intensity factor for base metal.

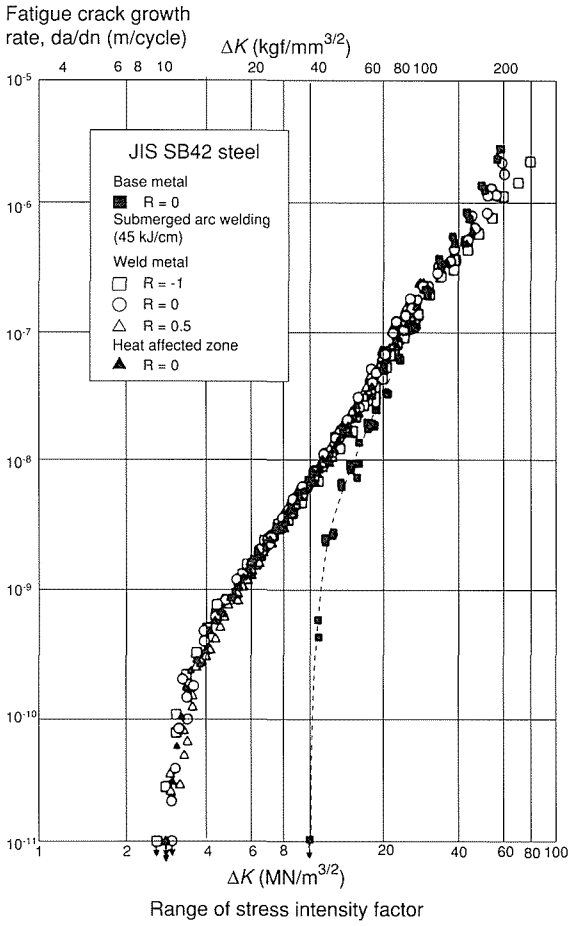

Fig. 2 Relationship between fatigue crack growth rate and range of stress intensity for welded joint.

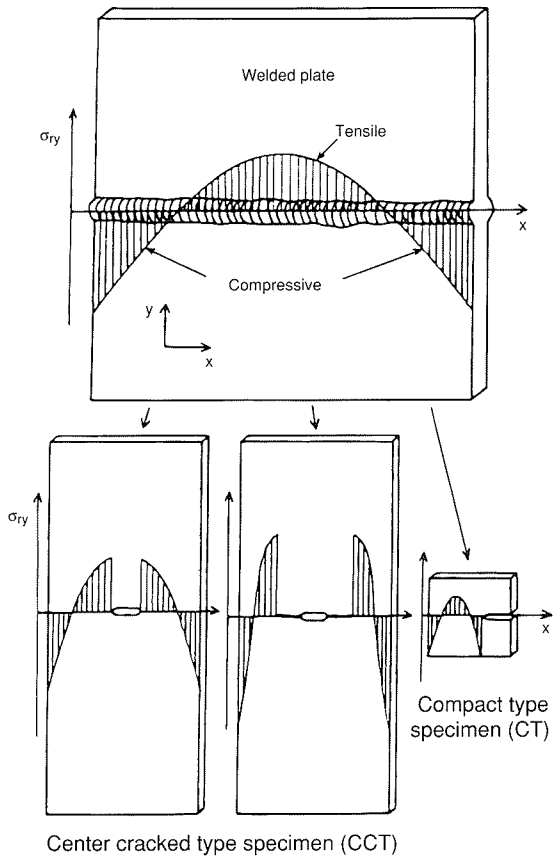

Fig. 3 Residual stress distribution in welded joint.

and the mean line for the relationship are given in the following formulas.

$$da/dn = 2.60\times10^{-11}\left(\Delta K^{2.75} - 2.00^{2.75}\right) \quad \text{for 99.5\% confidence limit} \tag{1}$$

$$da/dn = 1.45\times10^{-11}\left(\Delta K^{2.75} - 2.45^{2.75}\right) \quad \text{for mean line} \tag{2}$$

where the fatigue crack growth rate is represented in m/cycle, and the stress intensity factor, in $MN/m^{-3/2}$.

The loading condition in real structure is not constant amplitude but random loading. The influence of loading pattern on the fatigue crack growth properties was investigated. The employed stress distribution function was Rayleigh. The results show that the fatigue crack growth rate and the fatigue threshold under the random loading condition coincide with those for the constant amplitude test. This coincidence also occurs from the fatigue crack closure free condition. In this condition, the equivalent stress intensity factor range, ΔK_{eq}, and the mean fatigue crack growth rate, $\overline{da/dn}$, can be obtained as in the following formulas.

$$\Delta K_{eq} = \left\{\Sigma\left(\Delta K_i \cdot n_i\right)\right\}/\Sigma n_i \tag{3}$$

$$\overline{da/dn} = \Delta a/\Sigma n_i \tag{4}$$

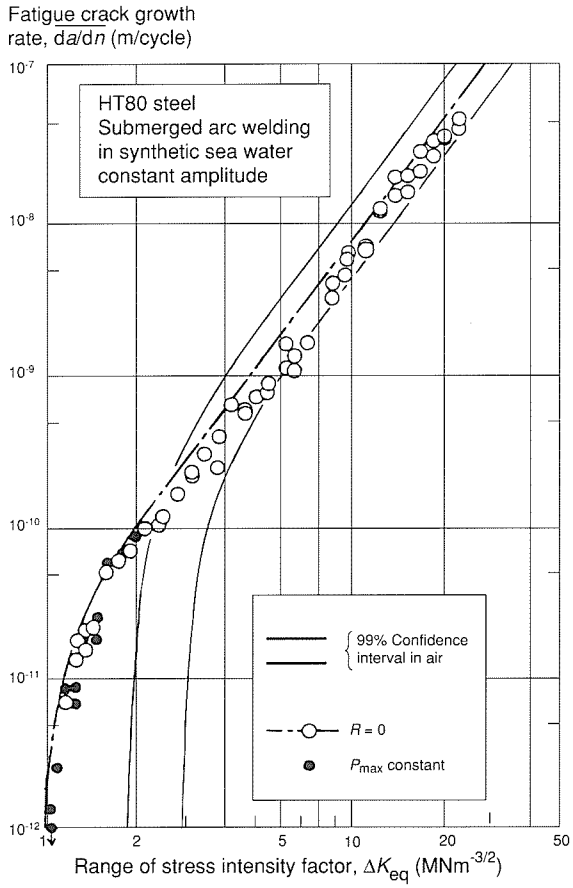

Fig. 4 Relationship between fatigue crack growth rate and range of stress intensity factor for welded joint in synthetic sea water.

where n_i is 0 for $\Delta K_i \leqq \Delta K_{th}$, Δa is the increment of crack length, ΔK_{th} is the fatigue threshold.

The fatigue crack growth properties of welded joints in synthetic sea water were also investigated. Figure 4 shows the results. The fatigue threshold in synthetic sea water is about a half of that in air. In the higher rates, the growth rate is similar for both environment. The properties under the random loading condition in synthetic sea water were also coincided with those at constant amplitude condition. When the environment varied periodically between the synthetic sea water and air, the properties were similar to those in synthetic sea water. Only under the environment where the drying time was longer than 30 minutes, the fatigue crack growth rate became slower compared with that in synthetic sea water. In this environment, once the growth rate became slow, the rate gradually decreased and finally became to be 0.

❒ Superplasticity of γ Base Titanium-Aluminides

M. Nobuki, D. Vanderschueren and M. Nakamura, 3rd Research Group*

Keywords: intermetallic compounds, titanium aluminides, superplasticity, flow stress, fracture strain

Recently, a great deal of efforts have been put into the research on TiAl base alloys. The objective of most of these investigations is to improve room temperature ductility, high temperature strength and oxidation resistance so that these intermetallics can be applied as a high temperature structural material.

The purpose of this research is to evaluate hot workability of Ti-Al-V alloys and to relate their properties to the microstructure controlled by thermomechanical processing. Special attention has been paid to the occurrence of superplasticity, because the superplasticity could be an important argument in considering the applicability of these alloys[1].

The compositions of the alloys used are TAV1/Ti-43.13Al-13.10V, TAV2/Ti-39.19Al-9.27V, TAV3/Ti-43.63Al-4.98V (mol%). Plasma arc melted ingots were homogenized in Ar at 1470 K for 86.4 ks and two sequential forgings were given at a strain rate of $10^{-3}s^{-1}$ in an Ar atmosphere. The first forging was carried out at 1470 K to a true strain of 1.0. The second forging was carried out at 1270 K to a true strain of 1.5 perpendicular to the first one.

After the second forging, grain sizes are about 10 μm in TAV1 and 6 μm in TAV2. TAV1 and TAV2 are mainly composed of the γ and β phases with a very small amount of the α_2 phase. TAV3 with a lamellar structure is not yet fully recrystallized even after the two step forging. The size of the equiaxed, recrystallized grains is 2 μm. In order to obtain a fully recrystallized TAV3 one should use numbers of forgings with lower deformation per forging at lower deformation rates and a temperatures below 1530 K. Since grains with lamellar orientation perpendicular to the forging direction are much more difficult to break down, the successive forgings should be given in different directions. TAV3 is composed of the γ phase with a small amount of the β and α_2 phases.

High temperature mechanical properties of the forged material were characterized using tensile tests at a strain rates between $3 \times 10^{-4}s^{-1}$ and $0.1s^{-1}$ and at temperatures between 1070 K and 1420 K in vacuum (2×10^{-3} Pa).

From the results of a series of tensile tests at different temperatures (T) and strain rates ($\dot{\varepsilon}$), material constant Q, A, α and n in equations 1 and 2, describing the flow stress (σ) were calculated.

$$Z = \dot{\varepsilon}\exp(Q/RT), \tag{1}$$

$$Z = A[\sinh(\alpha\sigma)]^{n}. \tag{2}$$

Here Z is Zener-Hollomon parameter, and R is the gas constant. The values of these constants are listed in table 1. The above equations were used to calculate hot deformation maps (Fig. 1).

It is generally considered that superplastic deformation takes place when the m-value is larger than 0.3. TAV2 exhibits the highest m-value that is slightly higher than that of TAV1 and significantly higher than that of TAV3. At $10^{-4}s^{-1}$ and at 1420 K the m-value of TAV2 is 0.8. At 1420 K the m-value is larger than 0.3 for all strain rates, even for a strain rate as high as $0.1s^{-1}$.

Superplastistic deformation is obtained in the γ plus α_2 and/or β phase alloys with the microstructure of consisting of equiaxed, recrystallized grains. This observation indicates that dynamic

Table 1 Material constants for flow stress of Ti-Al-V alloys.

Alloy	Q (kJ/mol)	A	n	σ
TAV1	484	6.98×10^{16}	1.79	9.95×10^{-3}
TAV2	426	9.91×10^{14}	1.74	8.75×10^{-3}
TAV3	363	2.24×10^{11}	1.57	9.67×10^{-3}

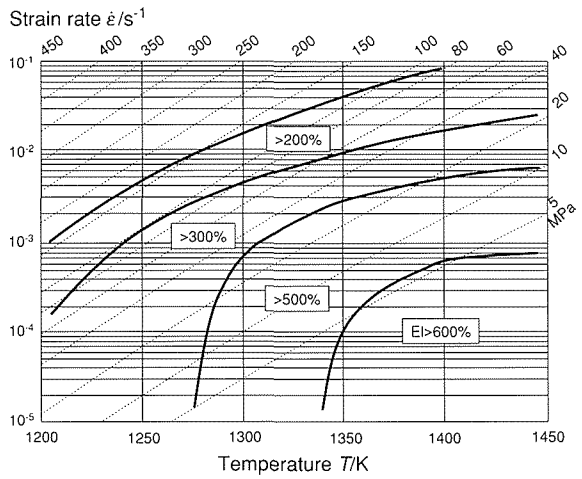

Fig. 1 Hot workability maps of alloy TAV2. Dotted lines represent the flow stress (σ) indicated by MPa at the end of each line. Solid lines represent the total elongation indicated by percentage at the lower side of each line.

*present address: Sidmar Arbed Alz, Belgium

recrystallization plays an important role in the superplastic deformation[2]. Therefore, the obvious conclusion is that the superplastic deformation in these materials is caused by grain boundary sliding accompanied with dynamic recrystallization which restores the inhomogeneous deformation microstructure and ensures the persistence of a fine grain structure.

In hot deformation of multi-phase ordered alloys, grain coarsening or refining depends on many various parameters, including crystal structure, deformation mechanism, phase distribution, initial grain size, temperature, strain rate and strain. A balance between grain coarsening and refining under these parameters results in an equilibrium grain size. For superplastic forming, it would be useful to establish the equilibrium grain size as a function of temperature, strain rate and strain.

References

1. *Status of R&D of High-Performance Materials for Severe Environments*, Y. Nakazawa, Proc. 4th Symp. High-Performance Mater. Severe Environments, Japan Industrial Technology Association, (1993): 165–68.
2. *Superplasticity of TiAl Intermetallics*, M. Nobuki and T. Tsujimoto, Advanced Structural Material, Proc. C-MRS Intern., ed. Y. Han, Elsevier Sci. Pub., 2 (1991): 791–96.

❒ Development of High Resolution Angle-Resolved Electron Spectrometer (HR-ARES) with Extremely Low Magnetic Field and Extremely High Vacuum for Surface Atomic Imaging

D. Fujita, T. Yakabe and K. Yoshihara, Fourth Research Group

Keywords: extremely high vacuum, Auger electron spectroscopy, X-ray photoelectron spectroscopy, angle resolved analysis, electron diffraction

Introduction

Top-most surface regions can be considered a new phase which has different chemical properties and atomic arrangements from those of the bulk. This unusualness of surface region is stem from the redistribution of surface atoms in order to minimize the surface free energy, which causes various interesting phenomena specific to the surface such as surface segregation, surface precipitation, surface reconstruction and so on. On the other hand, recent development of micro-electronics technology has enabled a monolayer-scale deposition of molecules or atoms, which has a possibility of development of artificially designed materials. Therefore, one of the main subjects of our research project is to establish original techniques for synthesizing such kinds of artificially nanoscale-controlled materials by using a thermodynamically equilibrium state or a molecular beam epitaxy (MBE) method. For example, we have succeeded in controlling the thickness of epitaxially grown graphite (0001) layers of the Ni (111) surface in monolayer-scale by using a precise temperature control[1]. With this surface precipitation technique, both monolayer graphite and multilayer graphite can be obtained. In order to clarify the details of the surface structures of the above nano-scale controlled materials or the surface reconstructed materials, a new and comprehensive surface analytical technique are required. Therefore, we have developed a new analytical principle for investigating both atomic concentrations and atomic arrangements within topmost few layers in a layer-by-layer manner, which is called atomic imaging, here. This methodology was named as SET (Surface Electron-spectroscopic Tomography).

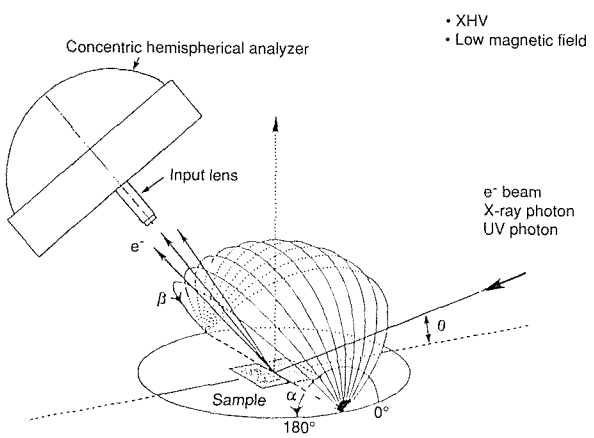

Fig. 1 Schematic picture of the angle-resolved measurements for SET analysis.

HR-ARES

Conventional electron spectroscopies such as AES (Auger Electron Spectroscopy), XPS (X-ray Photoelectron Spectroscopy), and UPS (Ultraviolet Photoelectron Spectroscopy) have potential ability to clarify atomic concentrations, atomic arrangements and electronic structures, if combined with an angle-resolved technique. Therefore, we have selected angle resolved electron spectroscopy for the base analytical technique to realize the SET principle. Schematic picture of the angle-resolved measurements for SET analysis is shown in Fig. 1. SET analysis is based on the measurements of angular distribution of both elastically and inelastically scattered electrons. Elastically scattered or diffracted electrons have been used for many surface analytical tools such as LEED (Low Energy Electron Diffraction), XPD (X-ray Photoelectron Diffraction), AED (Auger Electron Diffraction), and

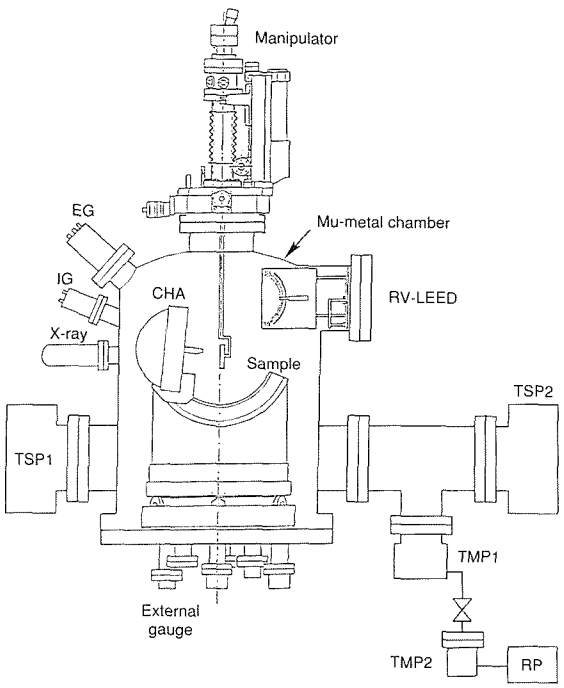

Fig. 2 Schematic diagram of a newly developed HR-ARES system.

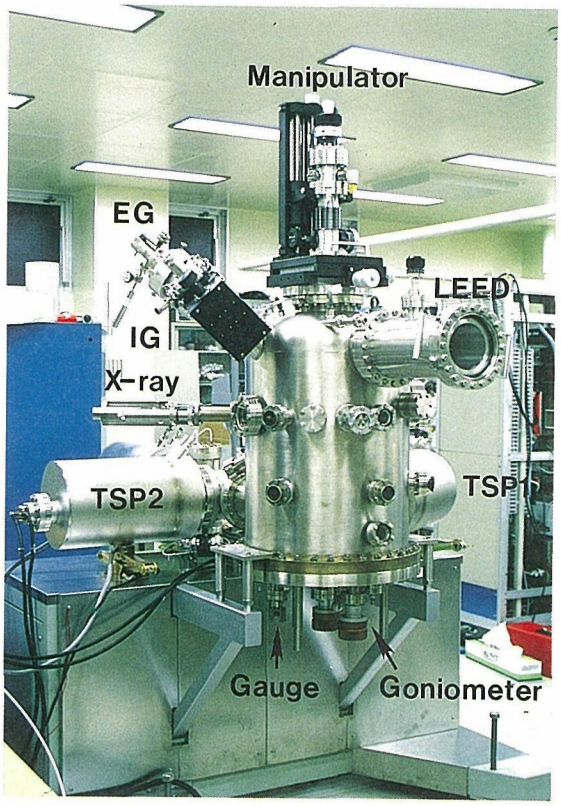

Fig. 3 Photograph of a newly developed HR-ARES system.

so on. Though inelastically scattered electrons have been little used for surface analysis, joint-analysis with elastically and inelastically scattered electrons is more attractive since latter electrons have more depth information.

Since 1992, we have been developing a high resolution angle-resolved electron spectrometer (HR-ARES) system with extremely high vacuum (XHV) and extremely low residual magnetic field[2, 3]. Schematic diagram and photograph of a newly developed HR-ARES system are shown in Fig. 2 and Fig. 3, respectively. This system can be used for the precise measurements of angular distribution of elastically or inelastically scattered electrons (photoelectrons, Auger electrons) excited by the incidence probes of X-ray (Mg Kα) photon, ultraviolet photon and electron beams with high energy resolution (20 meV) and high angular resolution (acceptance angle = ±0.4 deg.). Since the main chamber material was selected to be 5 mm-thick mu-metal alloy which has high magnetic-shielding ability, the residual magnetic field in the inner space was found to be decreased to less than 4 mG which is less than 1% of earth's magnetic filed. This extremely low magnetic field enables the precise angle-resolved measurements of ultra-low energy electrons of about 1 eV. Using our sophisticated XHV techniques, the HR-ARES system with many attachments for surface analysis and sample treatment has attained the extremely high vacuum of 10^{-10} Pa order.

References

1. *Surface Precipitation Process of Epitaxially Grown Graphite (0001) Layers on Carbon-doped Nickel (111) Surface*, D. Fujita and K. Yoshihara, J. Vac. Sci. Technol., A 12 (1994): 2134–39.
2. *Evacuation Properties of a Large Mu-metal Chamber for High Resolution Angle-Resolved Electron Spectroscopy (HR-ARES)*, T. Yakabe, D. Fujita, and K. Yoshihara, Journal of the Vacuum Society of Japan, 37 No. 3 (1994): 177–79 (in Japanese).
3. *Development of High Resolution Angle-Resolved Electron Spectrometer (HR-ARES) for Measurements of Angular Distribution of Elastically or Inelastically Scattered Electrons*, D. Fujita, T. Yakabe, and K. Yoshihara, Journal of the Surface Science Society of Japan, 15 (1994): 323–28 (in Japanese).

❒ Prediction of Fatigue Strength Properties using Materials Strength Database

M. Nihei, 4th Research Team

Keywords: life prediction, fatigue properties, materials strengths database, computer modeling

The safety and reliability of machinery and components are closely related to the technology of materials life prediction.

In this study, the integrated computerized system with the database was newly developed for the advanced materials life prediction, by combining the factual database on materials strengths and the knowledge obtained from the previously obtained scientific and empirical understanding for materials deformation and fracture process. By using the newly developed system, the new algorithm for predicting the fatigue strengths and fatigue lives of materials has been developed and been applied to construct the computer aided fatigue design system of machinery as a collaboration research with a private company.

Development of DIMS

The new system developed in this study was named as DIMS (Dialogical Integrated system for Material Strength database) and was build by using the engineering workstation, which connects with other terminals through the network communication system. This system can analyze the desired data set extracted from the materials strength database and can find the combinations among characterized items of materials on that strength. DIMS works under a UNIX operating environment with the X-Windows system and always offers the good man-machine interface to users.

In this system, many materials data items for searching and selection were involved on the materials strengths for 127 several types of materials and 750 different types of heats and were also applicable for analyzing to predict the fatigue life and/or creep strength. The architecture of this system was illustrated in figure 1. This system was composed from five different parts, which are

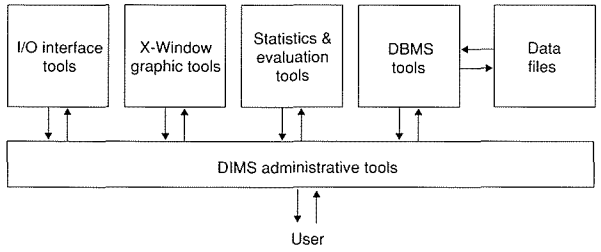

Fig. 1 Architecture of developed DIMS.

DBMS tools for searching and selection of data, statistically data operation/calculation for different type of evaluations of materials strengths such as high-cycle fatigue, low-cycle fatigue, crack propagation and creep strength properties, graphics tools for displaying the analyzed results, I/O tools for data handling and administration part for man-machine interface using X-Windows system on UNIX, respectively.

Modeling of Materials Strength

In this study, the following prediction model was used as the common basic model for strength properties, P.

$$P = f([C], [Si], [Mn], [Ni], [Cr], [Mo], Tp), \quad (1)$$

where [C], [Si], ... are the chemical composition of materials and Tp is the final heat treatment temperature respectively. In this modeling, it was assumed that the strength properties of materials are strongly related to materials structure.

The mathematical model for the prediction of materials strengths was assumed as following equation (2) by deforming the equation (1) to linear model obtained by multivariate analysis.

$$P_0 = A_0 + A_1[C] + A_2[Si] + \ldots + A_7[1/Tp]. \quad (2)$$

The materials parameters involved in the equation (2) can be obtained from the optimizing of data set by DIMS. However, it is considered that the equation (2) involves the estimation errors because of the linearization from equation (1) to equation (2).

In this study, therefore, the equation of modeling for materials strengths was corrected empirically as the following equation (3).

$$P = \beta P_0^{\gamma}, \quad (3)$$

where β and γ are correction factors and obtained empirically by using DIMS, respectively. The results for the prediction of the cyclic stress-strain curves are shown in figure 2 for a carbon steel and several low alloy steels under the axial strain-controlled low cycle fatigue test condition. It can be found that the predicted values of the cyclic stress-strain curves show a good agreement with those observed and the empirical modeling pro-

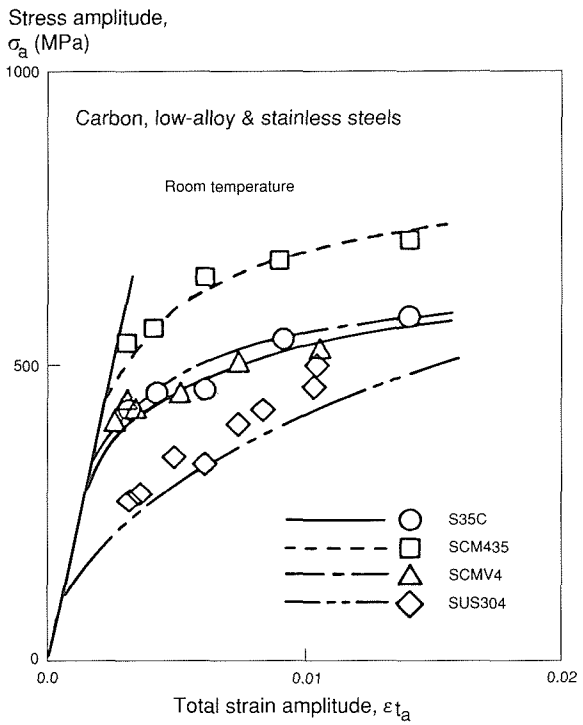

Fig. 2 Prediction of cyclic stress-strain curves.

cedure from equation (1) to (3) is quite suitable for the prediction of the fatigue strength properties of materials.

Prediction of S-N Curves

In this study, the prediction procedure of S-N curves for notched members was examined by applying the same analytical procedure developed in previous section. It was also assumed in accordance with the many knowledge on the fatigue strength properties; (1) the slope of S-N curves and fatigue limit are evaluated separately, (2) the fatigue life on the slope of S-N curves consisted of that of fatigue crack initiation and that of fatigue crack propagation, and (3) the fatigue limit corresponds to the threshold level of fatigue crack propagation. The fatigue initiation lives are estimated from the combination of Coffin-Manson relation, cyclic stress-stain relation of material and Neuber rule shown as equation (4)[1, 2], (5) and (6)[3] respectively.

$$\varepsilon_{ta} = \sigma_f / E(2N_c)^{-b} + \varepsilon_f (2N_c)^{-c}, \quad (4)$$

$$\varepsilon_{ta} = \sigma_a + (\sigma_a / K')^{1/n'}, \quad (5)$$

$$\sigma_a \varepsilon_{ta} = K_t^2 S_a^2 / E, \quad (6)$$

where N_c is the fatigue crack initiation life, S_a is the nominal stress, K_t is a stress concentration factor, and σ_a and ε_{ta} are local stress and strain amplitude, respectively. The crack propagation life is obtained from the integration of following nonlinear equation (7)[4].

$$da/dn = C(\Delta K^m - \Delta K_{th}^m), \quad (7)$$

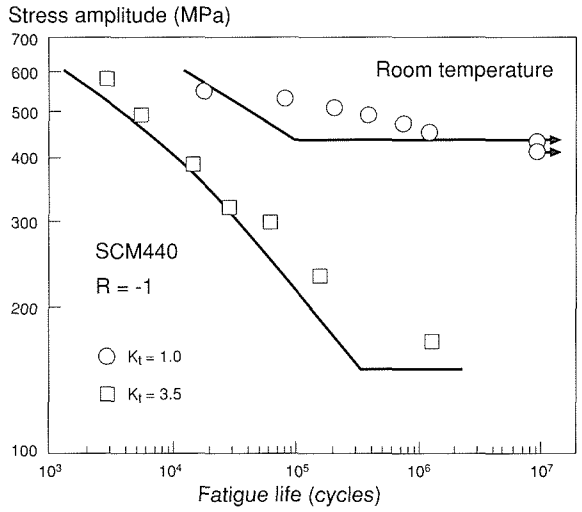

Fig. 3 Prediction results for S-N curves.

where da/dn is the crack propagation rate ΔK is the stress intensity factor and ΔK_{th} is the threshold of the crack propagation.

The fatigue limit was assumed to be related to the threshold level of crack propagation and the initial defect size was assumed to that of the mean grain size of materials, d. The fatigue limit, σ_w, of notched member was also assumed to decrease by the fatigue notch factor, K_f, which mathematical equation was proposed by Peterson[5]. $\Delta K_{th,R}$ is the threshold level of crack propagation with a stress ratio of R.

$$\sigma_w = \Delta K_{th,R} / 2\sqrt{(\pi \alpha d)} / K_f. \quad (8)$$

The results for the prediction of S-N curves is shown in figure 3. It is concluded from this figure that the prediction procedure developed in this study is quite suitable for the prediction of S-N curves.

References

1. *Behavior of Materials Under Conditions of Thermal Stress*, S.S. Manson, NACA Report, TN-2933 (1953).
2. *A Study of the Effects of Cyclic Thermal Stress on a Ductile Metal*, L.F. Coffin Jr., Trans. ASME, 76 (1954): 931–50.
3. *Theory of Stress Concentration for Shear-Strained Prismatical Bodies with Arbitrary Nonlinear Stress-Strain Law*, H. Neuber, Trans. ASME, J. App. Mech., 28 (1961): 544–50.
4. *Effect of Stress Cycle Asymmetry on Fatigue Crack Growth*, M. Klesnil and P. Lukas, Mater. Sci. Eng., 9 (1972): 231–36.
5. *Notch Sensitivity*, R.E. Peterson, Metal Fatigue, Sines and Waisemann ed., MacGrow-Hill, NY, Chap. 13 (1959): 293–306.

❒ Advancement of Mechanical Testing at Liquid Helium Temperature through VAMAS Round Robin Tests

T. Ogata, Mechanical Properties Division

Keywords: cryogenic temperature, tensile test, fracture toughness test

A series of interlaboratory comparisons of mechanical properties, tensile properties and fracture toughness, has been coordinated under the Versailles Project on Advanced Materials and Standards (VAMAS) in order to develop an understanding of mechanical-property determinations at liquid-helium temperature (4.2 K) and establish a unified method. This collaboration is called "Round-Robin Test." The first and the second Round-Robin Tests (RRT) were carried out so far. The first RRT[1, 2] focused on identifying problems and errors that might occur in testing. Some interesting results were discussed: the necessity of a basic approach to microstrain measurement at liquid helium temperature and load-cell calibration for tensile test, and the effect of the testing variables for fracture toughness test. Based on the results of the first RRT programs, the second programs specified the testing conditions in accordance with the latest draft of testing standards. The main purpose of the second RRT was refining the procedures of tensile tests and of fracture-toughness tests and draft document (1988) through clarifying remaining problems under the improved testing conditions.

Materials

For the first RRT, two austenitic steels were chosen as the test materials, SUS 316LN and YUS 170. The main reason for this selection was that they are commercially available and have a high yield strength and good fracture toughness favorable for cryogenic structural materials. Another reason was that they represent materials with a characteristic deformation behavior at liquid-helium temperature, so-called "serration." YUS 170 shows a less frequent and larger load-drop serration during the fracture-toughness test and is a less ductile material. On the other hand, SUS 316LN shows a more frequent and smaller load-drop serration and high toughness, even at liquid-helium temperature. For the second RRT, the test materials were SUS 316LN and Ti-5Al-2.5Sn ELI. SUS 316LN of the same heat of material used in the first RRT was chosen as the most appropriate material for the purposes of the second RRT. The Ti alloy was chosen for a new material for this RRT because it represents a high-strength and lower toughness material.

Test Procedure

Tensile and toughness specimens were machined at NRIM according to the geometry given by each participant.

In the first RRT, test conditions and procedures were more or less in accordance with room-temperature testing standards and were not intentionally unified among the institutes. In the second RRT, testing conditions and surroundings were improved and tensile tests were carried out in accordance with JIS[3] or the latest draft for ASTM.

For the tensile tests in the second RRT, test conditions were restricted such that and tests were carried out with constant crosshead control and nominal strain rate is less than 1×10^{-3} s^{-1} according to existing testing standards. The calibration of the load cell and extensometer was performed according to the standard procedure of each laboratory and the calibration charts were reported with the test results, yield strength, ultimate tensile strength, elongation, reduction of area, and Young' modulus.

Fracture-toughness tests in the first RRT were conducted by using a variety of techniques and systems: computer-aided single-specimen unloading compliance technique, multi-specimen method, key-curve method, and a combination of methods were used with a servohydraulic testing machine and a motor-driven screw-type machine. One institute attempted the load-control mode and specimen side-grooving. In the second RRT, test conditions and procedures were in accordance with the revised testing standards ASTM E813-87 and -88 ANNEX in principle. The stroke rate was limited to less than 1 mm/min. Calibrations of the load cell and extensometer were also carried out and reported.

Results of Tensile Tests

Figure 1 shows the results of tensile tests in the first and the second RRT on SUS 316LN: Ultimate tensile strength is plotted for each participant. Participants are in order of the average ultimate tensile strength obtained in the first RRT. Solid circles are the results of the first RRT and open triangles are the results of the second RRT. Scatter of the data obviously decreased in the second RRT. From the results of the first RRTs, it was evident that much of the data scatter could be attributed to the calibration errors of load-cell. So participants car-

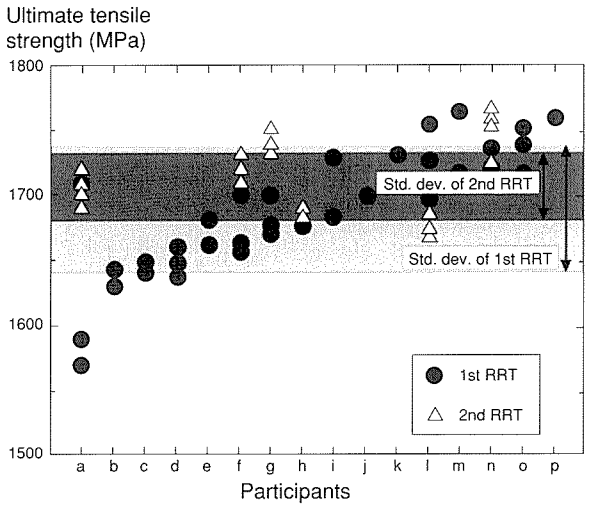

Fig. 1 Ultimate tensile strength of 1st and 2nd RRT of SUS 316LN.

ried out the second RRT by paying much more attention to the calibration. This improved preparation for the testing and the limited condition reduced the scatter of properties among participants. The average ultimate tensile strength was 1714 MPa with a standard deviation of 28 MPa (1.6% of the average).

These results and another report[4] proved that there would be almost no problem in cryogenic tensile tests for these kinds of materials under the improved conditions.

Results of Fracture Toughness Tests

Figure 2 presents the results of fracture toughness tests in the first and the second RRT on SUS 316LN. In the first RRT, the average fracture toughness was 247 MPa√m with a standard deviation of 31 MPa√m (12.6% of the average). In the second RRT, the average fracture toughness was 263 MPa√m with a standard deviation of 15.3 MPa√m (5.8% of the average). Scatter of fracture toughness also decreased in the second RRT. Strain rate and specimen thickness had no apparent effect on the fracture toughness of SUS 316LN in the first RRT and similarly, the effects were not clear in the second RRT. Further discussion has been done on the effects of the serration and testing variables: side-grooving, control mode and strain rate.

From these results, we confirmed that the fracture toughness deviated little under limited testing conditions; however, further study will be required to standardize the testing procedures for ductile-brittle materials.

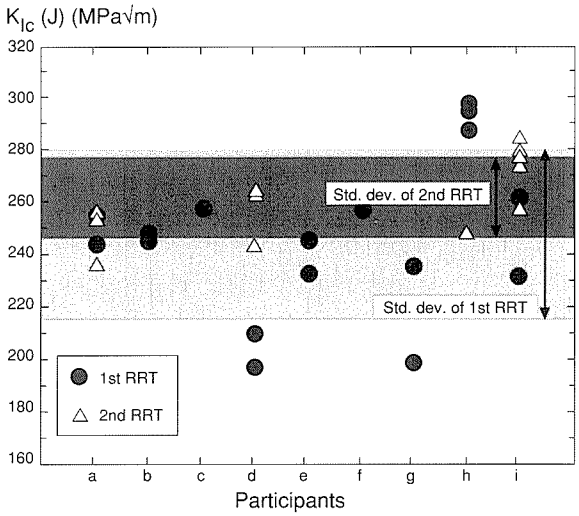

Fig. 2 Results of fracture toughness tests in the first and the second RRT on SUS 316LN.

Future Plan

The cryogenic structural group in VAMAS continues interlaboratory studies to develop an understanding of mechanical-property determination by starting an extended program on aluminum alloy and composite material.

References

1. *VAMAS Interlaboratory Tensile Test at Liquid Helium Temperature*, K. Nagai, T. Ogata, K. Ishikawa, K. Shibata, and E. Fukushima, Cryogenic Materials '88, 2 (1988): 893–900.
2. *VAMAS Interlaboratory Fracture Toughness Test at Liquid Helium Temperature*, T. Ogata, K. Nagai, K. Ishikawa, K. Shibata, and E. Fukushima, Adv. Cryo. Eng., 36 (1990): 1053–60.
3. *Tensile Testing Method for Metallic Materials in Liquid Helium*, Japan Industrial Standard, JIS Z 2277 (1990).
4. *Interlaboratory Tension and Fracture Toughness Test Results for CSUS-JN1 Austenitic Stainless Steel at 4 K*, H. Nakajima, Y. Yoshida, S. Shimamoto, R.L. Tobler, R.P. Reed, R.P. Walsh, and P.T. Purtsher, Adv. Cryo. Eng., 36 B (1990): 1069–76.

❒ Laser Deposition of $YBa_2Cu_3O_y$ Thin Films on Metallic Substrate with In-plane-textured YSZ Buffer Layers

M. Fukutomi, 1st Research Group

Keywords: $YBa_2Cu_3O_y$ thin film, laser deposition, bias sputtering, biaxially-textured YSZ buffer layer

The deposition of High T_c superconducting films on metallic substrates is technically important for the point of view of their future large scale applications such as conductors and electromagnetic shields. These applications, however, rely on the availability of high quality films on metallic substrates with high transport critical currents at 77 K. Suitable combinations of metal substrates and buffer layers have been investigated to date. One of the most promising choices is nickel-based superalloy (Hastelloy C) with a yttria-stabilized zirconia (YSZ) buffer layer for deposition of $YBa_2Cu_3O_y$ (YBCO) superconducting thin films.

The transport property of the films grown on polycrystalline substrates is, however, very poor because of the weak-link behavior of high-angle grain boundaries between misoriented superconducting grains. The polycrystallinity of the YSZ buffer layer is generally believed to be the reason of the existence of such high angle grain boundaries in YBCO film.

An attempt was made to control the crystal orientation of YSZ buffer layers using a new dc bias sputtering technique[1, 2]. Figure 1 shows a pair of specially devised electrodes (a substrate holder electrode and a hollow cathode electrode) installed in the sputtering system. The hollow cathode electrode consists of two pieces of rectangular plate, which were vertically installed below the substrate-holder electrode. A DC bias voltage applied to the substrate holder and the hollow cathode electrode are referred to as Vs and Vh, respectively. The substrate of Hastelloy tape, $3 \times 50 \times 0.3$ mm^3, was clamped on the tiltable specimen-holder electrode. The distance between the specimen holder and the target (8 mol% Y_2O_3-ZrO_2) was about 7 cm. Films were deposited at an ambient temperature. As is seen in figure 1, a characteristic parabola-shaped plasma was found to play an important role in achieving in-plane grain alignment of the films; the argon-ion flux extracted from this plasma appeared to impinge on the growing film at a channeling direction of the YSZ crystal structure, resulting in the occurrence of in-plane texturing.

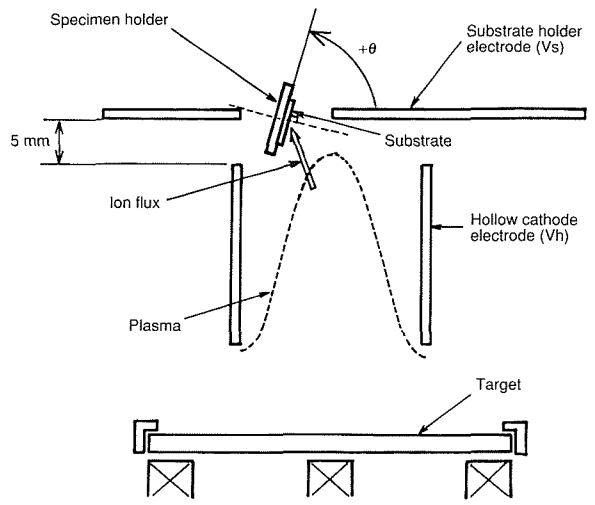

Fig. 1 Schematic representation of modified bias sputtering technique showing a cross-section view of the two electrodes installed in a magnetron sputtering system. The characteristic parabolic plasma-edge and the position of the tilted specimen are also shown.

A preliminary experiment showed that our YSZ thin films had the strongest (200) preferred orientation when films were grown at an RF power of 200 W and an Ar-2%O_2 pressure of 0.13 Pa while Vs and Vh were fixed at −200 V. Accordingly, a series of experiments was carried out under these deposition conditions while the specimen tilt angle θ were varied in wide range. It should be noted here the degree of in-plane texturing depended strongly on the specimen tilt angle θ. This enabled us to grow the YSZ buffer layer with different degrees of in-plane alignment controllably on Hastelloy substrates.

The Hastelloy tapes thus pre-coated with the YSZ buffer layer were then used for deposition of YBCO films using a laser ablation technique[3]. Figure 2(a) gives a typical pole figure for the (111) reflection plane of the cubic YSZ films grown at a specimen tilt angle θ of 75°. On the other hand, figure 2(b) is a pole figure for the (103) reflection plane of the YBCO film laser deposited on the Hastelloy substrate with the in-plane textured YSZ buffer layer shown in figure 2(a). A high degree of in-plane texturing in our YBCO films is evident. In figure 3 the transport J_c of the films is plotted against the degree of in-plane texture of YBCO, $1/\Delta\phi$. Here, $\Delta\phi$ is the full width of half maximum (FWHM) of the peak in the ϕ-scan of the YBCO thin films. This figure shows that the current-carrying capacity of the YBCO films grown on the polycrystalline metallic alloys depends strongly on the texturing of the films. An increase in J_c with

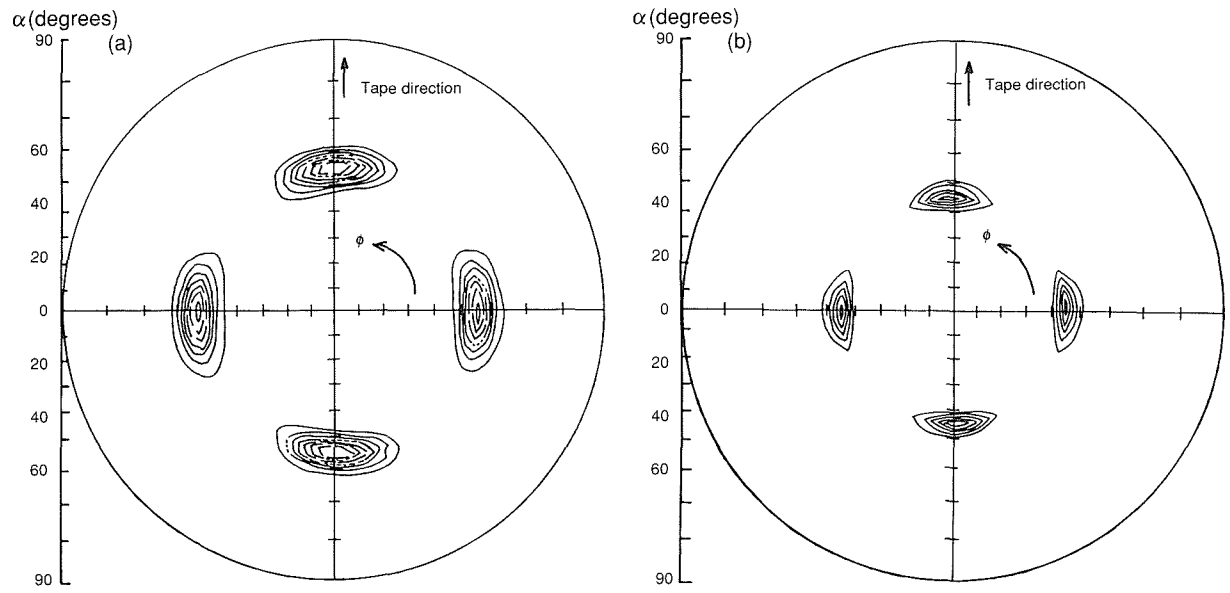

Fig. 2 Pole figure for (a) an YSZ film grown at a specimen tilt angle θ of 75° and (b) an YBCO film grown on an YSZ buffer layer as shown in (a).

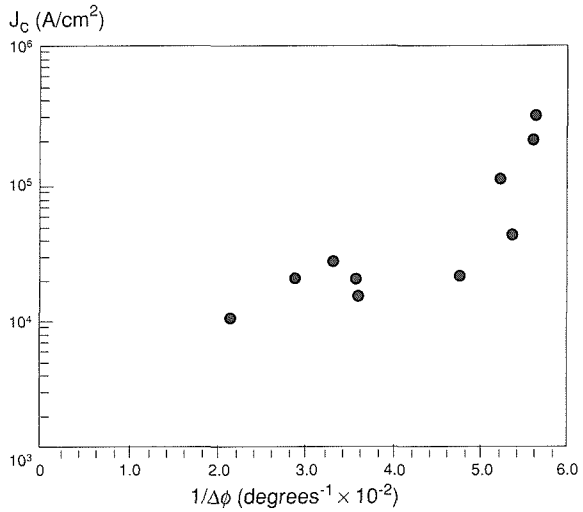

Fig. 3 Transport J_c at 77 K as a function of in-plane texturing of YBCO thin films.

improved texturing is due to a reduction of the weak links at high-angle grain boundaries of YBCO films. The best film thus prepared to date gave a T_c of 90 K and J_c of 3×10^5 A/cm^2 (77 K, 0 T). The results suggested that the new bias sputtering technique proposed here is considered to be valuable technologically and it offers a very convenient method for fabricating buffer layers with a desirable in-plane texture on long tape substrates.

This research was performed in collaboration with Mitsuba Electric Mfg. Co., Ltd.

References

1. *Control of Y_2O_3-Stabilized ZrO_2 Thin Film Orientation by Modified Bias Sputtering*, M. Fukutomi, S. Aoki, K. Komori, Y. Tanaka, T. Asano, and H. Maeda, Thin Solid Films, 239 (1994): 123–26.
2. *Preparation of In-Plane Textured Y_2O_3-Doped ZrO_2 Thin Film on Polycrystalline Metallic Tape by Modified Bias Sputtering*, S. Aoki, M. Fukutomi, K. Komori, and H. Maeda, J. Vac. Sci. Technol., A 12 (2) (1994): 501–05.
3. *Laser Deposition of $YBa_2Cu_3O_y$ Thin Films on a Metallic Substrate with Biaxially Textured YSZ Buffer Layers Prepared by Modified Bias Sputtering*, M. Fukutomi, S. Aoki, K. Komori, R. Chatterjee, and H. Maeda, Physica, C 219 (1994): 333–39.

❒ A System Mutually Making Use of Materials Information (Data-Free-Way)

M. Fujita, Second Research Group

Keywords: distributed database, advanced nuclear materials, data structure, to share data, computer network

A distribute database system named "Data-Free-Way (DFW)" is under development by the cooperation among National Research Institute for Metals (NRIM), Japan Atomic Energy Research Institute (JAERI) and Power Reactor and Nuclear Fuel Development Corporation (PNC). This project includes the construction of a database of specific nuclear materials research field in each organization and a computer network for mutual usage of each database.

Features of the System

Material behaviors under neutron irradiation environments in fission and fusion can be little understood because of little practical examination. Easily accessible material information system with huge material database by computers is efficient and necessary for design of the nuclear materials and analyses or simulations of the phenomena. According to these requirements, the project on the development of DFW was initiated in 1990 under the cooperation among NRIM, JAERI and PNC. In late 1993, other three research organizations: National Research Laboratory of Metrology (NRLM), Ship Research Institute (SRI) and the Japan Information Center of Science and Technology (JICST) joined in this system. Figure 1 shows the present status of the system construction of DFW. The computer network consists of six organizations. These computer system were introduced in each organization, and connected each other through "DDX-P" packet communication line. Accordingly, these databases and user-interface can be used mutually through the computer network.

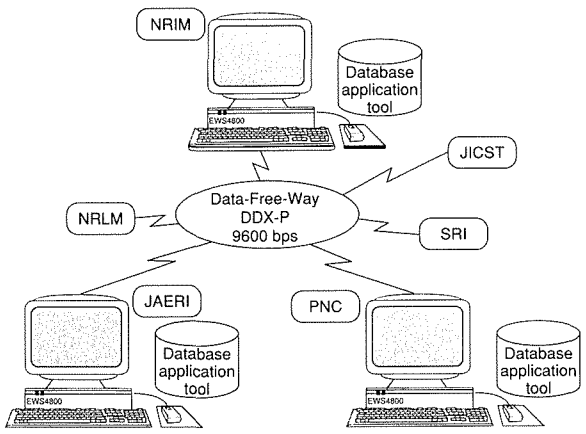

Fig. 1 Networking overview of Data-Free-Way system.

As engineering workstation (EWS) with "UNIX" operation system was selected as the computer system because EWSs had a superior capability to exchange any information with others through the computer network. The same types of EWSs and the other devices were introduced in each organization respectively. And they were connected with the network. The softwares such as network utilities, relational database management system (RDBMS), editors, and programming languages were also available.

Structure of Database and Data

Input data for the system are collected from the previous results obtained by the Fundamental Research on Nuclear Materials funded by the Science and Technology agency of Japan. The activities were focused on the advanced materials as nuclear structural materials, intermetallic compounds, ceramics and composites. So far, the data of 6600 specimens in the various kinds of materials are stored in the database having the structure as follows.

The system consists of a "Common database" and a "Generic database." The former is distributed to the three organizations and has the same data-structure. The data in the database can be used mutually by users in each organization without consciousness on the location of database storing the data. The latter contains meta-data and a data-dictionary. Furthermore, data sets of materials handbooks, reference books, catalogues and any other published data are stored into it. These databases are managed by RDBMS, and accessed through the user-interface systems like retrieval system, graphic tool and application program and so on.

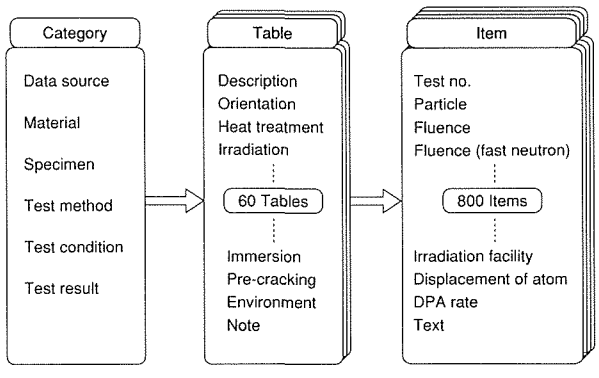

Fig. 2 The data structure of Data-Free-Way system.

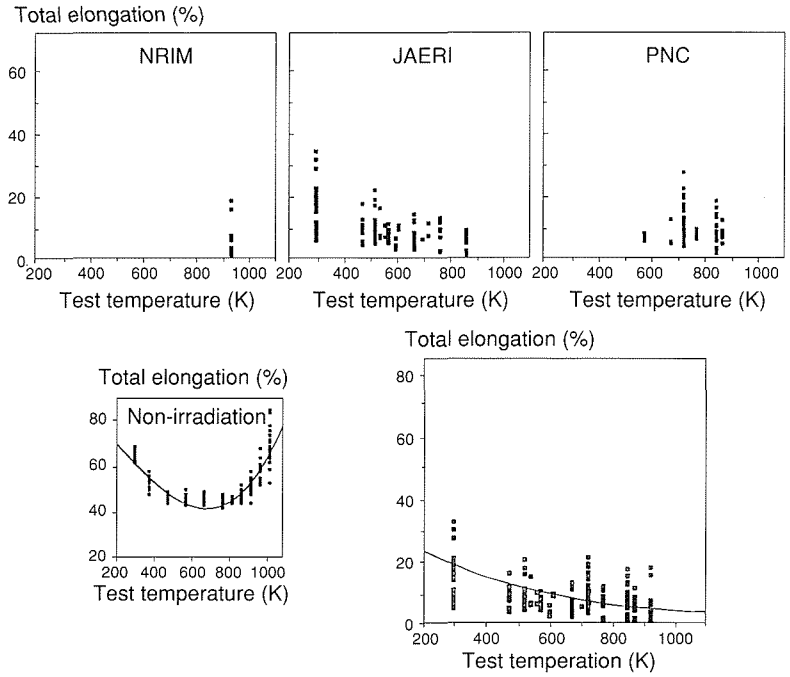

Fig. 3 Relation between elongation and test temperature on each organization on non and irradiated tensile test in type 316 steels.

The data structure of the "Common database" is originally designed as shown in Fig. 2. It is constructed with a three-level hierarchy. Database items are generally divided into six categories which are classified into the first level. Approximately 80 tables are considered to be in the second level. In the third level, more than 800 data items which contained numerical and character data are classified. This data structure is considered to include new materials data like ceramics and composites.

Functions of the System

Five functions such as (1) database on the base nuclear metals, (2) application software, (3) demonstration program, (4) mail and bulletin board, and (5) end of system. In the retrieval system of the database, users can easily access even the database of another organization as same as the in-house. They can easily select data items on the screen in accordance with the three level hierarchy which is same as the data structure.

An Example of the Merit by Using the System

The data for the database is collected from several research organizations under a certain cooperation to collect sufficient data and to maintain quality of data. A utilization technique of the system are also required to get refined information from the stored data. An example of the merit by using the system is discussed about tensile properties in Type 316 stainless steel.

So far, data on high temperature tensile properties of non-irradiated 316 steels have been collected by NRIM and JAERI. The data of irradiated steel have been collected by NRIM, JAERI and PNC under various irradiation conditions. Figure 3 shows both non-irradiated and irradiated data in the forms of relation between total elongation and test temperature. The elongation of non-irradiated data indicates minimum value at approximate 600 K. The irradiated data by NRIM are only at 1023 K, those by JAERI range from room temperature to 873 K, and those by PNC are at the middle range from 573 K to 873 K, although neutrons spectrum was different to each others. By combining those data corrected from three organizations through computer network, tensile properties in wide temperature range can be obtained. It can be easily seen that the macroscopic trend of the elongation on irradiated type 316 steels are similar non-irradiated one. As presented, dominant factors that control tensile properties of irradiated and non-irradiated steel can be examined using the data stored in the present system.

References

1. *Function and Utilization of Data-Free-Way,* M. Fujita, Y. Kurihara, H. Nakajima, N. Yokoyama, F. Ueno, S. Kano, and S. Iwata, Pro. of "Computer Aided Innovation of New Materials 92," North-Holland, Amsterdam (1992): 81.
2. *Present Status for Advanced Nuclear Materials,* H. Nakajima, N. Yokoyama, M. Fujita, Y. Kurihara, F. Ueno, S. Kano, and S. Iwata, Presented at 6th Int. Conf. on Fusion Reactor Materials (1993), to be published in J. Nucl. Mater.

❒ Fabrication of V_3Si Multifilamentary Superconductors by a Modified Bronze Process

T. Takeuchi, High Magnetic Field Research Station

Keywords: diffusion control, V_5Si_3, overall J_c, ac loss

Introduction

V_3Si shows excellent superconducting properties (H_{c2} (4.2 K): ~21 T, T_c: 17 K), being comparable to those of Nb_3Sn. The development of V_3Si for high-field d.c. magnet has been stopped for 20 years, since the "bronze process," established process to produce multifilamentary Nb_3Sn conductors, are not successfully applicable to V_3Si due to the preferential formation of V_5Si_3[1]. The V_5Si_3 layer initially formed around V_3Si filaments decreases eventually V_3Si volume fraction and hence overall critical current density J_c.

As for the a.c. use, V_3Si, however, seems to be rather superior to Nb_3Sn. For a.c. superconductors, the high resistivity barrier, like for cupro-nickel in NbTi conductors, is required to be arranged circumferentially around superconducting filaments in order to separate the filaments from each other for electromagnetic decoupling. It is impossible to utilize cupro-nickel in the Nb_3Sn conductors due to the reaction of Ni with Nb while the V_5Si_3 layer is expected to cut the coupling current between filaments because of the high resistivity of V_5Si_3 (~15 μΩcm at 4.2 K)[2] nearly equal to that of cupro-nickel. Thus, V_3Si are promising for a.c. applications, if the following items are satisfied,

1. overall J_c can be enhanced to the practical level more than 10^8 A/m^2,
2. thickness of the V_3Si layer can be easily adjusted,
3. V filaments can be drawn uniformly to less than 1 μm diameter for small hysteresis losses.

The present study was made to solve the above mentioned problems.

Approach to Solving the Problems

Realization of the item 1 requires the item 2. Livingston proposed a basic idea on this matter from a study on the ternary section of the Cu-V-Si phase diagram: the initially formed V_5Si_3 is eventually converted to V_3Si as long as the total proportion of V to Si in the composite (overall V/Si molar ratio) is kept around 3[3]. However, long times at high temperatures are necessary for appreciable V_3Si layer growth, thereby yielding grain growth of V_3Si and lowering the J_c of the V_3Si compound and the overall J_c accordingly. It is hence expected that the reduction of the V filament size to ~1 μm would decrease the diffusion spacing, bring about the completion of reaction in a short time without remarkable grain growth of mostly V_3Si layers, and thereby increase the overall J_c. Thus the item 3 is a key factor for the development of a.c. V_3Si superconductors from the standpoint of high-overall-J_c and small-a.c.-losses. We have realized ~1 μm filament diameter by preparing a double-stacked Cu-8.5at.%Si/V composite. The primary bundle is sheathed with a Ta tube.

Fabrication Process

The fabrication process for V_3Si multifilamentary wires started with reducing a Cu-8.5at.%Si alloy (bronze) tube which contained a high purity V rod, where the overall V/Si ratio was calculated at 3.3. Intermediate annealing at 520 °C for 1 h was made after every reduction of area (S_0/S) to 1.5. A bundle of 82 short-pieces of the single-core composite was then encased in a Ta tube for wire drawing.

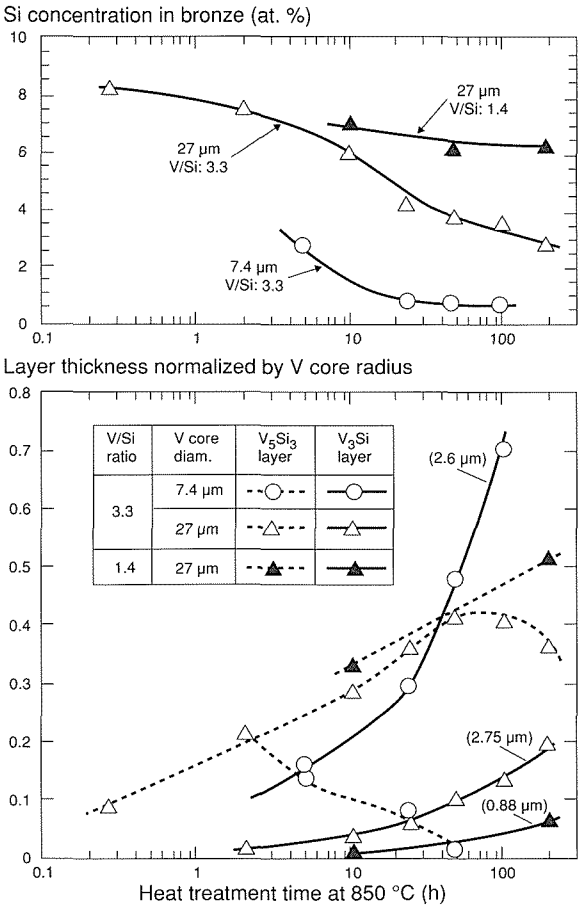

Fig. 1 Residual Si concentration in the bronze, and layer thickness of V_3Si and V_5Si_3 compounds normalized by V core radius as a function of heat treatment time at 850 °C for specimens with various V core sizes and overall V/Si ratios.

Finally, 134 pieces of the resulting single-stacked composite were assembled inside a bronze tube for wire drawing to the final V filament size ranging from 1.2 to 7.4 μm in diameter. Thus, we have prepared a 10988 (82 × 134)-filament double-stacked Cu-8.5at.%Si/Ta/[Cu-8.5at.%Si/V] composite with fine V filaments (~1 μm), where Si in the bronze inside of the Ta sheath is available only for the subsequent diffusion reaction, since Ta acts as a barrier of Si diffusion. Accordingly, the overall V/Si ratio in the double-stacked composite containing Ta was 3.3, which was equal to that of the single-core composite. Despite being grooved-rolled, individual V filaments are uniformly deformed with a rod-like shape and separated from each other. To investigate the effect of the overall V/Si ratio, we replaced a Ta sheath with a Cu-8.5at.%Si alloy sheath in the primary assembly, since Si in the bronze sheath contributes to the reaction with V. Thus, the overall V/Si ratio was 1.4 in the single-stacked composite and 0.81 in the double-stacked composite, respectively. Specimens, cut from the resulting composites, were heat treated for various periods at temperature ranging from 700 to 850 °C to form compound layers geometrically in the order V core/V_3Si/V_5Si_3/bronze.

Figure 1 shows the residual Si concentration in the bronze and thickness of both compound layers as a function of heat treatment time at 850 °C. For the single-stacked composite with 27 μm V filaments, the replacement of Ta with the bronze sheath brings about excess Si, resulting in the high level of Si concentration in the bronze, and hence a high chemical activity to produce the Si-rich compound V_5Si_3 even after long heat treatments. On the other hand, the adjustment of Si (overall V/Si ratio 3.3) using a Ta sheath brings about a decrease in chemical activity of Si in the bronze, decomposes the initially formed V_5Si_3 compound layer, and increases the thickness of the V_3Si layer. Long heat treatments are, however, necessary for appreciable V_3Si layer growth, which seems to yield grain growth of V_3Si. Reduction of filament size to 7.4 μm by double-stacking allows complete reaction to occur in a much shorter time: the residual Si concentration goes below 1 at.% at 24 h; the V_3Si layer becomes thicker than the V_5Si_3 even at 5 h. The volume fraction of V_3Si in the filaments reaches about 90% at 100 hr. The layer thickness within the parentheses is the absolute value for the V_3Si layer, which is rather large in specimens with fine V filaments at 100 h. This tendency would be promoted with decreasing V filament diameter to ~1 μm.

Overall J_c

Figure 2 shows the field dependence of the overall J_c optimized by varying reaction time at 850 °C for Si-adjusted specimens with different V core

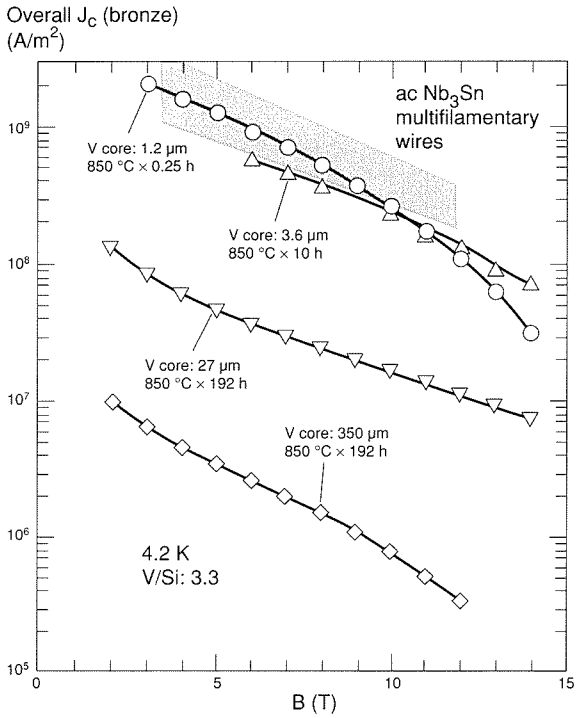

Fig. 2 Overall J_c(4.2 K) versus B curves for the V_3Si multifilamentary wires with various V core sizes. Overall J_c's of bronze processed Nb_3Sn multifilamentary wires for ac applications are shown in the figure for comparison.

sizes. The optimum reaction time, given in the figure, decreases with decreasing V core diameter. The reduction of the V core size brings about an increase in overall J_c, in particular, at a lower magnetic field. Large overall J_c in low fields for smaller V core specimens are probably due to the fine grain structure of V_3Si which is caused by shortening reaction time. $F_{p,\,max}$ (maximum in the overall J_c × H vs. H curve) reaches actually a peak against reaction time, suggesting that the grain-boundary pinning contribution becomes small at long heat treatment. On the other hand, there is a possibility of the enhancement of V_3Si-normal metal interface pinning which is also caused by reducing the V core size, in analogy with superconductors with submicron filaments for ac application. Preliminary experiments on anisotropy in J_c for a flattened multifilamentary conductor shows that overall J_c for magnetic fields parallel to the tape surface is larger than that for fields perpendicular to the surface, just like for an *in situ* Nb_3Sn tape conductor, supporting the above speculation on interface pinning.

We have achieved an overall J_c (4.2 K) of 1.3×10^9 A/m^2 at 5 T and 1×10^8 A/m^2 at 12.5 T, which are already comparable to those of Nb_3Sn multifilamentary wire for ac use. In the present V_3Si conductor, it is possible to achieve much smaller filament size and hence reduce hysteresis loss. The effective diameter of V_3Si filaments in 1.5–7 T is almost constant of 2.8 μm, which is already comparable to that of a.c. Nb_3Sn conductors. The combi-

nation of applying hydrostatic extrusion and alloying V with Ti would bring about uniform deformation of V filaments and decrease the effective diameter furthermore.

References

1. *Studies on the Formation of V_3Ga and V_3Si Superconducting Compounds by a New Diffusion Process*, K. Tachikawa, Y. Yoshida, and L. Rinderer, J. Mater, Sci., 7 (1972): 1154.
2. *Electric Transport Properties of V_3Si, V_5Si_3, and VSi_2 Thin Films*, F. Nava, O. Bishi, and K.N. Tu, Phys. Rev., B 34 (1986): 6143.
3. *V_3Si Formation by the Bronze Process*, J.D. Livingston, J. Mater. Sci., 12 (1977): 1749.

Research in Progress 1993–1994

❒ List of Research Subjects

Numbers with circle indicate subjects newly started from April 1994.

Numbers with square indicate subjects ended by March 1994.

Characterization/Properties

Electronic and nuclear properties

(1) Development of High Precision Detection Techniques for High Field Magnets

(2) Development of Common Interface to Two Different Types of Numerical Database

3 Pressure Effects on Physical Properties of Magnetic Materials

4 Electronic Structure and Superconducting Mechanism in High-Temperature Superconductors

5 Theory of Structure and Properties of Surfaces and Interfaces

6 Database Development in Assistance of New Superconducting Materials Research

7 Structure and Electronic Properties of Silicides

8 First-Order Phase Transitions in Magnetic and Superconducting Materials at Low Temperatures

9 Fundamental Studies of Electromagnetic Materials with Strong Electron Correlations

[10] Fermi Surfaces and Heavy Cyclotron Mass in the Molecular Conductor $(DMe\text{-}DCNQI)_2Cu$

Atomistic arrangement

(11) *In Situ* Observation and Structural Analysis of High T_c Superconductors at Low Temperature

12 Structures of Transition Metal Oxides from the Bonding View Point

13 Quantification Study on High Resolution Transmission Electron Microscopy

14 Synthesis and Characterization of Oxide Superconductors

15 Study on Fabrication Processes of High-T_c Oxide Superconducting Tapes by Means of Vapor Deposition and Powder-in-tube Methods

[16] Observation of Partial Density of States with X-ray Photoelectron Diffraction

Phase transformation and microstructures

17 Super-Microscopic Study on the Mechanism of Martensitic Transformation in Shape Memory Alloys

[18] A Molecular-Dynamics Study of the Nucleation Process at Liquid–Solid Interfaces

Surface and interface properties

(19) Research on Electrode Reactions between Metallic Ions and Carbonaceous Materials/Research on Electrochemical Characteristics of TiAl-base Alloys

20 Characterization of Composite Ultrafine Particles

21 Cooperative Phenomena of the Transformation Variants

22 Effect of Oxidation on Mechanical Degradation of Metallic Materials

23 Modeling and Electrochemistry of Corrosion under Thin Water Film

24 Evaluation of High-Performance Triazinedithiols as a Corrosion Inhibitor

25 Fabrication of Quantum Well Box Systems by Droplet Epitaxy for Advanced Optoelectronic Devices

[26] Fundamental Research on Adsorption under Electric Potential on Metal-atom-doped or Electron-doped Dispersed Carbons

[27] Studies of Local Corrosion Damage of Corrosion Resistant Alloys in High Temperature Water

Mechanical properties

(28) A Molecular-Dynamics Study on the Elementary Process of Fracture

(29) Detection and Healing of Damage in Materials

(30) Environmental Dependency of Cyclic Deformation Behavior

(31) Study on Transient Behavior of Deformation and Fracture at the Elevated Temperature

(32) Relationship between Fatigue Crack Propagation and Cyclic Deformation of Small Specimens

33 NRIM Fatigue Data Sheet Project IV

34 NRIM Creep Data Sheets IV

35 Fatigue Behavior of Brittle Materials at Elevated Temperatures

36 High Temperature Deformation and Fracture in Polycrystalline Oxide Ceramics

37 Study on Deformation and Fracture of Structural Materials at Cryogenic Temperatures

38 Study on Deformation and Fracture of Materials under Irradiation

[39] Effect of Surface Film on Deformation of Bulk Matrix Material

[40] Evaluation of Crack Initiation and Growth of Superalloys under Creep and Creep-Fatigue Conditions

[41] Real Time Evaluation of Fatigue Damage during Crack Propagation under Random Loadings

[42] Fatigue Crack Initiation Process in Corrosive Environment

[43] Controlling and Recovering Methods for High Temperature Damage

[44] Mechanism of Fretting Fatigue Failure in Metal Matrix Composite

Measurement and evaluation

(45) Atom Probe Microanalysis and its Use for Materials Design

(46) Fundamental Study on Advanced Techniques of Physical Characterization of Metallic Materials and their Application

(47) Research on the Development of Chemical Analysis and Characterization Techniques for Metallic Materials

(48) Fundamental Study for Electromagnetic Evaluation of Materials

(49) Nanoscopic Materials Damage Evaluation

50 *In Situ* Measurement of Local Strain at High Temperature by the Laser Speckle Method and its Application to Detection of Defects in Welding

51 Correlation between Plasma Parameters and Evaporation in Free-burning Arcs

52 Development of Advanced Technologies for Three Dimensional X-ray Microtomography

53 Study on the Image Measurement by Means of Fuzzy Logic

54 Study on Detection and Evaluation of Radiation Damages in Extreme Particle Fields

55 Study on Mechanism of Ion Production in Low Temperature Plasma

56 Modeling and Evaluation of Advanced Materials—A Coordinated Interlaboratory Research

57 Atomic Scale Evaluation of Material Damage in Aqueous Solution

58 Study on Design and Assessment Technology for Ecomaterials

59 The Control of Surface Atomic Layers of Solid Surfaces and the Development of Surface Electron Spectroscopic Tomography

60 Chemical Analysis of Organotin in Marine Environmental Samples

61 On-line Determination of Order Parameters in Alloys from Electron Diffraction by CCD Camera System and Its Application to Examination of Ordering Process

62 Characterization of Metals and Alloys using Synchrotron Radiation

63 Development of Extremely High Field Magnets

[64] Fundamental Study on Plasma Diagnostics in Free-burning Mixed Gas Arcs

[65] Advanced Techniques for Physical Analysis of Metals

[66] Sensitive Instrumental-Analysis by Direct Methods and Separation Methods of Metallic Materials

[67] Database System for R&D of Superconducting Materials

[68] Sensing and Analysis of Materials Damage Formation Process

[69] Quantitative Nondestructive Evaluation Techniques for Composite Materials

[70] Quantitative Evaluation of Fracture on Materials for Casks

Simulation and theory

(71) Establishment of Multidimensional Evaluation of Human Senses for Materials Design

(72) Thermodynamic Analysis of Transition Process from Metastable to Stable Phases

(73) Development of Data Modeling Method for Materials Strength Properties

74 Study on the Trend of Application of New Superconductors

[75] Computational Approach to the Mechanics of Heterogeneous and/or Anisotropic Microstructures in Advanced Materials

[76] Development of Material-design-technique for Mechano-chemical Attack on Lightweight Heat-resistant Materials

[77] Self-organizing Information-base System Used for Creative Research and Development

[78] Computer Aided Design Tools for the Development of Materials

[79] Basic Research to Establish Design Techniques for Advanced Materials

[80] Evaluation and Life Prediction of Material Strengths by "DIMS" System

Materials

Non-ferrous materials

(81) Relationships between Fatigue Softening/Hardening Behavior and TEM Structure of Titanium Alloys

82 Disintegration Phenomena in Intermetallic Compounds

[83] Microstructural Refinement and Mechanical Properties of Titanium Alloys

Intermetallic compounds

84 Fundamental Study of Microstructures to Develop High Performance Materials for Severe Environment (II-High Temperature Intermetallic Compound)

85 Sintering of TiAl Intermetallic Compound

86 Improvement of Mechanical Properties of Intermetallic Compounds by Crystal Growth Control

87 High Ionic Conductivity of Solid Electrolyte

88 High Performance Materials for Severe Environments I (Microstructure and Properties of Intermetallic Compounds with High Specific Strength)

89 Basic Research on Intermetallic Compounds for Structural Applications

Composites

90 Thermal Stability of Intermetallic Compound Matrix Composites Reinforced with Fibers

[91] Fatigue Fracture Mechanisms for TiAl Intermetallic Compounds at High Temperatures

Materials for mechanical application

(92) High Temperature Mechanical Properties of Particulate Reinforced Titanium-based Metal Matrix Composites

93 Intelligent Structural Materials

94 Toughness Improvement of Brittle Ceramics and Steels by Precipitation and Phase Transformation Control

[95] Development of Metal Matrix Composites for High Temperature Use Through Combinations of Advanced Powder Metallurgy Processes

[96] Production and Evaluation of Particulate-Reinforced Titanium Matrix Composites

Materials for electronics application

(97) Synthesis of Superconducting and Supermagnetic Ultrathin Films by Use of Ion Implantation

(98) Studies on Microstructure and Electromagnetic Characteristics of V_3Si Multifilamentary Superconductor

99 Synthesis of New Functional Materials by the Application of Host-Guest Reactions

100 Purification of Active Metals for the Preparation of Superconductive Materials

101 Structure Control and Electromagnetic Properties of High Temperature Superconductors

102 Development of $Bi_2Sr_2CaCu_2O_x$/Ag Coils for High Magnetic Field Application

103 Development of High-T_c Superconducting Bulk and Thick Films by Spraying and Internal Oxidation

104 Fabrication of Oxide Superconductors Using YAG Laser Irradiation

105 Development of Practical High-Field Multifilamentary Superconductors Made of Intermetallic Compounds

[106] Synthesis and Superconducting Properties of the Bi System Ultrathin Films of Thicknesses below 100 Å

[107] Development and Characterization of Superconducting Materials for Fusion Reactor Magnet Use

Magnetic materials

108 Research on Materials Synthesis to Control of Magneto-thermal Properties by Size Effects and on Low Temperature Production

[109] Research and Development of Systems and Materials for Magnetic Refrigeration

Materials for energy application

(110) Development of Third-Generation Nickel-base Single Crystal Superalloys

111 Thermal and Electrical Properties of II-IV and V-VI Thermoelectric Semiconductors

112 Energy Conversion Materials Fabricated with Functionally Gradient Structure

113 Environmental Degradation of Structural Materials for Light Water Reactors

114 Fundamental Research on Application of New Functional Materials to Passive Components

115 Assessment of Strength and Structural Materials Database for Weldment in FBR Components

116 Research on Distributed Database for Advanced Nuclear Metals

117 R&D of Advanced Heat-Resistant Structural Materials for Very High Temperature Gas-Cooled Reactors

[118] Study on Changing the Properties of Metallic-Oxide Films for Increasing the Hydrogen Permeability

[119] Material Chemistry in the Extreme Conditions under Irradiation

Bio-Materials

(120) Spectroscopic and Electrochemical Investigation of the Metal Complexes with an Unusual Electronic Structure

121 Bacteria Reaction on Materials

122 Fundamental Study on Biocompatibility of Materials

[123] Improvement of Wear Properties of Metallic Medical Materials

[124] Monitoring Reaction Rate of Bacteria

Processing

Separation and synthesis

125 Extraction from Metal to Gas Phase

[126] Fundamental Study on Preparation and Characterization of the Metal Complexes Possessing a Peculiar Molecular Structure

[127] Alloying Method Using Decomposition of Metal Halides

Gaseous process

128 Precise Composition Control of Ordered Alloys by Chemical Transportation Techniques

129 Processing and Development of Isotopically Controlled Materials (ICM)

130 Development of Shape Memory Thin Films Formed by PVD Method

Liquid state process

(131) Basic Study on Refining of Molten Metal and Controlling of Solidification by Electromagnetic Force

(132) Investigation on Nucleation and Crystal Growth Mechanism under Heterogeneous Ambient Phase

(133) Solidification Processing for Particle Dispersed Unidirectionally Grown Composites

134 Basic Technology Development of Materials Processing in a Short-Duration Microgravity Environment

135 Metastable Phase Solidification from Undercooled Liquid by Inducing External Nucleation Seed

[136] Purification of Metals by Non-Contacting Melting Method

[137] Solidification Processing for Fine-grain Structure Materials

[138] Measurements, Analyses and Evaluations of Specimens Made by FMPT

Solid state process

139 Metallurgical Analysis of Micro-Machining Region

Powder processing

140 Preparation and Characterization of Ultrafine Powders Used for Making Oxide Superconductors

141 Synthesis and Characterization of Advanced Materials Utilizing Colloidal Dispersed Systems

142 Study on Solid State Chemical Reaction, its Propagation and Materials Synthesis

143 Study on Properties of Raw Powder of Superconductor using High Pressure Forming

144 Development of Particles Assembly Technology for Integration of Functions

145 Fundamental Study on Creation of Micro Stereom Fabrics by Powder Technology

146 Study on Rapidly Solidified Powders for Superconductive Materials

147 Coating of Fine Powders by CVD Technique in Fluidized Bed

Joining

148 Corrosion of Dissimilar Metals Joints in Reactor Fuel Reprocessing Plants

149 Low Energy Joining with Controlled Surface Composition

150 Fundamental Research on Joining Technique in Microgravity

Composite process

151 Forced Infiltration Process for Making Composite Structures

152 Coating Formation by Molten and Electrified Powders

Process with aid of beam technology

153 Diagnostics of Laser Photoionization Induced Plasma

154 Study on Evaporation Process by High Energy Density Beams

155 *In Situ* Analysis/Evaluation of Radiation Damage in Materials

156 Characterization and Control of Elementary Functions of Materials in the Localized Fine Area

157 Synthesis of Special Compounds by a Combined Use of Ion Implantation and Deposition

Processing in special environment

158 Development of Quantum Microstructure in Ultra Clean Vacuum

❒ Research Programme

Characterization/Properties

Electronic and nuclear properties

① Development of High Precision Detection Techniques for High Field Magnets

April 1994 to March 1999

H. Aoki, High Magnetic Field Research Station

Keywords: high field magnet, high precision detection techniques, highly correlated electron system

In 1988 NRIM started a project to develop several types of high field magnets whose capabilities are of the highest class in the world. Most of the construction and installation of the planned magnets, i.e. the 40 T hybrid magnet, the 20 T large bore size magnet, the pulse magnets and the high resolution magnets, are now nearly completed. The purpose of the present project is to develop several kinds of high precision detection systems for the applications of these high field magnets to the researches of materials science.

We have already developed the high precision detection systems of the nuclear magnetic resonance, transport properties, quantum oscillations and so on for the high resolution magnets. These systems have been used for many cooperative researches as well as for in-house researches. An example of the products by the cooperative researches is given in Fig. 1.

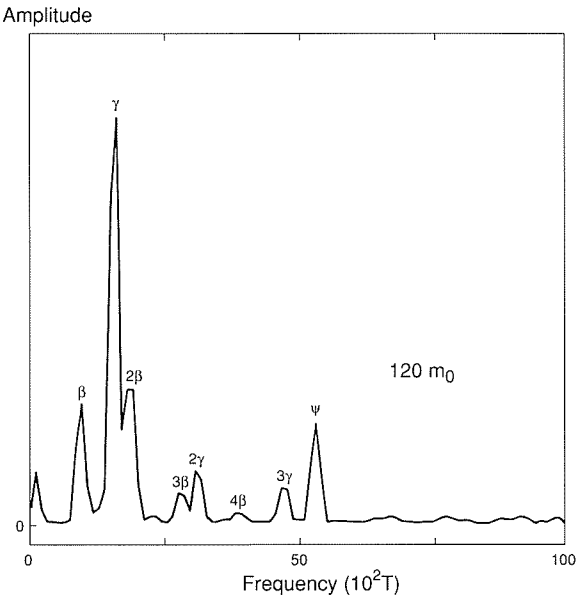

Fig. 1 Fourier spectrum of the de Haas-van Alphen effect signal from heavy fermion compound $CeRu_2Si_2$. This is the first successful observation of the heavy electrons whose effective masses exceed 100 m_0, where m_0 is the rest mass of an electron in vacuum. The frequency peak designated by ϕ is the signal from the heavy electrons. This study was performed in collaboration with the University of Tsukuba.

We will further develop such high precision detection systems for other high field magnets. The combination of other extreme condition such as ultra low temperatures, high pressures and so on with high magnetic fields are also planned. These systems will be mainly used for the study of the highly correlated electron systems, such as heavy fermion compounds, high T_c oxides and organic conductors.

② Development of Common Interface to Two Different Types of Numerical Database

April 1994 to March 1995

Y. Asada, Material Design Division

Keywords: oxide superconductors, database, network

We developed two types of numerical database for new high T_c superconducting materials. One is for the data from the published papers. There are so many fields that it is arranged to store any kind of data. Key item is sample number; If samples with different compositions appear in the same paper, then they have different sample numbers. Samples from different papers have different sample numbers even if they have the same composition. Using this key item, data are treated as individual data. This is important for data processing.

The other is for original data which we produced in our working group. We prepared samples well-characterized and measured many superconducting and normal state properties. The raw data are stored together with their detailed measuring conditions. We can make comparison among the data in various aspects.

These two databases are constructed using the same DBMS (DataBase Management System), but different in the database structure. It is desirable that these databases are used complementarily via network system. For this purpose we are going to develop user-friendly interface with common tools for access and data processing. We have a plan to introduce BBN/Cornerstone as a common tool for statistical processing. The result will contribute to the effective usage of the numerical databases with different database structure.

3 Pressure Effects on Physical Properties of Magnetic Materials

April 1993 to March 1996

T. Matsumoto, Materials Physics Division

Keywords: magnetic properties, Kondo effect, pressure dependence

Pressure is a clean and effective means to control the degree of hybridization of the 4f and conduction electrons which gives rise to various phenomena in rare earth intermetallic compounds such as heavy fermion state, mixed valence effect, Kondo-lattice behavior, long-range magnetic order and so forth. We have developed a high pressure technique that has yielded the most accurate measurement of magnetic susceptibility in this field. Using this technique, we can study the interplay between these competing states in a more controlled manner. One of our current interests centers on Ce intermetallic compounds. For example, we have investigated the magnetic susceptibility of CeP in detail under high pressures and have obtained numerous information about the ground state of Ce in this compound, pressure dependence of crystal field, that of the Kondo temperature and so on.

Our program also encompasses developing high pressure techniques. Present efforts in this area are directed toward constructing a new system that can measure some physical properties and crystal structure simultaneously.

Related Papers

Electrical Resistivity of the As-Grown $Gd_{1.92}Ce_{0.08}CuO_4$ Single Crystal under Pressure, A. Matsushita, S. Uji, and T. Matsumoto, Solid State Commun., 87 (1993): 321.

Effects of Pressure on Magnetic Susceptibility in α- and γ-Ce, T. Naka, T. Matsumoto, and N. Môri, Physica, B 194–196 (1994): 331.

Effect of Pressure on Crystal Field Splitting in CeP, T. Naka, T. Matsumoto, Y. Okayama, N. Môri, Y. Haga, and T. Suzuki, submitted to proceedings of ICSCES '93, San Diego.

4 Electronic Structure and Superconducting Mechanism in High-Temperature Superconductors

April 1989 to March 1995

T. Sasaki, Materials Physics Division

Keywords: high-temperature superconductor, theory, electronic structure

The high-temperature superconductor (HTSC) is a potential material for a variety of applications. Despite a great deal of effort of basic research on electronic structures and properties of HTSC's, the superconducting mechanism has not been clarified yet. In this work, we have studied the electronic structures and properties of HTSC's based on the first-principles calculations within the local-density approximation (LDA).

The electronic band structure of La_2CuO_4 has been calculated for two different crystal structures, K_2NiF_4 and Nd_2CuO_4, to clarify the role of oxygen atoms in its properties. The results show that the oxygen atoms outside CuO_2 planes realize the two-dimensional character of the electronic structure near the Fermi energy (E_F). The high density of states obtained just below E_F for the Nd_2CuO_4 structure implies its instability against hole doping, which is consistent with the observed fact that no hole-doping is possible in Nd_2CuO_4.

LDA band calculations have been performed for $YBa_2Cu_3O_y$ (y = 6 or 7) (abbreviated as Y123). Several characteristic aspects have been derived by comparing with other HTSC's. Importance of the energy separation between Cu-*d* and O-*p* states was pointed out in connection with photoemission experiments. Significance of the *p-p* hopping between the nearest oxygen atoms was also discussed.

The calculation for $YBa_2Cu_4O_8$ (Y124) has shown the similarity and dissimilarity between the electronic structures of Y123 and Y124. We found a large energy-level lowering of oxygen *p*-states at chain sites in Y124, which may explain the relative stability of the oxygen ions in Y124. Some differences in the Fermi surfaces between Y123 and Y124 were also suggested in conjunction with anisotropic transport properties.

The calculated Fermi surfaces of Y124 were utilized to calculate Hall coefficients in accordance with the Boltzmann transport theory. The obtained Hall coefficient is in good agreement with experiment in its sign (carrier character) and magnitude (carrier concentration). We have derived an important relation between the Hall coefficient and anisotropy of the in-plane resistivity. The mechanism of anomalous temperature behavior of the Hall coefficient was discussed based on the electronic structure.

Related Papers

Implications of Band-Structure Calculations for High-T_c Related Oxides, K.T. Park, K. Terakura, T. Oguchi, A. Yanase, and M. Ikeda, J. Phys. Soc. Jpn., 57 (1988): 3445–56.

Electronic Band Structure of $YBa_2Cu_4O_8$, T. Oguchi, T. Sasaki, and K. Terakura, Physica, C 172 (1990): 277–81.

Local-Density Band Structure of Y-Ba-Cu Oxides, T. Oguchi, T. Sasaki, and K. Terakura, Physica, C 185–189 (1991): 1733–34.

Calculation of the Hall Coefficient in $YBa_2Cu_4O_8$, T. Oguchi, T. Sasaki, and K. Terakura, in *Electronic Properties and Mechanisms of High-T_c Superconductors*, ed. by T. Oguchi, K. Kadowaki, and T. Sasaki, (Elsevier, 1992): 407–09.

Fermi Surface and Transport Properties of $YBa_2Cu_4O_8$, T. Oguchi and T. Sasaki, J. Phys. Chem. Solids, 53 (1992): 1525–32.

5 Theory of Structure and Properties of Surfaces and Interfaces

April 1993 to March 1996
T. Sasaki, Materials Physics Division
Keywords: electronic structure, structural stability, surface, interface

The aim of this study is to clarify theoretically the structural and electronic properties of solid surfaces and interfaces. The basic theory this study is standing on is the density-functional (DF) electronic theory within the local-density approximation (LDA).

We have extended the first-principles molecular dynamics formalism to the linear-augmented-plane-wave expression, which is expected to be one of the powerful tools to theoretically attack the physical problems.

By the application of the method to a Li-adsorbed Cu surface, we have successfully determined the position of the adsorbant on the surface and the rearrangement of the surface Cu atoms. It has been shown that the results can explain the experimental facts. Moreover, the calculations provided the mechanism of adsorption of the Li atoms on the Cu surface based on the electronic structure.

Further developments on methodological and numerical techniques will be also tried to make it possible to perform large-scale numerical calculations.

Related Papers

Density-Functional Molecular-Dynamics Method, T. Oguchi and T. Sasaki, Prog. Theor. Phys. Suppl., 103 (1991): 93–117.

Linear-Augmented-Plane-Wave Based Car-Parrinello Method and Its Application to Cu Surfaces, T. Oguchi and T. Sasaki, in *Computer Aided Innovations of Materials II*, ed. by M. Doyama, J. Kihara, M. Tanaka, and R. Yamamoto, (Elsevier, 1993): 107–10.

Augmented-Plane-Wave Force Calculations for Transition-Metal Systems, T. Oguchi, in *Interatomic Potentials and Structural Stability*, ed. by K. Terakura and H. Akai, (Spring-Verlag, 1993): 33–41.

6 Database Development in Assistance of New Superconducting Materials Research

April 1988 to March 1995
Y. Asada, Material Design Division
Keywords: oxide superconductors, database, graphic data, material design

Since the discovery of high-T_c oxide superconductors an enormous amount of research papers have been reported. Numerical database on these superconducting materials, therefore, is necessary for the researchers in this field. We developed in this study a numerical database "SUPERCON:" The data on superconducting properties (T_c, higher and lower critical magnetic fields, coherence length, penetration depth, energy gap, etc.) and related properties (Hall coefficient RH, thermopower s, thermal conductivity κ, specific heat C, etc.) are collected from the published papers. More than 5000 records of data are stored up to now in our database "SUPERCON." Graphic data of temperature dependence of RH, s, κ, C are also stored in the form of digital data.

We investigated the doping effect of elements on T_c in $Y_{1-x}R_xBa_2Cu_3O_z$, $YBa_{2-x}M_xCu_3O_z$ and $YBa_2Cu_{3-x}M_xO_z$ by retrieving the data from "SUPERCON." For each alloying system x dependence of T_c is fitted to the numerical equation using the least squares method. To construct a T_c calculation system these equations have been stored as basic data for superconducting materials design.

Related Paper

Numerical Database of High-T_c Oxide Superconductors, Y. Asada, to be published in Cryogenic Engineering (in Japanese), 28 (1993): 298.

7 Structure and Electronic Properties of Silicides

April 1993 to March 1996
T. Hirano, Chemical Processing Division
Keywords: silicides, single crystal, interface, high-pressure

The purpose of the study is to investigate the structure and the electronic properties of metal disilicides. We have been studying those two circumstances, i.e., at silicon/disilicide interface and under high-pressure.

In the former, the interface is formed by the growth of Si on single-crystalline substrates of transition-metal disilicides (M_TSi_2). M_TSi_2 is selected for the following reasons; (1) there are few experiments about semiconductor/metal interface formed on metal surface, and (2) Schottoky barrier height (SBH) of Si/disilicide interface is sensitive not only to the kind of metal but also to the structure of the interface. The structure of the interface is observed using transmission electron microscope, (TEM). The electronic property will be studied using SBH measurements.

The experiments under the latter condition are carried out using a multi-anvil apparatus. We use alkaline-earth metal disilicides (M_ASi_2, M_A = Ca, Sr, Ba) as samples because of their characteristic Si atom configurations and large compressibilities of M_A atoms. When the sample is compressed, it undergoes phase transition. The structure and electronic properties of the high pressure phase will be discussed using X-ray diffraction and electric resistivity measurements under pressure. Furthermore, we are going to discuss about the similarity among the transformation sequence under pressure in three M_ASi_2.

8 First-Order Phase Transitions in Magnetic and Superconducting Materials at Low Temperatures

April 1993 to March 1995

M. Uehara, Surface and Interface Division

Keywords: first-order phase transition, metastable state, quantum tunneling, magnetic relaxation

In disorder magnetic systems like SmCoCu, magnetic domain walls move between pinning centers provided by the disorder. At high temperatures this is known to occur via thermal activation: at low temperatures we have shown previously that there is a crossover to quantum tunneling. Such behavior due to magnetic relaxation is generally related to the nature of the first-order phase transition in which a macroscopic system in a metastable state undergoes transitions to a lower energy state. The decay of the metastable state in type II superconductors is also another typical example and it is indeed observed. We have studied the magnetic relaxation in high T_c superconductors. We have shown that the dynamics of vortices in Bi and Y-samples of high-T_c superconductors can be described on a very coherent way by using the mean relaxation time τ defined at a constant level of mixed state. The mean energy barrier E which is associated with this relaxation time is found to be proportional to the reciprocal magnetic field in both samples, $E \sim (1/H - 1/H_o)$. The temperature dependence of this energy barrier is also found to be the same for both samples above a crossover temperature T_{cr} = 6 K and 8 K, $E \sim [1 - (T/T_c)^2]$. Below their crossover temperatures both samples change the relaxation mechanism: the relaxation is no longer thermally activated but independent of temperature. This is attributed to the quantum tunneling of vortices. The studies on magnetic relaxation in conventional superconductors such as $Ti_{50}V_{50}$ and V_3Si single crystals are currently in progress.

Related Papers

Noncoherent Quantum Effects in the Magnetization Reversal of a Chemically Disordered Magnet, M. Uehara and B. Barbara, J. Physique, 47 (1986): 235–38.

Field and Temperature Dependence of the Mean Penetration Rate of Fluxons in the Mixed State of High T_c Superconductors, M. Uehara and B. Barbara, J. Phys. I. France, 3 (1993): 863–70.

Quantum Tunneling in Magnetic Systems of Various Sizes, B. Barbara, L.C. Sampaio, J.E. Wegrowe, Ratnam, A. Marchand, C. Paulsen, M.A. Novak, J.L. Tholence, M. Uehara, and D. Fruchart, J. Appl Phys., 73 (1993): 6703–08.

9 Fundamental Studies of Electromagnetic Materials with Strong Electron Correlations

April 1993 to March 1996

K. Kadowaki, 1st Research Group

Keywords: strong electron correlations, heavy fermions, Kondo effect, high quality single crystal growth

Strong electron correlation effects have been known to give rise to unusual physical properties in metals and intermetallic compounds with rare earth and actinide elements. The ground state of these materials at low temperatures could be superconducting, magnetic ordering, normal Fermi liquid with highly renormalized effective masses or insulating, depending upon the systems, and cannot be predicted by the properties at high temperatures, even at the best of our present knowledge. In order to better understand the fundamental driving mechanism of these ground states, a broad spectrum of materials has been investigated: heavy fermion compounds such as $CeRu_2Si_2$, $CeCu_6$, URu_2Si_2, UPt_3, etc., a new class of magnetic superconductors such as RET_2B_2C (RE = Rare earth elements, T = Ni, Pd, Pt), low carrier semiconductors (semimetals) such as CeP, CeAs, CeSb, etc., and Kondo insulators such as $Ce_3Bi_4Pt_3$, $Ce_3Sb_4Pt_3$, etc. For the study of physical properties of these materials it is essential to grow high quality single crystals. At the first year project we have set up two multi-purpose single crystal growing furnaces: one is the four-arc furnace to grow single crystals with low vapor pressures and the other is an induction furnace with vertical and horizontal zone refining functions and with bridgeman as well as Czochralski method. We have succeeded in preparing magnetic superconductors such as $Y(Ni, Pd, Pt)_2B_2C$, among which the highest T_c = 23 K was observed in the Pd compound. Single crystal growth of AEB_6 (AE = Ca, Sr, Ba) has been performed in order to study the doping effect of rare earth elements in relation to the formation of the heavy electron band with strong electron correlations.

10 Fermi Surfaces and Heavy Cyclotron Mass in the Molecular Conductor $(DMe\text{-}DCNQI)_2Cu$

April 1993 to March 1994

S. Uji, Materials Physics Division

Keywords: dHvA effect, organic conductor, electronic state

Recently, a novel molecular conductor containing Cu ions, $(DMe\text{-}DCNQI)_2Cu$ was synthesized. One of the striking features in the $(DMe\text{-}DCNQI)_2CU$ system is the fact that the drastic metal-insulator transition is induced by the substitution of the hydrogen atoms with the deuterium atoms in the DMe-DCNQI molecules. The transition is considered to be caused by the nesting of the one dimensional (1D) Fermi surface. The three dimensional static order of the valence of the Cu ions ($...Cu^+Cu^+Cu^{2+}...$) is found to take place without appreciable change in the average

valence when the 1D Fermi surfaces are nested. These characteristic properties are considered to be closely related to the structure of the Fermi surface in this system. In order to investigate the Fermi surface, we have carried out the de Haas-van Alphen (dHvA) measurements for the single crystals of the undeuterated $(DMe\text{-}DCNQI)_2Cu$.

We have found seven different oscillations with frequencies lower than 3000 T. These oscillations arise from the three dimensional (3D) Fermi surface which is dominated mainly by the Cu *3d* orbital character. Measuring the angular dependence of the frequencies, we determined the structure of the 3D Fermi surface. This is the first direct evidence of the existence of the 3D Fermi surface in molecular conductors. In addition to the low frequency oscillations, many oscillations with frequency higher than 3000 T are detected for the magnetic field in the *ab* plane. The observation demonstrates the coexistence of the 1D and 3D Fermi surfaces. The heavy cyclotron masses are found to result from the small energy dispersion due to the *3d* character. The results suggest that the effect of the mass enhancement due to the strong electron correlation is not appreciable.

Atomistic arrangement

⑪ *In Situ* Observation and Structural Analysis of High T_c Superconductors at Low Temperature

April 1994 to March 1999

T. Kimoto, 1st Research Group

Keywords: improvement of TEM image resolution at low temperature, high T_c superconductor, development of electron beam gun of high intensity, CCD camera, electron holography

Development of high T_c superconductors is very important for fusion reactors, but few principles for the development of higher T_c superconductors have been found because their mechanism of superconducting is not yet understood. One of the most effective approaches to the understanding is to carry out *in situ* observation of their crystal structures or magnetic fluxes under superconducting state with a transmission electron microscope (TEM). However there are several problems in TEM observation at low temperatures. The most important problem is the reduction of image resolution limit. The resolution limit at low temperatures is about ten times lower than that at room temperature because a TEM specimen is apt to drift easily due to the instability of temperature or vibrate due to liquid helium evaporation. Therefore, *in situ* low temperature TEM observation of high T_c superconductors has not been performed so far.

The objectives of the present research are to resolve the problems in low temperature TEM observation by developing both hardware and software. The improvement of image resolution limit at low temperature is planned to be realized mainly by reducing the exposure time for recording an image as short as possible by developing an electron gun of higher intensity and a cooled CCD camera of higher sensitivity and/or by controlling the specimen temperature with laser beam instead of electric heater. By developing a high intensity electron gun, the improvement of electron holography, which enables us to observe directly the fluxoid quanta in high T_c superconductors, is also aimed. An on-line system with CCD camera for the analysis of the diffraction patterns to determine the crystal structures of high T_c superconductors will be also developed.

The final goal which is expected to be approached by the present technological development for *in situ* low temperature TEM observation is to understand the mechanism of superconducting of high T_c superconductors for the first time and to establish the principles for the development of superconductors of higher T_c.

12 Structures of Transition Metal Oxides from the Bonding View Point

April 1992 to March 1995

M. Okochi, Materials Physics Division

Keywords: transition metal oxides, binding nature, γ-Mo_4O_{11}, ZrO_2-3mol% Y_2O_3, ZrO_2-12mol% CeO_2, X-ray photoelectron diffraction (XPD)

Transition metals oxides are characterized by the structures of crystalline coordination compounds with interatomic bonds by sharing of electrons between metallic atoms and the neighboring oxygen. The bonding view point is a potential conception to make the microscopic binding nature clear in three dimensional array of atoms and gives the conceptional understanding about the binding nature in the compounds like metal oxides.

We have determined valence states of molybdenum atoms in γ-Mo_4O_{11} by analyzing bond length between molybdenum and oxygen and besides that among metallic atoms. The analysis has been taken the coordination number and the maximum valency into consideration. The valence electrons of molybdenum have been estimated to be 4.72–5.52 in covalent bond of oxygen and to be 1.81 in metallic bond of the conduction band which is in agreement with metallic conduction of γ-Mo_4O_{11}.

Infrared and Raman spectroscopic studies of ZrO_2 doped with 3 mol% Y_2O_3 (Z-3Y) and 12 mol% CeO_2 (Z-12C) have been done with a conventional X-ray diffraction technique. Low-temperature infrared spectroscopy revealed that the 580 cm^{-1} and 725 cm^{-1} modes suddenly evolve at 123 K when the tetragonal(t)-monoclinic(m) phase transi-

tion is induced in Z-12C; the analysis of the oscillator strength of the B_u mode at 580 cm^{-1} indicated that the t-m phase transition occurred discontinuously with a narrow transition width about 2 K. It was concluded that the non-occurrence of the t-m phase transition in Z-3Y originated in its being less tetragonal (c/a = 1.012) than Z-12C(c/a = 1.018), in the context of the dependence of the transformability on the tetragonality.

A gas supply system and a refrigeration unit have been installed in our X-ray photoelectron diffraction (XPD) system. These new facilities make it possible to control oxygen contents at sample surface and to observe structure change as a function of temperature. The computer control and data analysis system has been improved for 2-dimensional XPD imaging of transition metal oxides.

13 Quantification Study on High Resolution Transmission Electron Microscopy

April 1993 to March 1996

S. Ikeda, Surface and Interface Division

Keywords: HRTEM, superconductor, YPd_2B_2C, cross section, ion irradiation, slow scan CCD camera

In the present study, we have tried to quantify, the high resolution electron microscopic image and electron diffraction intensity, with the aid of SSC camera, and to obtain much more information than the conventional use with photographic films. Light atoms, for example, oxygen atoms in a ceramic specimen can not be recorded on the film, in contrast with heavy atoms. A slow scan CCD camera-image processor with a dynamic range of 10^4 is attached to the high resolution electron microscope, JEM-4000EX, with a point to point resolution of 0.17 nm. Therefore, it is possible to detect the intensity contribution from oxygen atoms in oxides by image taken by the CCD camera.

We applied the above mentioned technique to identify the structure of recently discovered superconducting compound YPd_2B_2C. We performed electron diffraction experiments using the tilting stage and obtained performed 3D structure of the reciprocal lattice. We compared the high resolution images for the [100], [110] and [001] zones with the computed ones using MacTempas software and found that the structure of this compound is basically the same as that of $LuNi_2B_2C$.

It is known that ion irradiation enhances the irreversibility field of the superconducting material and increases intragrain critical current densities. We have examined irradiation induced structural damages in the BSCCO tapes with 15 μm thick using the cross-sectional TEM method. The results revealed that the long continuous cylindrical column defects with a diameter of 2 to 8 nm were produced by ion irradiations and the core of column is surrounded by an anisotropic strain field.

Related Papers

High Resolution Transmission Electron Microscopic Studies on a Superconductor YPd_2B_2C Compound, S. Ikeda, H. Fujii, T. Kimura, K. Kumakura, K. Kadowaki, and K. Togano, Jpn. J. Appl. Phys., 33 (1994): 3986–99.

HRTEM Observation of the Effects of 180MeV Cu^{11+} Ion-Irradiation on the Crystal Structure of $Bi_2Sr_2CaCuO_x$, B. Chenevier, S. Ikeda, H. Kumakura, K. Togano, S. Okayasu, and Y. Kazumasa, Materials Research Forum, 129 (1993): 17–30.

14 Synthesis and Characterization of Oxide Superconductors

April 1988 to March 1995

K. Nakamura, 1st Research Group

Keywords: high-T_c oxide superconductors, thin film, MBE, oxygen deficiency, intergrowth, super-lattice

Among various techniques in synthesizing films with multi-component layered structure, an alternate sequential deposition method using multi-evaporation sources and accurate shutter control is a most promising in controlling the structure of such systems. This method is used to control the number of CuO_2 layers in the Bi system to fabricate oxide superconductor films. The artificial superlattice structure with n up to 7 have been successfully prepared. We have investigated the structure of the films in detail and have found that intergrowth structure was often observed when the amount of evaporating flux from the source was somewhat different from the stoichiometric ratio. We also found that such intergrowth occurs periodically and can be characterized as a statistical mixture of neighboring two phases with different number of CuO_2 planes.

Another target in this study is to control oxygen deficiency and to characterize accurate oxygen content and structure change accompanied by oxygen deficiency in thin $YBa_2Cu_3O_{7-\delta}$(YBCO) films. We have found that not only the c-axial length but also the diffraction line intensity changes appreciably with oxygen deficiency. From this result we have proposed a new method to determine the degree of oxygen deficiency accurately from the intensity change. We also investigate in detail the structural change in thin YBCO films accompanied by the ordering of cations due to annealing of thin films.

Related Papers

Uniformly Layered Mixtures of the $Bi_2Sr_2Ca_{n-1}Cu_nO_{2n+4}$ Phases Formed in Artificially Layered Films-Structural

Analysis and Superconducting Properties, T. Hatano, K. Nakamura, H. Narita, J. Sato, S. Ikeda, and A. Ishii, J. Appl. Phys., 75 (1994): 2141–48.

Oxygen Potential Control in $YBa_2Cu_3O_{7-\delta}$ Thin Films, K. Nakamura, J. Ye, and A. Ishii, Physica, C 213 (1993): 1–13.

Quantitative Structure Analyses of $YBa_2Cu_3O_{7-\delta}$ Thin Films: Determination of Oxygen Content from X-ray Diffraction Patterns, J. Ye and K. Nakamura, Phys. Rev., B 48 (1993): 7554–64.

15 Study on Fabrication Processes of High-T_c Oxide Superconducting Tapes by Means of Vapor Deposition and Powder-in-tube Methods

April 1992 to March 1995
Y. Tanaka, High Magnetic Field Station
Keywords: YBaCuO film, deposition, BiSrCaCuO, AgCu sheath-tape, powder-in-tube technique

Fabrication processes for YBaCuO films and for Bi(Pb)SrCaCuO Ag-alloy-sheathed tapes have been studied. Deposition techniques are rf magnetron sputtering, excimer laser ablation, and low pressure thermal plasma flash evaporation. To obtain high critical current density, J_c, of YBCO films problems with respect to intergranular weak-links at high angle grain boundaries must be solved. Particular attention, therefore, has been given to prepare highly in-plain textured YSZ buffer layer in addition to c-axis alignment. A new bias-sputtering technique installed with a hollow-cathode type electrode has successfully been able for us to make triaxially aligned YSZ buffer layers on polycrystalline substrates. The critical temperature, T_c, of the YBaCuO thin films, which were laser-deposited on Hastelloy C with the in-plain textured YSZ buffer layer, is 90 K, and J_c was increased to as high as 2×10^5 A/cm^2 at 77 K.

Bi(Pb)SrCaCuO superconducting wires fabricated by the powder-in-tube technique using Ag-sheath are expected to be used in high-field magnet application, such as transmission cable and current leads conductors. Problems to be solved, however, in order to fabricate practical wires, are high homogeneity as well as sufficient mechanical strength in J_c in a long length. Problems we experienced that degrade J_c-value were Ag sheath swelling during sintering, cracks in oxide core, precipitations, non smooth sheath/oxide core interface and irregular deformation of the tape during partial melting process. The sheath swelling is caused by volume expansion of gases, mainly CO_2, H_2O or O_2, that are trapped in the soft Ag sheath, then can be eliminated by using carefully degas-treated calcined powder. Flatness of the sheath/core interface is very important for the formation of a highly oriented microstructures as well as free of precipitations. To keep the flatness it is important to roll the tape samples with the core microhardness less than about 150. Another problem, irregular deformation of the tape during partial melting process, has not been solved yet, probably related to a shrinkage of oxide core upon partial melting. AgCu alloy sheathed tapes for both Bi2212 and Bi2223 are useful to increase mechanical strength as well as high Jc, especially for Bi2223 with simultaneous addition of Cu (7 – 10at%) and small amount of Ti or Au.

16 Observation of Partial Density of States with X-ray Photoelectron Diffraction

April 1993 to March 1994
M. Shimoda, Materials Physics Division
Keywords: partial density of states (PDOS), X-ray photoelectron diffraction (XPD)

As one of the unique applications of photoelectron diffraction technique, a method of decomposition of state density in the valence and conduction bands has been recently proposed. This method is based on the fact that the photoelectron diffraction pattern of the conduction electrons in metal is the same as that of the core electrons. Actually, the results on some intermetallic compounds showed good agreement with the theoretical calculations. It is however not clear yet if this new technique works well for other materials, especially, metal oxides in which electrons in the valence band are strongly correlated with each other. Our purpose is thus to apply this method to some metal oxides and to compare the results with band calculations. For handling with oxides in a high vacuum chamber, we built a gas supply system to control oxygen contents at sample surface by adjusting oxygen pressure in the experimental chamber. We also installed a refrigerator to cool samples down to about 30 K both for stabilizing atoms at surface and for observing temperature dependent phenomena. At present, our target is a molybdenum bronze, a molybdenum-alkalinemetal-oxygen compound, which shows metal-insulator transition at low temperatures. We are trying to observe PDOS in both metal and insulator phases.

Related Paper

Two Dimensional Photoelectron Diffraction Images of a Single Crystal $Bi_2Cr_2CaCu_2O_{8+x}$, M. Shimoda, Butsuri, 48 (1993): 637.

Phase transformation and microstructures

17 Super-Microscopic Study on the Mechanism of Martensitic Transformation in Shape Memory Alloys

April 1992 to March 1995
S. Kajiwara, Physical Properties Division

Keywords: martensitic transformation, electron microscopic structure, stacking fault density, deformation band

In order to understand the formation process of martensite (h.c.p.) from austenite (f.c.c.) in an Fe-14Mn-6Si-9Cr-5Ni (mass%) shape memory alloy which is very low cost and has a property of corrosion-resistance, electron microscopic study has been performed on deformation structures formed by stepwise extension up to 4%. In the early period of the present study, using a high resolution differential interference optical microscope, we found that a martensite plate in this alloy which was induced by extension and seemed to be a single plate by conventional optical microscope, consisted of much smaller plates with the width of about 200 nm. On the other hand, in our previous study using a high resolution electron microscope, we have revealed by taking lattice images that deformation regions with 100–200 nm widths which were formed by 4% extension in a thermomechanically treated specimen consist of lamella structures having a mixture of f.c.c. phase and h.c.p. phase with 1–10 nm widths, but, in a specimen only solution heat-treated, no such mixtured structures are formed. A much better shape memory effect is obtained in the thermomechanically treated specimen than in the specimen only solution heat-treated.

This year we have examined the formation steps of martensite plates with conventional electron microscope in order to bridge a gap between the observations by optical microscope and high resolution electron microscope. After stepwise extension of 0.2, 0.4, 0.8, 1.6, 3.0 and 4.0%, deformation structures were observed by electron microscope for the thermomechanically treated specimens. Shifts of electron diffraction spots along c^*-axis in the diffraction pattern of the h.c.p. martensite were also measured to know stacking fault densities. The results are as follows. (1) In the earliest stage of deformation, a few h.c.p. martensite plates with the width of about 1.5 nm are formed in a group. As the amount of deformation is increased, the number of such groups is increased, but no appreciable thickening of the martensite plate itself has occurred. Such groups of martensite plates are scattered in a certain region which we call the "deformation band" hereafter. (2) The width of deformation bands is about 0.1 μm for 0.2% extension and increased to 1.3 μm for 4% extension. (3) The density of stacking faults in the h.c.p. martensite, which is expressed by fault parameter α, is increased somewhat (α: 0.05–0.1) in the early stage of deformation, but, in the later stage of deformation, no appreciable increase of α is observed. (4) Even in the martensite plates formed in the earliest stage of deformation, stacking faults exist in such an extent that the corresponding electron diffraction spots are shifted, though their density is small (α = 0.03).

Related Paper

HREM Study of Stress-Induced Transformation Structures in an Fe-Mn-Si-Cr-Ni Shape Memory Alloy, K. Ogawa and S. Kajiwara, Mat. Trans., JIM, 34 (1993): 1169–76.

[18] A Molecular-Dynamics Study of the Nucleation Process at Liquid–Solid Interfaces

April 1991 to March 1994

K. Kusunoki, Materials Physcis Division

Keywords: molecular-dynamics simulation, nucleation, liquid–solid interface, solidification, chaos

We have studied the solidification mechanism at liquid–solid interfaces using a molecular-dynamics simulation under the constant-pressure and the periodical boundary conditions (PBC). We applied the Lennard-Jones type interatomic potentials for the construction of a model system of stacking A- and B-monoatomic crystals with fcc structure. The interatomic potential between the B-atoms was set so that the melting temperature of the B-crystal was fairly higher than that of the A-crystal. The system was heated up to the melting temperature of the A-crystal, and then cooled down. In this process, the melt A-material was observed to crystallize at the A/B interface after creations and dissipations of clusters with an ordered structure. In addition, we observed that infinitesimal perturbations given to the initial state of the system caused remarkably the change in the final microstructure of the A-material. This phenomenon is attributed to a chaotic behavior of atoms emerging at the very early stage of the nucleation process.

Surface and interface properties

(19) Research on Electrode Reactions between Metallic Ions and Carbonaceous Materials/ Research on Electrochemical Characteristics of TiAl-base Alloys

April 1994 to March 1997

I. Tomizuka, Division of Physical Properties

Keywords: electrode reaction, metallic ion, carbonaceous material, electrochemical characteristics, TiAl-base alloy

The subject is concerned with the following three fields.

1. Investigation on effects of electrical potential on adsorption equilibrium and on rate of adsorption on solid carbons of metallic ions in an aqueous solution. The investigation includes:

(a) observation of chronological variation of concentration of solute ions in the aqueous phase under various acidities, various electrode potentials and various initial concentrations of the ion, and (b) discussion on electrochemical potential of metallic ions adsorbed on a carbon electrode, which may or may not be connected with the electric potential of the carbon electrode.

2. Investigation similar to that mentioned in item 1 where the solid carbon electrode is replaced by a liquid electrode composed of the fullerene dissolved in a polar and non-aqueous solvent, together with investigation on metallic salts which might be formed thereby in the liquid-electrode phase. The investigation includes: (a) observation of chronological variation of concentration of solute ions in the aqueous phase under various acidities, various electrode potentials and various initial concentrations of the metallic ion, and (b) discussion on formation of a fullerene-metal complex in the above non-aqueous phase, which will be based on the infrared-spectroscopy under an electrical potential.
3. Investigation on effect of cathode charge on polarization curves of TiAl-intermetallic-compounds-based alloys, on the surface layer formed thereby and on effect of mechanical elimination of surface film, together with basic analysis on corrosion-wear. In the investigation, following examinations will be performed on TiAl-intermetallic-compounds (TiAl, Ti_3Al, $TiAl_3$, etc.)-based alloys to be prepared in laboratory: (a) comparison between the polarization curves observed for the TiAl-base alloys which have been made free from absorbed-hydrogen by mechanically eliminating the passivating film and those observed for the alloys which have been made hydrogen-containing by cathodic-charging. Variation of the surface layer after each treatment will be checked by SEM, EPMA, EDAX X-ray diffractometry, chemical analysis, direct observation with an electron microscope and so on; (b) electrochemical analysis on corrosion wear; and (c) effect on corrosion-wear characteristics of alloying elements, hydrogen and structure.

20 Characterization of Composite Ultrafine Particles

April 1993 to March 1996

S. Ohno, Chemical Processing Division

Keywords: ultrafine particle, composite UFP, Ni-Ti-O system, plasma synthesis, catalytic property, photocatalytic decomposition

It is well known that the ultrafine particles (UFP) have many excellent physical and chemical properties. Further, the composite UFP formed by combining between foreign particles in the region of a UFP's size would be expected to improve the properties of UFP and to create a new function.

Recently, we found that the composite UFP of a Ni-Ti-O system have a good photocatalytic property for decomposition of water. In this study, the Ni-Ti-O UFP were synthesized by an RF-plasma CVD process and photocatalytic properties of the Ni-Ti-O UFP were determined by photocatalytic decomposition of trichloroethylene suspended in an alkaline aqueous solution.

From analysis of reaction products, it is presumed that the decomposition of trichloroethylene is caused by hydrogen and oxygen of nascent state, which is formed by photocatalytic decomposition of water, as the following equation

$$n\mathrm{C_2HCl_3} + 2m\mathrm{H} + m\mathrm{O} \rightarrow x\mathrm{CH_4} + y\mathrm{CO_2} + z\mathrm{CO} + w(\mathrm{Cl\ or\ Cl\text{-}compound}) \quad (1)$$

where chlorine or chlorine compounds such as HCl and $HClO_3$ is neutralized with an alkali in the solution. Furthermore, it is found that the $NiTiO_3$ phase in the composite UFP has the best photocatalytic property for above reaction.

21 Cooperative Phenomena of the Transformation Variants

April 1992 to March 1995

H. Miyaji, Advanced Materials Processing Division

Keywords: variant selection, martensitic transformation, Fe-30Ni alloy

The variant selection processes are studied on the martensite of ferrous alloys which have 3, 12, 24 crystallographically equivalent orientation relation with matrix crystal. In the present study we investigate the effect of the internal stress on the variant selection, which is induced during the processing of thin films.

The textures of Fe-30Ni alloy sheets rolled at a temperature above Md (γ) and subjected to a sub-zero treatment (α) were determined by an X-ray pole figure method. It is found that the rolled texture of γ phase is of the typical Cu-type. The transformation texture of α phase has the pole distribution of the shape of the numeral "8" by the effect of strong interaction with internal stress. On the other hand, the transformation texture of α phase, which was formed from γ phase annealed for a stress relieving, has the different pole distribution from the above one.

According to computer simulation of the transformation texture, it is considered that these differences arise from the change of the constraint stress in the parent phase; that is, the experimental

results are explained satisfactorily by supposing that the three-axial constraint stress acts to the α phase in the as-roll specimen, but that the stress along the normal direction of the sheet diminishes in the stress relieving treatment.

Related Papers

Effect of Specimen Size on the Variant Selection in Martensitic Transformation, H. Miyaji and E. Furubayashi, Textures Microstruct., 12 (1990): 189–97.

Transformation Texture Analysis of BCC and BCT Ferrous Martensite, H. Miyaji and E. Furubayashi, Textures Microstruct., 22 (1993): 43–51.

22 Effect of Oxidation on Mechanical Degradation of Metallic Materials

April 1991 to March 1995
Y. Ikeda, Failure Physics Division
Keywords: oxidation, fatigue, Y_2O_3 dispersion, mechanical alloying

Fe-20Cr alloys with and without dispersed oxide were prepared by mechanical alloying method. The dispersed oxides are Y_2O_3, Al_2O_3, ZrO_2 or SiO_2. These alloys were cyclically oxidized in a stream of dry O_2 up to 82 cycles. One cycle consisted of 10 ks (2 h 47 min) heating at 1100 K and 2 ks (33 min) cooling at R.T. The thermal cycling caused oxide scale cracking and produced oxide nodules. The metallic luster decreased with increasing heating cycles because of oxide nodule development. The decrease, however, was less extensive on Y_2O_3 dispersed alloys than the others. The reflectance after cyclic oxidation increased with increasing Y_2O_3 content. This result shows that dispersed Y_2O_3 suppressed scale cracking and hence oxide nodule development. The other oxides had no effect in suppressing the nodule development.

Fatigue test in air at 823 K showed that a lower limit of crack propagation was greater on Y_2O_3 dispersed alloys than the others. This result can not be explained by Orowan mechanism because dispersed oxides other than Y_2O_3 had no effect in fatigue crack propagation. It is more reasonably attributed to less extensive cracking of oxide film at fatigue crack tips of Y_2O_3 dispersed alloys than the other alloys, based on the oxidation result.

Cracking and spalling of oxide scale was less extensive on the alloy without dispersion prepared by mechanical alloying than that by melting. A similar result was obtained on type 316L stainless steels. These results suggest that excellent properties of oxide dispersion strengthened alloys are attributed to the process "mechanical alloying" also.

23 Modeling and Electrochemistry of Corrosion under Thin Water Film

April 1993 to March 1995
T. Kodama, Environmental Performance Division
Keywords: water film, vibration capacitance electrode, photodegradation, paint film

Water Film Corrosion

Such types of corrosion as atmospheric corrosion, indoor corrosion or dew-point corrosion are classified as water-film corrosion, where metal corrodes by electrochemical mechanism within a thin water film on metals. Corrosion in water film is thought to be much faster than that in bulk solution because of the accelerated diffusion and mass transfer. The mechanism of water-film corrosion has not been proven because of the difficulties in measuring electrode potential and current flow within water-film. In the present study we have developed a specially designed electrochemical cell and a non-contact reference electrode that is movable in x-y direction. The principle of the non-contact reference electrode is based on vibrating capacitance, in which alternating current proportional to the potential difference across the capacitor is generated by periodic change in its geometry. One electrode of the capacitor is flat metal specimen covered with thin water film and the other electrode consists of gold wire of 1 mm diameter. The latter is vibrated by an ac driven piezoelectricity ceramic. The generated ac current was detected with a lock-in amplifier. We have started measuring electrode potential of copper using the non-contact electrode. For comparison we also use a conventional immersion type tungsten electrode.

Atmospheric Corrosion in Tropics

Since 1989 we have been conducting atmospheric corrosion tests in the Philippines and Thailand under auspices of Japan International Cooperation Agency (JICA) as cooperative research works with governmental research institutes of these countries. Five-year plans of exposure are scheduled to be finished by fiscal year 1994. We will continue cooperation in the field of data analyses and human exchange program. In exposure test it has been shown that tropical climate is more aggressive to polymers than to metal because of UV intensity. For this simulation we have conducted photodegradation tests of polymer coatings. Three types of paints, namely, epoxy, alkyd and polyurethane were coated to 15 μm on glass plates. The effect of white pigment was also examined. Coated samples were exposed to xenon arc lamp up to 410 hrs. The UV intensity was 17 W cm^{-2} on coated surfaces. After irradiation paint film was scraped off and was subjected to structure analyses by FTIR. Within the exposure time no change was observed for polyurethane film indicating good

resistance to weathering. For epoxy new absorption band at 1700 cm^{-1} was apparent which is due to carbonyl radicals formed after photodegradation. For alkyd paint that contains carbonyl in its original form absorption band at 1167 cm^{-1} was used as an index to photodegradation. For epoxy and alkyd paints new absorption increased with time exponentially. In both epoxy and alkyd white paints are more resistant than clear ones owing to the UV absorption nature of pigment, particularly of rutile.

24 Evaluation of High-Performance Triazinedithiols as a Corrosion Inhibitor

April 1993 to March 1995
H. Baba, Environmental Performance Division
Keywords: triazinedithiole, corrosion inhibitor, copper

A new project on surfactants of triazinedithioles (RTDT) has started in cooperation with universities, governmental research institutes and industry under the auspices of Science and Technology Agency. The general targets of the project are designing molecular structure of high performance RTDT's with fluoride and silicious functional groups, and establishing synthetic methods of the compounds that give highly protective interfacial layers on surfaces of metals, rubbers and plastics. In NRIM we take part in clarifying the mechanism of corrosion inhibition and the nature of chemical bonding between metals and RTDT's. In the first year of the project our research concern is focused on the performance of conventional RTDT's on copper.

Copper specimens were electrochemically treated in several RTDT solutions with various radicals (R–), such as $-N(C_4H_9)_2$, $-N(CH_2CH = CH_2)_2$, –SH, $-N(n - C_8H_{17})_2$, $-NHC(CH_3)_2CH_2C(CH_3)_3$, $-N[CH_2 CH(CH_3)_3]_2$, $-NHC_{18}H_{35}$, $-N(CH_2C_6H_5)_2$, and $-N[CH_2(C_2H_5)CH(CH_3)_3CH_3]_2$, followed by characterization of surface layers and evaluation of corrosion resistance. By anodic polarization at 40 °C in alkaline solutions of various RTDT's, current peak owing to thiole oxidation appeared at around 1 V vs. SCE with potential dependence on the types of radicals (R–), indicating polymerization of thiole groups. Also it is known that at this current maximum the efficiency for the polymerization is the highest. We demonstrated that the oxidation current increased with increasing temperature and concentration, and prolonged electrolysis time, when copper anode was treated potentiostatically in Na_2CO_3 solutions containing RTDT-Na.

Chemical analysis by means of reflection FTIR was carried out for surface RTDT films prepared by electrochemical method. In IR spectra an absorption band at 1564 cm^{-1} was distinct indicating C = N stretching and the presence of thiole type radicals in the film. Obviously RTDT is incorporated into surface film as a result of electrolysis.

Corrosion performance of RTDT film was evaluated by anodic current change when copper specimens were polarized in air-saturated 3% NaCl solutions at a scan rate of 50 mV/min. Anodic polarization in this case was applied after the lapse of sufficient immersion time in the test solution for the stable corrosion potential. Untreated copper specimen showed a ready current increase by applying a small anodic potential shift, while treated samples showed high anodic current. From cathodic branch of polarization curves, we observed little effect of electrolytic treatment.

25 Fabrication of Quantum Well Box Systems by Droplet Epitaxy for Advanced Optoelectronic Devices

April 1991 to March 1996
N. Koguchi, Surface and Interface Division
Keywords: quantum well boxes, molecular beam epitaxy, GaAs, scanning tunneling microscopy

Predictions of enhanced electron mobility device and advanced semiconductor laser with highly-monochromized and low threshold current density have been made in the quantum well box structure. Although the molecular beam epitaxy (MBE) method is known to be successful in growing finely layered structures and quantum well wires, it has not yet been successful to obtain the quantum well box structure.

We have proposed a new MBE growth method named as Droplet Epitaxy for the fabrication of some III-V compound semiconductor quantum well box structures. This method is based on incorporating V-column elements with III-column elements in the periodic table droplets which were deposited on an inert surface of the substrate by monolayer adsorption of the III and V-column elements. Some III-V compound semiconductor surfaces terminated with a VI-column element like S, Se or Te have been reported to provide an inert surface with appropriate dangling bonds suitable for supporting the adhesion of foreign atoms. Such surfaces are thought to be suitable for the growth of epitaxial microcrystals by the Droplet Epitaxy method.

We have demonstrated three dimensional growth of GaAs epitaxial microcrystals on an S-terminated GaAlAs substrate by Droplet Epitaxy. At the end of the process of Droplet Epitaxy the GaAs microcrystals are covered by an MEE (migration enhanced epitaxy) grown GaAlAs layers. By this technique a number of epitaxial microcrystals with a pyramidal shape were successfully obtained on the S-terminated substrate. The size of the base of each epitaxial microcrystals was about 10 nm ×

10 nm and the standard deviation of the size distribution was about 5% only. We have also confirmed the S-terminated substrate surface by atomic-resolution images obtained by scanning tunneling microscopy.

Related Papers

Growth of GaAs Epitaxial Microcrystals on an S-terminated GaAs Substrate by Successive Irradiation of Ga and As Molecular Beams, N. Koguchi and K. Ishige, Jpn. J. Appl. Phys., 32 (1993): 2052–58.

New Selective MBE Growth Method for Direct Formation of GaAs Quantum Dots, N. Koguchi, K. Ishige, and S. Takahashi, J. Vac. Sci. Technol., B 11 (1993): 787–90.

Direct Formation of GaAs-GaAlAs Quantum Dots Structure by Droplet Epitaxy, N. Koguchi, K. Ishige, and S. Tsukamoto, MRS Symp. Proc., 326 (1994): 269–74.

26 Fundamental Research on Adsorption under Electric Potential on Metal-atom-doped or Electron-doped Dispersed Carbons

April 1993 to March 1994

I. Tomizuka, Division on Physical Properties

Keywords: adsorption, carbon, electric potential

This research is aimed at developing a new technology for waste-water treatment. It is based on an idea in which an electric field is applied on carbonaceous adsorbent.

Experiments were performed by immersing activated or inactivated carbon felt in acidic or neutral aqueous solutions of copper sulfate of various concentrations under various cathodic electric potentials, and then by repeating determination of concentration of the copper ion until an apparent equilibrium was established.

According to the experimental data in acidic solutions, it was found that the carbon felts, activated or inactivated, eliminated considerable amounts of ions from the solution when a cathodic potential was applied, while they hardly did so without electrical potential. Apparent equilibrium concentration depended on applied potential. Although the concentration was always larger than the theoretical value obtained from thermodynamic data cited in literatures, it was fairly smaller than the value obtained when the carbon felt was replaced by a copper plate and the same potential was applied for a comparable period of time. The reason for the difference is to be elucidated. Experimental data obtained from experiments in neutral solution are now under review.

The research subject includes some other missions in addition to those already mentioned. Some of them are investigations on adsorption under alternate potentials and absorption by a liquid-electrode comprising fullerene dissolved in a non-aqueous polar solvent. They are not completed at the time of going press of the manuscript. They are to be transferred to a new research subject starting from April 1994.

In the framework of the research, Prof. Kartel, vice director of Institute for Sorption and Problems of Endoecology in Kiev, Ukraine, was invited in order to exchange information in related fields. Staying in our institute for about three weeks, he visited National Institute of Radiological Science (Science and Technology Agency), Institute for Industrial Medicine (Ministry of Labor), Hokuetsu Carbons Co., Takeda Chemicals Co., Kansai Cokes & Chemicals and some other state-run or private-run institutions and exchanged information with professional persons on relevant topics.

Supported by the fund of the research, one of its staff, I. T. attended 21st Biennial Conference on Carbon held in Buffalo, NY, USA and collected information related with carbonaceous adsorbents.

27 Studies of Local Corrosion Damage of Corrosion Resistant Alloys in High Temperature Water

April 1993 to March 1994

N. Nagata, 5th Research Group

Keywords: high temperature water, corrosion fatigue, stress corrosion cracking

The objective of this research is to clarify the mechanism of degradation of structural materials for nuclear power plants in high temperature water.

Low cycle fatigue behavior of AISI316 stainless steel improved in China was tested in pressurized water at 573 K. Tests were conducted with fully reversed triangular wave form with 0.5 to 1.5% in total strain range and 0.1%/s in strain rate.

Since the elastic strain component, $\Delta\epsilon_e$, and the plastic strain component, $\Delta\epsilon_p$, exhibited a good linear relation to the fatigue life, N_{25}, in the S-N curves plotted on a log-log scale, the total strain range $\Delta\epsilon_t$ could be expressed as:

$$\begin{aligned}\Delta\epsilon_t &= \Delta\epsilon_e + \Delta\epsilon_p \\ &= AN_{25}^{-\alpha} + BN_{25}^{-\beta}\end{aligned} \qquad (2)$$

where A, B, α and β are constants. The value of exponent β was 0.69, which was approximately the same as 0.68 for SFVQ1A low alloy steel.

The S-N curves for the tested steel were not so different from the curve for ordinary AISI316 steel. In comparison with the design fatigue curves in the ASME Boiler and Pressure Vessel Code Sec. III, it was concluded that the tested alloy possesses safety margin to the integrity under high temperature water environments.

Stress corrosion cracking behavior of nickel alloys was tested in 10%NaOH solution of 573 K.

C-ring specimens stressed to 1.7 σ_y were tested under controlled potential of +100 mV positive. After 500 hours immersion, no cracks were present in the specimens for Alloy 600 as well as for Alloy 690. However, some corrosion pits were found in Alloy 600. It was implied that Alloy 600 may crack from these pits if the stress level is higher than 1.7 σ_y.

This research was performed in a collaboration program of NRIM with Shanghai Nuclear Engineering Research and Design Institute based on the Japan China Agreement on Cooperation in Research and Development in Science and Technology.

Mechanical properties

(28) A Molecular-Dynamics Study on the Elementary Process of Fracture

April 1994 to March 1997

K. Kusunoki, Materials Physics Division

Keywords: fracture mechanism, crack, ductility, atomistic model, molecular-dynamics simulation

Based on molecular-dynamics simulations, the present study aims at making definitions in an atomistic scale of the physical parameters such as stress, strain, and stress concentration/intensity factors appearing in the conventional macroscopic fracture mechanics. In addition, this study is also intended to make atomistic interpretations of the notions such as cracks and ductility of materials.

Atom displacements caused by an external force applied on a material are thought to be small and indefinable in the scope of the conventional continuum models and theories. Another target of this work is to elucidate how such small individual atomistic displacements evolve into the strain and stress which give rise to the macroscopic deformation and fracture of materials.

The molecular-dynamics simulations are to be carried out on the basis of a particle model with simple interatomic potentials.

(29) Detection and Healing of Damage in Materials

April 1994 to March 1997

N. Shinya, 5th Research Group

Keywords: damage detection, creep damage, creep cavities, healing of cavities

A new damage detection method, formation mechanisms of creep damage and a healing mechanism of creep cavities are being studied in this work. The main research program and results up to now are as follows.

Damage Detection Methods

A detection method for the localized strain and micro-cracks has been developed using a piezoelectric polymer. Formation of the localized strain and micro-cracks could be detected and determined quantitatively by measurement of electric charge evolved in the piezoelectric polymer.

Mechanisms of Creep Damage Formation

A new Moire method using the electron beam scan was developed for the measurement of localized deformation at high temperatures. The relation between the creep cavity formation and the inhomogeneous deformation by grain goundary sliding is studied experimentally using the electron Moire method and analytically by the calculation using a multi-grained finite element model.

Healing of Creep Cavities

In a previous work it was confirmed that a compound of BN forms at the cavity surface during creep in austenitic stainless steels. In order to shield all over the creep cavity surface by the stable compound, a new 18-8 stainless steel containing 0.07% B and 0.06% N was melted and creep tested. The steel showed high rupture strength and good ductilities. It was thought that the stable compound at cavity surface suppresses the cavity growth and brings about the superior rupture properties.

(30) Environmental Dependency of Cyclic Deformation Behavior

April 1994 to March 1996

R. Hamano, Mechanical Properties Division

Keywords: corrosive environment, crystallographic orientation, corrosion fatigue behavior

Fatigue lives of structural materials extremely decrease in corrosive environments, in comparison with laboratory air. However, we do not know any definite mechanisms to illustrate how the corrosive environments play an important role on the initiation or propagation process of fatigue crack. Therefore, it is needed to investigate the environmentally-assisted fatigue damages in the processes such as (a) pre-crack cyclic deformation, (b) microcrack initiation with its early propagation, and (c) long crack growth.

We have examined the fatigue crack initiation processes in the atmosphere of laboratory air and in a 3.5 pct NaCl aqueous solution at 293 K, using the specimens of high strength steels with the notch machined in the direction of 45 degrees to the axis of applied tensile direction. In the laboratory air, fatigue cracks initiated near the notch root and propagated in the same direction of notch plane, i.e., maximum shear stress direction. In the aqueous solution, however, the direction of fatigue crack propagation easily deviated from maximum shear stress direction to maximum tensile stress direction. This early transition of fatigue crack from shear stress mode to normal stress mode is

attributable to the environmental embrittleness susceptibility of materials in corrosive environment.

These results suggest that a systematic survey of environmental influence on crystallographic orientations of cracking might lead to a further understanding of the interrelationship between slip behavior and fatigue cracking, i.e., Stage I vs Stage II fatigue cracking.

In this study, the cyclic deformation behavior of the coarse-grained or single crystal high strength materials is investigated both in the presence and absence of hydrogen. Primarily using transmission or scanning electron microscopy, the orientation and environment dependence of the fatigue cracking of the materials is discussed altogether with the observational results of slip bands and plastic strain distribution.

(31) Study on Transient Behavior of Deformation and Fracture at the Elevated Temperature

April 1994 to March 1996

F. Abe, Environmental Performance Division

Keywords: creep deformation, inherent creep strength, creep crack growth, microstructural change

Complex transient behavior which does not obey classical form is observed on both creep deformation and creep crack growth of heat resistant steels and alloys at the elevated temperature. Creep deformation and creep crack growth are influenced by the changes in microstructure of materials. This study aims at giving a role of microstructural change in the transient behavior.

Anomalous Creep Deformation

Complex creep deformation which reveals multiple local minima in creep rate is observed for engineering heat resistant steels. The anomalous transient in creep rate is considered to be correlated with decrease in creep strength and an advent of inherent creep strength due to thermally induced changes in microstructure. The effect of microstructural change on anomalous transient in creep deformation behavior is investigated and discussed from a viewpoint of an inherent creep strength.

Early Stage of Creep Crack Growth

Nose region, in which two different creep crack growth rate are present for one value of C* parameter, is observed in the early stage of creep crack growth. Lower and higher creep crack growth rate in the nose region corresponds to transient and tertiary creep stage, respectively. Changes in microstructure at the vicinity of crack tips with the crack propagation are investigated. Mechanism of the nose in creep crack growth and assessment technic of creep crack growth rate in the early stage are discussed.

(32) Relationship between Fatigue Crack Propagation and Cyclic Deformation of Small Specimens

April 1994 to March 1997

A. Ohta, Environmental Performance Division

Keywords: fatigue crack, fatigue properties, cyclic deformation

The fatigue crack propagation properties in a crack closure free condition of steels are uniform in spite of the variation in kind of steels, heat treatment and stress ratio. The properties which are represented by the relationship between the stress intensity factor and the fatigue crack propagation rate change with the difference in elastic modulus. However, the relationship between the strain intensity factor, which is represented by the ratio between the stress intensity factor and the elastic modulus, and the fatigue crack propagation rate becomes uniform.

Though the relationship between the strain intensity factor and the fatigue crack propagation rate for titanium alloy which received the solution treated aging is similar to that for steel or aluminum alloy, the relationship between the strain intensity factor and the fatigue crack propagation rate for the titanium alloy which received annealing is superior to that for steel or aluminum alloy.

The differences in fatigue crack propagation properties resulting from these two heat treatments was analyzed in terms of the cyclic deformation properties of small, smooth specimens.

33 NRIM Fatigue Data Sheet Project IV

April 1990 to March 1995

S. Nishijima, Failure Physics Division

Keywords: fatigue of metals, standard reference data, steels and alloys, aluminum alloys

This project is aiming at the establishment of standard reference data on the basic fatigue properties of Japanese engineering materials most commonly used for machines and structures under fluctuating loads.

The work has been conducted since 1975 under successive five-year-term programs. In the present term IV, emphasis is put on the ambient temperature properties of high strength steels and aluminum alloys, intermediate temperature properties of steels for pressure vessels, and high-temperature time-dependent properties of heat-resistant alloys. A brief summary of NRIM Fatigue Data Sheets is given in table 1.

In parallel with the testing program, series of basic researches are being conducted to understand materials behavior and mechanisms of degradation under fatigue environment. Some of the latest concerns are: equivalence of steels and aluminum alloys in terms of strain based fatigue strengths, quantitative evaluation of the effect of

Table 1 Summary of NRIM Fatigue Data Sheets, as of March 1993

Subtheme	Items investigated	Issued
Machine structural materials	High-/low-cycle properties on: carbon/low-alloy steels, stainless steels, carburizing steels, spring steels, tool steels, aluminum alloys.	35
Welded joints of structural materials	High-/low-cycle and crack growth properties looking at the effect of: specimen size, welding procedure, stress ratio, weld/HAZ materials, and for aluminum alloys, as well.	21
Elevated temperature materials	Time dependencies in high-/low-cycle properties for: carbon/low alloy steels, stainless steels, and heat resisting alloys.	22

non-metallic inclusions in hard materials, cyclic softening mechanism of weld metals, interaction of strain aging at intermediate temperatures, elaboration of a new time-temperature parameter method predicting creep-fatigue interaction processes, and so on.

The output data thus validated by the basic researches have been published and exchanged worldwide with scientific and technical organizations. An on-line data service is available from the Japan Information Center for Science and Technology since 1990. It is anticipated that the NRIM Fatigue Data Sheet Project contributes largely to the safe and effective use of engineering materials.

Related Papers

Fatigue Properties of Butt-Welded Joints for 5083-0 Aluminum Alloy, H. Hirukawa, S. Matsuoka, E. Takeuchi, and S. Nishijima, Transactions of Japan Society for Mechanical Engineers, 58 (1992): 676–82 (in Japanese).

Effect of Yield Strength on Basic Fatigue Strength of Welded Joints, A. Ohta, Y. Maeda, and N. Suzuki, Fatigue and Fracture of Engineering Materials and Structures, 16-5 (1993): 473–79.

Parameter Analysis for Time-Temperature Dependent Low-Cycle Fatigue Life, K. Yamaguchi, K. Kobayashi, K. Ijima, and S. Nishijima, Transactions, ASME, Journal of Engineering Materials and Structures, 116 (1994): 479–82.

34 NRIM Creep Data Sheets IV

April 1991 to March 1996

K. Yagi, Environmental Performance Division

Keywords: NRIM Creep Data Sheets, heat-resistant steels and alloys, long-term creep and rupture tests

The objectives of this project are to obtain 10^5 h creep and rupture strength data in long-term creep and rupture tests on heat-resistant steels and alloys, to publish these data as the series of NRIM Creep Data Sheets, and to investigate long-term deformation behavior and creep rupture properties for these materials and the evaluation method of long-term creep and rupture strength at high temperature.

Table 2 NRIM Creep Data Sheets which were published in fiscal year 1993

NRIM/CDS/No.	Materials
17B	0.3%C steel plates for boilers and pressure vessels, JIS SB 480
20B	0.5Cr-0.5Mo steel tubes for boilers and heat exchangers, JIS STBA 20
13B	12Cr steel bars for turbine blades, JIS SUS 403-B
31B	1Cr-1Mo-0.25V steel castings for turbine casings, ASTM A356-9

This project has been continued since 1966 in order to obtain long-term creep data on many kinds of domestic heat-resistant steels and alloys. NRIM Creep Data Sheets on 4 kinds of materials as listed in table 2 were published in fiscal year 1993. These Data Sheets are B-version which contains the longer rupture data than 10^5 h. The manuscript of Technical Document on creep and rupture testing procedures, which have been accumulated in this project, is being produced.

Long-term creep rupture properties of steels and alloys at high temperature was investigated using the creep data and the specimens which have been tested in this project. The main subjects investigated are as follows; (1) the creep deformation behavior was evaluated using a modified θ projection concept. The complicated relationship between minimum creep rate and time to rupture for 1Cr-0.5Mo steel was clarified by the analysis of unusual creep curves using the modified θ approach. The creep deformation and rupture life for 12Cr steel was characterized by a parameter which was controlled by the stability of microstructure; (2) the creep deformation behavior of carbon steel (STB 410) was investigated on the basis of inherent creep strength concept. The creep rate at final stage in unusual creep curve was controlled by the inherent creep strength; (3) Iso-stress tests were conducted on carbon and low alloy steels in order to verify the applicability of this method to prediction of life.

This activities are expected to contribute to ensuring safety and reliability of structural components of high temperature plants and developing new materials.

Related Papers

Inherent Creep Strength for Ferritic Heat Resistant Steels, K. Kimura, H. Kushima, K. Yagi, and C. Tanaka, *Proc. of 5th Int. Conf. on Creep and Fracture of Engineering Materials and Structures,* ed. by B. Wilshire and R.W. Evans, London, The Institute of Materials, (1993): 555–64.

Characterization of Creep Deformation Behavior for Cr-Mo Steel, H. Kushima, K. Kimura, K. Yagi, C. Tanaka, and K. Maruyama (Tohoku Uni.), *Proc. of 7th JIM Int. Symp. on Aspects of High Temperature Deformation and Fracture in Crystalline Materials*, ed. by Y. Hosoi, H. Yoshinaga, H. Oikawa, and K. Maruyama, The Japan Institute of Metals, (1993): 609–16.

Creep Embrittlement of Structural Components in Catalytic Reformer Reactor, T. Nomura (Japan Energy), H. Tanaka, H. Kushima, M. Tabuchi, and K. Yagi, Trans. Jpn. Soc. Mech. Eng., A 59 (1993): 2066–73.

35 Fatigue Behavior of Brittle Materials at Elevated Temperatures

April 1992 to March 1996
Y. Kawabe, Mechanical Properties Division
Keywords: cyclic fatigue, elevated temperatures, ceramics

The development of ceramics is being watched with knee interest, because they are very promising as structural components for engineering applications where metallic materials are not available. Since many of them are subjected to static or cyclic loading at elevated temperatures for prolonged periods, it is important to understand fatigue behavior at elevated temperatures. Nevertheless, there are very few studies on the cyclic fatigue behavior of ceramics at elevated temperatures.

In a prior study, we had evaluated fatigue properties for various kinds of nontransforming ceramics at room temperature and suggested a crack resisting-reactivating model as fatigue mechanisms. However, it is doubted if this mechanism is available at elevated temperatures. Recent studies have shown that cyclic loading has a benificial effect at high temperatures, compared to static loading. Such results are inexplicable by any fatigue mechanisms proposed for room temperature so far. Systematical investigation for various kinds of ceramics is, thus, required to understand the difference at room and high temperatures.

In this study, cyclic fatigue crack growth behavior in normally sintered silicon nitride was investigated over a range of room temperature to 1200 °C. It was found that the crack growth rate does not show monotonical variation with temperature.

Related Papers

The Influence of Variable-Amplitude Loading on Cyclic-Fatigue Crack Growth in Silicon Nitride, G. Choi and S. Horibe, J. Mater. Sci. Lett., 12 (1993): 1886–87.

Cyclic Fatigue in Silicon Nitride Ceramics, G. Choi, S. Horibe, and Y. Kawabe, Acta Metal Mater., 42 (1994): 1407–12.

36 High Temperature Deformation and Fracture in Polycrystalline Oxide Ceramics

April 1992 to March 1995
K. Hiraga, Mechanical Properties Division
Keywords: oxide ceramics, superplasticity, cavitation

Concurrent cavitation in fine-grained superplastic ceramics is of practical importance because it degrades both high temperature tensile ductility and subsequent room temperature strength. Though earlier studies conducted at strains $\epsilon_{true} > 1.0$ showed that the level of cavitation defined as density loss or cavitated area fraction tended to increase with an increase in strain rate, extensive cavity interlinkage occurred to prevent detailed analysis available for cavity nucleation and growth mechanisms. Therefore, we have examined the cavitation behavior on the basis of cavity size distribution in an initial stage of superplastic deformation at 1573 K and at strains $\epsilon_{true} \leq 1.0$ where the influence of cavity interlinkage can be ignored.

Extensive observations with high resolution SEM have revealed that cavities nucleate mainly at multiple grain junctions and grow into fine crack-like shapes or facetted polyhedra in sizes of submicrometers followed by further growth into micrometer-sized rounded cavities. From the analysis of cavity size distributions, cavities with radii (R) greater than 1 μm were found to obey a growth law, $dR/d\epsilon \simeq R$, which indicates that the cavities grow by superplastic flow of the matrix. A steep change in cavity numerical density was also found to occur at about $R = 0.5$ μm. It suggests that a different growth mechanism prevails for the submicrometer-sized fine cavities. Detailed examinations on the growth of the fine cavities and the effects of intergranular glassy phase on cavitation are in progress.

Related Paper

Cavity Growth in a Fine-Grained Yttria-Stabilized Tetragonal Zirconia during Superplastic Deformation, K. Hiraga and E. Takakura, to appear in Proc. ICSMA 10, (Fundamental Physical Aspects of Strength of Crystalline Materials), 1994.

37 Study on Deformation and Fracture of Structural Materials at Cryogenic Temperatures

April 1993 to March 1996
K. Nagai, Mechanical Properties Division
Keywords: cryogenic temperature, fatigue strength, fracture toughness

Previous fatigue tests on structural materials were done at 4 K with a low frequency of 4 Hz to avoid specimen heating. In the present study, the effect of an increase in frequency to 20 Hz on fatigue behavior at 4 K was investigated

for two high strength materials: SUS316LN austenitic stainless steel and Ti-5Al-2.5Sn ELI alloy. In zero-to-tension cyclic stress condition, the former had a one-million-cycle fatigue strength comparable to the yield strength and, on the other hand, the latter had that fairy lower than yield strength. For each alloy, however, the 20 Hz S-N curve was identical to the 4 Hz one in the long life regime (more than 10^5 cycles to failure). And further, no difference was made on the behavior of fatigue initiation and propagation. Hence it can be concluded that the increase of frequency to 20 Hz is allowable for the determination of the fatigue behavior in long life regime with respect to high strength materials.

The accumulated operation time of recondensation refrigerating system that was installed first in 1980 into the cryogenic fatigue test machine reached ten thousand hours. Presumably this is the longest record among the active cryogenic fatigue testers.

Interrelationship between fracture toughness and impact value is controversial from alloy to alloy. An aluminum alloy, A2219, promising for cryogenic use showed increased fracture toughness at lower temperature. However, the impact value decreased as the temperature was lowered. These opposing effects of temperature on toughness parameters will be discussed in the light of difference in deformation behavior.

Related Paper

High Cycle Fatigue Properties of Ti-6Al-4V Alloys at Cryogenic Temperatures, K. Nagai, T. Yuri, O. Umezawa, K. Ishikawa, Y. Ito, and T. Nishimura, *Titanium '92, Science and Technology*, ed. by F.H. Froes and I. Caplan, The Minerals, Metals & Materials Society, (1993): 1827–34.

38 Study on Deformation and Fracture of Materials under Irradiation

April 1993 to March 1998

J. Nagakawa, 2nd Research Group

Keywords: irradiation, radiation damage, deformation, fracture

A change in mechanical properties induced by neutron irradiation is critically important for the structural materials of nuclear application. It influences significantly the endurance of structural components. In this research project, deformation and fracture of materials under irradiation has been studied both experimentally and theoretically. During the fiscal year 1993, the following research activities were accomplished.

Part of the in-beam creep-fatigue testing equipment, namely the loading train and the irradiation chamber, were made. The equipment will be connected to the NRIM small cyclotron after completion in the next fiscal year. The loading train is uniquely characterized by an automatic double-accuracy strain measurement system, which enables extremely high resolution in a creep mode and also very wide range in a fatigue mode.

Nuclear reaction products like helium and hydrogen are expected to be produced abundantly in fusion reactor materials. These gaseous products will influence the fracture properties directly by forming gas bubbles at grain boundaries or indirectly through affecting microstructure evolution. Fe-15Cr-20Ni ternary alloy specimens were irradiated with hydrogen ions with or without helium pre-injection at various temperatures. Both residual hydrogen and injected helium increase the density of point defect agglomerates, but the effect of hydrogen disappears above 800 K, while that of helium persists to higher temperatures. This indicates that it is harder for helium than for hydrogen to be released from the point defect traps.

Tokamak type experimental fusion reactors like ITER will be operated in a cyclic mode. Therefore, the effect of cyclic irradiation is important to the fusion reactor materials. Simple modeling and analytical calculation were carried out for cold-worked austenitic stainless steel at high temperatures. The calculation indicates that in a tokamak condition irradiation creep would be enhanced only by several times while nearly one order higher enhancement would be expected in the inertial confinement reactor condition, provided the same time-averaged atomic displacement rate.

39 Effect of Surface Film on Deformation of Bulk Matrix Material

April 1991 to March 1994

K. Kanazawa, Environmental Performance Division

Keywords: fatigue crack initiation, dynamic ultra micro hardness tester

Surface cracks are not easy to initiate under high-temperature and high-cycle fatigue in the atmospheric environment, because the oxide film formed on the specimen surface prevents dislocations from slipping off the surface. This project aims at studying the effect of surface film on the deformation of bulk matrix material for the purpose of evaluating the resistance of surface film to fatigue crack initiation from the surface.

On oxide film formed on the matrix of a low alloy steel was used as an example of surface films. Not only the hardness of the oxide film and its thickness but also the distribution of hardness from the surface film to the matrix was examined by using a dynamic ultra micro hardness tester. The hardness of the oxide film is higher than that of the matrix. The effects of hard thin oxide film on the deformation of bulk matrix were not clarified quantitatively yet.

40 Evaluation of Crack Initiation and Growth of Superalloys under Creep and Creep-Fatigue Conditions

April 1991 to March 1994

K. Yagi, Environmental Performance Division

Keywords: creep crack growth, creep-fatigue crack initiation and growth, superalloys

The understanding of crack initiation and growth behavior under creep and creep-fatigue loading conditions is important for the insurance of safety and reliability for high temperature structural components. In this work, the crack initiation and growth behavior of superalloys under creep and creep-fatigue conditions is being investigated in terms of microscopical creep damage mechanisms.

Creep Crack Growth Behavior

The creep crack growth behavior is affected by the damage modes which are formed at the crack tip. The crack growth rate under the damage mode condition where the cavities are initiated at the crack tip is the most severe, and the main creep crack is propagated by growth and linking of cavities. The creep crack growth rate was analyzed on NCF800H alloy for this damage mode condition. The creep crack growth behavior was estimated under the assumptions of uniform initiation of cavities and of cavity growth which is controlled by strain. The estimated growth rate agreed with experimental data in the case where 10 to 20 cavities were initiated uniformly on a grain boundary facet. However, many cavities were observed at the wide region of crack tip, and further investigation should be conducted on the creep crack growth for this damage mode.

Creep-Fatigue Life Evaluation

Creep fracture mode is a function of temperature and stress. Creep-fatigue life is affected by the change of creep damage mode. The cumulative creep-fatigue damage which was obtained in creep-fatigue tests was evaluated using a linear life fraction damage rule (LFR) and a ductility exhaustion approach (DEA). Both creep damage vs. fatigue damage relations obtained by LFR and DEA were dependent on the relevant creep damage mode. The relation obtained by DEA was also dependent on the loading type in creep-fatigue tests. The prediction of long-term creep ductility for DEA is not easier than that of creep rupture time for LFR. Therefore, long-term creep-fatigue life should be rather predicted by using creep-fatigue life criterion based on LFR.

Related Papers

Evaluation of Creep Crack Growth Behavior of NCF800H Alloy Based on Creep Fracture Mechanism, M. Tabuchi, K. Kubo, and K. Yagi, Tetsu-to-Hagané, 79 (1993): 732–38.

Relationship between Creep Damage Mode and Creep-Fatigue Interaction for SUS321 Steel, K. Kubo, O. Kanemaru, and K. Yagi, J. Soc. Mater. Sci. Jpn., 42 (1993): 1–7.

Long-term Creep-Fatigue Life Prediction, K. Yagi and K. Kubo, *Proc. of 7th Int. Symp. on Aspects of High Temperature Deformation and Fracture in Crystalline Materials*, ed. by Y. Hosoi, H. Yoshinaga, H. Oikawa, and K. Maruyama, The Japan Institute of Metals, (1993): 489–96.

41 Real Time Evaluation of Fatigue Damage during Crack Propagation under Random Loadings

April 1991 to March 1994

A. Ohta, Environmental Performance Division

Keywords: fatigue crack, random loading, crack closure, residual stress

The loading pattern in real structures varies randomly with time. However, most of fatigue crack propagation test is performed at constant amplitude. Therefore, it is necessary to reveal the relationship between the fatigue crack propagation properties in random loading condition and these at constant amplitude.

The fatigue crack usually initiates in welded part and in large structures. This occurs from the fact that the high tensile residual stresses exist in welded part. That is, the tensile residual stresses work as a mean stress and avoid the fatigue crack closure. The avoidance of fatigue crack closure accelerates the fatigue crack propagation rate.

In this study, the fatigue crack propagation properties under random loading condition are investigated, avoiding the fatigue crack closure.

The fatigue crack closure usually occurs in base metal where tensile residual stress does not exist. The fatigue crack propagation test was performed on base metal specimen keeping the maximum load to be a constant value while increasing the minimum load with the extension of fatigue crack.

The test results show that the fatigue crack propagation properties coincide each other among different high stress ratio conditions. The coincidence indicates that the fatigue crack closure was avoided by this test procedure.

The random loading test was performed with the loading pattern approximating the Rayleigh distribution of peaks. In this case, the maximum load was also kept to be a constant value while the minimum load was changed randomly. That is, the loading pattern resembles icicle from the ceiling. It is also revealed that the fatigue crack propagation rates and the fatigue threshold under random loading condition coincide with those at constant amplitude test.

Related Paper

Fatigue Crack Propagation in a Tensile Residual Stress Field under a Two-Step Programmed Test, A. Ohta, A.J. McEvily, and N. Suzuki, Int. J. Fatigue, 15 (1993): 9–12.

[42] Fatigue Crack Initiation Process in Corrosive Environment

April 1991 to March 1994

R. Hamano, Mechanical Properties Division

Keywords: corrosion fatigue, pre-crack deformation, early fatigue crack growth, high strength, slip localization

Fatigue lives of structural materials extremely decrease in corrosive environments, in comparison with ordinary laboratory air. However, we do not know any definite mechanism to illustrate how the corrosive environments play an important role on the crack initiation or crack propagation processes of fatigue. Therefore, it is neeeded to investigate the environmentally-assisted fatigue damages in the processes such as (a) pre-crack cyclic deformation, (b) microcrack initiation with its early propagation, and (c) long crack growth.

In the present study, the emphasis is put on the processes of pre-crack cyclic deformation and early crack propagation of high strength materials.

We have examined the fatigue crack initiation processes in the atmosphere of laboratory air and in a 3.5 pct NaCl aqueous solution at 293 K, using the specimens of high strength steels with the notch machined in the direction of 45 degrees to the axis of applied tensile direction. Load ratio of 0.1 and sinusoidal wave of a frequency of 1.0 Hz were employed. In the laboratory air, fatigue cracks initiated near the notch root and propagated in the same direction of notch plane, i.e., maximum shear stress direction. In the aqueous solution, however, the direction of fatigue crack easily deviated from the maximum shear stress direction to the maximum tensile stress direction. This early transition of fatigue cracks from shear stress mode to normal stress mode is attributable to the environmental embritleness susceptibility of materials in corrosive environment. The above results suggest strongly that environmental effects on pre-crack cyclic deformation and crack nucleation processes are of importance.

Related Paper

On the Transition of Fatigue Crack of Stage 1 to Stage 2 in Corrosive Environment, R. Hamano, to be published in Metall. Trans., A.

[43] Controlling and Recovering Methods for High Temperature Damage

April 1991 to March 1994

N. Shinya, Failure Physics Division

Keywords: grain boundary cavities, sintering, self-recovering, life extension

Low ductility fracture of metals after long term high temperature creep results from the progressive accumulation of grain boundary cavities throughout the creep process. So that, the acquirement of technologies for controlling and recovering the cavities are important for the development of reliable heat resisting alloys as well as for the maintenance of high temperature components. In this work, a sintering mechanism of grain boundary cavities, controlling methods for crack formation and life extension by sintering treatments have been studied.

Sintering Mechanism of Grain Boundary Cavities

Sintering rates of grain boundary cavities were measured using the highly sensitive density technique during annealing and compressive creep. The results showed that the grain boundary cavities are sintered and removed quickly by compressive creep, whereas the annealing causes only a slight sintering. The comparison between the experimental results and calculations using sintering and modified cavity growth models indicated that the sintering is controlled by the relaxing rate of tensile stress at grain boundary, which is caused by the atomic flow from the cavities to grain boundaries during sintering.

Controlling Method for Crack Formation

In order to prevent the creep crack formation at surface, a process of producing a grain size-gradient structure was developed. The grain size-gradient structure which combines a fine grain surface region and a coarse grain interior showed superior creep rupture and fatigue properties due to controlling surface crack formation

Extension of Creep Life

Repetitive creep/sintering tests were carried out to evaluate the effect of grain boundary cavity sintering on life extension. The results showed that the sintering treatments of hot isostatic pressing and compressive creep extend the creep rupture life considerably.

[44] Mechanism of Fretting Fatigue Failure in Metal Matrix Composite

April 1991 to March 1994

M. Sumita, Mechanical Properties Division

Keywords: MMC, SiC whisker, SiC particulate, fretting fatigue, fatigue

Aluminum alloy matrix composites reinforced with a discontinuous phase in the form of chipped fibers, whiskers or particles are considered to be candidates for many structural applications such as bodies of cars, airplanes, and so on, by virtue of high specific strengths and stiffnesses,

and high workability. As the addition of a second phase to aluminum alloys improves wear resistance performance, many application of these materials involve cyclic loading with fretting, and therefore, fretting fatigue properties are of critical interest.

Fretting damage is known to have a detrimental effect on fatigue behaviors of structural materials. Many factors control the fretting fatigue. This research was planned aiming a fundamental understanding of the mechanism of fretting fatigue failure from a microstructural viewpoint.

Fatigue tests and fretting fatigue tests (under contact pressure of 50 MPa) were carried out at a stress ratio of 0.1 using aluminum matrix composites. A method to evaluate the role of reinforcement phase in fatigue strength and fretting fatigue strength in a metal matrix composite was proposed. The fretting fatigue strength at 10^7 cycles in a 7075-T6 matrix composite reinforced with 20 vol% whiskers was about 60% higher than that estimated using the method proposed. However, the practical value of the plain fatigue strength at 10^7 cycles in the composite was nearly equal to the estimated value. The fretting fatigue strength and fatigue strength at 10^7 cycles in 2024-T6 metal matrix composites reinforced with 20 vol% SiC particulates with the mean size of 2 μm and 16 μm respectively, were 30% higher than those estimated and within the strengths estimated, respectively. The effect of SiC whisker and SiC particle reinforcement on friction coefficient, main crack initiation site at the fretted area, crack initiation and crack propagation in the composite materials were examined or discussed in order to explain fretting fatigue strength of the composite.

Related Papers

Role of Second Phase in Fretting Fatigue Strength in a Sic-Whisker-Reinforced Aluminum Alloy Composite, M. Sumita, N. Maruyama, and K. Nakazawa, J. Japan Inst. Metals, 57 (1993): 1141–48 (in Japanese).

Fatigue and Fretting Fatigue Behaviors of A2024-T6 Composite Materials Reinforced with 20 vol% SiC Particles, N. Maruyama, M. Sumita, and K. Nakazawa, J. Japan Inst. Metals, 57 (1993): 1268–74 (in Japanese).

Measurement and evaluation

(45) Atom Probe Microanalysis and its Use for Materials Design

April 1994 to March 1994

H. Harada, Materials Design Division

Keywords: Ni-base superalloy, NiTi-base alloy, phase equilibrium, atomic configuration, computer modeling

Microstructures of the third generation Re-containing Ni-base superalloys developed in NRIM for gas turbine blades are being analyzed by an Atom Probe Field Iron Microscope (APFIM) equipped with a Three Dimensional Atom Probe (3D-AP) shown in figure 2. The γ/γ' phase equilibrium in the alloys is determined on atomic scale by the analysis. Also the atomic configuration in the γ' phase is determined by layer-by-layer analysis. The results of the analysis are compared with estimations by computer modeling using Cluster Variation Method. So far we are obtaining a very good agreement between them.

The same approach is being made with Al-containing NiTi-base intermetallic alloys newly de-

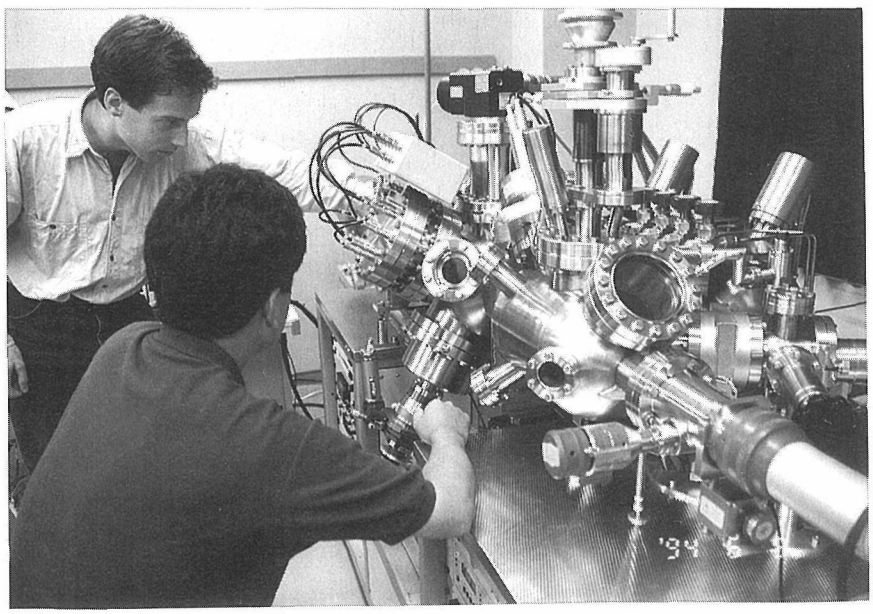

Fig. 2 APFIM/3D-AP installed in NRIM

veloped in NRIM for possible appreciation as gas turbine discs. The precipitation behavior of Ni_2TiAl phase, that is coherent with NiTi matrix, is thought to be the key to understanding the very high strength of the alloys. The APFIM/3D-AP is going to be used to analyze the very early stage of this precipitation in terms of the size, distribution and chemical composition of the precipitates.

㊻ Fundamental Study on Advanced Techniques of Physical Characterization of Metallic Materials and their Application

April 1994 to March 1996
R. Hasegawa, Materials Characterization Division
Keywords: EPMA, XRD, HRTEM, SEM

Fundamentals of the advanced techniques for the physical characterization of metallic materials and their application are studied.

Data Analysis and Image Processing of EPMA

We have built up the personal computer system for the rapid acquisition and accurate analysis of data of and electron probe microanalyser (EPMA) and applied successfully to actual analyses. Because of aging of the computer and the controller of EPMA, we are now renewing the hard and software of the system.

Improvement of Quantitative Analysis by XRD

The qualitative analysis by X-ray diffraction (XRD) method has been usually carried out by referring to the standard data (JCPD cards) in order to identify the materials in question. But unknown substances, such as reaction products and composite oxide compounds, can not be identified by referring the standard data. For such a quantitative analysis a computer software is developed, applying crystal structure analysis method for XRD.

Atomic Scale Observation by HRTEM

We have carried out the spatial structure analysis of lattice images obtained with a high resolution transmission electron microscope (HRTEM). In order to achieve a more accurate and time-saving analysis with atomic scale, a digital electron microscope system is now under construction, which is composed of imaging plate, slow scan CCD-camera, personal computer and engineering workstation connected by LAN.

Practical Application of ECP Method by SEM

The construction of ECP hardware has been almost finished as a pattern analysis system for the fine crystal structure characterization by a scanning electron microscope (SEM), connected to a digital image processing device. The software is now being developed for practical use.

㊼ Research on the Development of Chemical Analysis and Characterization Techniques for Metallic Materials

April 1994 to March 1997
R. Hasegawa, Materials Characterization Division
Keywords: GF-AAS, ICP-AES, GD-MS, TR-XRF, inert gas fusion

As a part of the characterization techniques of advanced metallic materials, instrumental chemical analyses become more important. In the previous research program (1991–1993) we have studied the procedures of high sensitive instrumental analysis of metallic materials. In this study (1994–1996), developments of analytical procedures with high accuracy and precision will mainly be carried out by using various state-of-the art analytical instruments. The study is divided into four items for the sake of convenience and main targets for each item in this fiscal year are as follows.

Elemental Analysis I (GF-AAS and Absorption Spectrophotometry)

1. Determination of lower boiling point elements in Ni-base superalloy by graphite furnace atomic absorption spectrometry (GF-AAS); particularly, determination of selenium.
2. Determination of trace Si and P in metallic materials by absorption spectrophotometry after the separation of matrix element.

Elemental Analysis II (ICP-AES)

1. Simultaneous determination of the trace impurities in titanium metals and silicides by inductively coupled plasma atomic emission spectrometry (ICP-AES) after the separation of titanium.
2. Comparison of a long plasma torch with a normal size plasma torch in "end-on" light measurement (observation of atomic emission in the direction along the plasma flame axis).

Solid Analysis I (GDMS and XRF)

1. Improvement of accuracy and precision in glow discharge mass spectrometry; particularly clarification of the experimental factors which give influence on the ion yield of an analyte.
2. Application of total reflection X-ray fluorescence analysis (TR-XRF) to the determination of trace elements in metallic materials; development of determination technique using an acidic solution in which solid sample is dissolved.

Solid Analysis II (Gas Analysis)

1. Application of inert gas fusion-infrared absorption method to the analysis of trace oxygen in a solder wire for IC use.

(48) Fundamental Study for Electromagnetic Evaluation of Materials

April 1994 to March 1997

I. Uetake, Failure Physics Division

Keywords: non-destructive evaluation, materials evaluation, electromagnetic method, magnetic flux leakage testing, leakage flux, multi-frequency magnetization, surface flaw

Flaws in structural materials decrease remarkably the materials strength. The detection of eventual flaws and material degradation is especially important for the security of important structures such as reactor pressure vessels and/or large constructions.

In this study the basic phenomena of electromagnetic evaluation method are investigated. The depth of magnetic flux penetration is variable according to the materials and the magnetization frequency. It is expected to get more information from different sites in the materials by the application of multi-frequency magnetization method. The detection and evaluation of flaws will be attempted at magnetization frequencies of several Hz to kHz. The evaluation and analysis of materials will be possible at higher accuracies by the introduction of multi-frequency magnetization technique.

(49) Nanoscopic Materials Damage Evaluation

April 1994 to March 1996

S. Matsuoka, Environmental Performance Division

Keywords: materials damage, STM, AFM, molecular dynamics

It is important to examine the materials damage in the vicinity of the crack tip or grain boundary for improving the reliability of structural materials. Recently, the damage in small-size structural components has also become a subject of much concern, as seen from an example of the stress- or electro-migration for aluminum thin-film conductors in the technology of integrated circuits.

A new research has been started since this year to develop the materials damage evaluation technique in the nanoscopic region. At first, the damage of metallic materials such as fatigue or creep, including the stress- or electro-migration for aluminum thin film conductors, is investigated by a scanning tunneling microscope (STM) and atomic force microscope (AFM) which have two excellent abilities of atomic scale imaging and nano-fabricating. On the basis of AFM, in particular, a nano-indentation method is developed to measure the hardness ahead of the crack tip or on the surface of thin films. Secondly, the process of damage or indentation is simulated, using a molecular dynamics. Finally, the nanoscopic materials damage evaluation is established by comparing the experiment and simulation.

50 *In Situ* Measurement of Local Strain at High Temperature by the Laser Speckle Method and its Application to Detection of Defects in Welding

April 1993 to March 1996

Y. Muramatsu, Advanced Materials Processing Division

Keywords: laser speckle method, dynamic strain, *in situ* strain measurement, high temperature

The laser speckle method has been developed to measure strains on the surface of any materials without contact. We have shown that the laser speckle method is also applicable to the *in situ* dynamic strain measurement in high temperature range during the welding process. We confirmed that our testing apparatus is able to follow the change of speckle patterns and many strain curves were obtained, which seem to have the correct tendencies qualitatively.

Some experiments, in which grids scratched on a metal plate were photographed continuously during welding, were carried out to examine the qualitative and quantitative measuring accuracy of the laser speckle method. Strains measured by the grid deformation agreed with those by the speckle method in the most time period during and after welding. Moreover, the good agreement in tendencies were also obtained between the speckle measurement and some numerical analyses using the thermal elasto-plastic finite element method.

A problem, however, was found that a different tendency exists between the laser speckle method and the sequential photographs in the strain curve just after the passing of the heat source through the measuring point.

We are examining whether the measuring accuracy depends on the expansion in the direction of the plate thickness just under the heating line or not. The effect of the formation of oxidation films on the accuracy is also examined.

By clarifying these points, we hope to obtain strain curves which are correct quantitatively throughout the welding period.

51 Correlation between Plasma Parameters and Evaporation in Free-burning Arcs

April 1993 to March 1996

K. Hiraoka, Advanced Materials Processing Division

Keywords: anode, trace element, cleaning action, current distribution, electron density, mixed gas

In this research, the effect of components of anode materials and shielding gases on the vaporization behavior has been investigated by using several kinds of measurements developed in the previous researches.

Firstly, the arc voltages in several anode materials were measured in detail, and the same time, the

current distributions on the anodes were estimated by the potential distributions measurements (as shown in 91's topics in NRIM Research Activities). From these measured results, it was found that the vaporization of trace elements in a water-cooled copper anode surface had influence on the arc voltage, and consequently the degree of the current concentration depended on the temperature gradient at the surface. It was cleared that there was the existence of the cleaning action on the anode plate related to the vaporization and consumption of a specific trace element. Furthermore, the behavior of a slag bit on the molten pool and the concentration of the current induced by the vaporization have been measured, and consequently it was concluded that the current distribution depended on the heat transport and the behavior of slag bits by the metal flow on the molten pool surface.

Secondly, the effect of the shielding gas composition on the anode modes and the electron density of the plasma was discussed. From the measurements of the current distribution, it was found that the current profiles at a water-cooled copper anode showed the same Gaussian distributions up to He contents of 75% from pure Ar, but the distributions in pure He and Ar-H_2 mixed gas arcs were clearly constricted. When the electron density profiles were measured using the stark broadening method and IR-radiation method first proposed by Ohji and Eager, it was found that the decrease in the electron density at the arc center with increasing the He content in Ar-He arcs was more remarkable than that at the peripheral region of the arc, and the distributions were defocussed at the anode center. On the other hands, the electron density near the anode in pure He and Ar-H_2 arcs was one order of magnitude smaller than the electron density in pure Ar arcs, and the distributions were focussed. It was suggested that the electron density profiles had the correlation with the anode modes.

Related Papers

Formation of Multiple Anode Spots in Stationary GTA Welding, A. Okada and H. Nakamura, Quarterly J. Japan Weld. Soc., 11 (1993): 253–59 (in Japanese).

Anode Behavior in GTA Welding and Its Effect on Melting Thin Plate, A. Okada and H. Nakamura, Quarterly J. Japan Weld. Soc., 12 (1994): 94–100 (in Japanese).

Current Distribution on Molten Pool in GTA Welding of Ti Alloy, A. Okada and H. Nakamura, Transaction Japan Weld. Soc., 24 (1993): 109–14.

Basic Parameters in Heat Transport in Argon-Helium Mixed Gas Arcs, J. Zijp and K. Hiraoka, Quarterly J. Japan Weld. Soc., 12 (1994): 21–29.

52 Development of Advanced Technologies for Three Dimensional X-ray Microtomography

April 1992 to March 1995

Y. Yamauchi, Materials Characterization Division

Keywords: CT, tomography, microtomography, X-ray, three-dimension

The X-ray computerized tomography has been widely utilized in the applications for relatively large objects, such as in medical diagnostics of human bodies or in industrial inspection of manufactured components. In those applications the required spatial resolution is usually in the order of 1 or 0.1 mm at most and is limited by the number of pixels on the image. The effective number of pixels is circumscribed by the dynamic range of the detected X-ray signal or the steepness of the X-ray absorption. Further a mass of data storage and computational power have to be considered. However, if it is allowed to restrict the size of objects fairly small, the constraints would be alleviated. The limited number of pixels may not affect the pixel size nor the resolution of image. Based on this idea, we are developing the X-ray microtomography device. In the previous project, high resolution tomographies of a small object were accomplished with the parallel beam projection using a conventional point X-ray source. Then we extended the function of the device to three-dimensional. In this project we have been studying advanced technologies which improve the spatial resolution of tomographs and which provide another function to analyze chemical composition.

We have tried to introduce a filtering technique into X-ray microtomography using conventional polychromatic sources for elemental evaluation of objects.

Results are summarized as follows.

1. Filter modulation of the incident beam yields slight modification of contrast in tomographs.
2. Postreconstruction subtraction between those tomographs extracts elemental information qualitatively.
3. Prereconstruction subtraction with initial projection data provides quasimonochromatic features to polychromatic CT.

53 Study on the Image Measurement by Means of Fuzzy Logic

April 1992 to March 1995

M. Fukamachi, Materials Characterization Division

Keywords: computer-image analysis, fuzzy logic, electron microscopy, distribution of chemical elements on metallurgical structures

In order to carry out an accurate and rapid computer-image analyses of metallurgical structures, the feasibility of an application of fuzzy logic to a computer-image simulation has been studied. Fine metallurgical structures can be revealed with the electron microscopy. Usually, the numerical computer-image simulation is necessary to analyze and to evaluate the fine metallurgical structures. It is difficult to give accurate numerical values to

many parameters which characterize the geometry of electron microscopy and the operating conditions to obtain a satisfactory image simulation.

The method to simulate microscope images of the secondary and the reflected electrons has been studied with an application of fuzzy logic. Only two parameters are used in the image simulation. These are the parameters to represent the amount of generation of the signal electrons and the efficiency of detector to collect the electrons. With this method, the distribution of chemical elements on metallurgical structures can be obtained rapidly by separating the image contrast caused by the local distribution of chemical elements from that of the uneven geometry of specimen surface.

54 Study on Detection and Evaluation of Radiation Damages in Extreme Particle Fields

April 1992 to March 1999

N. Kishimoto, Materials Characterization Division

Keywords: extreme particle field, *in situ* measurement, photoconductivity, critical fluence

Combined particle fields of ions and photons exert strong interactions with materials and are potent not only to detect elementary processes but also to explore novel properties of materials. Especially if both high energy and high density of ions and photons are attained, unexplored non-equilibrium effects will be expected, by virtue of their contrastive features of momentum, energy, excitation modes. The extreme particle field is also an important aspect for practical environments of high energy devices, such as fusion reactors, MHD generators, etc. The main purpose of this research program is to detect and evaluate non-equilibrium processes of materials in the extreme particle fields, associated with radiation damages.

Since 1992, techniques of combining irradiation and *in situ* measurements have been developed using high-energy light ions from the NRIM cyclotron. Damage concentration dependences of dark and photoconductivity have been studied in crystalline Si irradiated with 17 MeV protons. While the photoconductivity of the doped Si does not greatly change up to a certain irradiation fluence ϕ_c, it steeply decreases beyond the fluence ϕ_c. The tail spectrum of shallow impurities simultaneously vanishes at the critical fluence. It is clarified that the drastic decrease of the main peak results from the drops in the carrier density and the decay time, not in the carrier mobility. It is concluded from the results that a competitive process between shallow impurities and defects evolves and that the critical fluence ϕ_c corresponds to the damage concentration required to capture all the doped carriers.

As the first step toward the extreme particle fields a high-current negative ion injector of plasma-sputter type has been developed this year and has achieved the metal-ion flux more than 1 mA. The beam properties including the emittance are measured by the test-stand of the injector, and the data will be used for the development of high-current MeV accelerators.

Related Papers

A Fast and Accurate Infrared Pyrometer Combining Two-Wavelength Method and the Single Wave Band Detections, N. Kishimoto and H. Amekura, Japanese Sensor Newsletter, (Case Western Reserve University), 7 (1993): 27.

Resonant Creep of 316 Stainless Steel Under Pulsed Deuteron Irradiation, N. Kishimoto and H. Amekura, J. Nucl. Mater., in press.

55 Study on Mechanism of Ion Production in Low Temperature Plasma

April 1991 to March 1995

M. Saito, Materials Characterization Division

Keywords: direct current glow discharge, gas mixture, mass spectrometry

In order to clarify the ionization mechanism in a direct current glow discharge plasma under the pressure of about 10 Pa, the gas mixtures of Ar/CH_4, Ar/O_2, Ar/H_2, Ar/He, Ar/CO and Ar/CO_2 were used as a working gas. The ion intensity of elements was measured by a high resolution and precision mass spectrometer.

The magnitude of the decrease of the ion intensity of elements was in the order of Ar/H_2 gas mixture, Ar gas, Ar/CH_4 gas mixture, Ar/He gas mixture, Ar/CO gas mixture, Ar/CO_2 gas mixture and Ar/O_2 gas mixture, with that of the quenching of the argon metastable atoms (Ar^*) due to O_2, CO, CO_2, CH_4 and He. From these results, in a direct current glow discharge plasma, Penning ionization (metastable impact) is considered to be the dominant process for the ionization of the sputtered species.

56 Modeling and Evaluation of Advanced Materials—A Coordinated Interlaboratory Research

April 1992 to March 1996

S. Nishijima, Failure Physics Division

Keywords: advanced materials, property evaluation, modeling, VAMAS project, interlaboratory testing

Nature and Background

Research on advanced material will be one of the keys for continuing development of science and technology in the coming new decades. The present research aims at the development of models describing the behavior and properties peculiar to some selected advanced materials such as composites of high performances.

The approaches to establish the models are based on the detailed analysis and deep understanding of physico-chemical mechanisms in the elementary processes that allow the materials to exhibit their excellent properties.

The project also covers the establishment of rationalized methods for evaluating the performance of advanced materials. This work is a part of the international collaborative agreement of G7 countries since 1986: Versailles Project on Advanced Materials and Standards (VAMAS).

While the activities are organized as a nationwide coordinated research project and financed with the special coordination funds of the Science and Technology Agency (STA). NRIM participates in the project with the most important task force with 40 research staffs, and at the same time, serves as the key laboratory to harmonize the efforts of more than 50 participating research groups from industrial, university and national laboratories.

Materials Modeling

The objective of this STA Project is to develop materials models mainly about the strength properties of intermetallic compounds (IMC), metal matrix composites (MMC), ceramic matrix composites (CMC), and fiber reinforced polymer matrix composites (FRP). Four research groups of NRIM take part in these areas except for FRP. An X-ray micro-beam tomographic technique is also developed at NRIM to assist in analyzing those advanced materials.

Intermetallic compounds

Titanium aluminides are light-weight and heat-resisting material expected for high temperature applications. Two of NRIM laboratories are collaborating with Daido Steel Co., Ltd., to develop models explaining respectively the monotonic strength, fatigue strength and fracture toughness properties of TiAl. The problem here is to improve high temperature strengths without missing the room temperature ductility.

Microstructure change is investigated in detail for hot forged materials of Ti-49Al and Ti-51Al after different heat treatments. There are four types of microstructures for 49Al according to the heat treatment conditions: (1) single phase structure consisting of equi-axial γ grains, (2) γ structure with α_2 precipitates at the grain boundaries, (3) γ structure with platelets of α_2 precipitates in 3 to 4 different orientations within the grains, and (4) two phase lamellar structures of γ and α_2 phases. In case of 51Al, it appears only the single phase γ structure of equi-axial grains. The grain size can be controlled by selecting the heat treatment conditions for the two materials, except for the case of lamellar structure for which the grains tend to be coarser.

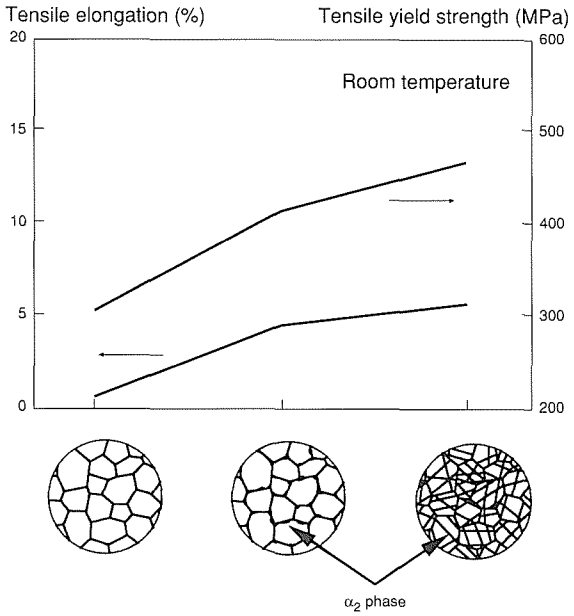

Fig. 3 Variation in tensile properties of Ti-49Al

Figure 3 shows the results of tensile tests of different materials at room temperature. The test shows that 49Al is superior to 51Al in the tensile and yield strengths, but inferior in the elongation, when the single phase γ structures with equi-axial grains are compared. The figure reveals, however, that the inter-granular α_2 precipitates can increase both the strength and elongation and the intra-granular precipitation of platelets at several orientations can result in a better improvement.

Metal matrix composites

Metal matrix composites are widely investigated for use in high temperature equipment because of the advantages in specific modulus and strengths at elevated temperatures. Interfacial reaction between reinforcing fibers and matrices is particularly important, because it may affect the strengthening mechanisms in the material model. NRIM is collaborating with Mitsubishi Heavy Industries and Tokyo University in this area.

Thermal cycling tests at 900–350 °C are being carried out on a SiC/Ti-15V-3Cr-3Al-3Sn composite, where the SiC fiber is fabricated by CVD process and carbon coated to 3 μm thickness. The material have been prepared by HIP at 880 °C and at 100 MPa for 1.5 h followed by various heat treatments to generate different thickness of reaction layers. It is found that a thin reaction layer of about 0.5 μm is already formed prior to the heat treatments. By heating the material for 26 h at 1000 °C, the thickness increases to 1.6 μm.

TEM observation and analyses conducted so far suggest that for a reaction thickness of 0.7 μm the interface includes several complex compounds such as TiC, TiSi, TiSiC, etc. Similar tests will be realized at different temperatures and under stresses for further analysis.

Ceramic matrix composites

There are hot expectations among industry people for ceramics matrix composites that could be used as materials for gas turbine blades working at 1500 °C, as the damage tolerant design seems to be applied for this type of materials. This area is studied in collaboration with Toshiba Corporation and Tokyo Institute of Technology.

The material for the investigation is made of laminated SiC textures filled with SiC matrix. Coupon specimens of various sizes are cut from the material at different orientations and examined in monotonic bending tests to look at the size and orientation effects.

Analysis of AE signals during the tests reveals that the delamination is predominant in the fracture process for out-of-plane bending of the composites, and the pull-outs and breakage of fibers for in-plane bending. The size effect is remarkable in case of the in-plane bend, i.e., the strength is lower for larger specimens; while it is not important in case of the out-of-plane bend, due to low inter-layer strengths of this composite. Anisotropy is notable for the in-plane bending, resulting lower strengths as the fiber orientation differs from the principal stress axis, but it is not observed for the out-of-plane bending.

The observations are being extended by further experiments and analyses at elevated temperature environments.

Micro-Beam X-ray Tomography

Micro-beam X-ray tomography is a unique microscopic analysis method that allows non-destructive 3-D observation of bulk samples. A high resolution tomographic technique is under development with particular attention for use in advanced materials research.

A high energy X-ray source is first developed by introducing special electric control system for ordinary rotating target. The generator can be operated at a power density of 12 kW/m^2 from 20 kV up to 120 kV. The source size achieved is effectively 0.1 mm × 0.1 mm at a takeoff angle of 6 degrees. This value is small enough to keep geometrical blurring of X-ray projection within a few microns.

New improvements are brought to the optical system projecting the image from a high resolution fluorescence plate newly developed by combining a thin reflector with aluminum coatings and an optical tube also originally designed. The system assures to release the hard X-rays transmitted through the microscope lenses that occasionally decrease the s/n ratio.

An improved rotating table of very high accuracy is also developed. It consists of air bearings on the main axis that is driven directly by a brushless motor and controlled by an optical non-contact encoder. An accuracy of sub-microns can be attained by this mechanism.

International Project VAMAS

The international cooperation of VAMAS Project started in 1986. It has today 14 Task Working Areas (TWA) as a whole, spreading from metals, polymers and ceramics (and their composites, as well), to different test techniques and problems related to materials classification and data. NRIM offers international chairpersons for 3 TWAs, respectively on: superconducting materials, cryogenic structural materials and materials property databases. It continues to be the leading member in other 4 TWAs each related to the standardization for: method of evaluating MMC, method of creep crack growth test, method of low cycle fatigue test, and method of surface chemical analysis.

57 Atomic Scale Evaluation of Material Damage in Aqueous Solution

April 1992 to March 1995

H. Masuda, Failure Physics Division

Keywords: *in situ* observation, STM, electrodeposition, image subtraction

The damage of metals in aqueous solution usually begins from the anodic dissolution around inclusions. In order to simulate the anodic dissolution around inclusions, we produced small copper particles (about 600 nm in diameter) on gold electrode in 0.1 M $CuSO_4$ + H_2SO_4 aqueous solution by the localized electrodeposition method found in the previous work[1].

The corrosion behavior of copper particles was studied as in the following. The local corrosion rate was estimated by the subtraction of STM images. The accuracy of estimated corrosion rate without the drift collection was also examined by measuring the drift of vertical direction with time. The drift of vertical direction in 15 minutes was less than 6 nm. The electrically deposited copper was consisted by 4 particles. The initial corrosion rate of particle was the biggest in the biggest particle. The particle size became the same as corrosion proceeded. However the average corrosion rate of whole particles was coincided well with the corrosion rate calculated from Faraday's conversion of the anodic current density. The local corrosion rate was found to be up to 3 times greater than the average corrosion rate. The corrosion behavior of small copper particles can not be explained by the existing theory of corrosion and further work is necessary to understand these phenomena.

Related Paper

Electrodeposition Phenomena of Cu Related to Tunnel Current, H. Masuda, N. Nagashima, and S. Matsuoka, Zairyo-to-Kankyo, 42 (1993): 648–52.

58 Study on Design and Assessment Technology for Ecomaterials

April 1993 to March 1996

K. Yagi, Environmental Performance Division

Keywords: evaluation of environmental load, ecomaterials data base, structural design of solid solution alloys, recyclable materials design, muliphase structure

Recent environmental problems in a global scale originate from strains existing in a large amount of materials and energy consumption. Although man-made materials have supported the society bringing advantages and conveniences to human life, they also impose a wide variety of burdens on the environment through each and every step of production, processing, consumption, use, recycling and disposal. Ecomaterials which would harmonize with the environment and minimize environmental load have to be developed as a new concept of materials design and materials technology. In this project, the study on three subjects as follows are being conducted.

Construction of Ecomaterials Data Base

The development of total evaluation method for environmental load through entire life cycles of materials served is a very important subject in this project. The objective of this work is to construct basic data base and their frame in order to establish a new ecobalance evaluation method in which environmental load and materials properties are evaluated. The fundamental frame for ecomaterials data base was studied, and the data of materials flows and environmental loads of materials were accumulated.

Structural Design of High Temperature Solid Solution Alloys

Strengthening mechanism of high temperature structural materials is investigated as the case study on ecobalance evaluation of materials developed. The factors of materials properties which affect the evaluation of ecobalance are examined. The long-term creep strength of carbon steels was strengthened by very dilute solid solution mechanism due to a slight amount of alloying elements.

Fracture Criterion for Multiphase Structure

For materials design of recyclable structural steels, lessening alloying elements and lessening their amount are strongly desired. Metal properties are generally made up by optimized alloying. For the ecomaterials, however, the properties are improved by microstructural adjustment. The relationship between microstructure and fracture criterion like fracture toughness and fatigue strength was studied on multiphase alloys.

Related Papers

Materials Development in Globally Environmental Problems, K. Yagi, Metals & Technology, 63–6 (1993): 5–10.

Ability of Life Cycle Analysis as Environmental Load Evaluation Method of Materials, K. Halada and R. Yamamoto (Tokyo Univ.), Bulletin of the Jpn. Inst. Met., 33–5 (1994): 516–23.

Complete Recycling System of Metals, K. Nagai, Metals & Technology, 63-10 (1993): 65–70.

59 The Control of Surface Atomic Layers of Solid Surfaces and the Development of Surface Electron Spectroscopic Tomography

April 1992 to March 1995

K. Yoshihara, 4th Research Group

Keywords: HR-ARES, extremely high vacuum, low residual magnetic field

The control of the surface atomic structure will be the key technology to develop modern new materials. Therefore, it is very important to develop the technology on creating very thin films and analyze the layered structure of the very thin film on atomic scale. Especially, the analytical technique must be a non-destructive one, because the properties of very thin films will be strongly affected by the interface structure between thin films and substrates.

The objective of the project is to establish the technology to create the very thin films on the solid materials and also to develop the new technique called "Surface Electron Spectroscopic Tomography (SET)." SET is the technique to make the surface atomic structure visible by analyzing the whole angle of energy spectrum of the electrons exited in the films. The electron exited in the bulk will loose the characteristic energy at the surface region. Therefore it will be possible to make the surface atomic structure visible when the tomographic technique is combined with electron spectroscopy.

The HR-ARES system with extremely high vacuum and extremely low residual magnetic field has been developed. This system can be used for the precise measurements of angular distribution of elastically or inelastically scattered electrons (photoelectrons, Auger electrons) excited by the incidence probes of X-ray (MgK α) and electron beams. Since the main chamber was made of 5 mm-thick μ-metal alloy which has high magnetic-shielding ability, the residual magnetic field in the inner space was found to be decreased to less than 4 mG. This extremely low magnetic field enables the precise angle-resolved measurements of ultra-low energy electrons of about 1 eV. Using our sophisticated UHV techniques, the HR-ARES system with many equipments for surface analysis and treatment has attained the extremely high vacuum of less than 10^{-9} Pa.

Related Papers

Evacuation Properties of a Large Mu-metal Chamber for High Resolution Angle-Resolved Electron Spectroscopy (HR-ARES), T. Yakabe, D. Fujita, and K. Yoshihara, Journal of the Vacuum Society of Japan, 37-3 (1994) to be published (in Japanese).

Development of High Resolution Angle-Resolved Electron Spectrometer (HR-ARES) for Measurements of Angular Distribution of Elastically or Inelastically Scattered Electrons, D. Fujita, T. Yakabe, and K. Yoshihara, Journal of the Surface Science Society of Japan, 15-5 (1994) to be published (in Japanese).

60 Chemical Analysis of Organotin in Marine Environmental Samples

April 1991 to March 1996

H. Okochi, Team of Director of Special Research

Keywords: ICP-MS, organotin, solid phase extraction, GF-AAS, sea water, deep sea sediments

Speciation of Organotin

For the analysis of ultra trace organotin compounds, separation and preconcentration such as organic solvent extraction are useful techniques. As compared with organic solvent extraction, solid phase extraction (SPE) is preferable from a point of view for environmental pollution. The SPE of organotin compounds in sea water has been developed using a polymer of styrene derivative/metacrylic ester as a solid phase sorbent. The recovery of organotin compounds was measured by atomic absorption spectrometry. The analytical procedures are as follows. To prepare the water samples, methanol was added to be 50% to sea water containing organotin compound standard solutions and pH was adjusted to ca. 0.5 with nitric acid. The water samples were forced through the cartridge at a flow rate at 8–9 ml/min. Elution was by gravity flow of 10 ml methanol. Recovery of TPT and TBT was almost 100%, while that of DPT and DBT was lower but the reproducibility was rather good.

ICP-MS has been used as a detector for organotin compounds which were separated with the use of miceller liquid chromatography. Each organotin compounds were separated with a 40 mM tris(hydroxymethyl)amino methane miceller mobile phase containing 75 mM NH_4NO_3, 3% acetic acid and 20% ethanol. The analytical column was YMC-Pack FL-C4, 30 × 4.6 mm and the injector with 50 µl sample loop was used. The proposed speciation method gave very good analytical results by using together with the SPE method.

Deep Sea Environmental Analysis

GF-AAS of Pb, Cd and Sn, and hydride generation/AAS of As in deep sea sediments were investigated. The optimum analytical conditions in GF-AAS were established by making ashing and atomizing temperature curves. In the case of the determination of As by GF-AAS, Al in sediments interfered As signals when the contents of Al was over 3%. Accordingly hydride generation/AAS of As in the presence of Al was investigated. The established analytical method was applied to the analysis of the various deep sea sediments.

61 On-line Determination of Order Parameters in Alloys from Electron Diffraction by CCD Camera System and Its Application to Examination of Ordering Process

April 1993 to March 1995

T. Kimoto, First Research Group

Keywords: order parameter, on-line determination, cooled CCD camera, ordering process

Long-range order (LRO) parameter can be determined from the ratio of intensities of superlattice and fundamental spots, whereas short-range order (SRO) parameter can be determined from the intensity distribution of diffuse scattering. If we use conventional films to record electron diffraction pattern, it is impossible to determine the order parameters by measuring the electron diffraction spot intensities, because the detectable range of intensities (dynamic range) on films is very small (usually 10–100). By this reason, quantitative examinations of order parameters have been performed so far by using X-ray and/or neutron diffraction. However, the X-ray or neutron diffraction technique has a disadvantage that it takes a long time (1–3 weeks) to determine order parameters and that it is practically impossible to determine order parameters in a very small region (less than 0.01 mm).

One of the objectives of the present research is to develop the on-line system to determine precisely LRO and SRO parameters from electron diffraction by using the cooled CCD camera detection system attached to a transmission electron microscope (TEM). The system has been developed from April 1992 to March 1993. The dynamic range of the cooled CCD camera is between 40,000 and 64,000. The following steps are necessary in order to develop so-called "on-line order parameter determination system:"

1. To make a theory which determines order parameters from the electron diffraction pattern on the basis of the fundamental diffraction theory, considering in inelastic scattering effects,
2. To make a computer program based on the theory in item 1 in order to realize the on-line determination of order parameters,
3. To improve the system by comparing the order parameters obtained by the system with those obtained by the X-ray diffraction technique.

The other objective in the present research is to examine ordering process by using the developed

"on-line order parameter determination system." The following researches are planned:

1. To examine how order parameter varies with location by determining order parameter in several small regions,
2. To examine the effects of super-saturated vacancies, which are introduced by annealing at high temperatures and rapid quenching, on ordering process,
3. To examine the effects of specimen thickness on the ordering speed, which is important in a thin specimen for electron diffraction.

62 Characterization of Metals and Alloys using Synchrotron Radiation

April 1993 to March 1997

K. Ohno, 1st Research Team

Keywords: near-surface analysis, EXAFS, synchrotron radiation

Characterization of near-surface has been performed by X-ray reflectometry in air.

An X-ray diffractometer was improved to make an advanced X-ray reflectometer. A pair of channel-cut Ge(111) monochromator attached to the X-ray source of the reflectometer made highly monochromatic and parallel X-ray beam. The divergence of the beam from the monochromator was 16 arc seconds. The incident beam intensity on the sample after slit selection of CuKα_1 radiation was about 10^{10} cps. The coaxial location of sample and detector axes was precisely adjusted with a specially designed tool. The sample holder was also designed to make fine translations and rotations of the sample for accurate 2:1 alignment of the surface of the sample.

The refractive index for all materials to X-rays is slightly below unity. This means that there is a region at very low angles in which total external reflection of the X-rays are observed. The reflected X-ray intensities were measured by using the θ–2θ scanning mode. Reflected X-rays from the top surface of the film and the interface between the film and the substrate interfered constructively and destructively. The interference gave rise to the "Kiessig" fringes observed at angles above the critical angle for total reflection. The surface roughness of some samples was measured by X-ray reflectometry and Atomic Force Microscopy (AFM). The determined surface roughness was highly reliable because the agreement of the results obtained from both methods was excellent.

The intermediate products in mechanical alloying processes were identified by using a laboratory scale EXAFS equipment.

Related Papers

Grazing Incident X-ray Reflectance Measurement of Surface and Interface Roughness on the Sub-nanometer Scale, M. Wormington, K. Sakurai, D.K. Bowen, and B.K. Tanner, (to be published in Materials Research Society Symposium Proceedings, 1994).

Characterization of Surfaces and Buried Interfaces of Thin Films by X-ray Reflectometry, K. Ohno, T. Yokokawa, and T. Saito, (to be published in Adv. X-ray Anal. Jpn, 1995).

63 Development of Extremely High Field Magnets

April 1992 to March 1995

H. Maeda, High Magnetic Field Research Station

Keywords: 80 T class long-pulsed magnet, 40 T class hybrid magnet, 20 T class large-bore superconducting magnet, high resolution magnet

For the purpose of evaluation of the high-field properties of high-T_c oxide superconductors, we are developing several high-field facilities, such as an 80 T class long-pulsed magnet, a 40 T class hybrid magnet, a 20 T class large-bore superconducting magnet, and high resolution magnets. We are also constructing an automatic helium refrigerator/liquefier to cool down the large superconducting magnets. For installing these facilities a new building with a floor space of 7,159 m^2 has been constructed this year.

We are developing a new Cu-Ag alloys, which is very interesting conductor material for a high-field long-pulsed magnet because of its promising combination of high conductivity and high mechanical strength. A small pulsed coil, wound of a Cu-16at%Ag wire with interlayer reinforcement of glass fiber, could generate 73.4 T with a pulse-length of 5 msec in an inner winding diameter of 12 mm. This is the new world record generated by a non-destructive pulsed magnet having a pulse-length longer than 1 msec. Using the pulsed fields we measured J_c of several kinds of superconductors. The J_c values of multifilamentary superconductors measured in the pulsed fields coincide well with those measured in steady fields.

This year we succeeded in generating 21.2 T in a 50 mm clear cold-bore of the superconducting magnet, when the No. 3 coil wound of (Nb, Ti, Ta)$_3$Sn wire was used as the inner coil. Under back-up fields of this magnet several small single-pancake coils, wound of Bi-2212 oxide superconducting tapes, have been excited. We could generate a field of 21.5 T in a 13 mm clear cold-bore through this interesting combination, which is the highest field record obtained by a full superconducting magnet system.

The first test operation of the superconductive part (a room-temperature bore of 400 mm) in the 40 T class hybrid magnet system has been performed recently. It took about 140 hr to cool down the superconductive part of 9.42 ton from room temperature to 4.2 K by using a helium refrigerator

of 200 W. We could excite the magnet up to 14.01 T without quenching, where the operation current was 1384.5 A with a helium evaporating rate of 18.8 l/hr. Although the designed highest field of this magnet is 15 T, we stopped the higher-field operation, because the 14 T is the guaranteed value of the superconducting part. After installing, piping, and cabling of all the system, the full operation of the superconducting part will be performed just before the full-system test operation.

By using the high resolution magnets we have collaborated with several institutions such as universities, national institutes, and private companies in more than 10 studies. The main themes of the collaborations are "Electronic structure in Cu of oxide superconductor measured by NMR," "Metamagnetic phase transition of heavy fermion compound, $CeRu_2Si_2$," Electronic structure of organic superconductor $(BEDT\text{-}TTF)_2MHg(SCN)_4$ (M = K, Rb, NH_4, Tl)," "Fermi surface of $CdCl_2$ graphite intercalation," "NMR measurement on catalyzer and grass," "Giant magnet resistance effect of metallic superlattice," and so on.

Related Papers

High Field Facilities under Development and Construction at the National Research Institute for Metals, Japan, K. Inoue, T. Asano, T. Kiyoshi, Y. Sakai, T. Takeuchi, K. Itoh, and H. Maeda, Physica, B 177 (1992): 7–15.

Present Status of High-Field Research Center under Construction in the National Research Institute for Metals, Japan, K. Inoue, T. Kiyoshi, T. Asano, Y. Sakai, T. Takeuchi, K. Itoh, M. Oshikiri, and H. Maeda, Advances in Cryogenic Engineering, 39 (1994): 419.

64 Fundamental Study on Plasma Diagnostics in Free-burning Mixed Gas Arcs

April 1993 to March 1994

K. Hiraoka, Advanced Materials Processing Division

Keywords: spectroscopy, argon, hydrogen, electron density, stark broadening

This research aims at developing the *in situ* spectroscopic measurement system and clarifying some basic plasma parameters (plasma gas temperature, plasma gas composition and electron density) in argon-hydrogen mixed gas tungsten arcs which have been utilized in the thermal plasma processing. A light spectroscopic analysis, developed under the assumption of the existence of the local thermal equilibrium (LTE) in the previous research, can be applied to the mixed gas arc plasma at more than 15,000 K where both of the exited argon line and the ionized line intensities can be measured (as shown in 93's topics in NRIM Research Activities). However, as introducing the hydrogen gas into the argon gas arc, it was difficult to measure the ionized argon line intensity except for the region near the cathode tip where the absence of the LTE had been proposed. Therefore, a new spectroscopic analysis was developed to estimate plasma parameters in the wide region from the cathode to the anode with the relative intensities of the exited argon (Ar I) and the exited hydrogen ($H\alpha$) line spectra which can be measured at the plasma above 10,000 K.

The results estimated by this new measurements led to the conclusions that the hydrogen gas concentrated at the arc center and that the plasma gas temperature at the arc center clearly decreased. Furthermore, the electron density profiles were estimated from the stark broadening of the exited hydrogen line spectrum $H\beta$. These results showed the agreement with the electron density profiles that were calculated from local plasma gas composition and temperature mentioned above. From the results, it was concluded that the new spectroscopic analysis was effective to estimate plasma parameters at the wider region of the argon-hydrogen mixed gas arc plasmas above 10,000 K.

Related Paper

Demixing in Argon-Helium Mixed Gas Tungsten Welding Arcs, K. Hiraoka, ISPC-11 Proc., Loughborough (U.K.), 1 (1993): 440.

65 Advanced Techniques for Physical Analysis of Metals

April 1991 to March 1994

R. Tamura, Materials Characterization Division

Keywords: XRD, HRTEM, EPMA, SEM

This work was carried out to develop new techniques for the physical analysis of metals by using an X-ray diffraction (XRD) facility, high resolution transmission electron microscope (HRTEM), electron probe microanalyzer (EPMA), and scanning electron microscope (SEM) for the purposes of advanced materials research. The results obtained so far are as follows:

XRD

In this study the X-ray diffraction method was improved and the new method was introduced to determine the site occupancy of the third elements by extending the method determining a long range order parameter in binary alloy systems. This newly developed method has been applied successfully to the study of Ti-Al compounds.

HRTEM

The structural analysis of lattice images obtained with HRTEM were investigated at the interface between metal and ceramic.

EPMA

In EPMA, we developed a new microcomputer system, by which speedy data acquisition and image processing can be carried out. This newly developed system has been applied successfully to the quantitative analysis of a very small amount of Ga in mining minerals.

SEM

It was clearly shown that the images overlapped secondary electron image and back scattered electron one are useful to identify the surface compositions of alloy powder. We are going to adopt ECP method for SEM to analyze a fine crystal structure.

[66] Sensitive Instrumental-Analysis by Direct Methods and Separation Methods of Metallic Materials

April 1991 to March 1994

R. Hasegawa, Materials Characterization Division

Keywords: inert gas fusion, GD-MS, GF-AAS, ICP-AES, separation

Aiming at the development of fundamental techniques for sensitive instrumental analyses of metals, alloys and related materials, studies on the following three items including direct methods and separation methods have been carried out. Main results obtained for each item are as follows.

Study on Direct Analysis of Solid Samples

1. Determination procedure of trace oxygen and nitrogen (ppm level) in iron and steels has been established by impulse heating-inert gas fusion method using a graphite capsule.
2. In order to apply glow discharge mass spectrometry (GD-MS) to the analyses of steels and titanium alloys, evaluated were the relative sensitive factors which could cover a wide concentration range from the determination of alloying elements to that of trace impurities.

Study on Direct Analysis of Liquid Samples

1. Analytical procedures to determine trace impurities in steels and refractory metals by graphite furnace atomic absorption spectrometry (GF-AAS) have been established; the procedures comprise ashing in hydrogen stream, platform atomization and background correction and optimum analytical conditions depend on the thermochemical properties of the analyte.
2. End-on and side-on observation of inductively coupled plasma (ICP) using electrothermal vaporization and time-resolved measurement were compared in the determination of refractory metallic impurities in a high purity iron sample and it was clarified that "end-on" is two-order sensitive than "side-on" observation.

Study on Separation Analysis of Liquid Samples

1. Simultaneous determination procedures of trace impurities in $MoSi_2$, Cr, $CrSi_2$, Ni, NiO and high purity iron samples were established by means of separation analysis followed by ICP atomic emission spectrometry (ICP-AES). Coprecipitation and ion exchange reactions were utilized to separate analytes from the large amount of matrix element which hinder sensitive analysis.
2. Fluoride separation-molybdosilicic acid blue spectrophotometry has been studied and the determination procedures of trace silicon in high purity iron and nickel samples were proposed.

[67] Database System for R&D of Superconducting Materials

April 1989 to March 1994

S. Nishijima, Failure Physics Division

Keywords: superconducting materials, high-T_c oxides, factual database, premier data

As one of the coordinated research programs of the Science and Technology Agency (STA), this research project aimed at the development of factual database systems on the high-T_c superconducting materials that would assist researchers with more ordered information. More than 30 research groups came together to share the work in industry, university and government laboratories. NRIM took part in the development of databases and acted as secretariat for the coordination of individual researches.

In the first three-year term ending at March 1992, the group work was rather oriented to improve the reproducibility of samples for common use, and to establish common practices for property evaluation, by replicated measurements of the common samples at the member laboratories. The second two-year term was used to enrich the core data in the system. This was made by the shared measurements of properties on common samples, as well as to develop application software for use and further development of the database systems.

The following is the main outcome of the database development work at NRIM. There are two types of data systems that are complementary to each other: one is based on the numerical data extracted from open literature and the other on the experimental raw data from the shared measurements of common samples. The former is a pilot database covering most properties that many people will be interested in. The latter can be used by researchers to evaluate samples, verify theories, check hyphothesis, and re-analyze the data at any time.

SUPERCON—A Property Database from Literature

Y. Asada, one of the co-workers of the author and originally the proposer of the present STA project, had been working on a model database, named SUPERCON, on the properties of oxide

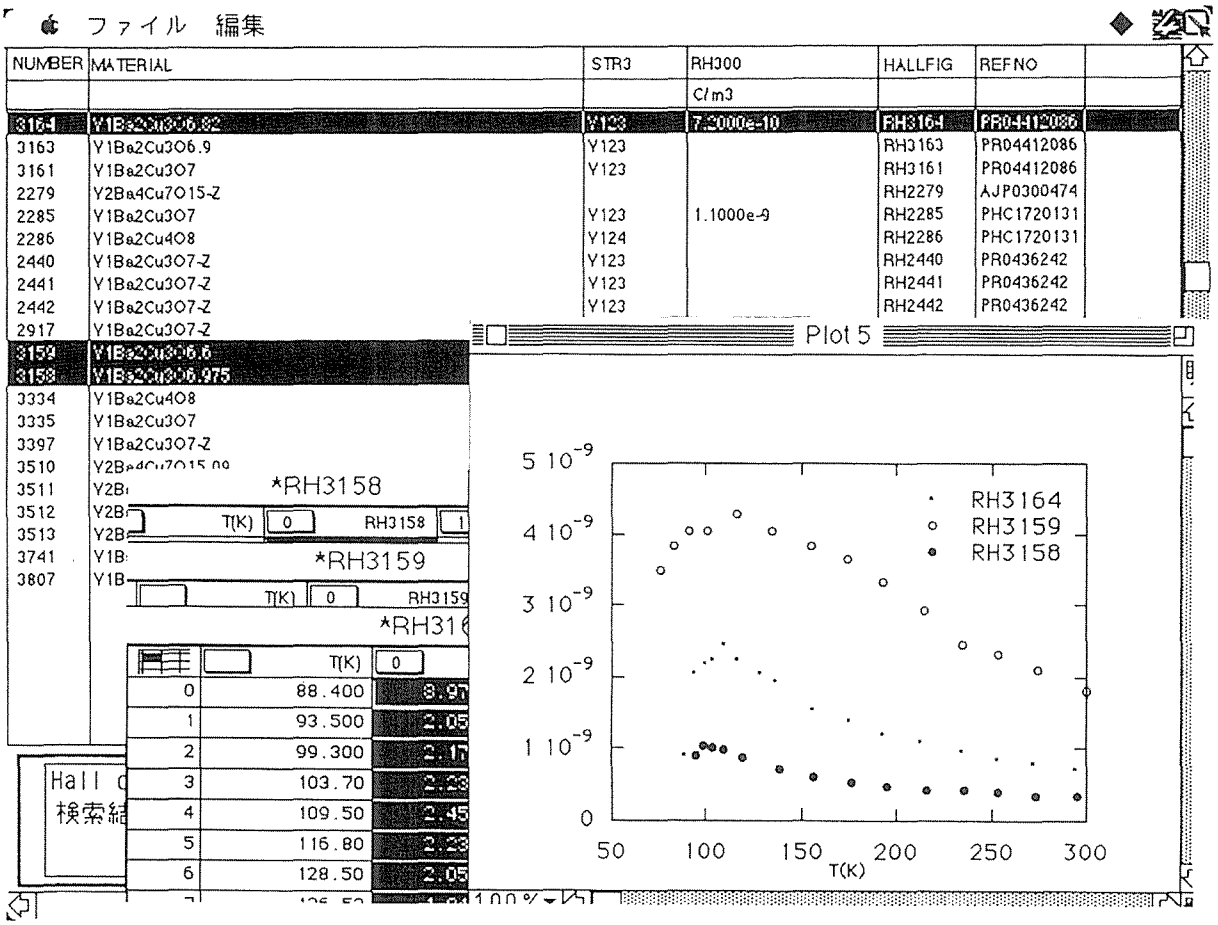

Fig. 4 Data retrieval and graph editing by SUPERCON: Hall coefficient of $YBa_2Cu_3O_7$ for 3 samples.

superconducting materials by collecting data from open literature. Although it was small and designed for personal use, his database was considered to be a good starting point for the cooperative project and worth for further development at NRIM.

It contains today a variety of numerical data on physical, chemical and structural properties about some 5000 different samples. All the data have been extracted from domestic and international journals in a traceable manner, so that eventual change of metadata can be reflected at future revision of that database.

The properties in SUPERCON system are categorized by 12 fields including: material description, crystalline structure, super and normal conducting properties, as well as properties for thermal, magnetic, mechanical, irradiation, corrosion, etc. It registers also the processes for data deduction that can be different by the authors.

Figure 4 demonstrates a working screen for data retrieval and graphs drawing. It shows temperature dependence of Hall coefficient for different samples of $YBa_2Cu_3O_7$ superconductor. The user can analyze those data selecting different deduction processes, if necessary, to find most appropriate values. It is also easy to check the quality and reliability of data and to seek for unknown factors that might affect those data.

Management System for Premier Data

The second database system is in principle consisting of the experimental raw data that are obtained from shared measurements of common samples in the STA project. It provides researchers with non-processed primary data, called premier data, that should contain maximum of hidden and non discovered information. Primary records are collected from member laboratories usually on floppy disks. A package of common format is used for easy storage and transfer of data.

Materials used for generation of core data includes: bulk polycrystals of $YBa_2Cu_3O_z$ with z = 6.9, 6.6, 6.4, single crystals of $YBa_2Cu_3O_7$, $Pr_{1.85}Ce_{0.15}CuO_4$, $Nd_{1.85}Ce_{0.15}CuO_4$, $Bi_2Sr_2CaCu_2O_8$, and $La_{2-x}Sr_xCuO_4$ with x = 0, 0.14, 0.15, 0.16, thin films of $RBa_2Cu_3O_7$ and $EuBa_2CuO_7$, thick films of $Bi_2Sr_2CaCu_2O_8$ and $Bi_2Sr_2Ca_2Cu_3O_{10}$, and Ag-sheathed tapes of $YBa_2Cu_3O_7$ and $Bi_2Sr_2Ca_2Cu_3O_{10}$.

The system has unique capabilities of describing and handling the premier data in the computer, in one hand, and treating, analyzing and evaluating them, on the other. Records are sometimes accompanied by complementary sub-items for adding value as, for example, the material name by its grouping criteria for easier inference, and the testing method by its procedure and accuracy for correct understanding. Fabrication processes and internal structures are recorded to allow interpretations between them and with other properties.

The system has already proved a full possibility of manipulating the variety of premier data to seek for the hints for materials research and development.

Related Papers

Numerical Database for High-T_c Oxide Superconductors, Y. Asada, Cryogenic Engineering, 28-6 (1993): 298–303 (in Japanese).

Database System Used for Research and Development of New Superconductors, K. Hoshimoto, T. Yokokawa, E. Nakada, and S. Iwata, Materiaux & Techniques, 80 No. 11–12 (1992): 27–29.

[68] Sensing and Analysis of Materials Damage Formation Process

April 1991 to March 1994

N. Shinya, Failure Physics Division

Keywords: damage monitoring system, piezoelectric polymer, electron Moiré method

In this work, a damage monitoring system and an advanced analytic technique have been developed. The main results are as follows.

1. Local strain sensing methods have been developed for damage detection in structural materials. As a strain sensor, piezoelectric polymers were coated on the surface of aluminum sheets. Local strains in the aluminum sheets were measured by an operational amplifier circuit with a scanning probe, and also observed using a scanning electron microscope as the image of voltage contrast. The experimental results demonstrate that these methods using piezoelectric polymers are sensitive and useful for the detection, measurement and monitoring of the local strain in structural materials.
2. An advanced Moiré method for the measurement of high temperature deformation, which uses electron beam lithography and scanning exposure of electron beam, has been developed. Micro-gratings are produced on the specimen's surface using electron beam lithography, and micro Moiré fringes (electron Moiré fringes) are caused by different amount of the secondary electrons when the primary electron beam is exposed to the micro-gratings. This new Moiré method makes them possible to observe the scanning electron microscope image and the electron Moiré fringes at the same time, to obtain clear Moiré fringes without any image processing system, and to determine the highly localized deformation at elevated temperature. Using this method, the micro-creep deformation such as grain boundary sliding, coarse slip and localized strain in pure copper specimens has been measured.

[69] Quantitative Nondestructive Evaluation Techniques for Composite Materials

April 1991 to March 1994

C. Masuda, Failure Physics Division

Keywords: nondestructive evaluation, frequency response, acoustic microscopy, laser-ultrasonics, composite materials, computer simulation

In this research, it was planned to develop nondestructive evaluation systems based on ultrasonic techniques to improve the reliability of newly developed structural materials including composites. The research was sponsored by STA and supported by members of various institutions, universities and companies. The following four sub-themes were carried out at NRIM.

Ultrasonic Measurement of Highly Attenuating Materials

A new improvement is achieved on the technique of the ultrasonic frequency response analysis that was developed in this research. It is used for quantitative measurement of microstructural properties such as grain size and density of inclusions. Theoretical analysis is made on the influencing factors, including surface roughness of specimens, thickness of ultrasonic couplant, ultrasonic wave forms and sound fields upon frequency response characteristics. It makes clear that the microstructural change can be identified precisely as the variation in the frequency response for highly attenuative materials.

Measurement Using Acoustic Microscopy

Microscopic elastic-properties of various advanced materials are investigated using a microscopic ultrasonic system. It is based on the measurement of Rayleigh wave velocities obtained from V-Z curve by scanning acoustic microscopic (SAM). The velocity change is investigated for samples with different thickness of titanium coating on sapphire substrate. It shows that the velocity decreases with increase of coating thickness. Similar analysis using a line-focus lens of SAM, reveals anisotropic property in a composite material of aluminum matrix with SiC whiskers. The bulk elastic property of the composite can be simulated as hexagonal presumably depending on its rotation-symmetric structure around whiskers.

Laser-Ultrasonics

Ultrasonic imaging system is under progress using laser-ultrasonic techniques. It succeeded the imaging of sub-surface small artificial defects using non-contact ultrasonic transmission and detection techniques. For the detection, an optical heterodyne interferometry system is used to simultaneous detection of longitudinal and shear vibrations. For the transmission, pulsed laser light is applied the sample surface through an optical fiber with large core diameter. Laser beam scanner

also employed for imaging, instead of x-y scanning of specimens. The resolution power is limited by frequency bandwidth of the detection that is 50 MHz in the present work, and is about 0.1–0.3 mm for defects just below surface of specimen.

Flaw Evaluation in Heterogeneous and Anisotropic Materials

Ultrasonic properties of carbon fiber reinforced plastic (CFRP) is analyzed using new 3-dimensional ultrasonic simulation technique that was developed in this research. The visualization of ultrasound in CFRP is first attained for unidirectional fiber arrangements. Promising results are obtained to simulate the ultrasonic behavior of composites having hexagonal and cubic properties. It is believed that the present analysis method is enough capable for the analysis of microscopic and macroscopic properties of materials.

This work will advance from the development stage of elemental techniques to the practical stage for evaluation of advanced materials during next 2 years term. It is intended to build an evaluation system for advanced materials, especially for metal matrix composites.

[70] Quantitative Evaluation of Fracture on Materials for Casks

April 1992 to March 1994
T. Yasunaka, Environmental Performance Division
Keywords: fracture toughness, low temperature embrittlement, carbon steel, ferritic nodular cast iron

Shipping containers for radioactive materials must maintain structural integrity even when subjected accident of impact loading at low ambient temperature. In ferritic steels, low temperature embrittlement occurs. Evaluation of materials against brittle fracture, therefore, is necessary.

The objective of this study is to characterize the behavior of dynamic fracture toughness of a carbon steel and a ferritic nodular cast iron and to develop the precise evaluation method for these materials.

In the transition region, the fracture toughness values of the carbon steel scattered largely, while those of the cast iron had a small amount of scatter. In the CT specimens of the cast iron, the occurrence of pop-in cracks preceded unstable fracture. This phenomenon leads to the conclusion that large scatter of fracture toughness values is attributed to the difference in the process of crack propagation.

Furthermore, an evaluation method of the cast iron by small bend specimens was proposed and the dependence of transition temperature on loading rates was discussed.

Related Papers

Dynamic Fracture Toughness and Evaluation of Fracture in a Ferritic Nodular Cast Iron for Casks, T. Yasunaka and K. Nakano, Proc. 10th Int. Sympo. on Packaging and Transportation of Radioactive Materials, (1992): L1304–10.

Dynamic Fracture Toughness and Evaluation of a Thick-walled Ferritic Spheroidal Graphite Iron, K. Nakano and T. Yasunaka, Tetsu-to-Hagane, 80 (1994): L330–35 (in Japanese).

Simulation and theory

(71) Establishment of Multidimensional Evaluation of Human Senses for Materials Design

April 1994 to March 1997
Y. Kurihara, Materials Design Division
Keywords: human senses, sensory test, multidimensional scaling method, materials design

The materials evaluation has been done up to now in respect of materials properties such as mechanical, chemical and physical properties. Recently, however, there are increasing demands for the material development and improvement from new aspects such as environment consciousness, amenity, and so on. When we investigate such new needs, most of information are provided mainly by language and human senses. However, generally speaking, the relationships among language information, the evaluation by human senses, and materials properties are not elucidated enough. Thus, the target of this study is to construct a quantitative evaluation method for the above relationships.

First, sensory information on materials will be collected by sensory test and Semantic Differential method. Second, characteristic vectors will be extracted from sensory information by multivariate statistical analysis. The relationship between these characteristic vectors and materials properties is examined by regression analysis to incorporate sensory information into materials design.

(72) Thermodynamic Analysis of Transition Process from Metastable to Stable Phases

April 1994 to March 1997
H. Onodera, Materials Design Division
Keywords: metastable phase, thermodynamic analysis, nucleation rate, T-T-T diagram, CVD, fluidized bed

Rapid solidification, mechanical alloying, sputtering and other non-equilibrium processing techniques have been employed during past few years to improve mechanical properties of various materials by refining the microstructure and reducing the extent of deleterious segregation during solidification. These techniques produce metastable phases such as supersaturated solid solutions,

crystalline intermediate phases and amorphous phase. For the effective utilization of these metastable phases to improve mechanical properties of materials, it is necessary to reveal the transition process from metastable to stable phases on the heat treatment. The target of this study is to construct a kinetic model which can describe the transition processes quantitatively.

In this study three subjects are stressed. First, the crystallization process of sputter deposited amorphous alloys is examined by electrical resistivity measurements, X-ray diffraction and transmission electron microscopy. In the preliminary study, we have found the formation of metastable α phase in preference to the stable γ phase in the crystallization process of amorphous TiAl alloys[1]. As the next step, high resolution electron microscope and atom-probe field ion microscope will be also used to analyze an initial stage of nucleation process. Kinetic analysis in terms of relative nucleation rate will be performed for the nucleation process. Secondly, theoretical derivations of time-temperature-transformation diagrams for multicomponent titanium alloys are aimed on the basis of the nucleation and growth theory. Third, a microstructural evolution in sintering of HfC coated tungsten powders, which are produced by CVD technique in fluidized bed, will be analyzed in terms of process conditions such as time, temperature and partial pressure of oxygen.

Related Paper

Crystallization of Sputter Deposited Amorphous Ti-52at%Al, T. Abe, S. Akiyama, and H. Onodera, ISIJ Int., 34 (1994): 429–34.

(73) Development of Data Modeling Method for Materials Strength Properties

April 1994 to March 1998

M. Nihei, 4th Research Team

Keywords: computational science, data modeling, prediction of strengths

The computational science is recently used for wide area of the materials science. We are planning to apply this computational science to the prediction of several materials strengths properties, by considering the mathematical/physical models for the strength properties with the combination to empirical understanding obtained through the advanced-integrated evaluation system named as DIMS with the factual database developed in the recent study, which works under a UNIX operating environment with the X-Windows system on LAN (Local Area Network) and has the evaluation function to analyze the desired data set extracted from the database and to find the combinations among characterized items of materials and that strengths properties. We are trying firstly to develop the new modeling technique for predicting the static strengths such as the tensile strength by considering the actual materials as the assembles of the small binding elements, whose sizes are much less than the grain size of the material and properties are calculated from that based on the dislocation theory, and by assuming that the calculated properties of whole elements are corresponding to that of actual materials. We are also trying to develop the knowledge base system to analyze the effect of the structures of materials by modeling that structure as an appropriate mathematical equation and are planning to predict the time-depend properties such as the creep strength by the combination of that knowledge base and computer calculation.

74 Study on the Trend of Application of New Superconductors

April 1988 to March 1995

K. Hoshimoto, Materials Design Division

The development of High T_c Superconductors will give revolutional influences on the fields not only of science but the economy or social affairs. The investigators of the new superconductors should recognize this fact. From this point of view, studies have been started on the trend of application of new superconductors, which include the investigation on the possibilities of application of new superconductors to the industries of energy and also to the future technology.

[75] Computational Approach to the Mechanics of Heterogeneous and/or Anisotropic Microstructures in Advanced Materials

April 1993 to March 1994

Y. Nakasone, 2nd Research Group*

Keywords: computational mechanics, micromechanics, heterogeneity

The present study proposes a new theoretical model of fatigue crack initiation in metallic materials. The extrusion can be often found in fatigued metallic materials and hence is regarded as one of the possible crack-initiation sites. The extrusion is a type of heterogeneity which causes local energy enhancement to bring about a crack or cracks in a metallic material. In the present theory, the heterogeneity is modeled by a dislocation dipole and analyzed theoretically by the use of the theory of continuously distributed dislocations.

The resultant governing equation was found a singular integral equation of the first kind with a generalized Cauchy kernel and a bounded Fredholm type kernel. The equation can not be solved theoretically, so that a computational method has been adopted using Erdogan's procedure. It was

*Present address: Science University of Tokyo

found that the crack initiation life N_f can be theoretically derived as a critical stress cycle number at which the Gibbs free energy reaches a maximum and where the system of interest becomes unstable. Furthermore, the present theory provides a theoretical interpretation of the fatigue limit as well as that of the microscopic type I crack. The theory can also derive the dependence of the fatigue limit on the yield strength and that of the fatigue strength on the grain size of a material considered.

Related Papers

Free Energy Formulation of Fatigue Crack Initiation along Persistent Slip Bands: Calculation of S-N Curves and Crack Depths, G. Venkataraman, Y.W. Chung, Y. Nakasone, and T. Mura, Acta Metall. Mater., 38 (1990): 31–40.

A Theory of Fatigue Crack Initiation in Solids, T. Mura and Y. Nakasone, Trans. ASME: J. Appl. Mech., 57 (1990): 1–6.

76 Development of Material-design-technique for Mechano-chemical Attack on Light-weight Heat-resistant Materials

April 1989 to March 1994

I. Tomizuka, Physical Properties Division

Keywords: material design, mechanochemical attack, light-weight heat-resistant material, intermetallic compound, C/C-composite material, oxide-dispersion strengthened superalloy

Mechano-chemical Attack on Intermetallic Materials

High temperature fatigue characteristics were observed in an oxidizing atmosphere on the heat-treated materials prepared from a Ni_3Al-based alloy. Obtained results were discussed with reference to their structure and hardness.

Electrochemical characteristics were observed for TiAl-based alloys in 5N-sulfuric acid. Their electrochemical behavior under anodic potentials was found to be extensively affected by the cathodic pretreatment performed for elimination of surface film.

Mechano-chemical Attack on C/C-composite Materials

This subject was performed with an intent of describing oxidation behavior of C/C-composite materials by a formula appropriate for material design technique. This attempt was successfully accomplished by our research based on the results obtained by oxidizing C/C-composite materials in a thermobalance. Oxidation behavior of a C/C-composite material was not found to be assessed from what was observed when the fiber and the matrix were oxidized separately. Oxidation behavior of various C/C-composite materials was observed under thermomicroscopes.

Mechano-chemical Attack on Light-weight Super-heat-resistant ODS-alloys

Investigations were carried out on effect on mechanical properties of nickel-based ODS-alloys of such minor alloying elements as carbon, and of gamma-prime phase content. Another investigation was carried out on effect of various dispersed oxides in an Fe-Cr alloy on its tensile deformation behavior.

Observation was performed on effect of dispersed yttria on hot-corrosion and high temperature oxidation behavior of a nickel-base alloy. Its addition was detrimental to both of them, presumably because the oxide hindered growth of nickel grains in the alloy.

77 Self-organizing Information-base System Used for Creative Research and Development

April 1992 to March 1994

K. Hoshimoto, Materials Design Division

Keywords: self-organizing, information-base, materials design, dictionary, knowledge converter

In the domain of metals and alloys one can never find any two species that have precisely identical internal structure even if the chemical composition and outer shape are the same; which means that one can not specify the object exactly in the database of materials properties. Therefore the specification of materials has inevitably somewhat ambiguity. Specialists create new materials by combining basic theories, factual data and qualitative knowledge with their full skill and experiences, while the information on materials today is increasing day by day beyond the quantity which one person can deal with. The objective of the present study is to develop a self-organizing information-base system for materials design. To realize the system, the investigation on fundamental procedures has been made to select and organize various types of information automatically with the aid of computer for producing new materials. Because the knowledge on materials being fuzzy ones, the information which the system can offer contains fuzziness inevitably to some extent. For this reason, a knowledge retrieval system has been constructed in the preceding study, by which the knowledge included in relative research articles are collected and stored in the computer, and in the response to the queries by user in his natural language (Japanese in this case) the system retrieves and shows the related knowledge to the user. Information on the data sources and experimental procedures are also stored together with the experimental results and conclusions.

The system to be accomplished in the study will treat collectively the fundamental knowledge on materials and the actual data of materials properties along with the above mentioned information.

In the first three years of the study, two tools for gathering information into the computer has been developed; the first one searches for new words from the text fed into the computer by using OCR and put them automatically in the internal dictionary. It also assists to construct a thesaurus in consultation with the user. The other one is a knowledge converter by which a text cut out from a document is transformed to a knowledge treatable by the computer.

On the basis of collected information, a prototype conversational system has been designed and realized to retrieve the information from the knowledge base by using natural English languages.

Related Paper

Development of a Knowledge Base System for Computer-Assisted Alloy Design, K. Hoshimoto, submitted to IUMRS-ICAM, August 31–September 4, 1993, Tokyo.

[78] Computer Aided Design Tools for the Development of Materials

April 1991 to March 1994

K. Hoshimoto, Materials Design Division

Keywords: computer aided development of materials, sensory test, micrographic data, materials database, knowledge on materials, materials design

The objective of the study is to extend the fundamental tools used for the computer aided development of materials. To develop an expert system of materials design and selection by using computer, it is necessary to obtain the quantitative correlation between microstructure and mechanical properties. Sensory tests followed by the analysis using a multi-dimensional scaling method have been adopted for the investigation of the relationship between the micrographic data of structure and various properties in a Ti-6Al-4V alloy. It has been concluded that specialists in the field of materials science evaluate the mechanical properties mainly from three kinds of extracted characteristics of geometry, anisotropy and size in a variety of microstructures. Moreover, good correlation was observed between the extracted characteristics of microstructures and mechanical properties.

A consultation system for the non-specialists with respect to the titanium alloy has been developed on the basis of the above mentioned analysis.

Related Paper

Characterization of Image data by Sensory Test, K. Kaneko, Y. Kurihara, K. Hoshimoto, M. Yamazaki, and M. Fujita, *Computer Aided Innovation of New Materials II*, (edited by M. Doyama et al.), Proc. of CAMSE '92, Yokohama, Sept. 22–25, 1992, 1501–04.

[79] Basic Research to Establish Design Techniques for Advanced Materials

April 1989 to March 1994

T. Yamagata, Materials Design Division

Keywords: intelligent computer program, parallel-beam X-ray diffractometry, lattice misfit, field ion microscope/atom prove

Establishment of structure design and property design sub-systems are carried out for each material, such as Ni-base superalloy, Titanium alloy and C/C-composite material. Establishment of alloy design expert system is carried out with alloy design program of Nickel-base superalloys. For expert system, intelligent computer program was developed. When the fundamental data such as chemical composition of γ and γ' phases analyzed by EPMA are added to old data. The equation of γ' surface, solubility index and mechanical property are modified by the intelligent program, and the accuracy and the reliability of alloy design program itself automatically are improved. In order to optimize prediction equation objectively, akaike information criterion was introduced in this system. High temperature creep rupture strength of Nickel-base single crystal superalloys is strongly dependent on lattice misfit, so that method for precise measurement of lattice misfit was developed using high temperature parallel-beam X-ray difractometory which was equipped with vertical scanning Ge(111) channel cut monochromatic beam monitor and using profile fitting method with a pseudo-Voigt function for resolution of overlapping pearks.

In collaboration research with University of Cambridge, the atomic structure of Nickel-base single crystal superalloy has been analyzed using a field ion microscope/atom-probe equipped with a reflection time-of flight mass spectrometer. The equilibrium pertaining coefficient defined as the ratio of the solute concentration in the γ' phase to that in the γ phase has been found to be 0.22, 0.27, 2.3 and 3.3 for Cr, Mo, Al, and Ta, respectively, in good agreement with our theoretical estimates. Ladder diagrams generated by progressively stripping the {200} planes of γ' revealed detail information about the position of solute atoms in the crystal structure. These data were found to compare well against estimates made using cluster variation calculation.

Related Papers

Towards an Intelligent Computer Program for the Design of Nickel-base Superalloys, T. Yokokawa, K. Ohno, H. Harada, S. Nakazawa, T. Yamagata, and M. Yamazaki, Proc. Fifth Inter. Conf. on Creep and Fracture of Engineering Materials and Structures, Swansea, U.K., March (1993): 245–54.

Atom-probe Microanalysis of a Nickel-base Single Crystal Superalloy, H. Harada, A. Ishida, Y. Murakami, H.K.D.H. Bhadeshia, and M. Yamazaki, Applied Surface Science, 67 (1993): 299–304.

Collaboration Research

Atom Arrangement Design and Control (Univ. of Cambridge, U.K.)

Computer Modeling of Alloys (Rolls-Royce plc, U.K.)

Single Crystal Superalloys for Future (IHI, JAPAN)

[80] Evaluation and Life Prediction of Material Strengths by "DIMS" System

April 1993 to March 1994

N. Nagata, 5th Research Group

Keywords: material strength, database, life prediction

The purpose of this research is to grade up the integrated database management system, "DIMS" (Dialogical Integrated system for Material Strength database) developed in the previous research titled "Development of knowledge based system for material life prediction" in which an integrated system for prediction of material strengths by combining the factual database on creep, fatigue and corrosion has been developed.

As research activities related to corrosion aspects in this year, a machine readable database associated with stress corrosion cracking of stainless steel was constructed by using related literature data. Based on the database, a new method for unified evaluation of SCC data of sensitized stainless steel obtained by different testing methods such as SSRT and U-bend tests was newly developed. SCC damages were analyzed by checking the correlation with several affected parameters. As a result, the upper boundary of an SCC fracture map can be predicted in terms of specific parameters such as DO concentration and pH.

In the fatigue aspects, a new method for predicting fatigue life by combining low cycle fatigue behavior, cyclic stress-strain behavior and fatigue crack growth behavior was developed. Based on this method, fatigue lives of ferritic steels can be predicted within the factor of 3 in precision in a wide range of temperature from room temperature to 873 K.

In the creep aspects, a new dialogical-type program was developed for prediction of creep rupture strength. By using this program, long time creep rupture strengths can be predicted in terms of a few parameter such as tensile strength, chemical compositions and so on.

Materials

Non-ferrous materials

(81) Relationships between Fatigue Softening/Hardening Behavior and TEM Structure of Titanium Alloys

April 1994 to March 1997

T. Kainuma, Mechanical Properties Division

Keywords: Ti-3-8-6-4-4, pure titanium, TEM structure, fatigue softening, fatigue hardening

The change of the width or area of the hysteresis loop during the fatigue testing of materials at constant stress amplitude is taken usually as a measure of dynamical changes in mechanical properties. By the testing at stress amplitudes higher than yield stress, fatigue hardening only takes place in alloys as well as pure metals (decrease in the width of hysteresis loop). While at stress amplitudes lower than the yield stress, fatigue softening occurs. Details of fatigue softening behavior have been reported for the materials such as aluminum, copper, silver and iron.

The aim of this work is to reveal the mechanisms of fatigue softening and hardening behavior of titanium alloys in connection with the characteristics of crystal structures, using transmission electron microscope (TEM).

Fatigue Softening and Hardening Behavior

We determined at first the specimen shape most suitable for tension-compression fatigue testing, then examined the crystal structure dependence of fatigue softening and hardening behavior using Ti-3Al-8V-6Cr-4Mo-4Zr (β-type titanium alloy, Ti-3-8-6-4-4) and pure titanium (α-type). The experiments for the fatigue softening and hardening phenomena were carried out on work-hardened and annealed materials, respectively.

Relation between Fatigue Behavior and Electron Microscopic Structure

We have shown previously that hydrogen absorption and subsequent formation of dislocation structures (ghost structure) occur in the beta-type titanium alloy during the specimen preparations, such as cold rolling, emery paper polishing, diamond blade cutting and water quenching.

In this work, we have established the preparation method for thin foils which are without ghost structures by the TEM observation; for example, the specimen cutting and mechanical polishing were performed either in argon gas atmosphere or in vacuum. The thin foils were prepared from the

fatigue-tested bulk specimens by cutting, mechanical polishing and jet-electropolishing. The TEM observation has been aimed to reveal the mechanisms of fatigue softening and hardening in titanium alloys.

82 Disintegration Phenomena in Intermetallic Compounds

April 1992 to March 1995
K. Kawahara, Physical Properties Division
Keywords: manganese intermetallic compound, disintegration, pulverization

We are engaged in an application and elucidation of natural disintegration phenomena occurring in some intermetallics. Other than MnAl-C intermetallics, the phenomena have been found in MeAl-C systems as well, where Me consists of carbide-forming elements, such as titanium, tantalum, nickel, hafnium, iron, cobalt, and chromium. Though silicon is the same kinds of elements its addition did not bring about any collapse. However, it has not been observed when Me was composed of non carbide-forming elements, such as zinc, tin, germanium, copper, and silver. These results suggest that the disintegration will be related closely to the coexisting of another carbides in addition to the aluminum carbide. It may be interesting to note why two kinds of carbides would be necessary to collapse. Although the hardness of the intermetallics will be considered to govern the disintegration, the phenomena occurred in soft NiAl-C systems with Hv140, whereas they did not in hard CrAl-C systems with Hv775. For MnAl-C systems, additional elements of iron and/or copper showed a tendency to depress the phenomena, implying that there will be a complex correlation with the hardness.

[83] Microstructural Refinement and Mechanical Properties of Titanium Alloys

April 1991 to March 1994
T. Kainuma, Mechanical Properties Division
Keywords: Ti-3-8-6-4-4, mechanical properties, microstructural refinement, hydrogen absorbing

Metastable beta-type titanium alloys recently have drawn attention because of their excellent formability. In the alloys, however, rapid grain growth tends easily to occurs when they are annealed at temperatures above the beta transition temperature Tβ. So then, a metastable beta-type alloy with a composition of Ti-3Al-8V-6Cr-4Mo-4Zr (Ti-3-8-6-4-4), being resistant to grain growth even at temperatures above Tβ, was developed for the applications requiring cold formability and high strength.

The aim of this work is to reveal the mechanisms of microstructural refinement of the Ti-3-8-6-4-4 alloy in grain size, substructure and alpha phase precipitation by thermomechanical treatment and hydrogen absorbing treatment. The mechanical properties of the alloy with the refined microstructures have also been evaluated.

Microstructural Refinement and Mechanical Properties

The grain size refinement for Ti-3-8-6-4-4 alloy was mainly achieved by heavy cold-rolling and following short time recrystallization treatment. An addition of a few percent of silicon to the alloy improved significantly the grain size refinement by suppressing grain growth, and enhanced age-hardening as well. A variety of substructural refinement of the alloy was achievable by different combinations of annealing condition and reduction ratio of cold-rolling. A relationship between the grain size refinement and the morphology of alpha phase precipitate was found and determined.

Microstructural Refinement by Hydrogenation

We have shown previously that penetration and consequent formation of dislocation structures, occur in the beta-type titanium alloys during the specimen preparations, such as cold rolling, emery paper polishing, diamond blade cutting and water quenching.

In this work, we have tried to understand the absorption mechanism of hydrogen by changing the composition of atmosphere. Besides, the dislocation structures have been examined for the Ti-3-8-6-4-4 alloy charged with hydrogen. It was shown that the high density of dislocation existing in the alloy was caused by the pinning effect of hydrogen atoms which retarding the recovery of dislocations introduced by thermomechanical treatments. Possibility of further refinement of the microstructures using the retardation effect of hydrogen has been studied.

Intermetallic compounds

84 Fundamental Study of Microstructures to Develop High Performance Materials for Severe Environment (II-High Temperature Intermetallic Compound)

April 1990 to March 1997
T. Yamagata, Materials Design Division
Keywords: Nb_3Al+ Nb two phase structure, mechanical properties, oxidation behavior

The project is a part of national research project to develop various heat resisting materials which withstand severe environment. Target of the project is to develop high temperature intermetallic compound such as niobium aluminides which possess 3 percent tensile elongation at room temperature and 75 MPa tensile strength at 2073 K. As intermetallic compound Nb_3Al(A15) is a typical brittle material with melting point of 2233 K, two

phase alloys composed of A15 and ductile A2 phase (Nb) and in equilibrium state at 2073 K, are searched in Nb-Al(16–23at%Al) binary and Nb-Al-X ternary alloys (X:Mo, Ta, W, Zr, Ti, Cr, Si, Co, Ni). Two phase structure was obtained at Nb-18at%Al in binary alloys, and in Ta and W added Nb-18Al-X ternary alloys. Effect of additional element on melting temperature also was examined with alloys heat treated between 2073–2473 K temperature range. It was cleared that Mo, Ta and W were most effective alloying elements for rise of melting point of Nb-Al-X ternary alloys. Mechanical properties of three two-phase alloy (Nb-18Al, Nb-18Al-Ta and Nb-18Al-W) were investigated at room temperature and 2073 K by compression test. At 2073 K, compressive strength at 10% strain increased by addition of Ta and W, but even the maximum strength obtained in Nb-18Al-W alloy was only 20% of target value. At room temperature, excellent compressive strain about 3% was obtained in three alloys.

About oxidation properties, weight change and surface morphology change were observed in Nb-19Al-binary alloy heating up to 1273 K at a rate of 2° K/min in oxygen, nitrogen and simulated air and Ar-20% O_2 gas. Variation of weight and surface morphology started at 1073 K and 623 K respectively. Surface morphology in the stage of variation-of-weight being observed is not uniform. Scale is thick in some places and thin in others. Cell structure of A15-phase with networks of A2-phase is formed. Variation of weight and surface morphology as well as formation of the cell structure are qualitatively almost similar, when the same alloy is heated in nitrogen, in simulated air and Ar-20% O_2 gas.

Observation on oxidation of series of alloys ranging from Nb-19Al through Nb-31Al in oxygen at 873 K or 973 K has revealed that increase in Al content generally increases incubation time and decrease weight gain.

Related Paper

High Temperature Reaction of Nb-19Al Alloy in Nitrogen of Technical Grade and in Simulated Air, I. Tomizuka, M. Okamoto, and A. Miyazaki, Gadin Conference on High Temperature Corrosion, New London, NH, USA, July 19, 1993.

85 Sintering of TiAl Intermetallic Compound

April 1993 to March 1996

Y. Muramatsu, Chemical Processing Division

The objective of this study is to produce highly densified TiAl through conventional sintering techniques. At first, sintering properties of various powders such as Ti+Al, Ti+$TiAl_3$ mixed powders and TiAl alloyed powder were investigated in order to find starting powders with excellent sinterability. Then, microstructures of sintered TiAl were examined.

Ti+$TiAl_3$ mixed powder was found to be promising as a starting powder. The sintering properties of this mixed powder were improved with the refinement of constituent powders, especially Ti powder. The sintering properties varied with the powder composition, and larger densification was achieved in Ti-rich compositions. The microstructures of sintered Ti-55at%Al consisted of a single γ-phase, and those of Ti-(45–50)at%Al were composed of equiaxis γ-phase and γ/α_2-lamellar structure. In the mixed structures, the amount of the lamellar structure increased with a rise of sintering temperature, and decreased with an increase of Al content.

Related Paper

Production of Highly Densified TiAl by Die Compaction-Sintering Method, Y. Muramatsu, T. Ohkoshi, and H. Suga, J. Japan Inst. Metals, 57 (1993): 944–51 (in Japanese).

86 Improvement of Mechanical Properties of Intermetallic Compounds by Crystal Growth Control

April 1992 to March 1997

T. Hirano, Chemical Processing Division

Keywords: unidirectional solidification, floating zone method, Ni_3Al, room temperature ductility

The objective of this study is to improve the mechanical properties of intermetallic compounds by crystal growth. Recently, we have found that unidirectional solidification using a floating zone method remarkably enhances the room temperature ductility of Ni_3Al without addition of alloying elements such as boron. We call this method FZ-UDS. Stoichiometric Ni_3Al grown by FZ-UDS exhibits larger than 60% tensile elongation at room temperature. Al-rich Ni_3Al also can be ductilized, indicating that FZ-UDS is a new promising method for improving brittle intermetallic compounds.

In this study three subjects are stressed. First, crystal growth technique is developed. Columnar grained structure is closely related to the large tensile ductility. Formation mechanism of this structure and favorable growth conditions are studied. Second, solidification structure, especially grain boundary character, is characterized. It has become clear that this structure consists of low energy boundaries. Third, the mechanical properties and deformation behavior are studied.

Related Papers

Unidirectional Solidification of Ni_3Al by a Floating Zone Method, T. Hirano and T. Mawari, Acta Metall. Mater., 41 (1993): 1783–89.

Microstructure and Room Temperature Ductility of Unidirectionally Grown Ni_3Al, T. Hirano and T. Mawari, Mat. Res. Soc. Symp. Proc., 288 (1993): 691–96.

Suppression of Environmental Embrittlement in Boron-Free Ni_3Al by Unidirectional Solidification, C. Nishimura, T. Hirano, and M. Amano, Scripta Metall. Mater., 29 (1993): 1205–09.

87 High Ionic Conductivity of Solid Electrolyte

April 1992 to March 1995

H. Nakamura, Environmental Performance Division

Keywords: ionic conductor, solid electrolyte, charge carrier, electrical conductivity

Recently, research works on solid high ionic conductor have been mainly focused on oxygen ion conductor such as ZrO_2, proton conductor such as $SrCeO_3$ and sodium ion conductor such as β-Al_2O_3.

One of the reasons why no other solid electrolytes have been developed as high ionic conductor is that cracks caused by grain growth or voids along grain boundaries tend to be initiated in the sintered materials prepared for the solid electrolyte.

The purpose of this study is to synthesize a new solid electrolyte consisting of oxides and sulfates ($M_2O - B_2O_3 - M_2SO_4$, M = Li, Na, K) of which grain boundaries or voids were decreased by a rapid quenching method, and to investigate the suitable composition of the compound in solid–liquid coexisting composition range by various thermal analytical methods.

Furthermore, the electrical properties of the electrolyte are evaluated by the measurement of electrical conductivity, the investigation of polarizing behavior, the determination of charge carrier, the comparison of electron motive force for concentration cell with that for theoretical one, etc.

Related Paper

Electrical Conductivity of Solid Beryllium Sulfide, A. Kasahara, Y. Ogawa, S. Iwasaki, and H. Nakamura, Mater. Trans., JIM, 34 (1993): 786–91.

88 High Performance Materials for Severe Environments I (Microstructure and Properties of Intermetallic Compounds with High Specific Strength)

April 1990 to March 1997

M. Nakamura, 3rd Research Group

Keywords: intermetallic compound, TiAl, microstructure, thermomechanical processing, high temperature strength, superplasticity, high temperature oxidation

Light-weight, heat-resisting intermetallic compound TiAl is a candidate for a structural use in severe environments, such as a space plane, etc., and the knowledge of various properties of TiAl base alloys is required for a practical use in such environments. In this research program, the mechanical properties are systematically studied for TiAl base alloys whose composition and microstructure are well controlled, and then the fundamental methods to control microstructure which gives the optimum properties for a practical use to materials are discussed.

TiAl base alloys with various microstructures and compositions have been prepared by heat-treatment and thermomechanical processing using isothermal forging above 1000 °C, and the effect of microstructure on mechanical properties like strength, ductility, etc. has been studied.

The effect of third elements on high temperature strength has been studied systematically for TiAl, and it has been found that the addition of a small amount of Sb improves the yield strength at 1000 °C. V-containing TiAl alloys with an equiaxed, fine grained and $\gamma + \beta$ phase structure have been prepared using thermomechanical processing. The alloys have exhibited the superplastic elongation of more than 600% at about 1150 °C. The oxidation behavior of TiAl containing a various amount of Y at high temperatures has been also studied.

Related Papers

Effect of Third Elements on High Temperature Strength of TiAl Base Alloys, K. Hashimoto, M. Nobuki, H. Doi, T. Kimura, T. Tsujimoto, and M. Nakamura, J. Japan Inst., 57 (1993): 898–904.

Superplasticity in a Vanadium Alloyed Gamma Plus Beta Phased TiAl Intermetallic, D. Vanderschueren, M. Nobuki, and M. Nakamura, Scripta Met. Mater., 28 (1993): 605–10.

Environmental Effect on Mechanical Properties of TiAl-Base Alloys, M. Nakamura, K. Hashimoto, and T. Tsujimoto, J. Mater. Res., 8 (1993): 68–77.

89 Basic Research on Intermetallic Compounds for Structural Applications

April 1993 to March 1996

M. Nakamura, 3rd Research Group

Keywords: intermetallic compound, TiAl, elongation, high temperature creep, grain morphology control, thermal shock

TiAl base intermetallic compounds have become of major interest as a candidate for high temperature structural applications. Although they have advantages of high melting point, high strength at high temperatures, high elastic moduli and reasonable oxidation resistance, improvement of both room temperature ductility and strength at temperatures above 1000 °C is required.

In this work, TiAl and Mn-containing TiAl alloys have been tested in tension in a temperature range

from room temperature to 500 °C in order to study the brittle-ductile transition in elongation. The elongation increased from 1% at room temperature to about 3% at 200 °C for the specimens with a small amount of the α_2 particles, while in the specimens containing the α_2 precipitates at the γ grain boundaries and grain interiors, the elongation increased from about 3% at room temperature with increasing temperature, and the Mn-containing alloy showed the elongation of more than 6% at 500 °C.

The knowledge of creep behavior at high temperatures is required for high temperature structural applications, but there are not many researches on tensile creep behavior of TiAl base alloys. The creep behavior in tension is studied at temperatures from 900 °C to 1100 °C in a He atmosphere and other atmospheres for a Ti-46at%Al alloy consisting of lamellar grains with a small amount of the γ grains at lamellar grain boundaries.

The microstructure control of TiAl base alloys is also studied for improvement of mechanical properties at high temperatures using a thermomechanical processing. We reported that alloys with an equiaxed, fine grained structure have relatively good ductility at room temperature and exhibit superplasticity at about 1000 °C. Plasma arc melted TiAl alloys containing V, Nb, Hf, C, and/or B exhibited a fine lamellar structure after homogenizing, and an equiaxed, fine grained structure of the alloys could not be obtained by the thermomechanical processing with which a fine grained structure of binary and ternary TiAl base alloys was obtained. Thus, the first isothermal forging at a α phase region followed by the second forging at a $\alpha + \gamma$ phase region has been found to be required in order to obtain a recrystallized and fine grained structure of the alloys.

The resistance to thermal shock of transition metal carbides and borides with a much higher melting point is also studied for much higher temperature structural applications using a HIP'ed mixture of W and TiB_2, etc.

Related Paper

Thermal Shock Behavior of Metal-Ceramics Mixtures for Ultrahigh Temperature Use, M. Fujitsuka, I. Mutoh, H. Nagai, and T. Tanabe, Proc. of the 3rd Japan Int. SAMPE Symp., *Advanced Materials-New Processes and Reliability*, ed. by T. Kishi, N. Takeda, and Y. Kagawa, SAMPE, Chiba, Japan, (1993): 641–46.

Composites

90 Thermal Stability of Intermetallic Compound Matrix Composites Reinforced with Fibers

April 1993 to March 1996

Y. Shinohara, Physical Properties Division

Keywords: TiAl matrix composite, B fiber, W fiber, protection layer, BN, TiB_2

Heat resistive materials which can be used above 1373 K are essential to the developments of the space-plane, the fusion reactor and the high-efficient turbine engine. TiAl intermetallic compounds have higher strength and toughness than metals and ceramics at elevated temperatures. TiAl matrix composites reinforced with fibers are hopeful for structural materials above 1373 K.

Reinforcements for TiAl matrix are SiC, B and W fibers. B and W fibers are tougher than SiC fibers, while are more reactive with TiAl. BN and TiB_2 have both little reactivity and good wettability with TiAl. We have studied on the B and W fibers with protection layers of BN or TiB_2.

Formation of BN and TiB_2 Layers and Optimization of Layer Thickness

The B fibers were coated with Ti by using PVD method, and were heat treated to form TiB_2 layers. The fiber strength deteriorated with the layer thickness. The thin layer may show little inhibitive action for the interfacial reaction between B and TiAl. The effect of TiB_2 thickness on the interfacial reaction will be investigated.

The CVD apparatus for W fiber was fabricated. Hg was used as the electrode, and served as the gas seal, also. W fibers were heated electrically to the desired temperature, and BN was deposited. The effect of BN thickness on the interfacial reaction between W and TiAl will be investigated.

Effect of Surface Morphology on the Strength of W Fiber

When the protection layer has insufficient shear strength, roughening of the fiber surface is effective in transferring stress between the fiber and the matrix. The surface of W fiber was successfully roughened by the following steps: (1) A fine W fiber is wound on the W fiber of reinforcement, (2) The surface of W fiber is oxidized, (3) The fine fiber and the W oxide are removed. The effect of the surface morphology on the fiber strength will be investigated.

91 Fatigue Fracture Mechanisms for TiAl Intermetallic Compounds at High Temperatures

April 1991 to March 1994

K. Yamaguchi, Failure Physics Division

Keywords: TiAl, intermetallic compounds, fatigue strength, fatigue crack

The TiAl intermetallic compound has a potential for high temperature structural applications due to its low density, high strength and good oxidation resistance. In this study the fatigue strength and fracture mechanism of the compounds were investigated.

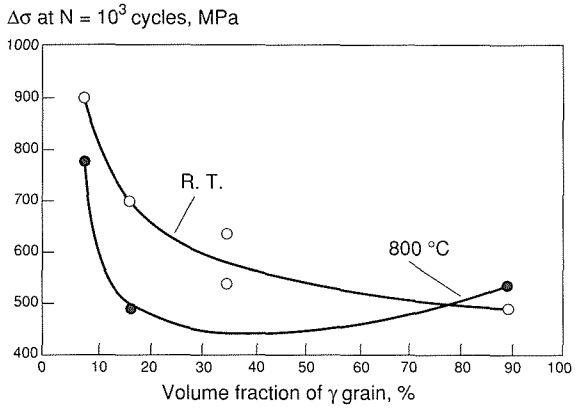

Fig. 5 Dependence of volume fraction of γ phase grains on the fatigue strength for TiAl alloys

Fatigue specimens were sampled from the alloys of Ti-33.9mass%Al, Ti-36.3mass%Al and Ti-34.7mass%Al-1.74mass%V. The heat-treatment conditions used were full-annealed and as-casted. Fatigue tests were carried out under strain-control at room temperature and at 800 °C, as well.

Figure 5 shows the dependence of the volume fraction of γ phase grains on the fatigue strength at 10^3 cycles for the alloys. This behavior could be considered to be due to the mechanism that the fatigue cracks were initiated by the persistent slip bands developed in γ phase grains.

Related Paper

Fatigue Properties and Its Mechanisms of Ti-Al-V Intermetallic Compounds, K. Yamaguchi, M. Shimodaira, and S. Nishijima, J. Iron and Steel Inst., 78 (1992): 134–40 (in Japanese).

Materials for mechanical application

(92) High Temperature Mechanical Properties of Particulate Reinforced Titanium-based Metal Matrix Composites

April 1994 to March 1997

M. Hagiwara, Mechanical Properties Division

Keywords: particulate-reinforced, titanium, MMC, mechanical properties, powder metallurgy

One of drawbacks of titanium alloys is that the service temperature is limited to 600 °C due to a degradation of tensile strength, creep resistance, thermal stability and environmental resistance. Moreover, titanium alloys exhibit lower stiffness and poor abrasion-related properties than nickel-based alloys. However, for future aircraft design, there is still demands for advanced titanium alloys having superior combinations of mechanical properties compared to the conventional counterparts in the temperature range above 600 °C.

Fabrication of titanium-based metal matrix composites (MMC) creates considerable potential for improvement in various properties. There are two basic types of MMC, i.e., long fiber reinforced and particulate reinforced. Of these, interest has increased in particulate reinforced MMC in recent years because these have isotropic characteristics and can be processed more easily using the conventional processing techniques.

Our research group has been devoted to the production of this type of titanium-based MMC using the advanced powder metallurgy (P/M) processes such as plasma rotating electrode process (PREP), melt spinning and proprietary blended elemental method. However, mechanical property data are still lacking. Particularly, creep and fatigue data at high temperatures, and the comparison with the unreinforced matrix alloys has received relatively little attention.

In this research program, titanium-based MMC reinforced with both large-sized ceramic particulates (1–10 μm in diameter) such as TiC and TiB and very fine oxide particulates (below 1 μm) such as Er_2O_3 will be produced using advanced P/M processes, and the creep and fatigue properties will be evaluated with emphasis on relating microstructural characteristics to these high temperature mechanical properties.

93 Intelligent Structural Materials

April 1991 to March 1995

S. Matsuoka, Environmental Performance Division

Keywords: intelligent material, material damage, self-sensing, self-restoring, nanotechnology

Recently, a new material concept, known as intelligent material or smart material, has been proposed and developed to establish the reliability of engineering structures such as air crafts, space structures and nuclear power plants. The intelligence of the material is defined as self-detectability for environmental changes and feasibility of sensing, processing and actuating.

In this study, fundamental research has been carried out in order to impart the intelligent functions to the metallic materials for structural use. Small cavities which do not deteriorate the mechanical properties exist in the materials. An attempt has been made to implant the sound-emitted material, phase transformed material or surface film controlled material into the cavities. The implantation could make the material possible to self-sense and self-restore the damage during operation. A nanotechnology based on the scanning tunneling microscope (STM) and atomic force microscope (AFM) has also been developed to evaluate the intelligent functions of the materials from atomic scale viewpoint.

In the current year, lead particles with about 2-μm-diameter dispersed in Fe-18Cr-8Ni steels were found to arrest the elevated-temperature fatigue crack growth. The arrest function was related to the fact that lead particles repaired the oxide film at the fatigue crack tip when the test temperature was higher than the melting point of lead. The fracture surfaces obtained were examined by an AFM/STM hybrid system. Using this system, topographic and current images of fracture surfaces were obtained at the same time in the AFM mode. These two images established the mechanisms that the oxide film at the crack tip were repaired by the melting lead.

94 Toughness Improvement of Brittle Ceramics and Steels by Precipitation and Phase Transformation Control

April 1993 to March 1996

F. Abe, Environmental Performance Division

Keywords: toughness, zirconia ceramics, martensitic steels, phase transformation

The purpose of the present research is to investigate the microstructural evolution in brittle materials, such as zirconia ceramics and neutron-irradiated martensitic steels, and to improve their toughness by microstructural control.

The transformation behavior of tetragonal (t) to monoclinic (m) phase was investigated by means of dilatometry for a sintered ZrO_2-9.7mol%MgO during cyclic annealing between room temperature and 1490 K. The amount of t $\leftrightarrow$ m transformation increased and the transformation temperature shifted to higher temperatures with increasing number of cyclic annealing up to about 40 cycles and then saturated. It should be noted that both the m $\rightarrow$ t and t $\rightarrow$ m transformation occurred in the two stages; m $\rightarrow$ t at 800–1050 K and 1350–1400 K on heating and t $\rightarrow$ m at 950–1200 K and 400–750 K on cooling. The low temperature stages were dominant in low cycle range below 10 cycles, while the high temperature stages were dominant in high cycle range. Transformation-induced microcracks were frequently observed along grain boundaries. The shift in transformation temperature correlated with the formation of the microcracks.

The effects of neutron-irradiation on the yield stress and ductility of newly developed 9Cr-1WVTa and 9Cr-3WVTa steels for fusion reactor were investigated over the temperature range from room temperature to 873 K after irradiation in Japan Materials Testing Reactor at 538 K to fast neutron fluences of 2×10^{23} and 3×10^{24} n/m^2. The yield stress increased proportionally with the 1/4 power of the neutron fluence. With increasing tensile-test temperature, the increase in yield stress caused by irradiation, $\Delta\sigma_y$, exhibited a further increase at 573–673 K and then decreased to zero over the range from 673–873 K.

Related Papers

Microstructural Control for Improving Creep Rupture Strength of Tempered Martensitic 9Cr-W Steels, F. Abe and S. Nakazawa, Proc. JIMIS-7, The Japan Institute of Metals, Nagoya, Japan (1993): 301–08.

Control of Precipitation and Phase Stability in Steels Consisting of Low Activation Elements, F. Abe, T. Noda, and M. Okada, Bull. JIM, 32 (1993): 543–52 (in Japanese).

Effect of Neutron Irradiation on Yield Stress and Ductility of Reduced-Activation Martensitic 9Cr-WVTa Steels, F. Abe, M. Narui, and H. Kayano, Mater. Trans. JIM, 34 (1993): 1053–60.

[95] Development of Metal Matrix Composites for High Temperature Use Through Combinations of Advanced Powder Metallurgy Processes

April 1991 to March 1994

M. Hagiwara, Mechanical Properties Division

Keywords: titanium, mechanical properties, powder metallurgy, titanium matrix composite

The conventional titanium alloys such as Ti-6Al-4V and Ti-6Al-2Sn-4Zr-2Mo exhibit poor high temperature properties and lower stiffness than nickel-based alloys.

The incorporation of relatively large-sized particulates which have superior high temperature properties relative to the matrix alloys is expected to overcome these drawbacks. In the present study, titanium alloy/particulate composites have been produced using two different kinds of powder metallurgy (P/M) processing techniques. Firstly, conventional titanium alloy matrix composites reinforced with either TiB or TiC particulates were produced using blended elemental P/M technique. Secondly, titanium alloy matrix composites reinforced with either Ti_3Al or TiAl were produced using plasma rotating electrode process (PREP) prealloyed P/M processing techniques.

It was found that the uniform dispersion of large-sized particulates is an effective method for improving properties such as elastic modulus, tensile and creep strength and room temperature high cycle fatigue properties of conventional titanium alloys, demonstrating that the sufficient load transfer from the matrix to the reinforcements have been achieved in the present composites. However, the composites produced in this study showed poor ductility at room and elevated temperatures. Because the fracture initiated from the cracking within the reinforcements, it was considered that more uniform dispersion and further refinement of the particulates through fabrication modifications such as the use of much smaller starting powder materials may lead to additional improvement in the mechanical properties of these composites.

Related Papers

Mechanical Properties of Particulate Reinforced Titanium-Based Metal Matrix Composites Produced by the Blended Elemental P/M Route, M. Hagiwara, S. Emura, Y. Kawabe, N. Arimoto, and H.G. Suzuki, ISIJ INT., 32 (1992): 906–16.

Microstructures and Tensile Properties of Titanium-Based Composites Produced by Powder Metallurgy, M. Hagiwara, S. Emura, J. Takahashi, Y. Kawabe, and N. Arimoto, Proc. 7th World Conf. Titanium, III (TMS) (1992): 2487–94.

[96] Production and Evaluation of Particulate-Reinforced Titanium Matrix Composites

April 1993 to March 1994

Y. Kawabe, Mechanical Properties Division

Keywords: particulate, composites, titanium, mechanical properties

This study is a part of "Investigation of High Temperature Titanium Alloys at above 600 °C," which is a joint research project determined by Chinese-Japanese Science and Technology Cooperation Committee. It was decided to be carried out by Northwest Institute for Non-Ferrous Metal Research (NIN) and National Research Institute for Metals (NRIM). The purpose of this program is (1) to study the techniques of preparing particulates-reinforced titanium-based metal matrix composites by both powder metallurgy (P/M) and ingot metallurgy (I/M) processes, (2) to evaluate the high temperature mechanical properties of these composites and (3) to discuss the strengthening mechanism by particulates.

The main results of joint research obtained by both institutes in the past year are as follows.

1. In Japan, three particulates-reinforced composites (1) Ti-5Al-2.5Fe/15%TiB, (2) Ti-5Al-13Cr/10TiC and (3) Ti-6Al-2Sn-4Zr-2Mo/10TiB have been produced using P/M process. In making these three composites, FeB, Cr_3C_2 and TiB_2 powder were used respectively as starting powder materials. The reasonably uniform dispersion of ceramic particulates was achieved in each of these composites. No obvious interaction zone was visible at resolution available in optical and scanning electron microscopy. The composites showed improved tensile strength, creep and room temperature high cycle fatigue strength over those for the unreinforced matrix alloys.
2. In China, two particulates-reinforced composites (1) Ti-15S/10TiC, (2) Ti-15S/10TiB_2 have been produced using I/M process. Ceramic particulates were added and dispersed randomly and homogeneously in matrix, and bound well with metal matrix. The former composite possesses good ductility (σ > 5%) at room temperature and high temperature strength; the latter has higher elastic modulus. Microstructure, interface reaction and structure, fracture behavior were also investigated.

Both institutes will further investigate the microstructures and mechanical properties of the composites processed in the other institute. High temperature fatigue test will be done extensively in NRIM, while NIN will concentrate on the study of creep properties of the composites.

Materials for electronics application

(97) Synthesis of Superconducting and Supermagnetic Ultrathin Films by Use of Ion Implantation

April 1994 to March 1996

K. Saito, Surface and Interface Division

Keywords: superconductivity, giant magnetization, ultrathin films, ion implantation

High quality superconducting or supermagnetic thin films of nanometer thicknesses are key materials for future applications of high density electric or magnetic devices. In this study we attempt synthesis of superconducting ultrathin films of BiSrCaCuO system and also supermagnetic ultrathin films of Fe-N system by means of ion implantation technique[1]. For film thicknesses below 10 nm, epitaxial growth mechanism is a most straightforward method for creating high quality crystalline films, since the depositing atoms may have a memory of the underlying substrate crystal structure and grow epitaxially on the substrate crystal. The deposited films can be modified by ion beams with various effects, i.e., atomic displacement, atomic mixing, thermal spike and channeling.

For the BiSrCaCuO system, we succeeded in obtaining superconducting transition temperature, $T_{c,o}$, higher than 80 K and the critical current, J_c, of the order of 10^4 A/cm^2 at 77 K. For the Fe-N system, we synthesize $Fe_{16}N_2$ phase films by nitrogen ion implantation into iron films. Multi-energy implantation is used in order to achieve uniform nitrogen concentration and hence to increase the volume fraction of the ordered martensite $Fe_{16}N_2$ phase for a film thickness of 50–250 nm. In this experiment it was very important to determine optimum annealing conditions. Magnetic response of these ultrathin films has been studied by a SQUID magnetometer.

Related Paper

Modification of Superconducting Thin Films by Means of Ion Implantation, K. Saito, Advances in Superconductivity VI, (Springer Verlag, Tokyo) (1994): 875–80.

(98) Studies on Microstructure and Electromagnetic Characteristics of V_3Si Multifilamentary Superconductor

April 1994 to March 1997

T. Takeuchi, High Magnetic Field Research Station

Keywords: flux pinning, ac loss, V_5Si_3, image analysis

V_3Si multifilamentary superconductors produced by a modified bronze process, developed at NRIM, are promising for ac applications. The combination of adjusting the total proportion of V to Si in the Cu-Si/V composite to ~3 and reducing V filaments to ~1 μm enables the completion of the reaction in a short time; the V_3Si_3 initially formed around V_3Si filaments appropriately decomposes and mostly V_3Si without grain growth is produced to achieve a high overall critical current density J_c (1.3×10^5 A/cm^2 at 5 T). In addition, the remaining V_5Si_3 layer is expected to act as an eddy-current barrier reducing ac losses, since the reported resistivity of V_5Si_3 (~15 μΩcm at 4.2 K) is likely to be high enough to separate the filaments from each other for electromagnetic decoupling.

In this study, with image analysis, we will perform quantitative analysis of microstructures that affect the electromagnetic characteristics of V_3Si multifilamentary superconductors. Flux pinning mechanisms would be clarified with precise measurements of cross-sectional area for V_3Si, and density, morphology and configuration for the grain boundary and V_3Si/normal-metal interface. Correlations between anisotropy in pinning force density and microstructures for a flattened multifilamentary conductor would give us an important information on flux pinning center. In order to confirm the effectiveness of V_5Si_3 layers as eddy-current barriers, we will measure the resistivity of V_5Si_3 layer in the composite. The superconducting effective diameter D_{eff} measured with a vibrating sample magnetometer would be compared with the designed diameter D_f and discussed with a result of image analysis for V_3Si filaments.

Related Papers

V_3Si Multifilamentary Superconductor Produced by a Modified Bronze Process, T. Takeuchi and K. Inoue, J. Appl. Phys., 74 (1993): 6454–56.

V_3Si Multifilamentary Superconductor with High Overall J_c, T. Takeuchi, K. Inoue, M. Kosuge, Y. Iijima, and K. Watanabe, to be published in Adv. Cryo. Eng., 40 (1994): 891–98.

99 Synthesis of New Functional Materials by the Application of Host-Guest Reactions

April 1990 to March 1995

M. Amano, Physical Properties Division

Keywords: insertion-extraction reaction, ionic conductor, hydrous pentavalent oxide, proton conduction

The aim of this project is to synthesize new functional materials by applying insertion-extraction reactions. We are trying to synthesize new ionic-conductor materials by using ion exchange processes. Hydrous pentavalent oxides have been selected as the object materials, because they are known to possess ion exchange property with ion memory effect and some hydrous oxide of Sb, Nb, and Ta, e.g., $HSbO_3.xH_2O$ and $HNbO_3.xH_2O$, are known as proton conductors. These compounds can be prepared by acid treatment of alkali metal compounds such as $LiSbO_3$, $KSbO_3$, $NaSbO_3$ and $LiNbO_3$. Different crystal structures of hydrous oxide can be obtained by changing the preparation process and starting materials. We have prepared monoclinic $HSbO_3.xH_2O$ (m-SbA) from $LiSbO_3$ and cubic $HSbO_3.xH_2O$ (c-SbA) from $KSbO_3$.

Temperature and humidity dependencies on the conductivity of two types of antimonic acid were investigated. The amount of absorbed water on c-SbA was larger than that of m-SbA. The conductivity of m-SbA is more sensitive to the amount of adsorbed water than that of c-SbA. The results suggest that the proton conductivity largely depends on the nanopore structure and the state of water in the antimonic acid. Further study on the correlation between proton conductivity and nanopore structure in the antimonic acid is now in progress.

100 Purification of Active Metals for the Preparation of Superconductive Materials

April 1987 to March 1995

T. Fujii, Chemical Processing Division

Keywords: sintering method, melt-growth method, $YBa_2Cu_3O_x$

In order to examine in more detail the superconducting characteristics of $YBa_2Cu_3O_x$ ceramics, effects of impurity contents in starting materials on superconductivity such as the critical transition temperature, T_c, and the critical current density, J_c, were investigated. Specimens for measurements of T_c and J_c were fabricated by the sintering and the melt-growth techniques using reagents of various purity grades. Superconducting properties were affected with the purity of starting materials as well as the preparation techniques. As far sintered specimens, T_c and J_c values increase 87.4–89.6 K and 140–317 A/cm^2 (at 77 K, OT), respectively, with a decrease in impurity contents in starting materials. In melt-grown specimens, both T_c and J_c values were improved to be 90.0–92.9 and 235–960 A/cm^2, respectively. In these specimens, with lowering impurity contents, T_c values increase whereas J_c values decrease. All the sentered specimens show similar microstructures with randomly

oriented plate-like 123 grains irrespective of impurity contents. On the other hand, fine grained needle-like 123 crystals and spherulitic microstructures were observed in the melt-grown specimens, in which the 123 grains became smaller with an increase in impurity contents.

101 Structure Control and Electromagnetic Properties of High Temperature Superconductors

April 1993 to March 1997
K. Togano, 1st Research Group
Keywords: structure control, melting process, vapor process, mixed state

The purpose of this study is to establish the basic technologies to control the structure of high temperature superconductors (HTSC) in synthesizing them by melt or vapor process. The relation between the structure and electromagnetic properties is also studied to understand the voltex state and pinning mechanism of HTSC. The informations obtained here are feedbacked to the processes to optimize their parameters. Following four subjects are being studied.

Relationship between Microstructure and Critical Current

Comprehensive work on the microstructure and phase changes during the partial melting process for $Bi_2Sr_2Ca_1Cu_2Ox$(Bi-2212) are being carried out. The result shows that the partial molten state is composed of liquid plus two solid phases of (Sr, Ca)mCunOx and Bi-Sr-Ca-O and their relative stability is influenced by the corporation of Ag and atmosphere (O_2 and Bi partial pressures). These knowledges have been applied to the process for Bi-2212 thick film/Ag composite tape and we have achieved large improvement of critical current density and the generation of high field using B1-2212/Ag coil at 4.2 K.

Elucidation of Electromagnetic Behavior

The purpose of this subject is to establish a new concept of mixed state of HTSC. Precise measurement of resistivity change in applied magnetic field has been carried out for various HTSC including a large and high-quality single crystal of Bi-2212 which has been prepared by zone melting technique with the infrared image furnace in our laboratory. The results can not be explained by the classical model of voltex motion. Our analysis indicates that the resistivity in mixed state is originated from the superconductivity fluctuation due to the strong two dimensionality.

Structure Control by Thin Film Synthesis

We are studying on the structure control and growth mechanism of Bi-system superconductors; $Bi_2Sr_2Ca_{n-1}Cu_nO_x$. By using alternative sputtering technique, we have already succeeded in preparing metastable structures up to n = 7 and superlattice structures with different n. Studies on their transport properties are now being carried out to understand the mechanism of superconductivity of this type of materials. The technology of atomic layer control established in this work will be applied for the fabrication of high quality devices.

Microstructure Control by Vapor Deposition Technique

Studies on the texture control of $Y_1Ba_2Cu_3O_x$ thin film are being carried out to overcome the weak link problem of this material. We have succeeded in obtaining three dimensionally controlled crystal orientation for YSZ buffer layer on a Hastelloy tape using a modified bias sputtering technique. The YBCO film deposited on this textured YSZ buffer layer shows in-plane alignment in addition to c-axis alignment, resulting in a large improvement of transport critical current density.

102 Development of $Bi_2Sr_2CaCu_2O_x$/Ag Coils for High Magnetic Field Application

April 1989 to March 1995
H. Kumakura, 1st Research Group
Keywords: pancake coil, generated magnetic field

We have fabricated small $Bi_2Sr_2CaCu_2O_x$ (Bi-2212)/Ag single pancake coils using Bi-2212/Ag tapes by dip-coating process, which are used as an insert coil of a conventional superconducting magnet. A wind, react and wind (W&R&W) process was applied for the fabrication of the coil. After the final winding of the tapes, the coil was encased into stainless steel tube and fixed with epoxy resin cured with acid-anhydride. The size of the coil were 47.5 mm in outer diameter, 14 mm in inner diameter and 40 mm in height. The critical current I_c and the critical current density J_c of this insert coil determined with the criterion of 10^{-13} Ω·m were 275 A and 36700 A/cm^2 respectively at a saturated superfluid helium temperature in a bias field of 20.8 T. Generated magnetic field by the coil was measured by a Hall probe set at the center of the coil. The I_c of 275 A generated a field of 0.7 T. Hence, the superconducting magnet system achieved a generation of total magnetic field of 21.5 T which was the highest magnetic field value ever obtained by the superconducting magnet system. The local I_c and J_c of the coil were higher than 400 A and 53000 A/cm^2 in 20.8 T, respectively, indicating that there was I_c scattering along the tape length due to inhomogeneity of superconducting oxide layer. This suggests that higher fields may be generated with better fabrication technology of the tapes and the coils. A larger double stacked Bi-2212/Ag pancake coil with outer diameter of 90 mm was also fabricated by a similar method, and was tested using a normal conducting bitter type magnet. This coil generated

higher field of 1.1 T at 4.2 K in a bias field of 20 T. These results demonstrate that Bi-2212 conductors are very promising for high magnetic field generation.

This research was performed in collaboration with Asahi Glass Co. Ltd. and Hitachi Cable Co. Ltd.

Related Papers

Properties of $Bi_2Sr_2CaCu_2O_x$/Ag Composite Tapes and Coils Melt-Solidified with $Bi_2Al_4O_9$, J. Shimoyama, N. Tomita, T. Morimoto, H. Kitaguchi, H. Kumakura, K. Togano, H. Maeda, and K. Nomura, Advances in Superconductivity V, (1993): 697–700.

Development of Superconducting Coil Using Bi-2212/Ag Tapes, N. Tomita, J. Shimoyama, H. Kitaguchi, H. Kumakura, K. Togano, H. Maeda, H. Fijii, and K. Nomura, Advances in Cryogenic Engineering 40, Plenum Press, New York, (1994): 297–303.

103 Development of High-T_c Superconducting Bulk and Thick Films by Spraying and Internal Oxidation

April 1989 to March 1995

H. Maeda, High Magnetic Field Research Station

Keywords: high-T_c oxide superconductor, plasma spraying, flame spraying, internal oxidation, magnetic shielding

We have studied the superconducting properties, compositions and microstructures of Bi-based and Y-based high-T_c oxide bulk and thick films prepared by plasma spraying, flame spraying and internal oxidation. Especially, we have tried to fabricate prototype superconducting magnetic shielding vessels, which are useful for medical applications of extremely weak neuromagnetics.

(Bi, $Pb)_2Sr_2Ca_2Cu_3O_{10}$ thick film cylindrical vessels with a thickness of about 700 μm were prepared by plasma spraying on the outer surface of a nickel alloy pipe (320 mm in outer diameter, 660 mm in length and 1.6 mm in thickness). A silver buffer layer with a thickness of about 50 μm was also plasma-sprayed to prevent the interdiffusion between the oxide layer and the substrate pipe. The vessels were post-annealed, and then their magnetic shielding effect, S, which is (applied magnetic field strength)/(measured magnetic field strength inside the pipe), were measured by an "RF-SQUID" magnetometer at an applied field of 0.3 G parallel to the pipe axis. The values of S show above 10^5 at the inside center position equal to the pipe diameter from the pipe end. We detect no different S in the frequency range of 0.1–10 Hz.

Flame spraying using a mixed gas of oxygen and propylene was also applied to fabricate Y-based high-T_c thick films. $YBa_2Cu_3O_7$ films with a thickness of 50 μm were prepared on a nickel plate substrate. The films have almost the same structure and superconducting properties as bulk oxides without post-annealing.

Three bulk types of Ag alloys including metallic compositions of YBa_2Cu_3, $Bi_2Sr_2Ca_1Cu_2$ and (Bi, $Pb)_2Sr_2Ca_2Cu_3$ were internally oxidized at temperatures of 973–1023 K and then annealed at various temperatures. Continuously connected high-T_c oxide layers are formed in the Ag matrix. T_c's of the samples are almost equal to those of bulk samples, although the Bi2223 composition samples have a mixed phase of Bi2212 and Bi2223. Especially, some of the Bi2212 samples show a critical current, I_c, of 10^3 A.

104 Fabrication of Oxide Superconductors Using YAG Laser Irradiation

April 1986 to March 1995

H. Wada, High Magnetic Field Station

Keywords: yttrium-based superconductor, 211 phase, YAG laser

Research efforts have been made to explore and fabricate oxide superconductors with high critical temperatures and large critical currents. Recently, the so-called QMG (Quench and Melt Growth) method has been applied to the fabrication of yttrium-based oxide superconductors. The superconducting phases resulted contain dispersed fine precipitates and strongly textured, which leads to a remarkable increase in critical current density. In this method samples are heated above 1,273 K where a liquid phase coexists with Y_2O_3. When samples are quenched to low temperatures, fine particles of Y_2BaCu(211 phase) precipitate and act as pinning centers. If samples are cooled by about 100 K and kept there, YBa_2Cu_3 (123 phase) grows from a mixture of liquid phase and 211 phase. Thus, cooling process determines microstructures, such as distribution, size and texture of superconducting and non-superconducting phases.

Laser irradiation is one of the possible techniques one can heat and quench materials. In this study yttrium containing samples of a Y:Ba:Cu composition ratio of 1:2:3 were irradiated using a YAG laser machine at an irradiation power of 50 W and a sample traveling speed of 0.5 mm/sec.

The X-ray diffraction analysis on an irradiated and quenched sample revealed the formation of 211 phase. It seems, therefore that laser irradiation maybe one possible technique to introduce pinning centers into yttrium-based oxide superconductors. Further work is needed to optimize irradiation conditions to obtain a maximum critical current density.

105 Development of Practical High-Field Multifilamentary Superconductors Made of Intermetallic Compounds

April 1992 to March 1995
K. Inoue, High Magnetic Field Research Station
Keywords: multifilamentary superconductor, Nb_3Al, diffusion reaction, supersaturated bcc phase

The Nb tube process has recently been developed at NRIM for fabricating Nb_3Al multifilamentary superconductors, which are characterized by the ultra-fine microcomposite of Nb/Al-Mg (Al-Mg core size of 0.1 μm) and the heat treatment at low temperatures below 1000 °C. However, the fabrication of ultra-fine microcomposite requires stacking-processes more than 3 times, which make the commercial production of the Nb_3Al wires difficult. Therefore, in order to reduce this difficulty we studied the superconducting properties of Nb/Al-Mg composite (Al-Mg core size of 1–2 μm) made by double-stacking and heat-treated at high temperature for very short time. To realize the very short heat treatment, we developed a continuously rapid-quenching process described as follows.

The long double-stacked composite wire was moved continuously with high speed, heat treated by ohmic-heating, and then quenched into a molten Ga bath to be cooled down rapidly with cooling rates of 15,000 °C/sec or faster. The molten Ga bath plays a role not only as an electrode for ohmic-heating but also a coolant for rapid-quenching. As quenched the composite shows only a T_c of about 9 K, which is that of Nb. According to the X-ray diffraction study, metastable bcc Nb-Al solid solution filaments were formed in the composite due to the rapid-quenching. However, subsequent annealing (post annealing) was found to cause the transformation from the metastable solid-solution to the Nb_3Al A15 phase with fine grain structure. Typical ohmic heating temperature and heating time were about 2000 °C and 0.1 sec, respectively. The post annealing were performed at 700–900 °C for 0.5–200 hr.

The highest T_c and J_c(20 T, 4.2 K) obtained so far were 17.3 K and $2 \times 10^8 A/m^2$, respectively. These values are much higher than those for the ultra-fine Nb_3Al composite heat treated at relatively low temperature, and comparable to those of the commercially available Nb-tube processed (Nb, Ti)$_3$Sn multifilamentary wires, which is known to have the highest J_c in high fields. Thus the Nb_3Al multifilamentary wire is very promising as a practical high field superconducting cable.

Related Paper

Nb_3Al Multifilamentary Wires Continuously Fabricated by Rapid-Quenching, Y. Iijima, M. Kosuge, T. Takeuchi, and K. Inoue, to be published in Advances in Cryogenic Engineering, 35 (1994): 899–905.

106 Synthesis and Superconducting Properties of the Bi System Ultrathin Films of Thicknesses below 100 Å

April 1993 to March 1994
K. Saito, Surface and Interface Division
Keywords: superconductivity, ultrathin films, Bi system

Synthesis of ultra thin films below 100 Å thickness is an essential subject for fabricating advanced integrated electric devices. For film thickness below 100 Å, however, it was difficult to produce high quality superconducting thin films because of experimental difficulties of controlling film compositions and microstructures.

In our study we utilized the epitaxial growth mechanism for thin films on MgO(100) substrates and synthesized ultrathin films with thicknesses from 150, 100 and down to 70 Å. To make ultrathin films superconducting, it was necessary to elaborate short-time and multistep annealing with controlled rates of cooling[1]. Even for a film thickness of 70 Å, we could attain zero resistance transition temperature, $T_{c,o}$ of 106 K[2]. The transition was confirmed by magnetization measurements using a SQUID magnetometer. SEM examination revealed that a directional array of thin crystals with very fine steps was formed along two well defined crystallographic directions, probably along the a and b axes of the thin crystals. The critical current density J_c was about 10^4 A/cm^2 at 77 K.

Related Papers

Fabrication of 30 nm Thick Superconducting BiSrCaCuO Thin Films by Single-Target Magnetron Sputtering Method, M. Kaise and K. Saito, J. Jpn Inst. Metals, 1 (1993): 103–07.

Modification of BiSrCaCuO Thin Films by Ar Ion Implantation, K. Saito, Advances in Superconductivity VI, (Springer Verlag, Tokyo, 1994): 875–80.

107 Development and Characterization of Superconducting Materials for Fusion Reactor Magnet Use

April 1989 to March 1994
H. Wada, High Magnetic Field Station
Keywords: Nb_3Al wires, neutron irradiation, critical current, tensile strain

The purpose of this study is to develop high-field superconducting materials for fusion reactor magnet use. New, promising superconducting materials are characterized and evaluated under conditions that such materials may experience when wound to a superconducting magnet which should confine and control plasma in the reactor.

In fiscal year 1993 effects of neutron irradiation and applied tensile strain on the critical current of Nb-tube processed Nb_3Al wires were studied. Critical currents of multifilamentary Nb_3Al wires were almost unchanged up to a neutron fluence of 1.4×10^{18} n/cm^2 (E > 0.1 MeV) and then decreased abruptly with increasing neutron fluence. The decreases in critical current at a magnetic field of 8 T relative to unirradiated values were about 13% and 90% at neutron fluences of 3.9×10^{18} n/cm^2 and 1.2×10^{19} n/cm^2, respectively.

The critical currents of both unirradiated and irradiated wires were monotonically decreased with applied tensile strain. For all the wires tested, the decreases in critical current at 8 T relative to unstrained values were about 10% and 25% at strains of 0.5% and 1.0%, respectively.

Magnetic materials

108 Research on Materials Synthesis to Control of Magneto-thermal Properties by Size Effects and on Low Temperature Production

April 1993 to March 1996

M. Sato, T. Numazawa, H. Kimura, Physical Properties Division

Keywords: low temperature, fine magnetic particles, garnet solid solution

The magnetic entropy properties of fine magnetic particles have been investigated. A mean field approximation is used to calculate the entropy change-temperature curve at different magnetic fields. The result shows that the entropy change of a magnetic system consisting of 100 fine particles with 1/2 magnetic moment has a broad peak around T_c, but the entropy change is enhanced 3 times larger above T_c than that of bulk system. For the synthesis of fine magnetic particles, an 11%Fe silica gel is grown by sol gel processing. Because the gel processing largely depends on catalysts, several catalysts are investigating.

$(Dy_{0.4}Y_{0.6})_3Ga_5O_{12}$ solid solution single crystal has been developed as magnetic refrigerants in order to obtain temperatures less than 1 K. It was grown using the Czochralski technique. It is difficult to control the crystal diameter because of an instability of solid–liquid interface during the growth. Doping effects of Ca in the garnet will be investigated to reduce the instability.

Thermal switch properties of Graphite have been investigated. Thermal conductivity of Graphite largely depends on temperatures below 4 K and it is useful to work as a thermal switch to control the heat flow.

This research was partly performed in collaboration with the Institute for Materials Research, Tohoku University.

Related Paper

Growth of Dysprosium Garium Garnet Single Crystals, H. Kimura, T. Numazawa, M. Sato, and H. Maeda, Cryst. Res. Technol., 29 (1994): 317–23.

109 Research and Development of Systems and Materials for Magnetic Refrigeration

April 1993 to March 1994

M. Sato, T. Numazawa, H. Kimura, Y. Iwasa, Physical Properties Division*

Keywords: magnetic refrigeration, Garnet magnetic materials, low temperature

This cooperative research project has been focused on the tandem magnetic refrigeration system and the magnetic materials for production of low temperatures below 1 K. The tandem magnetic refrigerator using the active regenerators has been developed and tested. The refrigerator consists of regenerative magnetic cores (magnetic material + heat exchangers), pulsed superconducting magnets and heat transfer fluid of He^3. Operating the Carnot magnetic cycle, we use the tandem connecting superconducting magnets. The magnets provide variational magnetic fields periodically by transferring the electrical energy alternate via bipolar power supply. The refrigerator obtained 1.65 K at 2 T and 0.2 Hz cycle operation. $(Dy_xGd_{1-x})_3Ga_5O_{12}$ $(0 \leq x \leq 1)$ Garnet single crystal was grown by the Czochralski technique and thermomagnetic properties of the material are measured. A magnetic transition temperature can be controlled by substitution of Dy^{3+} for Gd^{3+} and increasing x decreases the transition temperature below 0.85 K. Thermal conductivity of $Dy_3Ga_5O_{12}$ is decreased largely by applying magnetic fields and consequently, low thermal conductivity reduces the heat transfer rate and the efficiency of magnetic refrigerator. On the other hand, it is found that decreasing x enhances the thermal conductivity. Therefore, the optimization of x can be decided by considering the refrigeration temperature and thermal efficiency of the magnetic refrigerator.

This research project was performed with Francis Bitter National Magnet Laboratory of MIT under U.S.-Japan S&T agreement.

Related Papers

Carnot Magnetic Refrigerator between 1.4 K and 10 K, T. Numazawa, H. Kimura, M. Sato, and H. Maeda, Cryogenics, 33 (1993): 547–54.

A Tandem Magnetic Refrigerator for 1.8 K, S. Joeng, J.L. Smith Jr., Y. Iwasa, and T. Numazawa, Cryogenics, 34 (1994): 263–69.

---

*Francis Bitter National Magnet Laboratory, MIT

Materials for energy application

⑪⓪ Development of Third-Generation Nickel-base Single Crystal Superalloys

April 1994 to March 1997
T. Yamagata, Materials Design Division
Keywords: alloy design, lattice misfit, specific gravity, Rhenium, low density

First-generation Nickel-base Single Crystal Superalloy (SC-alloy) was developed on the basis of new metallurgical concept in the late '70 and the first production single crystal turbine airfoil entered service in 1982. After that, several SC-alloys, CMSX-4, PWA1484, etc. were developed and significant increases in high temperature strength capability have been achieved. This improvement, however, was realized by empirical addition of large amount of heavy refractory element such as Ta, W and Re at the cost of increase in density (8.9). Increase of density causes decline of heat efficiency of turbine, because lord on turbine disc increase. The purpose of this work is to develop new type SC-alloy with relatively low density (8.5) and with excellent high temperature strength using alloy design computer program developed by us. Search program in alloy design computer program, in this case, is used to find out optimum alloy composition which satisfy the alloy design conditions fixed by structural parameters of lattice misfit and γ' volume fraction, composition of alloy elements such as Cr and Re content, solubility index, density, heat treatment window. Single crystal of designed alloy is directionally solidified and mechanical properties and structural parameters are evaluated, and these data are fed back to the alloy design program to improve predictive accuracy of alloy design program.

Collaboration Research

Computer Modeling Alloys (Rolls-Royce plc, U.K.)
Single Crystal Superalloys for Future (IHI, Japan)

111 Thermal and Electrical Properties of II-IV and V-VI Thermoelectric Semiconductors

April 1993 to March 1996
I.A. Nishida, Physical Properties Division
Keywords: thermal conductivity, thermoelectric property, energy conversion, $Bi_{2-x}Sb_xTe_{3-y}Se_y$, $Pb_{1-x}Sn_xTe$, $Mg_2Si_{1-x}Ge_x$

Thermoelectric (TE) materials have been widely used for the direct energy conversion systems. These materials convert thermal energy to electric power with quick response and without noises and mechanical vibration. Recently, the thermoelectric generator is mainly used for the electric source in the space, marine and polar region, and the thermoelectric cooling system is mainly used for the precise controlling of the temperature of semiconductor processing equipments, optical and electronic devices. Therefore, the TE materials with high conversion efficiency have drawn a strong attention.

The TE materials high efficiency are given by the three characteristics, i.e., high thermoelectric power (α) and electric conductivity (σ) and low thermal conductivity (κ). For the TE materials with very low values of κ, such as $Bi_{2-x}Sb_xTe_{3-y}Se_y$, $Pb_{1-x}Sn_xTe$ and $Mg_2Si_{1-x}Ge_x$, etc., it is very difficult to obtain the reliable value of κ.

The aim of this study is to establish more precise technique for the measurement of κ by means of the static comparative method, Harman's method and PAS (Photo Acoustic Spectroscopy).

Related Papers

Anisotropic Galvanomagnetic and Thermoelectric Properties of n-Type B_2Te_3 Single Crystal with the Composition of a Useful Thermoelectric Cooling Material, H.T. Kaibe, Y. Tanaka, M. Sakata, and I.A. Nishida, J. Phys. Chem. Solids, 50 (1989): 945–50.

Preparation and Thermoelectric Properties of $Mg_2Si_{1-x}Ge_x(x = 0.0–0.4)$ Solid Solution Semiconductors, Y. Noda, H. Kon, Y. Furukawa, N. Otsuka, I.A. Nishida, and K. Matsumoto, Materials Transactions JIM, 33 (1992): 845–55.

112 Energy Conversion Materials Fabricated with Functionally Gradient Structure

April 1993 to March 1996
I.A. Nishida, Physical Properties Division
Keywords: energy conversion, thermoelectric materials, functionally gradient materials

Thermoelectric (TE) materials have been widely used for the direct conversion of thermal energy to electric power without noise and mechanical system. For a given alloy system with homogeneous matrix and dopant distribution, the optimized figure of merit Z is limited to a narrow characteristic temperature range, apart from the fact that the TE conversion efficiency η is comparatively small. Since the temperature of the thermocouple legs distribute continuously from the top (high temperature) end to the bottom (low temperature) end, the maximum value of η can be obtained with the functionally gradient TE material, in which the carrier concentration of the TE material is changed continuously with the exposed temperature along the thermocouple leg. In this way, the mean value of η can be increased as much as double. In addition, Z can be increased by controlling the alloy composition with fine grained structure. This is because the lattice component of thermal conductivity can be decreased by the phonon scattering at the lattice defects such as the crystal distortion and grain boundary.

The purpose of the present study is to establish the fabrication technology of the functionally gradient TE material with high η by controlling the carrier concentration, alloy composition, crystal texture and grain size.

Related Paper

A Try for Thermoelectric Conversion Materials with a Super High Energy, I.A. Nishida, New Ceramics, 7-1 (1994): 49–52 (in Japanese).

113 Environmental Degradation of Structural Materials for Light Water Reactors

April 1991 to March 1996

N. Nagata, 5th Research Group

Keywords: light water reactor, high temperature water, SCC database

A modeling for stress corrosion cracking (SCC) of structural materials for LWR in high temperature water and systematization of the related data for SCC were conducted.

1. The propagation of SCC in high temperature water should be consisted of three unit processes. These are break down of oxide film, dissolution of fresh surface appeared and repassivation of the fresh surface. We educed an equation which shows the relationship between the fracture strain $\in_{SCC}$ and the dissolution and repassivation rates, R_d and R_o for constant strain rate condition.
   In high temperature water, both R_d and R_o should increase as the dissolved oxygen concentration is higher. Aggressive ions such as Cl^- may increase R_d and decrease R_o. On the basis of these considerations, assuming the values of R_d and R_o, we obtained relations between $\in_{SCC}$ and the strain rate for various oxygen and chloride concentrations. These relations agreed with the experimental results of 304 stainless steel in water containing 0.2–40 ppm of oxygen or 5 ppm of chloride.
   R_d and R_o are going to be measured by strain electrode technique.
2. Based on the SCC database, a method of unified evaluation for SCC data of sensitized stainless steel obtained by different test methods such as SSRT and U-bend test was newly developed. In this database SCC damages were evaluated in terms of SCC crack depth, area fractions of intergranular and transgranular fracture, respectively. Several parameters which affect SCC behavior such as temperature, dissolved oxygen (DO) concentration, pH, maximum stress, conductivity and so on were analyzed by means of correlation with the SCC damages. As a result, the upper bound of a SCC fracture map can be predicted in terms of specific parameters such as DO concentration and pH.

114 Fundamental Research on Application of New Functional Materials to Passive Components

April 1990 to March 1995

T. Ishihara, 5th Research Group

Keywords: shape memory alloy, cyclic transformation, SCC

To apply shape memory alloys to the nuclear power plant, it is necessary to evaluate the characteristics of the shape memory alloys in some environments. In this study, (1) effects of water temperatures on stress corrosion cracking (SCC) susceptibilities in high temperature water and (2) effects of cyclic transformation on the shape memory characteristics were evaluated in a Fe-14Mn-6Si-9Cr-5Ni(wt.%) shape memory alloy.

1. The effects of dissolved oxygen and test temperature on SCC behavior of Fe-14Mn-6Si-9Cr-5Ni shape memory alloy (M_s:307.7 K, A_f: 413.7 K) were investigated in high temperature pure water. The specimens were strained at the rate of $8.3 \times 10^{-7} s^{-1}$ in water of 383 K–56 K. The shape memory alloy showed high susceptibility to SCC in high oxygen concentration (>0.2 ppm) and high temperature range (473 K–563 K), similarly to the case of 304 stainless steel. On the other hand, shape memory alloy showed remarkable behavior that SCC susceptibility increased below 423 K in deaerated water (<10 ppb O_2). Referring to transformation temperature, the mechanism of cracking in this temperature range is considered to be hydrogen embrittlement.
2. Some specimens were solution treated at 1420 K for 1.8 ks. Other specimens were solution treated, cold-rolled by 10% and heat treated at 970 K for 0.6 ks. The cyclic transformation was repeated 20 times. After cycling, the martensite phase was observed by TEM. To make clear the effect of cyclic transformation on microstructure, the density of stacking disorders of ε martensite was measured. The diffraction patterns with many streaks were analyzed to determine the density of stacking disorders in ε martensite. The main results obtained are as follows. (1) The M_s and A_s temperatures decrease with increasing in number of the cyclic transformation in the solution treated specimen. (2) The A_s temperature decreases drastically with increasing number of the cyclic transformation, but the A_f temperature is almost constant. (3) The density of stacking disorders in ε martensite decreases with increasing in number of the cyclic transformation in both of solution-treated and thermomechanically treated specimens.

115 Assessment of Strength and Structural Materials Database for Weldment in FBR Components

April 1991 to March 1996
Y. Monma, Failure Physics Division
Keywords: welded joint, creep, FBR, stainless steel

The mechanical behavior of welded joint under creep loading is one of great concerns for the integrity of important components of the FBR (fast breeder reactor) such as the reactor vessel. Welded joints by gas tungsten arc welding for plates with 50 mm thickness from a heat of type 304 (17Cr-10Ni-0.04C) and 316FR (17Cr-11Ni-2Mo-0.01C-0.07N) stainless steels were prepared for the study. The joints were "overmatching," or the strength of the weld metal was higher than that of the base metal. Full-thickness joint specimens were subjected to creep tests at 550 °C in addition to conventional small specimens at 500–600 °C up to about 20,000 h.

A new method of the measurement using the Moiré interferometry of CCD camera and digital image processing allows us to determine the strain distribution of welded joints. On the basis of FEM calculation we can predict the strain distribution from the creep constitutive equation, which can be obtained from the creep strain-time data of small specimens cut from the base metal and the weld metal. The thermal cycling history of welding introduces the local variability of properties in the thickness direction: the creep resistance of weld metal in central parts is stronger than that of the surface portion. We can improve the accuracy of prediction for creep strain by incorporating the concept of "damage parameter" and three dimensional FEM models. The accuracy of prediction we could achieve so far is the factor of two.

Related Paper

Creep Behavior of 304 Stainless Steel Welded Joints Composed of Two Different 308 Weld Metals, Proc. IUTAM Symposium on Mechanical Effects of Welding, Springer-Verlag (1992): 231–38.

116 Research on Distributed Database for Advanced Nuclear Metals

April 1991 to March 1996
M. Fujita, 2nd Research Group
Keywords: Data-Free-Way, distributed database, advanced nuclear materials, to share data, transmutation

New material-searching using database systems is required for nuclear technology. But it is very difficult at present to describe numerous nuclear materials properties because of their complexity in nature and pre-standardized status of information on new materials. The stored data consist of the properties under environments from normal to severe states, such as high temperature, stress loading and/or corrosive ones under heavy irradiation. Therefore, a wide spectrum of special knowledge of different fields is necessary.

A distributed database system, for designing and selecting has been built under the cooperation of National Research Institute for Metals (NRIM), Japan Atomic Energy Research Institute (JAERI) and Power Reactor and Nuclear Fuel Development Corporation (PNC). In 1993, other three research organizations: National Research Laboratory of Metrology (NRLM), Ship Research Institute (SRI) and the Japan Information Center of Science and Technology (JICST); were connected to this system. The system is called as "Data-Free-Way" and has been built since April of 1990. This project is to build the system within five years, focusing on advanced nuclear materials, such as new structural metals, intermetallic compounds, ceramics and composites. Input data will be captured from results of Fundamental Research on Nuclear Materials supported by Science and Technology Agency of Japan.

In the pilot system, a new method to share data and meta-data among the databases of the respective institutes is demonstrated. The merits to share data and the methods to obtain the knowledge in the distributed data system were discussed through irradiation data on tensile and creep properties of type 316 stainless steel.

In NRIM besides the cooperated construction of distributed database for nuclear materials a simulation system of nuclear transmutation and radioactivation is being created.

Related Papers

Present Status of Data-Free-Way (Distributed Database for Advanced Nuclear Materials), H. Nakajima, N. Yokoyama, F. Ueno, M. Fujita, Y. Kurihara, and S. Iwata, J. of Nuclear Materials, 191–94 (1992): 1046–50.

Simulation System of Nuclear Transmutation and Radioactivation for Material Design, M. Fujita and T. Noda, Proc. of COMP '93 (1993): 404–09.

117 R&D of Advanced Heat-Resistant Structural Materials for Very High Temperature Gas-Cooled Reactors

April 1990 to March 1995
T. Tanabe, 3rd Research Group
Keywords: high temperature gas-cooled reactor (HTGR), materials-design, testing-and-evaluation

In order to fulfill the national demand for advanced structural materials for high temperature gas-cooled reactors, we have carried out the R&D of new heat-resistant materials for very high temperature use up to 1373 K by combining the

materials-design and the testing-and-evaluation technologies. The present status of the R&D is as follows.

Development of Advanced Material Testing-and-Evaluation Technologies

The investigations on the creep crack growth rate anisotropy of Inconel MA754 at 1273 K in air were done by using CT specimens with the stress axis parallel (L direction) and perpendicular (LT direction) to the elongated grains of the alloy. The results obtained were as follows.

1. In the specimens with L direction, side grooves hinder the crack growth along the elongated grain boundaries effectively.
2. Creep crack growth rates in the accelerated region of crack growth can be evaluated by C* parameter and the rates are faster in LT direction of the alloy than in L direction, of Inconel 713C and of Ni-26%Cr-17%W (1408).

Development of Advanced Heat-Resistant Materials

Trials to manufacture ODS Ni-Cr-W alloys were carried out by mechanical alloying of powders of the constituent elements in Ni-26%Cr-17%W and those of Y_2O_3. In spite of their high values in hardness (Hv > 400), their creep rupture lives at 1373 K in an HTGR He environment were extremely inferior to those of 1408 because of their small grain sizes. From these results, efforts to get the alloy with large elongated grains are being done. Further, the effect of Ta addition on the creep rupture lives of 1408 was investigated at the same condition mentioned above. The results show that the lives of 1408 with 1wt% Ta will be longer at the lower stress levels than those of MA754 in the LT direction.

Related Papers

Creep Properties under Varying Stress/Temperature Conditions on Nickel-Base Heat-Resistant Alloy Hastelloy XR, H. Tsuji, T. Tanabe, Y. Nakasone, and H. Nakajima, J. Nucl. Sci. Tech., 30 (1993): 768–76.

Corrosion Behavior of Ni-Base Superalloys at 1373 K in Simulated HTGR Impure Helium Gas Environment, I. Mutoh, Y. Nakasone, K. Hiraga, and T. Tanabe, J. Nucl. Mater., 207 (1993): 212–20.

Creep Rupture Properties under Varying Load/Temperature Conditions on a Nickel-Base Heat-Resistant Alloys Strengthed by Boron Addition, H. Tsuji, T. Tanabe, and H. Nakajima, J. Nucl. Mater., 208 (1994): 111–18.

Cavitated Creep Fracture in a Ni-Base ODS Alloy at 1273 K, K. Hiraga, T. Iwama, and T. Tanabe, *Proc. 3rd Japan Int. SAMPE Sympo. "Advanced Materials"—New Process and Reliability*, edit. by T. Kishi, N. Takeda, and Y. Kagawa, (1993): 2040–45.

Effect of Carbon Content and Helium Gas Environment on Creep Crack Growth Properties of Ni-26% Cr-17%W-0.5%Mo Alloy at 1273 K, M. Tabuchi, Y. Nakasone, T. Ohba, K. Yagi, and T. Tanabe, Metall. Trans., to be published.

[118] Study on Changing the Properties of Metallic-Oxide Films for Increasing the Hydrogen Permeability

April 1991 to March 1994

M. Amano, Physical Properties Division

Keywords: oxide film, hydrogen penetration, reaction method, hydrogen separation

It has been found that palladium-coated V-15at%Ni alloy membrane is a promising material for hydrogen separation. It shows good resistance to hydrogen embrittlement with hydrogen permeability larger than those of Pd-Ag alloy membranes. However it reveals a conspicuous hydrogen trapping phenomenon below 473 K. The phenomenon is mainly caused by the oxide film under the palladium overlayer. It is difficult to remove oxide film before palladium coating even in a high vacuum. The aim of this study is to increase the hydrogen permeability of oxide films on metals and alloys based on V_a elements by changing the composition and structure of the films through a reaction method. It has been found that the deposition of a few nanometer lanthanum or yttrium before palladium coating markedly suppresses the hydrogen-trapping phenomenon below 473 K for the V-15at%Ni alloy membrane. The depth profile of Auger electron spectroscopy analysis for the oxide film revealed that the vanadium oxide was reduced and the oxide consisting mainly of lanthanum or yttrium was formed underneath the palladium overlayer. The reaction method was not useful for palladium-coated vanadium and niobium membranes. The cause of the difference in hydrogen permeation between the alloy membrane and vanadium or niobium membrane is now studied.

[119] Material Chemistry in the Extreme Conditions under Irradiation

April 1989 to March 1994

M. Kitajima, 2nd Research Group

Keywords: irradiation, dynamic process, surface reaction, surface lattice disordering

Materials are subject to both chemical and physical attacks by particle bombardment at the same time under irradiation. The purpose of this research is to elucidate mechanisms of the irradiation activated surface reaction and to develop new analytical techniques for that with emphasis of real-time observation of dynamic process. Kinetic or phenomenological modeling on the surface reaction and surface damage processes is also our target. From this viewpoint we're investigating time-dependent behaviors for surfaces of graphite,

silicon and other materials during and after ion irradiation, by using a real-time Raman technique which we had developed in this research project, and have got very new information on ion-mass dependence of lattice disordering rate and the relaxation processes of defects produced by ion irradiation. *In situ* real-time ellipsometry was also performed to study growth kinetics of ultra thin oxide during oxygen plasma discharge, and plasma characteristics were examined using the Langmuir probe, emission spectroscopy and mass spectroscopy to compare with the surface reaction rate. We have found a surface orientation effect of the plasma oxidation rate of silicon using the real-time ellipsometry, and recently have started a study on sample bias effect on the ultra thin silicon oxide growth. In addition to these studies, we are measuring TOF spectra of molecular intermediates emitted from surface through chemical reaction between the surface and molecular beam using laser chemistry.

Related Papers

Thermal Relaxation of Ion-Irradiation Damage in Graphite, E. Asari, M. Kitajima, K.G. Nakamura, and T. Kawabe, Phys. Rev., B47 (1993): 11143–48.

Lattice-Disordering in Graphite under Rare-Gas Ion Irradiation Studied by Raman Spectroscopy, K.G. Nakamura and M. Kitajima, Phys. Rev., B449 (1994): 1011–15.

Silicon Wafer Orientation Dependence in The Initial Plasma Oxidation Processes, H. Kuroki, K.G. Nakamura, T. Kawabe, and M. Kitajima, Solid St. Commun., 88 (1993): 487–89.

Real-Time Observation of Refractive Index Change under Ultra Thin Oxide Film Growth, H. Kuroki, T. Kawabe, and M. Kitajima, Solid St. Commun., 88 (1993): 785–88.

Multiphoton Ionization Detection of SiO Molecules Formed by O_2 Oxidation of Silicon Surface, K.G. Nakamura, H. Kuroki, and M. Kitajima, J. Appl. Phys., 75 (1994): 4261–63.

Bio-Materials

⑫⓪ Spectroscopic and Electrochemical Investigation of the Metal Complexes with an Unusual Electronic Structure

April 1994 to March 1997

H. Isago, Chemical Processing Division

Keywords: metal complex, antimony, phthalocyanine, electronic structure

The fabrication of molecular devices, where one molecule functions as one device, is one of the most attractive and challenging theme in current and future science. Some materials in biological systems, such as proteins (including enzymes), can be considered as well-designed molecular devices. In numbers of such materials in biological systems, unusual electronic structures have been often observed. Therefore, it is a key step to the fabrication of molecular devices to find out compounds with an unusual electronic structure. In this meaning, metal complexes are particularly of interest as model compounds for such materials in biological systems because numbers of such materials contain some metal ion(s) in their reaction centers which have an unusual electronic structure.

We have investigated some metal complexes of phthalocyanine, which have attracted much attention as a group of new advanced materials in recent years. For example, it was found in this laboratory that bis(phthalocyaninato)lanthanoids(III) exhibited remarkable electrochromic properties in organic solvents and in solid state as thin film. In these compounds, unlike usual molecular compounds, a hole is created in the complex molecule. This work is intended to understand the unusual electronic structures of the above-mentioned bis(phthalocyaninato)lanthanoids(III) complexes from the view points of $\pi - \pi$ interaction between the two cofacial phthalocyanine chromophores mainly by using spectroscopic, electrochemical, and spectroelectrochemical techniques. Furthermore, we will try to prepare previously unknown antimony-phthalocyanine complexes. It is because that antimony is stable in trivalent oxidation state and has a close ionic radius to those of lanthanoids(III), and hence, bis(phthalocyaninato)antimony(III), which has a hole in the molecule, is expected to form.

The results of this work will serve not only for the fabrication of molecular devices but also for further understanding of supramolecular chemistry.

121 Bacteria Reaction on Materials

April 1993 to March 1995

H. Masuda, Failure Physics Division

Keywords: Cu, QCM, bacteria

The reaction caused by bacteria is safe to the environment. This reaction is intended to be applied to the various processes, such as refining process. However this reaction is too slow to use for the industrial purpose. Our main purpose in this study is such that, using new measurement device such as the quartz crystal microbalance (QCM) and the atomic force microscope (AFM), we analyze the behavior of bacteria in various environment and finally control the behavior of bacteria.

This year we developed the QCM system to measure the bacteria reaction. 10 MHz quartz crystal coated with electrically deposited Cu was used to measure the reaction rate of bacteria (Thiobacil-

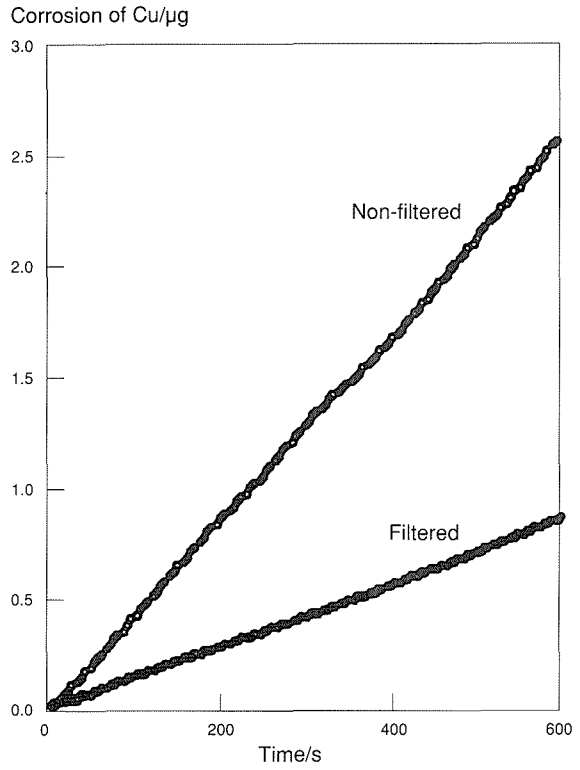

Fig. 6 Corrosion rate of Cu in culture solution after 240 h cultivation.

lus ferrooxidans). In this QCM system, the mass change of 450 ng for Cu can be detected by the frequency shift of quartz crystal. The bacteria oxidized Fe^{2+} into Fe^{3+}, and the Fe^{3+} oxidized Cu into Cu^{2+}. The oxidation rate of Cu depends on the amount of Fe^{3+} when the amount of Fe^{3+} is small. Figure 6 shows the bacteria reaction measured by QCM system. The reaction rate difference between the filtered and the non-filtered environment corresponds to the rate of bacteria reaction. Thus the rate of bacteria reaction can be measured by this system.

122 Fundamental Study on Biocompatibility of Materials

April 1993 to March 1999

M. Sumita, Mechanical Properties Division

Keywords: biomaterial, pseudo-body fluid, cytotoxicity, cell adhesion, debris, corrosion, fretting fatigue

With the increase in the number of the aged, those who have to be implanted biomaterials in their body increase. It is important that the materials exist and function in their body without any trouble for many years until they die. Release of metallic ions and debris from materials implanted in body should be avoided, because they always or infrequently cause carcinogenicity, physical deformity enhancement and allergies. Unexpected failure of materials implanted also should be avoided, because the resultant reoperation forces the patient physical and mental pains. Therefore, non toxicity, adhesion to tissue, control in bioreaction caused by foreign bodies, sufficient resistance to corrosion and wear, and long fatigue life are considered as necessary characteristics for the biomaterials used in vivo conditions.

As metallic materials had the higher strength and the higher toughness than all of the other materials, 316L stainless steel, Co-Cr-Mo alloy, Ti-Al-V alloy, etc. have experimentally been used as the biomaterials. However, no biomaterials, which have no problems in biocompatibility exist.

The content of the present research subject is as follows.

1. Quantitative evaluation of toxicity of materials through cell culture method, and analysis of the relationship between the critical value of toxicity and state analysis of a very small amount of material in the pseudo-body fluid in which wear test and fretting fatigue test performed.
2. Measurement of the adhesion force of a cell to the surface of a material, and observation of cell degeneration caused by foreign body and mechanical stimulus.
3. Evaluation of wear strength, fatigue strength, and fretting fatigue strength of materials in a pseudo-body fluid.

123 Improvement of Wear Properties of Metallic Medical Materials

April 1992 to March 1994

A. Hoshino, Physical Properties Division

Keywords: medical material, titanium alloy, stainless steel, fretting corrosion, tribological properties

Although titanium alloy exhibits a good combination of both mechanical and corrosion resistance under static condition, the resistance to fretting corrosion under dynamic condition is less than that of stainless steel group.

In order to understand the degradation mechanism and improve the tribological properties of titanium alloys for surgical implants, the fretting corrosion test of α/β type Ti-6Al-4V was conducted in saline solution at 37 °C.

It has been found that the corrosion potential of titanium alloy during the fretting corrosion test becomes less noble than 316L stainless steel and the anodic current (metal ions release) of titanium alloy is remarkable compared with stainless steel. The increase in surface hardness by means of heat treatment of the α/β type titanium alloy was not controlling factor for fretting corrosion loss of metallic biomaterials.

Related Papers

Consideration on Coupling Application of Biomedical Titanium Alloy with Stainless Steel, A. Hoshino, Zairyo-to-Kankyo, 42 (1993): 291–96.

Application of Biomedial Titanium Alloy Coupled with Stainless Steel, A. Hoshino, Corrosion Engineering, 42 (1993): 341–50.

124 Monitoring Reaction Rate of Bacteria

April 1993 to March 1994
H. Masuda, Failure Physics Division
Keywords: Cu, QCM, Bacteria

The reaction caused by bacteria is safe to the environment. However this reaction is too slow to use for the industrial purpose. Our main purpose is monitoring the bacteria reaction and finding the best environment for bacteria reaction.

First we developed the QCM system to measure the bacteria reaction. 10 MHz quartz crystal coated with electrically deposited Cu was used to measure the reaction rate of bacteria (Thiobacillus ferrooxidans). In this QCM system, the mass change of 450 ng for Cu can be detected by the frequency shift of quartz crystal. The bacteria oxidized Fe^{2+} into Fe^{3+}, and Fe^{3+} oxidized Cu into Cu^{2+}. The oxidation rate of Cu depends on the amount of Fe^{3+} when the amount of Fe^{3+} is small. The reaction rate difference between the filtered and the non-filtered environment corresponds to the rate of bacteria reaction. Figure 7 shows the change of the rate of bacteria reaction with the culture time. The rate of bacteria reaction increased exponentially and then saturated. These phenomena are coincident with the reported phenomena.

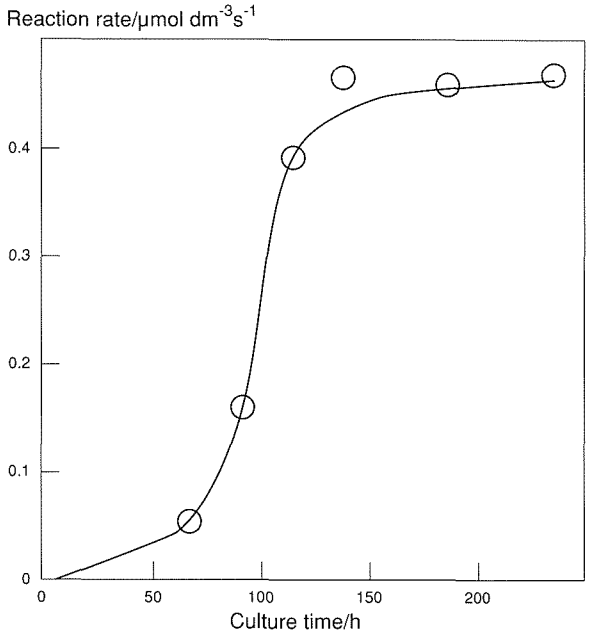

Fig. 7 Change of reaction rate of T. ferrooxidans with culture time

Processing

Separation and synthesis

125 Extraction from Metal to Gas Phase

April 1992 to March 1995
A. Fukuzawa, Chemical Processing Division
Keywords: thermal plasma, low pressure plasma jet, vaporization

Thermal plasma produced by transfer or non transfer type torch is widely used for melting metals and lining. However, its operating pressure is usually at atmospheric pressure, and in some case low pressure plasma jet is used, but its pressure is not less than 100 torr.

This research work is to investigate the behavior of plasma jet in lower pressure of 10 torr order and apply to the gaseous extraction of tramp elements like Cu, Sn, Ga or Cr from liquid iron or steel by the help of ultra high temperature of plasma jet. As in the preliminary test, glow discharge was observed at around 10 torr, later gaseous extraction experiments were carried out over 20 torr. It became clear that the extraction of Cu in iron is much higher than that of Sn at the same temperature and pressure, as expected from the difference of activity coefficients at dilute solution between both elements. However, as the relation between their extraction rates is not proportional to the activity coefficient, further consideration based on the kinetics should be taken as the other factors which affect the vaporization of these elements.

This technology can be applied for the extraction of various kinds of elements from molten steel, especially from steel scrap, by installing plasma torch at the top of RH degassing process.

126 Fundamental Study on Preparation and Characterization of the Metal Complexes Possessing a Peculiar Molecular Structure

April 1991 to March 1994
H. Isago, Chemical Processing Division
Keywords: metal complex, bismuth, cerium, phthalocyanine, preparation

Phthalocyanines and their metal complexes have attracted much attention as a group of new advanced materials in recent years. For example, it was found in our laboratory that bis(phthalocyaninato)lanthanoids(III) exhibited remarkable electrochromic properties in organic solvents and in solid state as thin film

In this work, we have investigated preparation and characterization of (1) bis(phthalocyaninato)cerium complex and its derivatives and (2) bismuth(III)-phthalocyanine complexes.

In subject (1), it was found that the cerium ion in the cerium complex, which showed exceptional properties among a series of bis(phthalocyaninato)lanthanoids(III), was in mixed valence state between trivalent and tetravalent states mainly by spectroscopic techniques. The Ce 4f orbital was found to be covalently hybridized with a phthalocyanine π orbital. In subject (2), we were able to isolate bismuth(III)-phthalocyanine complexes for the first time as a phthalocyanine complex of group-15 elements and successfully characterize them by chemical and spectroscopic techniques. It is noteworthy that only monophthalocyaninato complexes were isolated and no experimental evidence for the formation of bisphthalocyaninato complex was obtained whereas lanthanoids readily formed bisphthalocyaninato complexes under the same conditions although both bismuth and lanthanoids are stable in trivalent oxidation state and have a close ionic radius to each other.

Related Papers

Mixed Valence State of Cerium in Bis(phthalocyaninato)cerium Complex, H. Isago and M. Shimoda, Chem. Lett., (1992): 147–50.

Syntheses and Characterization of Bromo- and Chloro(phthalocyaninato)bismuth(III) Complexes, H. Isago and Y. Kagaya, Bull. Chem. Soc. Jpn., 65 (1994): 383–89.

127 Alloying Method Using Decomposition of Metal Halides

April 1991 to March 1994

G. Omori, Advanced Materials Processing Division

Keywords: alloying, decomposition, metal halides, zirconium, magnesium

The purpose of this work is to obtain basic information for developing new alloying techniques which use decomposition phenomena of metal halides; an investigation was conducted for making Mg-Zr alloys.

Mg-Zr alloys are rather promising in various applications that require low density and high strength, because magnesium is a light element and zirconium is an effective grain refiner of magnesium. There are, however, knotty problems in practical alloying procedures; zirconium of elemental form, for example, is not suitable for alloying because of its high melting point and high oxidation tendency.

It was found that a mixture of $ZrCl_4$ and ZrF_4 was excellent as an agent for Mg-Zr alloy making. Using an electric furnace, a block of magnesium was melted in a crucible of low nickel stainless steel under SF_6 atmosphere to prevent the melt from oxidation, and the addition of zirconium to magnesium was done by putting in it the powder or briquette of the blend of $ZrCl_4$ and ZrF_4 fixed with a sort of phosphorizer.

It was realized that $ZrCl_4$ played an important role in the alloying reactions; the compound $ZrCl_4$, compared with ZrF_4, has relatively low physicochemical stability, as it shows sublimation at 604 K and easy hydrolysis as well as deliquescence, and it reacts with Mg exothermically at temperatures lower than that of the reaction between ZrF_4 and Mg.

Based on the obtained experimental data, it is supposed, as a scenario of the alloying reaction, that a small part of $ZrCl_4$ is reduced by magnesium at first, resulting in the dissolution of Zr in magnesium and the formation of $MgCl_2$, and this reduction supplying heat, triggers off further reduction of $ZrCl_4$ and formation of $MgCl_2$. While, a part of this $MgCl_2$ will react with ZrF_4 resulting in the formation of MgF_2 and $ZrCl_4$, and this $ZrCl_4$ subsequently reacts with Mg.

As the total of this cyclic reaction of the mixture of $ZrCl_4$ and ZrF_4 with Mg and $MgCl_2$, the concentration of $ZrCl_4$ fairly decreases relative to ZrF_4, and this inspissation of ZrF_4 is found to be effective further in suppressing the size growth of $MgCl_2$ inclusion particles dispersed in Mg-Zr alloys.

Gaseous process

128 Precise Composition Control of Ordered Alloys by Chemical Transportation Techniques

April 1992 to March 1995

H. Sasano, Physical Properties Division

Keywords: ordered alloys, shape memory alloys, reversible color change alloys, chemical transportation technique

Ordered alloys are expected to have attractive properties. However, the properties are very sensitive to the composition of the alloys. It is hard to control the composition precisely by conventional methods. We succeeded in controlling zinc or cadmium concentration in shape memory alloys and reversible color change alloys with accuracy of 0.1 percent by solid–vapor diffusion couple method. In this method, components to be applied are restricted to elements which have high vapor pressure. In this study we try to control the concentration of elements which have low vapor pressure.

We attempted to control aluminum concentration in nickel alloys by controlling heating temperatures of pure nickel plates and mixture of aluminum powder and ammonium chloride placed in a closed alumina tube independently. It was expected that aluminum chloride gas formed by the reaction of aluminum with ammonium chloride would decompose on the nickel surface and then

aluminum would diffuse into nickel. Aluminum concentration on the nickel plates lay only in the single gamma, delta, epsilon phase regions and the region of solid solution of nickel side in the aluminum-nickel binary phase diagram and kept constant values even when the heating duration changed. From these results it was found that aluminum concentration in nickel alloys could be precisely controlled by this method.

129 Processing and Development of Isotopically Controlled Materials (ICM)

April 1992 to March 1997
T. Noda, 2nd Research Group
Keywords: isotopically controlled materials, ICM processing facility, laser CVD, chemical vapor infiltration

Materials composed of isotopically selected elements realize the essential solution of subjects such as induced activity, He embrittlement, and compositional change caused by reactions with energetic particles.

The objectives of the program are (1) R&D of *in situ* ICM processing facility (ICMPF) utilizing infrared multi-photon decomposition reaction, (2) search of working materials for isotope separation, (3) development of *in situ* synthesis of isotopically controlled SiC, Si_3N_4, BN, etc. and (4) development of ceramics and their composites with advanced properties.

The following results were obtained.

1. The isotope separation experiment using Si_2F_6 was conducted under the irradiation of pulse infrared laser with an energy range of 3.0–6.3 kJ/m^2/pulse. SiF_4 with condensed ^{29}Si and ^{30}Si was produced by the irradiation of the laser at 944–967 cm^{-1} while ^{28}Si was concentrated in the residual Si_2F_6 gas.
2. Si_2F_6, working gas for Si isotope separation, was synthesized with 80% of efficiency from Si_2Cl_6 and ZnF_2. Infrared spectroscopy showed a typical spectrum of Si_2F_6 and no other impurities disturbing above experiments were found.
3. The simulation code, IRAC, calculating transmutation and induced activity, and decay heat under various neutron irradiation conditions covering thermal to 14 MeV neutrons predicted superiority of ICM to conventional materials.
4. The examination of SiC film synthesis from SiF_4 gas and SiF_2 polymer was started using excimer laser CVD technique.
5. Chemical vapor infiltration process to obtain SiC composite with a high purity and improved mechanical properties is being developed. Pre-carbon coating around carbon fibers was found to be effective to improve the strength and toughness of carbon fiber/SiC composite.

Related Papers

Microstructure and Growth of Sic Film by Excimer Laser CVD at Low Temperatures, T. Noda, H. Suzuki, H. Araki, F. Abe, and M. Okada, J. Mat. Sci., 28 (1993): 2763–68.

Effect of Incident Direction of ArF Laser to Graphite Substrate on the Formation of Photo-CVD SiC Film, H. Suzuki, T. Noda, H. Araki, J.J.A.P. Part 1, 32 (1993): 3566–71.

Isotope Controlled Materials, T. Noda, Kinzoku, (1993): 32–37.

130 Development of Shape Memory Thin Films Formed by PVD Method

April 1993 to March 1998
A. Takei, 3rd Research Group
Keywords: micromachine, shape memory, Ti-Ni, sputtering

Micromachines such as micromanipulators and fluid microvalves are expected to be used in the near future in various fields such as biotechnology, medicine and the semiconductor industry. In order to produce such a micromachine, the development of an effective microactuator is essential. Recently we demonstrated that Ti-Ni thin films formed by sputtering could be a promising candidate for such an actuator due to their shape memory effect.

In this research work the factors that affect shape memory characteristics of thin films have been investigated. The results showed that aging effect is an important factor to obtain perfect shape memory effect. A plastic strain after a thermal cycle was decreased from 0.4% to 0.1% by annealing at 500 °C for 1 h for a Ti-51at%Ni thin film. This film exhibited perfect superplasticity as well as perfect shape memory effect.

This research was performed in collaboration with Tsukuba University.

Related Papers

Shape Memory Characteristics of Sputter-Deposited Ti-Ni Thin Films, S. Miyazaki and A. Ishida, Materials Transactions, JIM 35 (1994): 14–19.

Shape Memory Thin Film of Ti-Ni Formed by Sputtering, A. Ishida, A. Takei, and S. Miyazaki, Thin Solid Films, 228 (1993): 210–14.

Liquid state process

(131) Basic Study on Refining of Molten Metal and Controlling of Solidification by Electromagnetic Force

April 1994 to March 1997
A. Fukuzawa, Chemical Processing Division

Keywords: cold crucible, levitation melting, electromagnetic force

Cold crucible type levitation melting method using high frequency electric power is known as non-contacting melting method. Therefore, this melting method is advantageous for melting of high purity metals, chemically reactive metals and refractory metals.

In these several years, we have made various kinds of trials on the cold crucible type non-contacting induction furnace and many fundamental results concerning with the cold crucible have been obtained.

One of other advantages of this melting method is to have the separating ability of inclusions from the molten metal, because magnitude of electromagnetic force working toward the molten metal is different from that of inclusions by the physical properties of metal and inclusions. So the shape of the cold crucible, high frequency coil and the electric output power are to be examined to obtain the optimum levitating conditions for separating inclusions from molten metal considering physical properties of materials for melting. Separating mechanism and separating rate of inclusions from levitated molten metal are to be also examined.

⑬② Investigation on Nucleation and Crystal Growth Mechanism under Heterogeneous Ambient Phase

April 1994 to March 1996

T. Fujii, Chemical Processing Division

Keywords: nucleation, crystal growth, peritectic reaction, secondary recrystallization, exaggerated grain growth

The purpose of the present study is to obtain the fundamental knowledges for controlling the following crystal growth processes, which occur in the circumstances containing other solid phases of foreign particles.

1. Nucleation and crystal growth with peritectic reaction.
2. Nucleation in solid state reaction and exaggerated grain growth.

Recently, high J_c values have been obtained in the bulk specimens of high T_c oxide superconductors fabricated by means of peritectic solidification process. However, the growth mechanism of these crystals and the role of peritectic reaction in the growth process have not been revealed. In the first subject, we intend to clarify such a growth mechanism on $YBa_2Cu_3O_x$ crystals which melt incongruently at 1000 °C through the metallographic observation and the measurement of growth parameters on the quenched specimens grown at various temperatures.

Investigation will be also made on salicylic acid-acetamid system, in which a peritectic compound at the composition of 1:1 ratio forms at 65 °C. It is possible to observe *in situ* the crystal growth process by means of optical microscopy in this experiment.

In the second subject, we aim to develop the theory of the normal and abnormal grain growth process so as to apply it to the growth of single crystals of intermetallic and ceramic materials as well as metallic materials.

⑬③ Solidification Processing for Particle Dispersed Unidirectionally Grown Composites

April 1994 to March 1996

A. Sato, Advanced Materials Processing Division

Keywords: solidification processing, unidirectional solidification, composite, particle dispersion

Many kinds of composite materials combined various matrix alloys with numerous reinforcing materials are being produced by multitudinous processings. Therefore, the cost performance of the processing and the properties of the composite material are the most important factors in production of composite materials. Particle dispersed composites of these composite materials can be manufactured at the lowest cost by solidification processings. The properties of particle dispersed composites can be improved by controlling the structure of the matrix alloy. The purpose of this study is to obtain basic knowledges and fundamental techniques on the followings.

1. The optimum conditions of the mechanical alloying to make particle uniformly dispersed powder samples.
   a. matrix alloys; composition, size, configuration,
   b. reinforcing particle; composition, size, configuration, volume fraction, and
   c. mechanical alloying; strength of stirring, duration of stirring, size and number of balls.
2. The optimum conditions of sintering to produce samples to be used in the following solidification experiment: porosity, temperature, duration of sintering.
3. The optimum conditions of solidification of powder and sintered samples in unit gravity environment on the earth: solidification velocity, temperature gradient, volume fraction of dispersed particle, size and configuration of particle.
4. The optimum condition of unidirectional solidification: solidification velocity, temperature gradient, volume fraction of dispersed particle, size and configuration of particle.
5. Effect of wettability of the particle added on the engulfment/pushing particle at the unidirectional solidification interface as a function of solidification conditions.

6. Effect of gravity on the engulfment/pushing particle at the unidirectional solidification interface as a function of solidification conditions.

134 Basic Technology Development of Materials Processing in a Short-Duration Microgravity Environment

April 1992 to March 1995

A. Sato, Advanced Materials Processing Division

Keywords: microgravity, solidification, combustion synthesis, superconductor

This project is designed in order to use the drop tower facility at Kami-sunagawa in Hokkaido (μG for 10 s) and Toki in Gifu (μG for 4.5s). This project consists of 19 sub-themes, and three of them are being carried out in NRIM.

A Study on Double Combustion Synthesis Apparatus

Combustion syntheses of TiNi from Ti and Ni mixture powder were studied in this fiscal year. The experiments were carried out using the same combustion synthesis apparatus in order to compare 1 G and micro-G result exactly. The velocities of propagation of combustion synthesis were measured by two sets of W-Re thermocouple. The velocity of propagation in 1 G experiment was 1.59 mm/sec and 1.03 mm/sec in micro-G. The velocity reduction in micro-G was due to the lack of convection of the liquid Ni phase.

Observation of Harbingering Phenomena of Solidification/Crystallization

The purpose is to clarify how the macroscopic structure of solidified materials is formed. In 1993, we performed experiments using transparent materials, and results obtained were as follows. The nucleation occurred at the contact point of liquid meniscus and the mold wall. Then, number of crystals were formed by the detachment of dendrites grown. Three mechanisms of the dendrite detachment were observed: fluid flow, collision among dendrites, and collision with mold wall.

Study on the Synthesis of High Temperature Superconductors

The purpose of this subject is to investigate the influences of gravity on various solidification phenomena of oxide high temperature superconductors (HTSC), because the solidification is one of the most promising processes to fabricate wire, thick film and bulk materials of HTSC. In 1993, we have focused on the investigations on the phase and microstructural changes during melting and solidification of $Bi_2Sr_2Ca_1Cu_2O_x$ and its composites with Ag and MgO. We have found that Ag and the free surface of liquid phase have great effects on the melting point, the stability and the grain alignment.

135 Metastable Phase Solidification from Undercooled Liquid by Inducing External Nucleation Seed

April 1993 to March 1996

S. Tsukamoto, Advanced Materials Processing Division

Keywords: solidification, metastable phase, levitation melting, undercooling

Metastable metallic materials produced from deeply undercooled melts can provide some interesting materials properties. In the previous work, we indicated that the metastable phase solidification could be induced with relative ease if the barrier to the nucleation could be avoided due to an epitaxial growth from pre-existing matrix of different solidification mode in rapid solidification of electron beam skin melting. The aim of this investigation is to elucidate the role of nucleation during the solidification of undercooled melts and to develop a new technique for producing metastable bulk materials using a levitation melting method and an external seeding.

In the present year, the correlation between undercooling and competitive phase selection of equilibrium and metastable phases was examined using AISI 316 stainless steel with primary ferritic solidification mode. The 700 mg samples were melted and solidified in the levitation coil by controlling the flow rate of cooling gas under the constant power of the induction coil. When a recalescence event was recognized, the power was shut down and the sample quenched in a tin bath. The undercooling varied from 20 to maximum value of 220 K depending on the cooling rate in the range 1–65 Ks^{-1}. The solidification mode changed from primary ferritic to austenitic (metastable phase) when the undercooling exceeded 180 K in spite of the facts that $T_{0\gamma}$ of the material is only 10 K below the liquidus and the growth velocity of the austenite is larger than that of ferrite. This means the ferrite is more favored in regard to the nucleation over a wide range of undercoolings.

This research was performed in collaboration with Research Development Corporation of Japan and University of Cambridge.

Related Paper

Metastable Phase Solidification in Electron Beam Welding of Dissimilar Stainless Steels, S. Tsukamoto, H. Harada, and H.K.D.H. Bhadeshia (Univ. of Cambridge), Mater. Sci. and Eng., A 178 (1994): 189–94.

136 Purification of Metals by Non-Contacting Melting Method

April 1991 to March 1994

A. Fukuzawa, Chemical Processing Division

Keywords: cold crucible, levitation melting

The purpose of this study is to develop the electromagnetic levitation melting process of reactive metals and refractory metals using the cold crucible type non-contacting induction furnace. Up to now, the reaction between metal and crucible has made it difficult to purify the reactive metals and there has been no crucible materials for homogeneous melting of refractory metals. The cold crucible type melting method will solve these problems.

In these several years, we have made various kinds of trials on the cold crucible type non-contacting induction furnace and many fundamental results concerning to the cold crucible have been obtained. Moreover, we have developed the levitation control techniques; supplying different two frequencies in order to obtain optimum levitation conditions corresponding to any molten metals and alloys that have various physical properties such as density, electrical resistance, and melting point.

A new conception of levitation controlling is that two sets of coils are arranged around the cold crucible and two high-frequency currents are supplied from two electric power sources which have different frequency. The higher frequent currency is supplied to the upper coil, and the rather lower frequency current is supplied to the lower coil. The role of the lower coil is mainly levitation of material, for the levitation force is proportional to the square root of reciprocal of electric source frequency. The role of the upper coil is mainly heating of material, for the eddy current in the material to be melted is more converged to the surface of the material and heating efficiency is improved with the increase of electric source frequency.

[137] Solidification Processing for Fine-grain Structure Materials

April 1991 to March 1994

A. Sato, Advanced Materials Processing Division

Keywords: solidification processing, fine grain structure, rapid solidification, vigorous agitation

Many kinds of materials composed of various grain structures can be produced by solidification processings. Grain structures can be divided roughly into following three categories: (1) A coarse-grain structure, or a single-crystal structure in the extreme case; (2) A fine grain structure, or an amorphous structure in the extreme case; (3) A usual poly-crystal structure found in conventional castings. The coarse-grain structure or the single-crystal structure can be obtained by slow undirectional solidification, while the fine-grain structure or the amorphous structure can be realized by rapid solidification. The usual poly-crystal structure is acquired at a common solidification rate.

The research on the production of ingots composed of the fine-grain structure was carried on by rapid solidification process along with vigorous agitation. An apparatus for this process was constructed, and experiments using Al-20 mass%Si alloys were carried out. The results obtained shows that the grain size of the primary silicon decreases at a higher revolution speed and a bigger diameter of the stirring rod, and at a more rapid cooling of the mold.

The effect of the ultrasonic vibration added during solidification of cast irons were examined through the inspection of their microstructures and the grain size of graphite particle crystallized. The ultrasonic vibration was added onto the molten cast iron through the SIALON horn vibrated at 18.7 kHZ × 13 μm. The results obtained showed that the size of graphite in C/V and ductile cast irons vibrated are smaller by 2 or 3 times than that in those without vibration.

[138] Measurements, Analyses and Evaluations of Specimens Made by FMPT

April 1992 to March 1994

A. Sato, Advanced Materials Processing Division

Keywords: microgravity, solidification, fluid flow, superconductor, diffusion

FMPT (First Material Processing Test of Japan) was performed in September, 1992, in Space Shuttle (SL-J mission). Researchers of our Institute are responsible for the following 5 themes out of 22 materials processings in the total 34 themes.

Production of Compound Semiconductor Crystals by Floating Zone Melting

The crystal of InSb processed in space was ϕ 20–30 mm × 100 mmH. This experiment was the first experiment aimed at growing a single crystal of a compound semiconductor by floating zone method. The surface of the molten zone was covered with an oxide thin film during growing in space. Floating liquid column was sustained not only by its surface tension, but also by the thin oxide film. Solidification was proceeded in the skin. Nucleations and growth twins were generated from the oxide film. X-ray topography shows that most portion of the crystal is of high quality and of low dislocation density. Characteristic growth striation patterns by the convection flows were not observed on the X-ray topographies. The values of the electric resistivity were from 4×10^{-5} Ωm to 8×10^{-5} Ωm along the growth axis. The thin oxide film served as a flexible container which gives the crystal no stress and suppresses the Marangoni convection flow.

Production of News Superconducting Materials

The samples examined were monotectic Al-Pb-Bi alloys and eutectic Ag-Ln-Ba-Cu (Ln = Y, Yb) and

Ag-Cu alloys. The experiment was done by using continuous heating furnace (CHF) of FMPT. For Al-Pb-Bi alloys, we obtained uniform dispersion of Pb-Bi particles in Al matrix by the flight experiment, while the ground samples showed a large gravitational segregation. By deforming the flight Al-Pb-Bi alloy samples, and by oxidizing Ag-Ln-Ba-Cu alloy samples, we succeeded to fabricate *in situ* composite superconductors, fine Pb-Bi superconducting filaments in Al matrix and high temperature oxide superconductors in Ag matrix.

Formation Mechanism of Deoxidation Products in Iron Ingot Deoxidized with Two or Three Elements

To reduce the oxygen level in steel, deoxidation with two or three elements (hereafter combined deoxidation) is usually taken instead of an element because of its high deoxidation ability. But the contribution of each element to the combined deoxidation is not clear enough. Since a perfect still bath condition is presented in space or under micro gravity circumstance, deoxidized products are expected to grow at its nucleation site. Al, Si and Mn were chosen as the deoxidizing elements, and iron alloys containing these elements and their mixtures were used. Alloys were sandwiched between iron rods of 5 mmϕ with three levels of oxygen content. Then the sample cartridge was heated in LIF at the programmed heating profile up to around 1600 °C in 54 min. A successful operation in space was reported, but the sample was heated up about 5 min faster than the program according to the record. Samples could be examined, but the occurrence of turbulent flow during melting was obvious after EPMA analysis. There was no significant difference in inclusion shape deoxidized between in space and on ground.

Preparation of Particle Dispersion Alloys

A melting and solidification experiment of TiC dispersion nickel base alloys under microgravity was conducted in order to investigate the effect of gravity on the dispersion of TiC particles and mechanical properties. The inspections and temperature profile confirmed that all systems and devices worked correctly, and that melting and solidification were performed successfully in spite of the melt leakage in FMPT. Experimental results disclosed some definite differences of microstructure and hardness between alloys solidified in FMPT and on the ground. The FMPT processed alloys exhibited a more homogeneous structure and a higher hardness. The macroscopic segregation in the ground samples is caused by thermal convection, bubble motion, and the structural coarsening due to the Ostwald ripening. These experiments demonstrate that the melting and solidification under a microgravity environment promotes a uniform dispersion.

Diffusion in Liquid State of a Binary Alloy System

The concentration profiles of FMPT specimens along their axes (diffusion couple of Au and Ag) were determined by EPMA quantitatively. The following three results were obtained: The diffusion in the flight specimens proceeded much faster than that in the ground ones. The reproducibility of result in the flight ones was less sufficient than that in the ground ones. Diffusion curves of the flight ones were less smooth than that of the ground ones. These results suggest that Marangoni convection occurred at the quasi-free surface near the interface of diffusion specimens.

Solid state process

139 Metallurgical Analysis of Micro-Machining Region

April 1993 to March 1996

S. Yamamoto, Advanced Materials Processing Division

Keywords: micro-machining, metallurgical factor, TiAl, finished surface region

The purpose of this research is to obtain a sound surface region of metallic compound (TiAl) by machining and to microfy the mechanical system.

Decreasing the flaw in the finished surface region of the metallic compound (TiAl) by micro-machining was investigated. If it is possible to produce machine parts of the TiAl having a flawless finished surface region, their production must be increase very much.

The chip form of TiAl changed from needle type to continuous type with decreasing the cutting volume. The tool wear indicated the minimum value at the speed of the chip redness. Such cutting condition is expected to decrease faults of cracks so forth in the finished surface region. On the otherhand, the finished surface by the micro-machining is different for the specific crystal orientation. This is related to the twinning of crystals.

Powder processing

140 Preparation and Characterization of Ultrafine Powders Used for Making Oxide Superconductors

April 1988 to March 1995

S. Ohno, Chemical Processing Division

Keywords: superconducting oxide, superconductive phase, ultrafine powder, Al_2O_3, Ag

Improvement of homogeneity, sinterability, and preferable orientation are expected using finer powders as raw materials for superconducting oxide. One objective of this study is to synthesize the ultrafine powders suitable for making supercon-

ducting oxide. Various preparation methods are conducted such as reactive plasma-metal reaction, RF-plasma CVD, oxalate coprecipitation and citrate sol-gel methods. Then the factor affecting the superconductivity properties is examined, especially on the appropriate composition, particle size, and sintering conditions.

In this study, we have examined the effect of aluminum oxide (Al_2O_3) on the formation of superconductive phases in Bi-Sr-Ca-Cu-O ceramics [Bi:Sr:Ca:Cu = 4:3:3:6] prepared from ultrafine powders. It was found that the formation of superconductive phases was accelerated significantly by adding about 0.2 mass% of Al_2O_3 powder (50 nm) into the mixed oxide, but the addition of Al_2O_3 powder more than 0.5 mass% decreased dramatically the formation of superconductive phases. It was shown by chemical analysis of sintered ceramics that Al_2O_3 has a greater effect on the doping of Ag into the ceramics from a sintering Ag substrate.

141 Synthesis and Characterization of Advanced Materials Utilizing Colloidal Dispersed Systems

April 1993 to March 1995

Y. Sakka, Chemical Processing Division

Keywords: colloid, fine powder, consolidation, gas desorption, nanocomposite

Key developments in processing of fine powders are (1) synthesis of fine powders with controlled sizes, shapes and chemistries, (2) consolidation techniques to control pore volume and pore size distribution, and (3) the role of powders and compacts on the evolution of microstructures during sintering. Although many kinds of techniques in preparing fine powders have been reported, little efforts have been paid on the consolidation of fine powders. In the present study, the emphasis will be on the second and third development.

Colloidal processing of nano-sized powders such as Al_2O_3, ZrO_2, SiC and Si_3N_4 is conducted to obtain green bodies with controlled pore sizes. The most important factor is how to disperse the powders. In the present study, stable suspensions with a solid content of 45 vol% are prepared by adjusting pH and adding appropriate amount of electrolyte.

Electro-discharge sintering is applied to obtain the nanophase materials using ultrafine powders. In this procedure, the powders are heated by instantaneous high electric pulsed power application under a uniaxial pressure.

Characterization of the synthesized materials is another subject. The gas (especially H_2, H_2O, CO and CO_2) sorption-desorption experiments of metal-ceramics nanocomposite particles are conducted for characterizing the catalytic properties.

Related Papers

Processing of Nanocomposite Silicon Nitride-Mullite-Alumina by Reaction Sintering, Y. Sakka and I.A. Aksay, Nanostructured Mater., 4 (1994): 169–82.

Fabrication of Porous Materials by Consolidating Ultrafine Metal Powders, Y. Sakka, T. Uchikoshi, S. Ohno, and H. Okuyama, Proc. Powder Metal. World Congress, (1993): 792–95.

Adsorption of Hydrogen on Ni and Ni-TiO_2 Composite Ultrafine Particles, T. Uchikoshi, Y. Sakka, S. Ohno, H. Okuyama, and K. Yoshihara, Surface Sci., 287–88 (1993): 1082–86.

142 Study on Solid State Chemical Reaction, its Propagation and Materials Synthesis

April 1993 to March 1996

Y. Kaieda, Chemical Processing Division

Keywords: combustion synthesis

The fundamental study to reveal the reactions between solids (powder), solid and liquid, and solid and gas is carried out. The propagation of the reaction and the synthesis process of the materials synthesized through the reaction are also studied. The field of the study covers not only the grasp of the phenomena but the comprehensive understanding of the chemical reaction, the heat transfer, the mass transfer and the other aspects of the synthesis of materials in the solid phase system.

The selection of the combinations of elements, which is focused in the present study, will be investigated. The system of the combination that might exhibit the effect of convection and pressure during the reaction and synthesis process is selected considering the system that performs the effect of liquid and gaseous phase. The system of elements, in which the safety during the experiment is assured, is selected.

Investigation by the thermal analysis with rising temperature in constant speed and/or in alternating speed is carried out to reveal the conditions for the initiation of the reaction, the propagation and the synthesis. The influence of pressure and convection on the phenomena in the reaction process of the system containing gaseous phase or liquid phase is studied using a high gaseous pressure apparatus.

Combustion syntheses of mixture of Ni and Ti powder are carried out in a 100 kg batch scale. The synthesized materials were worked to be wires. The wire samples were examined by a measurement of thermal analysis. The chemical compositions of the sample were as follows: Ni = 56.68 mass%, Ti = 44.11 mass% and O = 0.0677 mass%. The most important Af transformation temperature was decreased with the increase of heat-treating temperature.

143 Study on Properties of Raw Powder of Superconductor using High Pressure Forming

April 1988 to March 1995

Y. Kaieda, Chemical Processing Division

Keywords: combustion synthesis, superconductor, Y-Ba-Cu-O system

National Research Institute for Metals developed the combustion synthesis process for industrial production process to produce many kinds of ceramics and intermetallic compounds using the heat of formation of the combination of the elemental powders in the system. If the combustion synthesis is applied for making Y-Ba-Cu-O system superconductor, the elemental powders should be used to get a heat of formation in the reaction between the starting metallic powders and an oxygen gas in order to ignite and propagate the combustion synthesis. However the pure metallic yttrium powder is unstable and easily oxidized in the air at room temperature and reactive to water. Pure metallic barium is also unstable and oxidized in the air at room temperature and reactive to water and toxic to human body. To the contrary, pure copper is relatively stable in the air and not reactive to water. It may be instinctive to use pure copper powder as a key material for performing combustion synthesis of Y-Ba-Cu-O system superconductor. The values of the heat of formation of copper oxides are 155.3 kJ/mol for CuO.

The combustion synthesis of Y-Ba-Cu-O system superconductor was performed, using the heat of formation of copper oxide, under the absolute pressure range of pure oxygen gas at 1.3 kPa to 12.6 MPa to examine whether the heat of formation of copper oxides is enough for sustaining the propagation of the combustion synthesis and synthesizing the Y-Ba-Cu-O system superconductor. The process of combustion synthesis of Y-Ba-Cu-O system superconductor using pure copper powder and pure oxygen gas was revealed and the samples made by combustion synthesis were characterized.

144 Development of Particles Assembly Technology for Integration of Functions

April 1992 to March 1996

N. Shinya, Failure Physics Division

Keywords: intelligent materials, multiple functions, particle assembly, technology

For creation of intelligent materials, technologies for systematization and integration of multiple functions should be developed in advance. Systematically coordinated multiple functions will lead to manifestation of intelligent functions, such as self-repair, self-diagnosis, feedback and so on, which can respond to environmental conditions.

In order to provide materials with the systematically coordinated multiple functions, a new approach is made through a development of particles assembly technology in this work. Each particle has a primitive function such as sensor, processor and actuator. Therefore coordinations and systematizations of these primitive functions may be realized through three dimensional particles arrangement. For the arrangement it is necessary to develop the technology which make it possible to assemble several kinds of particles according to structural designs for the manifestation of the coordination and systematization. As elemental technologies for the three dimensional particles arrangements, particle designs, particle preparation, controls of particle movement and treatments of assembled particles are being studied at the first stage.

Main results up to now are as follows;

1. Powder particles of Au(40 μm) and SiO_2(5 μm) were electrified positively and negatively, respectively. The SiO_2 particles attached to the Au particles and covered almost their surfaces by mixing of both powder particles. These ordered mixtures are expected to be applied to development of the multifunctional materials.
2. Powder particles of Au(400 μm) were coated with a conducting polymer, polypyrrole. The coated particles showed non-linear current-voltage behaviors by Shottky barrier at metal/conducting polymer contacts. This suggests that a new type of varistor can be developed using the coated particles.
3. Electrified patterns were drawn on $CaTiO_3$ substrates using electron beam scanning. SiO_2 powder particles, which were scattered over the electrified patterns, formed to the figures of patterns. It was thought that this technique makes it possible to assemble powder particles into devices and multi-functional materials.

145 Fundamental Study on Creation of Micro Stereom Fabrics by Powder Technology

April 1993 to March 1996

K. Halada, 4th Research Team

Keywords: powder, porosity, sintering, structure control, ecomaterial

Minerals of biological origin have the microstructure to perform functions efficiently. It is well-known that spicules or echinoderms have three dimensional framework or porous structures, e.g. microperforate, labyrinthic, retiform fascicular etc., to perform efficient mechanical properties. We have started this study as a first step with an ambitious to acquire or mimic the design and construction of materials of natural origin in the field of the inorganic materials technology.

Powder technology is noteworthy technology to create the mimetic microstructure of natural materials, because the powder can be divided to small elemental particles and can be synthesized under optional controllings. Prediction of microstructures and stereom morphologies of sintered materials is important to design such microstructures. One part of this study is that on arrangement; to develop the way of prediction for the microstructure and the stereom morphology of sintered materials.

The feature of powder particle is also important as the element of synthesis. Embellishment of particles with finely controlled qualities is expected to enlarge the possibility of the design of stereom fabrics. The second part of the study is that on assembling; to inquire the way of combination of various type of particles and to inquire the production method of appropriate powder or embellished particles for assembling.

Related Papers

Study on the Creation of Micro-porous-sphere by Ultrafine Particles, H. Okuyama, S. Ohno, K. Minagawa, and K. Halada, Funtai Oyobi Funmatsuyakin, 40-12 (1993): 1174–78 (in Japanese).

Relation between the Particle Size and Shape of Metal Powders by High Pressure Water Atomization, K. Chiba, K. Minagawa, K. Halada, and T. Nakata, Funtai Oyobi Funmatsuyakin, 40-12 (1993): 1170–73 (in Japanese).

146 Study on Rapidly Solidified Powders for Superconductive Materials

October 1988 to March 1995
K. Halada, 4th Research Team
Keywords: superconductive materials, rapid solidification, powder, sintering

Rapidly solidified Bi-Sr-Ca-Cu-O glassy ceramics was produced by gas atomization and centrifugal atomization from molten oxide. By the centrifugal atomization ligaments and spherodized glassy powder 0.1 to 1 μm in diameter were obtained. Gas atomized powder composed of fine spherical powder less than 20 μm in diameter and thin fiber with round heads at the end. All of them were amorphous, which had the crystallization temperatures around 500 °C.

While the mixed powder showed a simple shrinkage behavior above 700 °C, the atomized powder once shrank above 500 °C, followed by the second shrinkage around 700 °C, and characteristically expanded from 820 °C before rapid shrinkage above 860 °C. From the atomized powder $Bi_2Sr_2CuO_6$ crystallized above 500 °C. $Bi_2Sr_2CaCu_2O_8$ (superconductive phase) appeared above 800 °C, and the partial melting took place around 860 °C. Below the temperature of the remarkable partial melting extraordinary growth of Ca_2CuO_3 phase was observed. The phase separation generated Bi-rich part as the counter result of the growing of Ca_2CuO_3 phase. These phase separation was confirmed by newly developed EPMA composition analysis. The Bi-rich part was prevented from producing the stable high-T_c phase, because the liquid phase broke out from the Bi-rich part below the temperature to make the high-T_c phase stable.

Related Papers

Sintering of Bi-Sr-Ca-Cu-O Superconductive Material Atomized from Molten Oxide, K. Halada, K. Minagawa, H. Suga, H. Okuyama, S. Ohno, and Y. Muramatsu, Advances in Powder Metallurgy & Particulate Materials, 8 (1992): 281–92.

EPMA Composition-coordinate Mapping Analysis of the Phase Change of Atomized Bi-Sr-Ca-Cu Oxide, K. Halada, K. Honma, K. Minagawa, and H. Okuyama, Funtai Oyobi Funmatsuyakin, 39-5 (1992): 390–96.

147 Coating of Fine Powders by CVD Technique in Fluidized Bed

April 1991 to March 1994
T. Itagaki, Materials Design Division
Keywords: fluidized bed, CVD, HfC, tungsten powder

This research is aimed at preparing various types of very fine powders coated with very thin layer of a second substance. The fine coated powders have various advantages when they are used for sintering. For example, if the powder is coated with a sintering agent, the sintering will finish in much shorter time or will be performed at a lower temperature as compared with the case when the agent is added as powder, because the agent is much more finely dispersed. When an alloying element is coated on powder of a refractory metal, the alloying will be more homogeneous by the same reason.

A chemical vapor deposition technique in a fluidized bed is planned to be applied to make the coating layer comprising ceramic materials. The particle size of the powder will be 1–10 microns, and thickness of the coated layer will be several nanometers. Based on the research work performed previously, we have been convinced that coating by CVD technique in a fluidized bed is technically feasible.

The first experiment was concerned with coating of HfC on tungsten powder. Until present, we attained coated layer of about 7 nanometers thickness on the surface of tungsten powder in diameter of 4 microns. The obtained powder will be sintered at a high temperature to obtain tungsten alloy dispersed with HfC.

Next experiment will be concerned with coating of sintering agent on ceramics such as silicon ni-

tride or silicon carbide. This coating will be more difficult because the density of the powder is much smaller than that in the first experiment.

Joining

148 Corrosion of Dissimilar Metals Joints in Reactor Fuel Reprocessing Plants

April 1991 to March 1996

H. Irie, Advanced Materials Processing Division

Keywords: diffusion bonding, titanium, zirconium, stainless steel, laser speckle method

Dissimilar metals joints are to be used in a new reactor fuel reprocessing plant in Japan. The joints composed of stainless steels and valve metals such as zirconium and titanium alloys are produced by a solid state joining. It is necessary for the safety of plant to assure sufficient mechanical strength and at the same time corrosion resistance to condensed nitric acid.

According to the experimental results until last year, a diffusion bonded metal joint of stainless steel to zirconium with sufficient strength could be obtained with inserting an annealed tantalum foil between well polished joint surfaces and at 1123 K. The direct bonding produced a wide diffusion layer and brittle intermetallic compounds. The joint with tantalum at a higher temperature also produced iron-zirconium and nickel-zirconium compounds. At lower temperature such as 1073 K, unbonded interface area were left and weakened joint strength. The thickness of diffusion layer under direct bonding was about 100 nm. However, that of the tantalum inserted bonding was only 40 nm at each side of tantalum.

In order to decrease bonding temperature and suppress formation of intermetallic compounds, elimination of oxide film on interfaces is effective. An argon ion spattering method has been investigated. Only to eliminate oxide film, a higher accelerating voltage of 5 kV was effective. The strength of bonded joint, however, was not sufficient because of ion implantation of argon into matrix metals. Then 1 to 2 kV voltage was more effective for joining. Another method is used a bombardment of hydrogen because of strong affinity with oxygen. But the formation of hydrogen ion by discharge is a big barrier at present.

Corrosion property of diffusion bonded joints have been investigated under 3 N nitric acid at 60 °C. Under this weak corrosion environment, it depended strongly upon the finished surface condition, that is, the plastically deformed state.

An adequate diameter of irradiated laser of laser speckle method for measurement of local distortion of diffusion bonded joint has been investigated.

149 Low Energy Joining with Controlled Surface Composition

April 1993 to March 1995

O. Ohashi, Advanced Materials Processing Division

Keywords: joining, surface composition, argon ion bombardment, direct bonding of silicon, hydrogen permeability

As a part of a National Project in Japan which focuses on "Materials Interconnection" there is an interest in fundamental research designed to create new functional materials by controlling the surface composition, structure and shape of joining surfaces. Research work undertaken at NRIM aims to develop low energy joining techniques based on the control of surface composition. Furthermore, work is being carried out to develop materials for a special function, i.e., hydrogen purification and silicon devices for semi-conductor applications. The characteristics of the prepared surfaces are examined using an ultra high vacuum equipment that enable surface control and analysis. In addition, surface modification techniques by vapor deposition have been examined to improve the hydrogen permeability of some developed membranes.

We have obtained the following results:

1. When bonding single silicon crystals, joints with high strength were made in vacuum. High joint strength is attributed to forming SiO_2 of cristobalite type at the bonding surface.
2. Argon ion bombardment had the effect of cleaning bonding surface, but also increased argon ion plantation as the accelerating voltage was increased. Copper bonds could be made using an accelerating voltages of 2–3 kV. But, copper failed to bonding an accelerating voltage of 4 kV. High accelerating voltage planted argon in surface layer. Argon came out from surface layer during bonding, prevented bonds at contact area from forming.
3. Yttrium-deposition was demonstrated to be effective in modifying the interface between palladium-overlayer and vanadium-based alloys (V-15NI-0.05Ti). The hydrogen permeability of this membrane increased markedly with yttrium-deposition. But changing vanadium-based alloy into pure niobium, the hydrogen permeability decreased with yttrium-deposition.

150 Fundamental Research on Joining Technique in Microgravity

April 1993 to March 1996

K. Sasabe, Advanced Materials Processing Division

Keywords: joining in space, microgravity, brazing, electron beam welding

Brazing and electron beam welding are thought to be the most practical joining methods for the construction or repair of structures and experimental equipments in space, because the particular conditions of vacuum and microgravity in space can be used positively for those techniques. The purpose of this study is to analyze the flowing phenomena of molten metals contacting with a solid, which is the most fundamental phenomena for brazing and electron beam welding, and to make clear the mechanisms of it.

Brazing

A simulation program for penetration of molten filler alloy into a brazing gap was developed using the theory of thermal conduct by way of trial. The properties of thermal field changed during penetration of molten alloy into a capillary gap was investigated based on the simulation results. Moreover, the initiation conditions of penetration, i.e., the process to determine free surface shape of molten alloy in a gap and the relationships of mass transfer and heat transfer were analyzed by model experiments using epoxy resin plates and paraffin.

Electron beam welding

In order to carry out electron beam welding successfully, a small and light welding machine is desirable. A low accelerating voltage electron beam of 20 kV was able to be obtained by reconstructing a 60 kV machine. The weld penetration depth by this machine was about 10 mm at a low welding speed. Recent rapid development of semiconductor technology can accomplish an adequate welding machine of 20 kV.

The influence of surface-activation elements such as sulfur and oxygen on molten metal flow was investigated using stainless steels of different sulfur content levels. The critical content value of sulfur was 50 ppm. At more than 50 ppm, the width of molten zone on specimen surface was narrow and at less than 50 ppm it was widened and flat. The penetration depth did not depend upon the sulfur content, then the sulfur does decide the molten metal flow. However, this effect was not coming simply from the surface tension flow (Marangoni flow).

Composite process

151 Forced Infiltration Process for Making Composite Structures

April 1992 to March 1996

T. Dendo, Advanced Materials Processing Division

Keywords: infiltration, semi-molten state, intermetallic compound

Forced infiltration technique is applied to two different processing purposes in this theme.

The first is to make a composite layer structure in surface portion of a porous ceramic compact by infiltration under semi-molten state. The infiltrating metals employed are Pb-Sn alloys which have a wide range of semi-molten state in which liquid and solid co-exist. The porous compacts used are made of alumina powder having mean particle size of 1 μm, and their porosities are controlled in the range of 75 to 95% in relative density by choosing sintering condition. The composite layer structure consisting of metal and ceramic can be formed in the outer portion of the alumina compact. Infiltrating behavior and morphology of the layer structure are investigated in relation to the process parameters such as volume fraction of liquid, porosity of ceramic compact, infiltration pressure and so on.

The other is to synthesize intermetallic compounds by infiltration into a porous metallic preform. At present, some attempts are being made for synthesizing Ti-Al compounds by solid–liquid reaction through infiltrating process. It is confirmed that three kinds of compounds i.e., Ti_3Al, TiAl and $TiAl_3$, are synthesized in this process and each fraction of them is mainly affected by the thermal conditions such as pre-heating temperature and pouring temperature. Besides, effects of additive elements and particle size of titanium powder are examined with respect to the structural morphology.

Related Papers

Synthesis of Ti-Al Intermetallic Compounds by Reaction during Pressure Infiltration, T. Shirota, T. Hashimoto, M. Nakamura, H. Doi, T. Kimura, and T. Dendo, Proc. 43rd Join. Conf. Tech. Plast., (1992): 483–86 (in Japanese).

Pressure Infiltration under Semi-molten State for Making Composite Layer Structure, T. Dendo, T. Shirota, and M. Kiuchi, Proc. 4th Int. Conf. Tech. Plast., (1993): 194–99.

152 Coating Formation by Molten and Electrified Powders

April 1991 to March 1995

S. Kuroda, Advanced Materials Processing Division

Keywords: plasma spray, surface coating, deposition phenomena, interface, mercury porosimetry

This research aims to clarify the **deposition phenomena** of molten particles onto solid surface with a special interest in spray deposition of coatings in mind. The collision of a high velocity molten particle onto a solid surface and the subse-

quent solidification are very fast and complicated phenomena, on which various coating processes such as plasma spraying are based. With the aid of a technique developed to measure the velocity and temperature of flying particles, morphology of quenched splats as well as the pore structure of the deposited coatings have been related to those parameters.

The mechanical property as well as the bonding between sprayed particles are examined by using various mechanical testing methods and microscopic techniques. Mercury porosimetry combined with pore visualization by impregnation techniques was found to be a sensitive technique to detect the changes in the pore structure within sprayed deposits caused by different spraying conditions such as spray distance and substrate temperature. In addition, feasibility of employing electrostatic force to control the motion of fine powders are under investigation.

Related Papers

The Quenching Stress in Thermally Sprayed Coatings, S. Kuroda and T.W. Clyne, Thin Solid Films, 200 (1991): 49–66.

Measurement of Temperature and Velocity of Thermally Sprayed Particles using Thermal Radiation, S. Kuroda, H. Fujimori, T. Fukushima, and S. Kitahara, Trans Jpn. Welding. Soc., 22 (1991): 82–89.

Significance of the Quenching Stress in the Cohesion and Adhesion of Thermally Sprayed Coatings, S. Kuroda, T. Fukushima, and S. Kitahara, J. Thermal Spray Technol., 1 (1993): 325–32.

Evaluation of the Pore Structure in Plasma-sprayed Coatings, to be published in Proc. of the 8th Cimtec, June 1994, Florence, Italy.

Process with aid of beam technology

153 Diagnostics of Laser Photoionization Induced Plasma

April 1992 to March 1995

Y. Ogawa, Chemical Processing Division

Keywords: laser photoionization, laser induced plasma, drift velocity, ion and electron temperatures, plasma density

Resonance stepwise photoionization method has acquired a wide variety of applications. Novel applications of laser photoionization include its emergence as a feasible method for the processing of high-purity materials and the separation of commercially valuable isotopes, when using as the detection of trace elements, and ion sources for ion implantation, etc. Furthermore, the extraordinary sensitivity and versatility of resonance photoionization spectroscopy have already applied to the identification of high-lying atomic levels, the measurement of transition cross sections, and the studies of chemical reactions, etc.

These applications are mainly based on laser stepwise excitation of atoms and on extraction of ions from weakly ionized plasma produced by the photoionization. The method of laser stepwise resonant photoionization of atoms was suggested more than ten years ago and the basic features and characteristics of this method have been fundamentally realized. However, little is known about the microscopic and even macroscopic properties of the laser induced plasma (such as drift velocity, ion and electron temperatures, plasma density and so on) or about the extraction behavior of ions under the applied electric field. We have planned this research work to establish the diagnostic techniques for the weakly ionized plasma, which will contribute to the understanding of ion extraction behavior.

Related Paper

Laser Material Purification of Neodymium, Y. Ogawa et al., J. Jpn. Inst. Met., 55 (1991): 545–52.

154 Study on Evaporation Process by High Energy Density Beams

April 1992 to March 1995

H. Irie, Advanced Materials Processing Division

Keywords: electron beam, laser, evaporation, laser induced plasma, electron density

The electron beam evaporation process has been widely used in coating industry, but it has been used at very low evaporation rate because of large production rate of sputter. These coating process has been done on the base of experiences owing to shortage of knowledge of evaporation mechanism. On the other hand, laser has been considered as a good heat source to produce material vapor in controlled environment. But laser itself is the same kind of heat source as the electron beam and it will face the same problem as the electron beam does.

In process of high power carbon dioxide laser, the interaction of laser with induced plasma of ionized vapor and environment gases occurs. The evaporation rate and velocity of evaporated metal atom have been investigated in a controlled atmosphere using a chamber. The electron density of laser induced plasma rapidly changed with respect to time and location. Then a CCD camera with infrared ray was used for measurement of radiated energy, and electron density was calculated from the results. The electron density strongly depended upon the environment gas rather than chemical composition of evaporated metallic vapor. It was highest in a mixed gas of argon and hydrogen and decreased in order of pure argon and helium. The radiation from metallic ion could be also recog-

nized by an optical analysis. The higher electron density in the mixed gases indicated that hydrogen promoted the evaporation of metal.

In electron beam process, the optical measurement was very difficult because of lead included window glass. Then it needs stationary evaporation to investigate evaporation process. For this purpose, the irradiation method of electron beam was developed. A high speed oscillation of Lissajou' figure of focused beam accomplished a relatively stationary evaporation. In addition to this oscillated beam, another electron beam has been used for observation of evaporation and diffusion process of materials.

155 *In Situ* Analysis/Evaluation of Radiation Damage in Materials

April 1988 to March 1995

K. Furuya, Materials Characterization Division

Keywords: radiation damage, *in situ* analysis, dual-beam ion irradiation, SUBNANOTRON, 1 MV TEM, 200 keV ion implanter, 30 keV ion sputter source

Radiation damage of metallic materials is characterized by the atomic displacements associated with the destruction of the crystalline structure by irradiation of energetic particles such as neutrons and ions. Many types of defects and defect clusters are supposed to be produced by this atomic process and the resultant microstructure generally becomes complicated with the formation of dislocation loops, voids, precipitates and so on. For the basic understanding of radiation damage, it has been strongly desired to clarify the process of atomistic displacement. *In situ* observation in the transmission electron microscope (TEM) is one of the fascinating method to investigate the structural evolution induced by particle bombardments and implantation.

The purpose of this research is to develop a new facility for *in situ* analysis of the microstructural aspects of materials under dual beam ion irradiation. The facility so called "SUBNANOTRON" consists of 1 MeV TEM with two ion accelerators. The voltage of 1 MeV for electrons was chosen for the resolution lower than 0.15 nm, for enough thickness of the specimen and enough volume at the specimen position where stressing, heating and cooling will be conducted. The analytical tools such as MAD, EDS and EELS are essential to characterize the complicated structural changes of irradiated materials. The construction of the SUBNANOTRON is now in the final stage for installing dual ion beams interface.

Dual ion accelerator systems consist of 200 keV and 30 keV implanters with a hollow cathode heavy ion source and RF discharge light ion source, respectively. The high energy beam was selected through a 1.5 T analyzing magnet at an angle of 45 degrees, and then deflected vertically by an angle of 44 degrees for introducing into the TEM. The low energy beam was vertically analyzed before entering the port of the TEM. The beam lines were carefully controlled by electrostatic lens and evacuated by the ion pumps and magnetically suspended turbo pumps for keeping the resolution of the TEM. TEM images were collected and magnified directly in a fiber optically coupled TV camera, and recorded with an S-VHS type VTR through a real time processor.

The whole system will be completed and ready for operation in the middle of this year, and will be opened for the research collaborations between Japanese and overseas materials scientists.

156 Characterization and Control of Elementary Functions of Materials in the Localized Fine Area

April 1989 to March 1994

K. Furuya, Materials Characterization Division

Keywords: cathodoluminescence (CL), TEM, micro-hardness, GaAs

Functions of materials in a bulk state are controlled by the physical and chemical properties in a localized fine area ranging from 10^{-6} to 10^{-9} m. Especially, the electronic properties of metals and semiconductors are influenced by the lattice distortion associated with the heterogeneity in the materials such as surfaces, grain boundaries and the interface of multilayers. Cathodoluminescence (CL) has been used to characterize the photoelectronic properties of semiconductors. However, the microstructural aspect and elementary functions of micro mechanically fabricated area such as by the hardness indentor could not be well analyzed in the previous studies. The purpose of this research is to demonstrate the usefulness of micro-hardness test for characterizing the effects of the surface fabrication on the photoelectronic properties of GaAs.

The material in this study is Si doped N-type GaAs (100) wafers. 10 to 100 g loads of Vickers indentors were applied on the surface of GaAs for 10 s to introduce mechanical strain depending upon the resultant indentation size varying from 5 to 20 μm. CL measurements at room temperature were carried out by 200 kV TEM equipped with a light collecting device and monochrometer, which was operated at 100 kV with a beam current of 100 nA. Particularly seen on the surface of GaAs were micro cracks initiated at the four corners of an indentation and a large amount of quench of CL intensity both inside and outside of an indentation. The degree of this quench in the compressive strained area was much larger than that in the tensile strained area where the clacks were located.

Taking into account for the peak shift of CL spectrum, the relaxation of strain by cracking may be concluded to result in the recovery of CL intensity. This result implies the importance of the residual strain at the interface of multilayer structures of semiconductors. For the next step, CL measurements at low temperatures will be carried out on the double layer thin film semiconductors.

157 Synthesis of Special Compounds by a Combined Use of Ion Implantation and Deposition

April 1992 to March 1994

K. Saito, Surface and Interface Division

Keywords: ion implantation, deposition, BiSrCaCuO, $Fe_{16}N_2$

A combined use of ion implantation and sputter deposition is a unique technique for synthesizing novel materials by means of atom injection, atom mixing and radiation induced or enhanced effects in highly controlled manner. In this study we have synthesized high-quality superconducting BiSrCaCuO thin films of thicknesses below several tens of nanometers. For film thicknesses of 30, 15 and 7 nm, we obtained the superconducting transition temperatures T_c, 108 K, 86 K and 85 K, respectively. The mechanism of ion beam induced film modification was based on the formation of unit cell-scales of collision cascades and their reordering at relatively low temperatures. On the other hand, we synthesized a magnetic film of $Fe_{16}N_2$ nitrides with giant magnetization by means of multi-energy nitrogen ion implantation. Although the volume fraction of $Fe_{16}N_2$ was still small, about 60% for a film thickness of 250 nm, the saturated magnetization of the nitrogen ion implanted films was 230 emu/g, a few percent larger than that of unimplanted iron films. A considerably high coercive force H_c of 200 Oe was obtained at 5 K.

Related Papers

Fabrication of 300 Å Thick BiSrCaCuO Thin Films with T_c of 108 K by Use of Ion Implantation, K. Saito and M. Kaise, Jpn. J. Appl. Phys., 31 (1992): L1047–50.

Thermal Spike and Displacement Damage Effects in BiSrCaCuO Thin Films by Ar Ion Beams, K. Saito and M. Kaise, Jpn. J. Appl. Phys., 31 (1992): 3539–45.

Fabrication of 30 nm Thick Superconducting BiSrCaCuO Thin Films by Single-Target Magnetron Sputtering Method, M. Kaise and K. Saito, J. Japan Inst. Metals, 57 (1993): 103–07 (in Japanese).

Processing in special environment

158 Development of Quantum Microstructure in Ultra Clean Vacuum

April 1990 to March 1995

K. Yoshihara, 4th Research Group

Keywords: quantum microstructure, ultra clean vacuum, levitation transport

Materials with quantum microstructure are expected to have new and excellent functional properties. Creation of these materials requires extremely clean and high vacuum environment in order not to deteriorate the materials properties with impurities from the environment. The project has completed the first phase of fabrication of sample transfer system by magnetic levitation. We could successfully transfer samples from one station in a main chamber to another station in an intro chamber without any exposure to contaminable environment. The second phase of the project is carried out to create materials with quantum microstructure with the ultra vacuum system. We have manufactured an apparatus for the preparation of super thin film controlled on an atomic scale.

An extremely high vacuum system has been developed in order to transfer specimens from one instrument to another without any contamination of the ultra clean surface. Two chambers for instruments can join with the main chamber in transport through intro chambers. The main chamber without transport system achieved 9×10^{-10} Pa. One transport system in the main chamber can levitate a carrier with specimens about 2 mm above stators by electromagnets in stators and transfer the carrier by linear motor drive. Operation of the system increased base pressure from 2.43×10^{-8} Pa to 2.56×10^{-8} Pa. The other transport system in an intro chamber can levitate the carrier by $YBa_2Cu_3O_{7-x}$ superconducting magnet and transfer it with permanent magnet discs of SmCo mechanically by a belt conveyor. Meissner effect and pinning effect of superconductor discs provide the carrier with stable levitation transfer. Operation of the system increased base pressure of 2.45×10^{-8} Pa little. The total system could transfer specimens from an intro chamber to a station in the main chamber in the vacuum of less than 10^{-8} Pa.

An apparatus has been developed in order to prepare super thin film on an atomic scale in an extremely high vacuum. The apparatus consists of three chambers to maintain extremely high vacuum in the main chamber for film preparation. The main chamber is evacuated by an ion pump system with effective performance even in 10^{-8} Pa. Specimen is heated by concentration of infrared radiation and the temperature change is measured by infrared radiometer using PbS detector. Film is prepared by electron beam bombardment system with ±5° angle directivity. The crystal structure of substrate and prepared film is observed with RHEED system.

Publications

❒ Papers Published in 1993

Characterization/Properties

Electronic and nuclear properties

1. *Anisotropic Vortes State of Single Crystalline $Bi_2Sr_2CaCu_2O_{8+\delta}$*, K. Kadowaki and T. Mochiku, Advanced in Superconductivities V, (1993): 187–90.
2. *Curie Paramagnetism of Chromium Ultrafine Particles*, T. Furubayashi and I. Nakatani, J. Appl. Phys., 73 (1993): 6412–13.
3. *Mossbauer Studies of Iron Magnetic Fluids Prepared by Evaporation Method*, T. Furubayashi and I. Nakatani, J. Mag. Mag. Mater., 122 (1993): 74–77.
4. *Ce3d and Zr3d XPS Spectra of ZrO_2-12mol% CeO_2 after Heat Treatments and Ar^+ Etching*, H. Zhu (Zhejiang Univ.) and T. Hirata, J. Mater. Sci. Lett., 12 (1993): 749–51.
5. *On the Electric Field Gradient at Copper Nuclear in Oxides*, T. Shimizu, J. Phys. Soc. Jpn., 62 (1993): 772–78.
6. *Ionic Model of Some Aspects of Cu NQR Spectra in Oxides Superconducting*, T. Shimizu and H. Yasuoka (Univ. of Tokyo), J. Phys. Soc. Jpn., 62 (1993): 779–83.
7. *dHvA Effect Study of Metamagnetic Transition in $CeRu_2Si_2$*, H. Aoki, S. Uji, *A.A. Keiko, and *Y. Onuki (*Univ. of Tsukuba), J. Phys. Soc. Jpn., 62 (1993): 3157–71.
8. *Orbital and Spin Susceptibilities of the Pyramidal ^{63}Cu Sides in $Y_1Ba_2Cu_3O_x$ System*, T. Shimizu, H. Aoki, †H. Yasuoka, †K. Yoshimura, †K. Kosuge (†Kyoto Univ.), and *T. Tsuda (*Univ. of Tokyo), J. Phys. Soc. Jpn., 62 (1993): 3710–20.
9. *Field and Temperature Dependence of He Mean Penetration Rate of Fluxons in the Mixed State of High-T_c Superconductors*, M. Uehara and B. Barbara, J. Phys. 1 France, 3 (1993): 863–70.
10. *Isotope Controlled Materials*, T. Noda, Metals & Technology, 63 (1993): 32–37 (in Japanese).
11. *Itinerant 4f Electron in $CeRu_2Si_2$*, *A.A. Keiko, *T. Ebihara, *I. Umehara, *K. Sato, *Y. Onuki (*Univ. of Tsukuba), H. Aoki, S. Uji, and T. Shimizu, Physica, B 186 (1993): 147–49.
12. *High Quality Single Crystal Growth and Fermi Surface Property of UGe_2*, *S.W. Yun, *K. Sato, *Y. Fujimaki, *I. Umehara, *Y. Onuki, *S. Takayanagi (*Univ. of Tsukuba), H. Aoki, S. Uji, and T. Shimizu, Physica, B 186 (1993): 186–88.
13. *de Haas-van Alphen Oscillation in the Superconducting Mixed State of 2H-$NbSe_2$ and Nb*, *Y. Onuki, *I. Umehara, *T. Ebihara, *A.A. Keiko, *K. Sato, *K. Takita (*Univ. of Tsukuba), H. Aoki, S. Ujia, and T. Shimizu, Physica, B 186 (1993): 1050–52.
14. *Electrical Resistivity of Some Uranium Compounds*, K. Kadowaki, Physica, B 186–88 (1993): 727–29.
15. *Mossbauer Studies of Superconducting $La_{2-x}Ca_{1+x}Cu_2O_6$ Doped with ^{57}Fe*, T. Furubayashi, *K. Kinoshita, *T. Yamada (*NTT Basic Res. Lab.), and T. Matsumoto, Physica, C 204 (1993): 315–21.
16. *Flux Creep by Quantum Tunneling in $YBa_2Cu_3O_{7-\delta}$*, S. Uji, H. Aoki, *S. Takebayashi, *M. Tanaka, and *M. Hashimoto (*Nippon Steel Corp.), Physica, C 207 (1993): 112–18.
17. *Transition of f Electron Nature from Itinerant to Localized—Magnetic Transition Studied via the dHvA Effect*, H. Aoki, S. Uji, *A.A. Keiko, and *Y. Onuki (*Univ. of Tsukuba), Phys. Rev. Lett., 71 (1993): 2110–13.
18. *Local Epitaxy of Ag on $Bi_2Sr_2CaCu_2O_{8+\delta}$*, P. Schwaller, P. Aebi, J. Osterwalder, L. Schlapbach, M. Shimoda, T. Mochiku, and K. Kadowaki, Phys. Rev., B 48 (1993): 6732–35.
19. *de Haas-van Alphen Effect of Single-1 $CdCl_2$ Intercalated Graphite*, *W.R. Datars, *P.K. Ummat (*McMaster Univ.), H. Aoki and S. Uji, Phys. Rev., B 48 (1993): 18174–77.
20. *Flux Dynamics and Dissipation in Vortex States in High T_c Superconductors*, K. Kadowaki, T. Mochiku, H. Takeya, Y. Saito (Univ. of Tsukuba), and S.L. Yuan (Univ. of Tokyo), Proc. of 1993 Int. Workshop on Superconductivity, (1993): 234–35.
21. *Tunnel Diode Oscillator Application to High Sensitivity dHvA and Superconducting Critical Field Studies of Anisotropic Organic Conductors*, *G.J. Athas, *J.B. Brooks (*Boston Univ.), S.J. Klepper (MIT), S. Uji, and M. Tokumoto (Electrotechnical Lab.), Rev. Sci. Instrum., 64 (1993): 3248–51.
22. *Magnetic Breakdown in the Organic Conductor $(BEDT\text{-}TTF)_2KHg(SCN)_4$*, S. Uji, H. Aoki, *J.S.

Brooks, *A.S. Perel, *G.J. Athas (*Boston Univ.), S.J. Klepper (MIT), †C.C. Agosta, †D.A. Howe (†Clark Univ.), **M. Tokumoto, **N. Kinoshita, **H. Anzai (**Electrotechnical Lab.), Solid State Commun., 88 (1993): 683–86.

Atomistic arrangement

23. *Atom-Probe Microanalysis of a Nickel-Base Single Crystal Superalloy,* H. Harada, A. Ishida, Y. Murakami (JRDC), H.K.D.H. Bhadeshia (Univ. of Cambridge), and M. Yamazaki, Appl. Surf. Sci., 67 (1993): 299–304.
24. *High-Strength (5 GPa) Steel Wire: an Atom-Probe Study,* H.K.D.H. Bhadeshia (Univ. of Cambridge) and H. Harada, Appl. Surf. Sci., 67 (1993): 328–33.
25. *X-ray Photoelectron Diffraction Image of a $Bi_2Sr_2CaCu_2O_{8+x}$ Single Crystal,* M. Shimoda, Butsuri, 48 (1993): 623–36 (in Japanese).
26. *X-ray Photoelectron Diffraction Studies on a Single Crystal $Bi_2Sr_2CaCu_2O_{8+x}$,* M. Shimoda, Butsuri, 48 (1993): 637–39 (in Japanese).
27. *Low-Temperature Structural Phase Transition in ZrO_2-12mol% CeO_2 Studies by IR Spectroscopy and X-ray Diffraction,* T. Hirata, H. Zhu (Zhejiang Univ.), T. Furubayashi, and I. Nakatani, Commun. Am. Ceram. Soc., 26 (1993): 1361.
28. *A Fast Response and Accurate Infrared Pyrometer Combining the Two-Wavelength Method and the Single-Band Detections,* N. Kishimoto and H. Amekura, Japanese Sensor Newletter, 7 (1993): 27–30.
29. *Crystal Structure of the Ferromagnetic Copper Oxide $La_{1.8}Ba_{1.2}CuO_5$,* T. Mochiku, H. Asano, F. Izumi, F. Mizuno, H. Masuda, I. Hirabayashi, and S. Tanaka, Kens Report, 9 (1993): 37.
30. *HREM Observation of the Effects of 18MeV $Cull^+$ Ion-Irradiation on the Crystal Structure of $Bi_2Sr_2CaCu_2O_x$,* B. Chenevier, S. Ikeda, H. Kumakura, K. Togano, *S. Okayasu, and *K. Kazumata (*JAERI), Mater. Sci. Forum, 129 (1993): 18–30.
31. *Quantitative Structure Analyses of $YBaCu_3O_{7-\delta}$ Thin Films: Determination of Oxygen Contents from X-ray Diffraction Patterns,* J. Ye and K. Nakamura, Phys. Rev., B 48 (1993): 7554–64.
32. *Determination of Site Occupation of Alloying Elements in γ′ Phase of Ni-Base Superalloy by Atom Probe,* A. Ishida, H. Murakami, H. Harada, M. Yamazaki (JRDC), and H.K.D.H. Bhadeshia (Univ. of Cambridge), Report of 123rd Committee on Heat-Resisting Metals and Alloys Jpn. Soc. for the Promotion of Sci., 34 (1993): 71–76 (in Japanese).
33. *The Atomic Location of Multi-Component Nickel-Base Single-Crystal Superalloys,* H. Murakami, H. Harada, M. Yamazaki (JRDC), and H.K.D.H. Bhadeshia (Univ. of Cambridge), Report of 123rd Committee on Heat-Resisting Metals and Alloys Jpn. Soc. for the Promotion of Sci., 34 (1993): 315–23 (in Japanese).
34. *Electrical Resistivity of the As-Grown $Gd_{1.92}Ce_{0.08}CuO_4$ Single Crystal under Pressure,* A. Matsushita, S. Uji, and T. Matsumoto, Solid State Commun., 87 (1993): 321–24.

Phase transformation and microstructure

35. *Zirconium-Hafnium Interdiffusion in Polycrystalline Fluorite-Cubic CeO_2-ZrO_2-HfO_2 Solid Solution,* Y. Sakka, Y. Ohishi (Kyocera Corp.), K. Ando (Toshiba Corp.), and Y. Ikeda (Kyushu Univ.), J. Am. Ceram. Soc., 76 (1993): 1381–83.
36. *Superplasticity of Low Carbon HSLA Steel during Baivite Transformation,* H. Nakajima, S. Yamamoto, H. Miyazi, and E. Furubayashi, J. Iron and Steel Inst. Jpn., 79 (1993): 1345–49 (in Japanese).
37. *Application Modes of Ultrasonic Vibration to Molten Metal and Their Effect on Solidification Structures,* Y. Ohsawa, A. Sato, T. Namai, and G. Aragane, J. Jpn. Found. Soc., 65 (1993): 289–93 (in Japanese).
38. *Surface Modification of Intermetallic Compound TiAl by Nitrogen Ion Implantation,* T. Matsushima and K. Saito, J. Jpn. Inst. Met., 57 (1993): 325–31 (in Japanese).
39. *Effect of Third Elements on the High-Temperature Strength of TiAl Base Alloy,* K. Hashimoto, M. Nobuki, H. Doi, T. Tsujimoto, and M. Nakamura, J. Jpn. Inst. Met., 57 (1993): 898–904 (in Japanese).
40. *Shape Memory Effect and Related Transformation Behavior in an Unausaged Fe-Ni-Co-Ti Alloy,* T. Kikuchi and S. Kajiwara, Mater. Trans., JIM 34 (1993): 907–18.
41. *HREM Study of Stress-Induced Transformation Structures in an Fe-Mn-Si-Cr-Ni Shape Memory Alloy,* K. Ogawa and S. Kajiwara, Mater. Trans., JIM 34 (1993): 1169–76.
42. *A Structure Image of R-Phase in a Ti-Ni Alloy,* K. Ogawa and S. Kajiwara, Mater. Trans., JIM 34 (1993): 1223–25.
43. *Nonuniform Recrystallization in a Mechanically Alloyed Nickel-Base Superalloy,* *Y. Murakami, *K. Mino (*JRDC), H. Harada, H.K.D.H. Bhadeshia (Univ. of Cambridge), Metall. Trans., A 24 (1993): 1049–55.

44. *Japanese Approaches to Ferritic/Martensitic Steel Development for Fusion Reactor*, F. Abe, A. Kayama, M. Tamura, and A. Hishinuma, Proc. of IEA Workshop on Ferritic/Martensitic Steels, (1993): 106–24.

45. *Cooling Rate Dependence of α/γ Phase Transformation in Titanium Aluminides and its Application to Alloy Development*, M. Takeyama, T. Kumagai, M. Nakamura, and M. Kikuchi (Tokyo Inst. Technol.), Proc .of Int. Sympo. on Structural Intermetallics, (1993): 167–76.

46. *Transformation Texture Analysis of B.C.C. and B.C.T. Ferrous Martensite*, H. Miyazi and E. Furubayashi, Textures and Microstructures, 22 (1993): 43–51.

Surface and interface properties

47. *Diffusion of Alloying Elements into Al_2O_3 Coating Films on ODS Alloys*, Y. Ikeda and N. Washizu, Detect and Diffusion Forum, 95–98 (1993): 1089–94.

48. *Y_2O_3 Dispersion Effect on Al_2O_3 Protective Coating Examined on the Basis of Five Models*, Y. Ikeda, K. Nii, and M. Yata, ISIJ Int., 33 (1993): 298–306.

49. *Effect of Dissolved Oxygen Concentration on Fatigue Crack Growth Behavior of A533B Steel in High Temperature Water*, Y. Katada, N. Nagata, and S. Sato, ISIJ Int., 33 (1993): 877–83.

50. *Photoelectron Emission during Initial Oxidation at Elevated Temperature of Fe-Cr Alloys in Air*, N. Washizu, Y. Ikeda, and H. Masuda, J. Jpn. Inst. Met., 57 (1993): 914–18 (in Japanese).

51. *Performance of Oxide Coating Films on ODS Alloys*, Y. Ikeda, H. Sumiyoshi, S. Matsuoka, and E. Takeuchi, Proc. of 2nd Int. Conf. on Mechanical Alloying for Structural Applications, (1993): 125–29.

52. *Localized Corrosion of Copper in Wet Organic Acid Vapor*, H. Baba and T. Kodama, Proc. of 8th Asian Pacific Corrosion Control Conf., (1993): 98–104.

53. *Study of Photodegradation of Paint Films using FTIR*, T. Kodama and W. Rungruangkannokul (Chulalongkorn Univ.), Proc. of 8th Asian Pacific Corrosion Control Conf., (1993): 437–51.

54. *Mechanism by Which Dispersed Y_2O_3 Exerts Beneficial Effect on High Temperature Ceramic Coating*, Y. Ikeda and N. Washizu, Processing and Fabrication of Advanced Materials for High Temperature Applications II, (1993): 435–48.

55. *Adsorption of Hydrogen on Ni and Ni-TiO_2 Composite Ultrafine Particles*, T. Uchikoshi, Y. Sakka, S. Ohno, H. Okuyama, and K. Yoshihara, Surf. Sci., 287–88 (1993): 1082–86.

56. *Hot Corrosion in a Burner Rig Tester of the Ni-Base Alloy on a Single Tie Line*, Y. Koizumi, I. Tomizuka, S. Nakazawa, and H. Numata, Zairyo-to-Kankyo, 42 (1993): 86–92 (in Japanese).

57. *The Effect of Ultraviolet Radiation on Corrosion of Painted Steels*, K. Kurosawa, V. Loha (KMITT), E.G. Mamaril (ITDI), and P. Buranawanich (DMR), Zairyo-to-Kankyo, 42 (1993): 297–304 (in Japanese).

58. *High Temperature Oxidation and Hot Corrosion of an Yttria ODS Alloys*, I. Tomizuka, Y. Koizumi, S. Nakazawa, and H. Numata, Zairyo-to-Kankyo, 42 (1993): 514–20 (in Japanese).

59. *Dissolution Behavior of MnS Inclusions in Low Alloy Steel in High Temperature Water*, S. Matsushima, Y. Katada, S. Sato, and N. Nagata, Zairyo-to-Kankyo, 42 (1993): 636–40 (in Japanese).

60. *Reaction Phenomena Related to Tunnel Current*, H. Masuda, N. Nagashima, and S. Matsuoka, Zairyo-to-Kankyo, 42 (1993): 648–52.

61. *Electrochemical Behavior of TiAl-Base Alloys in Sulfuric Acid*, H. Numata, I. Tomizuka, and T. Tsujimoto (Ibaraki Univ.), Zairyo-to-Kankyo, 42 (1993): 782–89 (in Japanese).

Mechanical properties

62. *Intelligent Structural Materials*, S. Matsuoka, Ceramics, 28 (1993): 581–84 (in Japanese).

63. *Creep Crack Growth Behavior of Creep Brittle Alloy*, M. Tabuchi, K. Kubo, and K. Yagi, Creep and Fracture of Engineering Materials and Structures, (1993): 449–58.

64. *Inherent Creep Strength for Ferritic Heat Resistant Steels*, K. Kimura, H. Kushima, K. Yagi, and C. Tanaka, Creep and Fracture of Engineering Materials and Structures, (1993): 555–64.

65. *Effect of Yield Strength on the Basic Fatigue Strength of Welded Joints*, A. Ohta, Y. Maeda, and N. Suzuki, Fatigue Fract. Eng. Mater. Struct., 16 (1993): 473–79.

66. *High Temperature Creep Damage in Steels and Superalloys*, K. Hiraga, R. Lombard (Stabilus GmbH), *H. Vehoff and *P. Neumann (*Max-Plank-Institut fur Eisenforschung GmbH), Steel Research, 64 (1993): 449–53.

67. *Fatigue Crack Propagation in a Tensile Residual Stress Field under a Two-Step Programmed Test*, A. Ohta, A.J. McEvily (Univ. of Connecticut), and N. Suzuki, Int. J. Fatigue, 15 (1993): 9–12.

68. *Creep Rupture Properties of a Nickel-Base Great-Resistant Alloy Hastelloy XR under Varying Temperature/Stress Condition*, *H. Tsuji, T. Tanabe, Y. Nakasone, and *H. Nakajima (*JAERI), JAERI-M, 93–105 (1993): 1–32.

69. *Creep Properties with Short Period Excessive Loading on a Nickel-Base Heat-Resistant Alloy Hastelloy XR*, *H. Tsuji, T. Tanabe, Y. Nakasone, and *H. Nakajima (*JAERI), JAERI-M, 93–144 (1993): 1–69.

70. *Creep Rupture Properties under Varying Load/Temperature Conditions on a Nickel-Base Heat-Resistant Alloy Strengthened by Bron Addition*, *H. Tsuji, T. Tanabe, and *H. Nakajima (*JAERI), JAERI-M, 93–173 (1993): 1–19.

71. *Evaluation of Some Heat Hastelloy XR as the Material Used for High-Temperature Components of the High-Temperature Engineering Test Reactor*, *H. Tsuji, T. Tanabe, *T. Nakanishi, Y. Nakasone, and *H. Nakajima (*JAERI), JAERI-M, 93–209 (1993): 1–64.

72. *Damage Evaluation of Metallic Materials—STM Images of Slip Lines, Fracture Surface and Micro Indentations*, S. Matsuoka, J. Crystallographic Soc. Jpn., 35 (1993): 97–98 (in Japanese).

73. *Sintering Rate of Creep Cavities in Heat Resisting Steel*, J. Kyono, N. Shinya, H. Kushima, and R. Horiuchi (Nihon Univ.), J. Iron and Steel Inst. Jpn., 79 (1993): 604–10 (in Japanese).

74. *Evaluation of Creep Crack Growth Behavior of NCF800H Alloy Based on Creep Fracture Mechanism*, M. Tabuchi, K. Kubo, and K. Yagi, J. Iron and Steel Inst. Jpn., 79 (1993): 732–38 (in Japanese).

75. *Effect of Fretting on Fatigue Strength of a Ti-6Al-4V Alloy under a Number of Environments*, N. Maruyama, M. Sumita, and K. Nakazawa, J. Iron and Steel Inst. Jpn., 79 (1993): 1374–79 (in Japanese).

76. *Role of Second Phase in Fretting Fatigue Strength in a SiC-Whisker-Reinforced Aluminum Alloy Composite*, M. Sumita, N. Maruyama, and K. Nakazawa, J. Jpn. Inst. Met., 57 (1993): 1141–48 (in Japanese).

77. *Fatigue and Fretting Fatigue Properties of a 2024-T6 Aluminum Alloy Reinforced with 20 wt. pct. SiC Particles*, N. Maruyama, M. Sumita, and K. Nakazawa, J. Jpn. Inst. Met., 57 (1993): 1268–74 (in Japanese).

78. *Static Fatigue in Ceramic Materials: Influences of an Intergranular Glassy Phase and Fracture Toughness*, G. Choi and S. Horibe (Waseda Univ.), J. Mater. Sci., 28 (1993): 5931–36.

79. *The Influence of Variable-Amplitude Loading on Cyclic Fatigue Crack Growth in Silicon Nitride*, G. Choi and S. Horibe (Waseda Univ.), J. Mater. Sci. Lett., 12 (1993): 1886–87.

80. *Relationship between Creep Damage Mode and Creep-Fatigue Interaction for SUS321 Steel*, K. Kubo, O. Kanemaru, and K. Yagi, J. Soc. Mater. Sci. Jpn., 42 (1993): 1–7 (in Japanese).

81. *Evaluation of Strength of Welded Joints by Maximum Stress Constant Fatigue Test*, A. Ohta, Y. Maeda, and N. Suzuki, J. Soc. Mater. Sci. Jpn., 42 (1993): 1167–71 (in Japanese).

82. *Fractal and Fractography*, S. Matsuoka, J. Soc. Mater. Sci. Jpn., 42 (1993): 1245–46 (in Japanese).

83. *Fatigue Crack Propagation in Welded Joints in Synthetic Sea Water*, A. Ohta, J. Soc. Naval Architects Jpn., (1993): 316–20 (in Japanese).

84. *Effect of Neutron Irradiation on Yield Stress and Ductility of Reduced-Activation Martensitic 9Cr-WVTa Steels*, F. Abe, *M. Narui, and *H. Kayano (*Tohoku Univ.), Mater. Trans., JIM, 34 (1993): 1053–60.

85. *Static and Cyclic Fatigue in Ceramics*, G. Choi and S. Horibe (Waseda Univ.), Metals & Technology, 63 (1993): 15–26 (in Japanese).

86. *Material Evaluation with STM Technology—Measurements of Hardness and Strain*, S. Matsuoka, Metals & Technology, 63 (1993): 52–7 (in Japanese).

87. *Microstructures and Room-Temperature Ductility of Unidirectionally Grown Ni_3Al*, T. Hirano and T. Mawari, MRS Sympo. Proc., 288 (1993): 691–96.

88. *High Cycle Fatigue Properties of Beta Titanium Alloys*, S. Muneki, F. Morito, J. Takahashi, N. Kainuma, and Y. Kawabe, Proc. of 3rd Jpn. Int. SAMPE Sympo., 2 (1993): 1784–89.

89. *Properties of P/M Processed Titanium Alloy/Particulates Composite*, M. Hagiwara, S. Emura, Y. Kawabe, *N. Arimoto, and *S. Mori (*Sumitomo Sitic Corp.), Proc. of 3rd Jpn. Int. SAMPE Sympo., 2 (1993): 1836–43.

90. *Role of Second Phase in Fatigue and Fretting Strengths in a SiC-Particle-Reinforced Aluminum Alloy Composites*, M. Sumita, N. Maruyama, and K. Nakazawa, Proc. of 3rd Jpn. Int. SAMPE Sympo., 2 (1993): 1993–98.

91. *Cyclic Fatigue in Silicon Nitride Ceramics: Effects of Environment, Microstructure and Fracture Toughness*, G. Choi and S. Horibe (Waseda Univ.), Proc. of 3rd Jpn. Int. SAMPE Sympo., 2 (1993): 1999–2004.

92. *Cavitated Creep Fracture in a Ni-Base ODS Alloy at 1273 K*, K. Hiraga, T. Iwama (Meisei Univ.), and T. Tanabe, Proc. of 3rd Jpn. Int. SAMPE Sympo., 2 (1993): 2040–45.

93. *Bimodal Creep Cavitation in Nickel Base Oxide Dispersion Strengthened Inconel Alloy MA754*, K. Hiraga and H. Vehoff (Max-Plank-Institut fur Eisenforschung GmbH), Proc. of 7th JIM Int. Sympo. on Aspects of High Temperature Deformation and Fracture in Crystalline Materials, (1993): 229–36.

94. *Microstructural Control for Improving Creep Rupture Strength of Tempered Martensitic 9Cr-W Steels*, F. Abe and S. Nakazawa, Proc. of 7th JIM Int. Sympo. on Aspects of High Temperature Deformation and Fracture in Crystalline Materials, (1993): 301–08.

95. *Fundamental Aspects of Inherent Creep Strength for Ferritic Steels*, K. Kimura, H. Kushima, K. Yagi, and C. Tanaka, Proc. of 7th JIM Int. Sympo. on Aspects of High Temperature Deformation and Fracture in Crystalline Materials, (1993): 309–16.

96. *Long-Term Creep-Fatigue Life Prediction*, K. Yagi and K. Kubo, Proc. of 7th JIM Int. Sympo. on Aspects of High Temperature Deformation and Fracture in Crystalline Materials, (1993): 489–96.

97. *Characterization of Creep Deformation Behavior for Cr-Mo Steel*, K. Yagi, H. Kushima, C. Tanaka, and K. Maruyama (Tohoku Univ.), Proc. of 7th JIM Int. Sympo. on Aspects of High Temperature Deformation and Fracture in Crystalline Materials, (1993): 609–16.

98. *Intelligent Structural Materials and Scanning Tunneling Microscopy*, S. Matsuoka, Science of Machine, 45 (1993): 500–06 (in Japanese).

99. *Strain Distribution Measurement System Using CCD Camera*, H. Hongo and H. Masuda, Sensor Technology, 13 (1993): 28–32 (in Japanese).

100. *High Cycle Fatigue Properties of Ti-6Al-4V Alloys at Cryogenic Temperature*, K. Nagai, T. Yuri, O. Umezawa, T. Ogata, K. Ishikawa, Y. Ito and T. Nishimura, Titanium '92 Science and Technology, (1993): 1827–34.

101. *Fracture Characteristics of Solution-Treated Ti-1SV-3Cr-3Sn-3Al Alloys*, K. Nagai, K. Ishikawa, T. Horiya, and H. Suzuki, Titanium '92 Science and Technology, (1993): 1875–82.

102. *Creep Embrittlement of Structural Components in Catalytic Reformer Reactor*, T. Momura (Nikko Kyodo Co., Ltd.), H. Tanaka, H. Kushima, M. Tabuchi, and K. Yagi, Trans. Jpn. Soc. Mech. Eng., A 59 (1993): 2066–73 (in Japanese).

103. *Effect of Yield Strength on Basic Fatigue Strength of Welded Joints*, A. Ohta, Y. Maeda, and N. Suzuki, Q. J. Jpn. Weld. Soc., 11 (1993): 185–89 (in Japanese).

Measurement and evaluation

104. *A Super High-Power Rotating Anode X-ray Source for EXAFS Measurement*, K. Sakurai, Advances in X-ray Chem. Anal. Jpn., 24 (1993): 187–98 (in Japanese).

105. *Influence of Operating Parameters on Ion Intensity in Glow Discharge Mass Spectrometry*, M. Saito, Anal. Chim. Acta, 274 (1993): 327–34.

106. *Simultaneous Determination of Sub* $\mu g\ g^{-1}$ *Levels of Impurities in High Purity Iron by Inductively Coupled Plasma-Atomic Emission Spectrometry after Circulation of Eluant through Anion Exchange Resin Mini-Column*, K. Yamada, O. Kujirai, and R. Hasegawa, Anal. Sci., 9 (1993): 385–90.

107. *Atomic-Scale Structure Analysis in a Laboratory—A New EXAFS Facility*, K. Sakurai, Boundary, (1993): 40–46 (in Japanese).

108. *Grazing Incidence X-ray Fluorescence Spectrometry and Reflectometry with Synchrotron Radiation—A New Tool for Characterization of Thin Films*, K. Sakurai, Bull. Jpn. Inst. Met., 32 (1993): 323–30 (in Japanese).

109. *Ion Induced Auger Spectra*, M. Yoshitake, Bunseki, (1993): 828–30 (in Japanese).

110. *Analysis of Trace Elements by Glow Discharge Mass Spectrometry using Doped Electrode Technique*, M. Saito, Bunseki Kagaku, 42 (1993): 21–25 (in Japanese).

111. *Determination of Trace Silicon in Graphite Molybdosilicate Blue Spectrophotometry after Fluoride Separation*, H. Yamaguchi, K. Yamada, H. Okochi, and R. Hasegawa, Bunseki Kagaku, 42 (1993): 141–44 (in Japanese).

112. *Determination of Trace Impurities in Tungsten Disilicide by Graphite Furnace AAS and ICP-AES*, H. Yamaguchi, K. Yamada, O. Kujirai, and R. Hasegawa, Bunseki Kagaku, 42 (1993): 145–50 (in Japanese).

113. *Determination of Trace Silicon in High Purity Iron by Molybdsilicic Acid Blue Spectrophotometry following Fluoride Separation*, M. Kiyokawa, H. Yamaguchi, and R. Hasegawa, Bunseki Kagaku, 42 (1993): 219–22 (in Japanese).

114. *Determination of Trace Amounts of Sodium and Potassium in High-Purity Tantalum by Graphite-Furnace Atomic Absorption Spectrometry*, S. Hasegawa, T. Kobayashi, K. Ide, and R. Hasegawa, Bunseki Kagaku, 42 (1993): 643–47 (in Japanese).

115. *Problems of Low Cycle Fatigue Test at High Temperature*, K. Yamaguchi, M. Kitagawa (Ishikawajima-Harima Heavy Industries Co., Ltd.), Y. Fukuda (Hitachi, Ltd.), R. Komine

(PNC), and H. Hirata (Toshiba Corp.), ISIJ Int., 33 (1993): 817–24.

116. *EXAFS Experiments with High-Power Rotating Anode X-rays*, K. Sakurai, Jpn. J. Appl. Phys., 32 (1993): 261–63.

117. *Simultaneous Determination of Trace Impurities in High-Purity Chromium Metal and Chromium Disilicide by Inductively Coupled Plasma Atomic Emission Spectrometry after Coprecipitation*, O. Kujirai, K. Yamada, and R. Hasegawa, J. Anal. Atomic Spectr., 8 (1993): 481–85.

118. *Local Strain Sensing using Piezoelectric Polymer*, M. Egashira and N. Shinya, J. Intelligent Material Systems and Structures, 4 (1993): 558–60.

119. *X-ray Fluorescence Analysis on mg Order of Oxide Super Conductors by Glass Bead Technique and Matrix Correction using Theoretical Alpha Coefficients*, K. Sato, S. Itoh, and H. Okochi, J. Iron and Steel Inst. Jpn., 79 (1993): 948–54 (in Japanese).

120. *Parameter Analysis for Temperature and Strain Rate Dependence of Low-Cycle Fatigue Life at High Temperature*, K. Yamaguchi, K. Kobayashi, K. Ijima, and S. Nishijima, J. Iron and Steel Inst. Jpn., 79 (1993): 1284–87 (in Japanese).

121. *Low-Cycle Fatigue Life Analyzed by Parameter Method for Various High Temperature Materials*, K. Kobayashi, K. Ijima, K. Yamaguchi, and S. Nishijima, J. Iron and Steel Inst. Jpn., 79 (1993): 1288–92 (in Japanese).

122. *Interface Structure in Sintered Fe-Y203 Powder Studied by High Resolution Electron Microscopy*, K. Ogawa, J. Jpn. Inst. Met., 57 (1993): 706–13 (in Japanese).

123. *Analysis of Titanium Alloys by Glow Discharge Mass Spectrometry*, S. Itoh, F. Hirose, S. Hasegawa, and R. Hasegawa, J. Jpn. Inst. Met., 57 (1993): 1186–91 (in Japanese).

124. *Magnetic Flux Leakage by Adjacent Parallel Surface Cracks and Its Evaluation Methods*, I. Uetake and T. Saito, J. JSNDI, 42 (1993): 455–63 (in Japanese).

125. *Effects of Composition and Helium Injection on Dislocation Loop Development in Pure Fe-Ni-Cr Alloys under Ni Ion Irradiation*, T. Kimoto, J. Nucl. Mater., 203 (1993): 164–71.

126. *Auger Depth Profiling of a GaAs/AlAs Superlattice Structure by using Factor Analysis*, D. Fujita and K. Yoshihara, J. Surf. Sci. Soc. Jpn., 14 (1993): 32–29 (in Japanese).

127. *A New and Practical Energy Calibration Method using Spectrometer Offset Function in Auger Electron Spectroscopy*, D. Fujita and K. Yoshihara, J. Surf. Sci. Soc. Jpn., 14 (1993): 429–35 (in Japanese).

128. *Determination of Ultra Low Contents of Oxygen in High Purity Iron*, T. Yoshioka, H. Okochi, and R. Hasegawa, Mater. Trans., JIM 34 (1993): 504–10.

129. *Laboratory EXAFS*, K. Sakurai, O Plus E, (1993): 109–13 (in Japanese).

130. *Microcreep Deformation Measurements by a Moire Method using Beam Lithography and Electron Beam Scan*, T. Kishimoto, M. Egashira, and N. Shinya, Optical Eng., 32 (1993): 522–26.

131. *Evaluation of Composition by Microtomography using Conventional X-ray Sources*, Y. Yamauchi, N. Kishimoto, T. Ikuta (Osaka Electro-Communication Univ.), and T. Saito, Proc. of 3rd Jpn. Int. SAMPE Sympo., 2 (1993): 2137–40.

132. *In Situ Observation of MMC under Tensile Loading by Synchrotron X-ray CT*, Y. Tanaka, C. Masuda, *T. Hirano, *K. Usami (*Hitachi, Ltd.), and S. Nishijima, Proc. of 3rd Jpn. Int. SAMPE Sympo., 2 (1993): 2141–46.

133. *Measurement of Sound Velocity of High Sound Attenuation Materials by Frequency Response*, H. Fukuhara, Proc. of 3rd Jpn. Int. SAMPE Sympo., 2 (1993): 2207–11.

134. *Strain Measurement in Nanometer Scale with a Computer-Aided Scanning Tunneling Microscope*, K. Miyahara, S. Matsuoka, N. Nagashima, and H. Masuda, Proc. of Joint JSME/KSME Conf. on Recent Progress in Fracture Mechanics, (1993): 111–16.

135. *High-Intensity X-ray Line Focal Spot for Laboratory Extended X-ray Adsorption Fine Structure Experiments*, K. Sakurai, Rev. Sci. Instrum., 64 (1993): 267–68.

136. *High-Intensity Low Tube-Voltage X-ray Source for Laboratory Extended X-ray Adsorption Fine Structure Measurements*, K. Sakurai and H. Sakurai (Rigaku Denki Co.), Rev. Sci. Instrum., 64 (1993): 2702–03.

137. *Superplasticity in a Vanadium Alloyed Gamma Plus Beta Phased Ti-Al Intermetallics*, D. Vanderschueren (Catholic Univ. Leuven), M. Nobuki, and M. Nakamura, Scr. Metall., 28 (1993): 605–10.

138. *Nanoscopic Hardness Measurement by Scanning Tunneling Microscope*, N. Nagashima, S. Matsuoka, K. Miyahara, and H. Masuda, Trans. Jpn. Soc. Mech. Eng., A 59 (1993): 2005–10 (in Japanese).

139. *Current Distribution on Molten Pool in Stationary GAT Welding of Ti Alloy—Study on Behavior of Anode on Molten Pool in GAT Welding (Report 1)*, A. Okada and H. Nakamura, Trans. Jpn. Welding Soc., 24 (1993): 109–14.

140. *Anodic Spot Current on Molten Pool in Stationary GAT Welding—Study on Behavior of Anode on Molten Pool in GAT Welding (Report 2)*, A. Okada and H. Nakamura, Q. J. Jpn. Weld. Soc., 11 (1993): (in Japanese).

141. *Formation of Multitype Anode Spots in Stationary GAT Welding—Study on Behavior of Anode on Molten Pool in GAT Welding (Report 3)*, A. Okada and H. Nakamura, Q. J. Jpn. Weld. Soc., 11 (1993): 253–59 (in Japanese).

Simulation and theory

142. *Database System for Basic Studies of New Superconductors*, K. Hoshimoto, E. Nakata, T. Yokokawa, and S. Iwata (Univ. of Tokyo), Computer Aided Innovation of New Materials II, (1993): 69–72.

143. *Thermodynamics Aided Design of Multicomponent High Temperature Titanium Alloys (Ti-Al-Sn-Zr-Nb-Si System)*, H. Onodera, S. Nakazawa, T. Abe, T. Tsujimoto, and M. Yamazaki (Nishi Tokyo Univ.), Computer Aided Innovation of New Materials II, (1993): 1495–500.

144. *Characterization of Image Data using Sensory Test*, R. Kaneko, Y. Kurihara, K. Hoshimoto, M. Fujita, and M. Yamazaki (Nishi Tokyo Univ.), Computer Aided Innovation of New Materials II, (1993): 1501–04.

145. *Database for New Superconductors*, Y. Asada, Cryogenics Eng., 28 (1993): 298–303 (in Japanese).

146. *Impurity Diffusion Behavior in β-Titanium*, H. Onodera, H. Ohyama (Kobe Steel Ltd.), H. Nakajima (Iwate Univ.), H. Takatori (Nippon Mining Co., Ltd.), H. Fujii (Nippon Steel Corp.), T. Maeda (Sumitomo Metal Industries, Ltd.), H. Takahashi (NKK Co.) and S. Watakabe (Kawasaki Steel Corp.), Defect and Diffusion Forum, 95–98 (1993): 729–34.

147. *Creep Properties of $\alpha + \alpha_2$ Type Ti-Al-Sn-Zr-Nb-Si Alloys Designed with the Aid of Thermodynamics*, H. Onodera, T. Abe, S. Nakazawa, T. Yamagata, M. Yamazaki (Nishi Tokyo Univ.), and T. Tsujimoto, ISIJ Int., 33 (1993): 793–98.

148. *Study of Creep and Rupture Behavior for a Ni-Base Heat Resistant Alloy Improved for High Temperature Gas-Cooled Reactor*, H. Yoshizu, Y. Monma, E. Baba, *Y. Kurata, *H. Nakajima, and *T. Suzuki (*JAERI), JAERI-M, 93–231 (1993): 1–133 (in Japanese).

149. *Development of Simple Strain Distribution Measurement System by Interferometry using CCD Image Elements*, H. Hongo, H. Masuda, and Y. Monma, J. Iron and Steel Inst. Jpn., 79 (1993): 504–09 (in Japanese).

150. *In Situ Measurement of Strain Distribution using CCD Moire Interferometry*, H. Hongo, H. Masuda, and Y. Monma, J. Mat. Testing Research Association, 38 (1993): 13–17 (in Japanese).

151. *Materials Development towards the Reduction of Environmental Load—Design and Assessment of Metallic Materials for ECOMATERIALS*, K. Kimura and K. Yagi, J. M. E. S. J., 28 (1993): 540–47 (in Japanese).

152. *Analysis of Preferential Substitution Site of the Third Element in TiAl(L1o) Compound by the Cluster Variation Method*, T. Abe, T. Yokokawa, and H. Onodera, Proc. of Int. Conf. on Computer-Assisted Materials Design and Process Simulation, (1993): 308–13.

153. *Simulation System of Nuclear Transmutation and Radioactivation*, M. Fujita and T. Noda, Proc. of Int. Conf. on Computer-Assisted Materials Design and Process Simulation, (1993): 404–09.

154. *Characterization of the Microstructure in a Ti-6Al-4V Alloy by the Sensory Test and Its Application*, R. Kaneko, Y. Kurihara, M. Yamazaki (Nishi Tokyo Univ.), and M. Fujita, Proc. of Int. Conf. on Computer-Assisted Materials Design and Process Simulation, (1993): 492–97.

155. *New Design Concept of Material with Minimized Environmental Load*, K. Yagi and K. Kimura, Proc. of Int. Workshop on Environmentally Compatible Materials and Recycling Technology, (1993): 105–10.

156. *Reliability of Creep Rupture Lives Extrapolated by Time-Temperature Parameter Methods*, K. Maruyama (Tohoku Univ.), E. Baba, K. Yokokawa, H. Kushima, and K. Yagi, Report of 123rd Committee on Heat-Resisting Metals and Alloys Jpn. Soc. for the Promotion of Sci., 34 (1993): 257–64 (in Japanese).

157. *Prediction of Fatigue Strength Properties using Materials Strength Database (2nd Report, Prediction of Low-Cycle Fatigue Strength)*, M. Nihei and T. Konno, Trans. Jpn. Soc. Mech. Eng., A 59 (1993): 1390–94 (in Japanese).

158. *Characterization for Each Group Having Same Type Microstructures in Ti-6Al-4V by Sensory Test*, R. Kaneko, Y. Kurihara, and M. Fujita, Zairyokagaku, 30 (1993): 315–21 (in Japanese).

Materials

Non-ferrous materials

159. *Characteristics of EB Weldable PM Mo and Mo-Re Alloys*, F. Morito, JOM, 45 (1993): 54–58.
160. *Preparation and Characterization of Sintered Mo-Re Alloys*, F. Morito, J. de Physique, 3 (1993): 553–56.
161. *Microstructures and Mechanical Behaviors of Mo-Re Welds*, F. Morito, Proc. of 13th Int. Plansee Seminar, 1 (1993): 585–95.

Intermetallic compounds

162. *Electrical Conductivity of Solid Beryllium Sulfide*, A. Kasahara, Y. Ogawa, S. Iwasaki, and H. Nakamura, Mater. Trans., JIM 34 (1993): 786–91.
163. *Effect of Microstructure on Oxidation Behavior of TiAl Inter Metallic Compound*, K. Kasahara and A. Takei, J. Jpn. Inst. Met., 57 (1993): 544–48 (in Japanese).
164. *Effect of Third Elements on Damping Capacity of Mn-20Cu Alloy*, K. Kawahara, N. Sakuma, and Y. Nishizaki (Chiba Inst. Technol.), J. Jpn. Inst. Met., 57 (1993): 1089–96 (in Japanese).
165. *Effect of Fourth Elements on Damping Capacity of Mn-20Cu-5Ni Alloy*, K. Kawahara, N. Sakuma, and Y. Nishizaki (Chiba Inst. Technol.), J. Jpn. Inst. Met., 57 (1993): 1097–100 (in Japanese).
166. *Effect of Surface Roughness on High-Temperature Oxidation of γ-TiAl Alloy*, K. Kasahara and M. Takeyama, J. Jpn. Inst. Met., 57 (1993): 1288–92 (in Japanese).
167. *Environmental Effect on Mechanical Properties of TiAl Base Alloy*, M. Nakamura, K. Hashimoto, T. Tsujimoto, and T. Miura, J. Mater. Sci., 8 (1993): 68–77.

Composite materials

168. *Thermal Stability of FRM*, Y. Shinohara, Zairyokagaku, 30 (1993): 130–35 (in Japanese).
169. *Consideration on Coupling Application of Biomedical Titanium Alloy with Stainless Steel*, A. Hoshino, Zairyo-to-Kankyo, 42 (1993): 291–96 (in Japanese).

Materials for mechanical application

170. *Strengthening Capability of Beta Titanium Alloys*, Y. Kawabe and S. Muneki, Beta Titanium Alloys in the 1990's, (1993): 187–97.
171. *Thermal Stability of Plasma Sprayed Ni-Cr-Al-Y/YSZ PGM in Uniform and Gradient Temperature Fields*, Y. Shinohara, Y. Imai, S. Ikeno, I. Shiota (Kougakuin Univ.), and T. Fukushima, Ceram. Trans., 34 (1993): 255–62.
172. *Effect of Beta Grain Size and Aged Structures on Strength and Toughness in a Ti-3Al-8V-6Cr-4Mo-4Zr Alloy*, S. Muneki, Y. Kawabe, and J. Takahashi, J. Jpn. Inst. Met., 57 (1993): 268–73 (in Japanese).
173. *Metal-Ceramics Composites*, Y. Shinohara, Metals & Technology, 63 (1993): 72–77 (in Japanese).
174. *Mechanical Properties of Ti_2AlNb Intermetallics Produced by Blended Elemental and Prealloyed P/M Methods*, S. Emura, M. Hagiwara, Y. Kawabe, and S. Mori (Sumitomo Sitix Corp.), Proc. of 1993 Powder Metall. World Cong., (1993): 1160–63.
175. *Condition Mechanism of Iron Disilicides Doped with Aluminum*, Y. Shinohara, Y. Imai, I. Shiota (Kougakuin Univ.), M. Okamoto, and I. Nishida, Proc. of 6th Sympo. on Functionally Gradient Materials, (1993): 169–74.
176. *Mechanical Properties of Ceramic Particulates-reinforced Titanium-Based Composites Produced by Blended Elemental Powder Metallurgy*, M. Hagiwara, S. Emura, Y. Kawabe, *N. Arimoto, and *S. Mori (*Sumitomo Sitix Corp.), Proc. of Int. Sympo. on Light Materials for Transportation Systems, (1993): 903–10.

Materials for electronics application

177. *Phase Studies and Superconducting Properties of Ag-Added $Bi_2Sr_2CaCu_2O_y$/Ag Tapes*, T. Hasegawa, H. Kobayashi, H. Kumakura, H. Kitaguchi, and K. Togano, Advanced in Superconductivities V, (1993): 737–40.
178. *Fabrication Conditions and Superconducting Properties of Ag-Sheathed Bi-Sr-Ca-Cu-O Tapes Prepared by Partial Melting and Slow Cooling Process*, *K. Nomura, *M. Kiyofuji (*Hitachi Cable, Ltd.), H. Kitaguchi, H. Kumakura, K. Togano, and H. Maeda, Appl. Phys. Lett., 62 (1993): 1–13.
179. *Growth of GaAs Epitaxial Microcrystals by Droplet Epitaxy*, N. Koguchi, Bull. Jpn. Inst. Met., 32 (1993): 485–94 (in Japanese).
180. *Axial and Transverse Stress/Strain Dependence of Critical Temperature in Bronze Processed Nb_3Sn Wires*, T. Kuroda and H. Maeda, Cryogenic Eng., 28 (1993): 274–80 (in Japanese).

181. *Effects of Transverse Compressive Stress on the Critical Current in Nb_3Sn and Nb_3Al Wires*, T. Kuroda and H. Maeda, Cryogenic Eng., 28 (1993): 439–45 (in Japanese).

182. *High-T_c Oxide Superconducting Tapes and Wires*, H. Kamakura, Cryogenic Eng., 28 (1993): 484–91 (in Japanese).

183. *Critical-Current Degradation in Nb_3Al Wires Due to Axial and Transverse Stress*, T. Kuroda, H. Wada, S. Bray, and J. Ekin, Fusion Engineering and Design, 20 (1993): 271–75.

184. *Multifilamentary Nb_3Al Wires Reacted at High Temperature for Short Time*, M. Kosuge, Y. Iijima, T. Takeuchi, K. Inoue, T. Kiyoshi, H. Irie, and K. Watanabe (Tohoku Univ.), IEEE Trans. on Applied Superconductivity, 3 (1993): 1010–13.

185. *Superconductivity of Nb_3Al Formed by Solid State Reaction of Nb with Ag-Based Alloy*, T. Takeuchi, M. Kosuge, Y. Iijima, and K. Inoue, IEEE Trans. on Applied Superconductivity, 3 (1993): 1014–17.

186. *Preparation of Ag-I Intercalated $Bi_2Sr_2CaCu_2O_y$ Superconductor*, H. Kumakura, J. Ye, H. Kitaguchi, K. Togano, and J. Shimoyama (Asahi Glass Co, Ltd.), Jpn. J. Appl. Phys., 32 (1993): 894–97.

187. *Structural Changes and Annealing Behavior of Ar-Ion-Irradiated Superconducting BiSrCaCuO Thin Films*, M. Kaise and K. Saito, Jpn. J. Appl. Phys., 32 (1993): 942–48.

188. *Growth of GaAs Epitaxial Microcrystals on an S-Terminated GaAs Substrate by Successive Irradiation of Ga and As Molecular Beams*, N. Koguchi and K. Ishige, Jpn. J. Appl. Phys., 32 (1993): 2052–58.

189. *Effect of High Energy Ion Irradiation and Electron Irradiation on Textured $Bi_2Sr_2CaCu_2O_x$*, H. Kumakura, H. Kitaguchi, K. Togano, H. Maeda, J. Shimoyama (Asahi Glass Co, Ltd.), *S. Okayasu, and *Y. Kazumata (*JAERI), J. Appl. Phys., 74 (1993): 451–57.

190. *V_3Si Multifilamentary Superconductor Produced by a Modified Bronze Process*, T. Takeuchi and K. Inoue, J. Appl. Phys., 74 (1993): 6454–56.

191. *Fabrication of 30 nm Thick Superconducting BiSrCaCuO Thin Films by Single-Target Magnetron Sputtering Method*, M. Kaise and K. Saito, J. Jpn. Inst. Met., 57 (1993): 103–07 (in Japanese).

192. *New Selective Molecular-Beam Epitaxial Growth Method for Direct Formation of GaAs Quantum Dots*, J. Vac. Sci. Technol., B11 (1993): 787–90.

193. *A Selective Growth of GaAs Microcrystals Grown on Se-Terminated GaAlAs Surface for the Quantum Well Box Structure*, T. Chikyow and N. Koguchi, Mater. Res. Soc. Sympo. Proc., 283 (1993): 765–70.

194. *Growth of GaAs Epitaxial Microcrystals on a S-Terminated GaAs(001) by VLS Mechanism in MBE*, N. Koguchi, K. Ishige, and S. Takahashi, Mater. Res. Soc. Sympo. Proc., 283 (1993): 815–20.

195. *Microstructural Aspects of Materials for Nondestructive Long-Pulse High-Field Magnets*, J.D. Embury, M.A. Hill, W.A. Spitzip, and Y. Sakai, MRS Bull., 18 (1993): 57–60.

196. *Present Status of High-T_c Oxide Superconducting Wires and Tapes*, H. Kumakura and H. Maeda, Oyobutsuri, 62 (1993): 455–58 (in Japanese).

197. *Arsenic Absorption on GaAs(001)*, H. Norenberg and N. Koguchi, Surf. Sci., 296 (1993): 199–212.

198. *Growth of GaAs Epitaxial Microcrystals on an S-Terminated GaAs Substrate in MBE*, N. Koguchi, K. Ishige, and S. Takahashi, 12th Record of Alloy Semiconductor Physics Electronics Sympo., (1993): 217–22.

Magnetic materials

199. *Iron-Nitride Ultrafine Particles and Iron-Nitride Magnetic Fluids*, I. Nakatani, Ceramics, 28 (1993): 1056–64 (in Japanese).

200. *Thermal Switch Properties of $Dy_3Ga_5O_{12}$ Garnet Single Crystal*, T. Numazawa, H. Kimura, M. Sato, and H. Maeda, Cryogenic Eng., 28 (1993): 588–92 (in Japanese).

201. *Iron-Nitride Magnetic Fluids Prepared by Vapor-Liquid Reaction and Their Magnetic Properties*, I. Nakatani, M. Hijikata, and K. Ozawa, J. Mag. Mag. Mater., 122 (1993): 10–14.

202. *Effects of Heat Treatment on Properties of Magnetic Fluids*, I. Nakatani, *H. Yamamoto, and *T. Sugano (*NOK Corp.), J. Mag. Mag. Mater., 122 (1993): 15–18.

Materials for energy application

203. *Control of Precipitation and Phase Stability in Steels Consisting of Low Activation Elements*, F. Abe, T. Noda, and M. Okada, Bull. Jpn. Inst. Met., 32 (1993): 543–52 (in Japanese).

204. *Present Status and Future Prospect of Reduced-Activation Ferritic/Martensitic Steels*, F. Abe, Fusion Reactor Materials Forum, 8 (1993): 13–45 (in Japanese).

205. *Thermal Relaxation of Lattice Disorder in Graphite under Ion Irradiation*, *E. Asari, M. Kitajima, K. Nakamura, and *R. Kawabe (*Univ. of Tsukuba), J. Jpn. Soc. Surf. Sci., 14 (1993): 301–06 (in Japanese).

206. *Corrosion Behavior of Ni-Base Superalloys at 1373 K in Simulated HTGR Impure Helium Gas Environment*, I. Mutoh, Y. Nakasone, K. Hiraga, and T. Tanabe, J. Nucl. Mater., 207 (1993): 212–20.

207. *Thermal Relaxation of Ion-Irradiation Damage in Graphite*, *E. Asari, M. Kitajima, K. Nakamura, and *R. Kawabe (*Univ. of Tsukuba), Phys. Rev., B 48 (1993): 11143–48.

208. *Japanese Approaches to Ferritic/Martensitic Steels*, F. Abe, A. Kayama, M. Tamura, and A. Hishinuma, Proc. of IEA Workshop on Ferritic Martensitic Steels, (1993): 106–24.

209. *Silicon Water Orientation Dependence in the Initial Plasma Oxidation Processes*, *H. Kuroki, K. Nakamura, *R. Kawabe (*Univ. of Tsukuba), and M. Kitajima, Solid State Commun., 88 (1993): 487.

Materials for environmental application

210. *Evolution of Material into Ecomaterials*, H. Harada, Kagaku to Kogyo, 67 (1993): 418–25 (in Japanese).

211. *New Materials Development Concept from Global Environment—Ecomaterials and Metallic Materials*, K. Yagi, Metals & Technology, 63 (1993): 5–10 (in Japanese).

Intelligent materials

212. *Research and Development of Intelligent Materials*, N. Shinya, J. Jpn. Hydraulics and Pneumatics Soc., 24 (1993): 65–73 (in Japanese).

Processing

Separation and synthesis

213. *Bath Vibration in Bottom Blowing Through Type Reactor*, Y. Fukuzawa, S. Furuyama, S. Iwasaki, and A. Fukuzawa, J. Iron and Steel Inst. Jpn., 79 (1993): 464–71 (in Japanese).

214. *Solid State Deoxidation of Some Rare Earth Metals and Reduction of Their Interstitial Impurity Concentrations by Electron Beam Melting*, K. Kamihira, R. Hasegawa, and O. Ogawa (Univ. of Tokyo), Mater. Trans., JIM 34 (1993): 243–47.

Gaseous process

215. *Effect of Incident Direction of ArF Laser to Graphite Substrates on the Formation of Photo-Chemical Vapor Deposition SiC Film*, Y. Suzuki, H. Araki, and T. Noda, Jpn. J. Appl. Phys., 32 (1993): 3566–71.

216. *Removal of Oxygen from Praseodymium by Calcium Vapor*, *O. Ogawa, K. Kamihira, *A. Ando (*Univ. of Tokyo), and R. Hasegawa, J. Alloys and Compound, 193 (1993): 17–19.

217. *Control of Zinc Concentration and Growth Rate of Beta Phase in Copper-Zinc Alloy by Heating Pure Copper in Zinc Vapor*, H. Sasano, *H. Arai, and *T. Suzuki (*Kougakuin Univ.), J. Jpn. Inst. Met., 57 (1993): 440–44 (in Japanese).

218. *Preparation and Characterization of Cu-Zn-Al Shape Memory Alloy by Heating in Zinc Vapor*, H. Sasano, *H. Arai, and *T. Suzuki (*Kougakuin Univ.), J. Jpn. Inst. Met., 57 (1993): 445–48 (in Japanese).

219. *Microstructure and Growth of SiC Film by Excimer Laser Chemical Vapor Deposition at Low Temperatures*, T. Noda, Y. Suzuki, H. Araki, F. Abe, and M. Okada, J. Mater. Sci., 28 (1993): 2763–68.

220. *Processing of Carbon Fiber/SiC Composite for Low Activation*, T. Noda, H. Araki, F. Abe, and Y. Suzuki, Mater. Trans., JIM 34 (1993): 1122–29.

221. *RBS-PIXE Analysis on Thin Films of High-T_c Oxide Superconductors*, A. Ishii and K. Nakamura, Nuclear Instruments and Methods in Physics Res., B 75 (1993): 388–91.

222. *Preparation of $YBa_2Cu_3O_y$ Superconducting Thin Films by Radio-Frequency Plasma Flash Evaporation Apparatus*, K. Komori, *W. Fukunaga, M. Fukutomi, Y. Tanaka, T. Asano, H. Maeda, and *N. Hosokawa (*Anelva Corp.), Phase Transitions, 42 (1993): 117–22.

223. *Oxygen Potential Control in $YBa_2Cu_3O_{7-\delta}$ Thin Films*, K. Nakamura, J. Ye, and A. Ishii, Physica, C 213 (1993): 1–13.

224. *Characterization of Ti-Ni Shape Memory Thin Films Formed by Sputtering*, A. Takei, A. Ishida, and S. Miyazaki (Univ. of Tsukuba), Proc. of 1st Int. Conf. on Processing Materials for Properties, (1993): 1177–80.

225. *SiC Film Formation by ArF Laser CVD*, Y. Suzuki, H. Araki, and T. Noda, Proc. of 3rd Jpn. Int. SAME Sympo., 2 (1993): 1135–40.

226. *Shape Memory Thin Film of Ti-Ni Formed by Sputtering*, A. Ishida, A. Takei, and S. Miyazaki (Univ. of Tsukuba), Thin Solid Films, 228 (1993): 210–14.

227. *Formation of Thin Films by Dry Processing (PVD, CVD)*, A. Takei, Zairyokagaku, 30 (1993): 53–60 (in Japanese).

Liquid state process

228. *Unidirectional Solidification of Ni_3Al by a Floating Zone Method*, T. Hirano and T. Mawari, Acta Metall. Mater., 41 (1993): 1783–89.
229. *Application Modes of Ultrasonic Vibration to Molten Metal and Their Effect on Solidification Structures*, Y. Ohsawa, A. Sato, T. Namai, and G. Aragane, J. Jpn. Found. Soc., 65 (1993): 288–93 (in Japanese).
230. *Production of Aluminum Alloy Profile Rods by a Moldless Upward Continuous Casting Process*, A. Sato, Y. Ohsawa, and G. Aragane, J. Jpn. Inst. Met., 57 (1993): 93–98 (in Japanese).
231. *Attack on Magnesia Crucible by Molten Iron*, T. Dan. N. Aritomi, K. Ogawa, K. Honma, and T. Kimura, Mater. Trans., JIM 34 (1993): 460–66.
232. *Suppression of Environmental Embrittlement in Boron-Free Ni_3Al by Unidirectional Solidification*, C. Nishimura, T. Hirano, and M. Amano, Scr. Metall. Mater., 29 (1993): 1205–09.

Powder processing

233. *Reactive Sintering of Ni_3Al under Compression*, C. Nishimura, C.T. Liu (Oak Ridge Natl. Lab.), Acta Metall. Mater., 41 (1993): 113–20.
234. *Composite Ultrafine Particles*, S. Ohno, Ceramics, 28 (1993): 1175–82 (in Japanese).
235. *Characterization of the Surface Oxide Layer of Iron Ultrafine Particles*, T. Uchikoshi. M. Yoshitake, Y. Sakka, T. Furubayashi, and K. Yoshihara, J. Chem. Soc. Jpn., (1993): 92–97 (in Japanese).
236. *Production of Highly Densified TiAl by Die Compaction-Sintering Method*, Y. Muramatsu, T. Ohkoshi, and H. Suga, J. Jpn. Inst. Met., 57 (1993): 944–51 (in Japanese).
237. *Solidified Structure of Centrifugally Atomized Alloy Powder*, K. Halada, H. Suga, and K. Minagawa, J. Jpn. Soc. Powder Powder Metall., 40 (1993): 1154–59 (in Japanese).
238. *Solidified Microstructure of Zn-Al Alloy Powder Produced by Various Atomization*, K. Halada, K. Minagawa, K. Chiba (Shibaura Inst. Technol.), and J. Bie (Delft Inst. Technol.), J. Jpn. Soc. Powder Powder Metall., 40 (1993): 1160–65 (in Japanese).
239. *Measurement of Water Jet Properties of High Pressure Water Atomization*, K. Minagawa, K. Halada, and K. Chiba (Shibaura Inst. Technol.), J. Jpn. Soc. Powder Powder Metall, 40 (1993): 1166–69 (in Japanese).
240. *Study on the Creation of Micro-Porous-Sphere by Ultrafine Particles*, H. Okuyama, S. Ohno, K. Minagawa, and K. Halada, J. Jpn. Soc. Powder Powder Metall., 40 (1993): 1174–78 (in Japanese).
241. *Effect of Water Jet on the Formation of Super Fine Powders by High Pressure Water Atomization*, K. Minagawa, K. Chiba (Shibaura Inst. Technol.), and K. Halada, J. Jpn. Soc. Powder Powder Metall., 40 (1993): 1231–37 (in Japanese).
242. *The Vaporization Phenomenon of Molten Metal during "Hydrogen Plasma-Metal" Reaction*, S. Ohno, J. High Temperature Soc. Jpn., 19 (1993): 105–11 (in Japanese).
243. *Combustion-Synthesized Functionally Gradient Refractory Materials*,, *S.E. Niedzialek, *G.C. Stangle (*New York State College), and Y. Kaieda, J. Mater. Res., 8 (1993): 2026–34.
244. *Sintering Characteristics of Fe and FeCo Alloy Ultrafine Powders*, Y. Sakka, T. Uchikoshi, and E. Ozawa (K. K. L' Air Liquid Lab.), J. Mater. Sci., 28 (1993): 203–17.
245. *Surface Chemistry and Sintering Characteristics of Nickel Ultrafine Powders*, Y. Sakka and T. Uchikoshi, Powder Metall, 36 (1993): 179–85.
246. *Effect of Water Jet on the Formation of Super Fine Powder by High Pressure Water Atomization*, Proc. of 1993 Powder Metall. World Cong., (1993): 78–81.
247. *Self-Propagating Reaction Sintering of Intermetallic Compounds*, Y. Kaieda, Proc. of 1993 Powder Metall. World Cong., (1993): 395–400.
248. *Fabrication of Porous Materials by Consolidating Ultrafine Metal Powders*, Y. Sakka, T. Uchikoshi, S. Ohno, and H. Okuyama, Proc. of 1993 Powder Metall. World Cong., (1993): 792–95.

Joining

249. *Diffusion Bonding*, O. Ohashi, J. Jpn. Weld. Soc., 62 (1993): 512–17 (in Japanese).
250. *Interface Structure at Wetting Tip of Molten Sn-Pb Alloy on Pure Cu-Plate—Wetting of Sn-Pb Alloys on Cu Plate (1)*, K. Sasabe and O. Ohashi, Q. J. Jpn. Weld. Soc., 11 (1993): 401–04 (in Japanese).
251. *Interfacial Energy and Wetting of Cu/Sn-Pb Alloy—Wetting of Sn-Pb Alloys on Cu Plate (2)*, K. Sasabe and O. Ohashi, Q. J. Jpn. Weld. Soc., 11 (1993): 405–09 (in Japanese).
252. *Diffusion Welding of Laminated Stainless Steel Wafers*, O. Ohashi, Q. J. Jpn. Weld. Soc., 11 (1993): 489–93 (in Japanese).

Composite process

253. *Pressure Infiltration under Semi-Molten State for Making Composite Layer Structure*, T. Dendo, T. Shirota and M. Kikuchi (Univ. of Tokyo), Advanced Technology of Plasticity, 4 (1993): 194–99.

Process with aid of beam technology

254. *Influence of Ion Implantation and Etching on the Photoluminescence from Porous Silicon*, A.K. Kuprin, N. Ishikawa, K. Furuya, and T. Saito, Proc. of 3rd Jpn. Int. SAMPE Sympo., 2 (1993): 976–81.

255. *Demixing in Argon-Helium Mixed Gas Welding Arcs*, K. Hiraoka, Proc. of 11th Int. Sympo. on Plasma Chemistry, (1993): 440–45.

256. *Melting Process and Spiking Phenomenon in Electron Beam Welding*, S. Tsukamoto and S. Irie, Trans. Jpn. Weld. Soc., 24 (1993): 18–23.

257. *Evaluation of Local Plasma Composition and Temperature in Mixed Gas Tungsten Arc Plasma Column by Light Spectroscopy—Study on Characteristics of Gas Tungsten Arc Shielded by Mixed Gases (Report 2)*, K. Hiraoka, Q. J. Jpn. Weld. Soc., 11 (1993): 68–74 (in Japanese).

Processing in special environment

258. *Development of High Field Magnets at the National Research Institute for Metals*, T. Kiyoshi, K. Inoue, and H. Maeda, Bull. Jpn. Inst. Met., 32 (1993): 409–16 (in Japanese).

259. *Development of 20 T Large Bore Superconducting Magnets (I)—Design for Coils*, T. Kiyoshi, K. Inoue, K. Itoh, T. Takeuchi, H. Wada, H. Maeda, *K. Kuroishi, *T. Takizawa, *F. Suzuki, and *N. Tada (*Hitachi, Ltd.), Cryogenic Eng., 28 (1993): 253–59 (in Japanese).

260. *Development of 20 T Large Bore Superconducting Magnets (II)—Design for Cooling Systems*, T. Kiyoshi, K. Inoue, K. Itoh, T. Takeuchi, H. Wada, H. Maeda, *K. Kuroishi, *T. Takizawa, *F. Suzuki, and *H. Mori (*Hitachi, Ltd.), Cryogenic Eng., 28 (1993): 260–67 (in Japanese).

261. *Development of 20 T Large Bore Superconducting Magnets (III)—Operation Results*, T. Kiyoshi, K. Inoue, K. Itoh, T. Takeuchi, M. Kosuge, Y. Iijima, *K. Kuroishi, *T. Takizawa, *F. Suzuki, and *Y. Sato (*Hitachi, Ltd.), Cryogenic Eng., 28 (1993): 268–73 (in Japanese).

262. *Generation of Magnetic Fields Over 20 T using Developed Superconducting Magnet System*, T. Kiyoshi, K. Inoue, K. Itoh, T. Takeuchi, H. Wada, H. Maeda, *K. Kuroishi, *F. Suzuki, *T. Takizawa, *N. Tada, and *H. Mori (*Hitachi, Ltd.), IEEE Trans. on Applied Superconductivity, 3 (1993): 78–81.

263. *High Field Pulsed Magnet Wound of Cu-Ag Alloy Wire*, T. Asano, Y. Sakai, K. Inoue, M. Oshikiri, and H. Maeda, Jpn. J. Appl. Phys., 32 (1993): 1027–29.

264. *Auger Electron Spectroscopy Analyses of the Interface of Titanium-Clad Steels with Ultra-Low-Carbon Contents*, D. Fujita and K. Yoshihara, J. Iron and Steel Inst. Jpn., 79 (1993): 1088–94 (in Japanese).

265. *Melting and Solidification of Y-Ba-Cu-O Ceramics in Microgravity by Utilizing TR-1A Sounding*, H. Kitaguchi, K. Togano, *S. Yoda, *M. Machida, and *H. Nishimura (*NASDA), J. Jpn. Soc. Microgravity Appl., 10 (1993): 15–25 (in Japanese).

266. *Melting and Solidification of Dispersion Alloys in Microgravity Environment*, Y. Muramatsu, K. Halada, T. Dan, S. Yoda (NASDA), and S. Anzawa (Ishikawajima-Harima Heavy Industries Co., Ltd.), J. Jpn. Soc. Microgravity Appl., 10 (1993): 26–37 (in Japanese).

267. *Magnetic Levitation Transport System for Extremely High Vacuum*, M. Tosa, A. Itakura, and K. Yoshihara, J. Vac. Soc. Jpn., 36 (1993): 253–56 (in Japanese).

268. *Extreme High Vacuum and Baking*, D. Fujita, Netsu Shori, 33 (1993): 139–43 (in Japanese).

269. *GaAs/AlAs Superlattice as a Proposed New Reference Material for Sputter Depth Profiling*, K. Yoshihara, *D.W. Moon, D. Fujita, *K.J. Kim (*Korea Res. Inst. Standards and Science), and K. Kajiwara (Sony Corp.), Surface and Interface Analysis, 20 (1993): 1061–66.

❒ NRIM Publications (Apr. 1993 to Mar. 1994)

1. Bulletin of National Research Institute for Metals, in Japanese.
   No. 15 (Mar. 1994)
2. Annual Report of National Research Institute for Metals, in Japanese.
   For fiscal year of 1992 (Nov. 1993)
3. Kinzaigiken News, in Japanese.
   Nos. 4 to 12 (1993) and Nos. 1 to 3 (1994)
4. NRIM Research Activities, in English.
   (Oct. 1993)
5. NRIM Special Report, in English.
   Nos. SR-94-1 and 2 (Mar. 1994)
6. Material Strength Data Sheet, in English.
   NRIM Creep Data Sheet,
   Nos. 17B and 20B (Jan. 1994)
   Nos. 13B and 31B (Mar. 1994)
   NRIM Fatigue Data Sheet,
   Nos. 73 to 78 (Dec. 1993)

International Exchange Apr. 1993 to Mar. 1994

❒ International Collaboration Research

Australia

1. Study on Surface Modification of Metals with Ultra-High Temperature Heat Sources. (CSIRO)

Brazil

1. Study on Ni-Base Superalloys. (Fundacao de Technologia Industrial)

Canada

1. Damage Evaluation and Remaining Life Prediction of Structural Materials. (Canadian Center for Mineral and Energy Technology)

China

1. Investigation of High Temperature Titanium Alloy for Application over 600 °C. (Northwest Institute for Non-Ferrous Metal Research)
2. Studies on Structural Control and Superconducting Properties of High Temperature Superconductors. (Institute of Metal Research Academia Sinica)
3. Study on the Combustion Synthesis of Intermetallic Compounds. (Northwest Institute for Non-Ferrous Metal Research)
4. Fundamental Study on the Improvement of Superconductivity for High-T_c Oxide. (Northwest Institute for Non-Ferrous Metal Research)
5. Study of Localized Corrosion Damage of Corrosion Resistance Alloys in High Temperature Aqueous Solution. (Shanghai Jiao Tong University)

Finland

1. Development of Superconductive Thin Oxide Coatings. (Tampere University of Technology)

France

1. Superconducting and Cryogenic Magnetic Materials. (Service National des Champs Intenses, Centre National de la Recherche Scientifique Grenoble and Others)

Germany

1. Development of Superconducting Materials. (Kernforschungszentrum Kerlsruhe)
2. Exchange of Creep and Fatigue Data Sheet. (5 Institutes)

Italy

1. Superconducting Properties of Advanced Superconductors in Time-Varying Magnetic Fields. (CISE Spa, Technologia Innovative Thermophysics & Cryogenics Sec.)
2. Intercomparison of Methods and Materials for Strain Measurements at Cryogenic Temperatures. (Instituto di Metrogia "G. Colonettie"-C.N.R.)
3. Study on the Mechanism of Deformation, Fracture and Corrosion in Ni-Based Superalloys. (Instituto per la Tecnologia dei Materiali Metallicinon Tradizionali)

Korea

1. Development of the Aluminaid-Base Intermetallic Compounds for Structural. (Korea Institute of Machinery and Metals)
2. Characterization of the Composite Film with Dispersion of Carbide Phase by PVD and CVD Process and the Establishment of the Process Parameters Leading to Fabrication Techniques. (Korea Institute of Machinery and Metals)
3. Performance Characterization of Materials at High-Temperature. (Korea Standards Research Institute)
4. Development of Metallic Superconducting Materials. (Korea Research Institute of Standard Science)

Russia

1. Research Cooperation on Materials Property Data Modeling. (Institute Inorganic Chemistry, Academy of Science, Siberia)
2. Water Purification through Adsorptive Electrochemical Dispersed Systems. (Frumukin Institute of Electrochemistry)

Sweden

1. Application of Advanced Electromagnetic Technology to the Metallurgical Processing. (Royal Institute of Technology)

U.K.

1. Evaluation of Life and Remaining Life Prediction of Huge Structures under Service Operation. (Welding Institute)

U.S.A.

1. Combustion Synthesis for Production of Ceramic, Intermetallic and Composite Materials. (Alfred University)
2. Research and Development on Systems and Materials for Magnetic Refrigerators. (Francis Bitter National Magnet Laboratory)
3. Database of Properties for High-Temperature Superconducting Materials. (National Institute of Standards and Technology)
4. Studies of High-Strength/High Conductive Materials and Their Application to High-Field Magnets. (Francis Bitter National Magnet Laboratory)
5. Fundamental Studies on the Conductor Fabrication of High Temperature Oxide Superconducting Materials. (University of Illinois)
6. Evaluation Methods for Superconductors. (National Institute of Standards and Technology)

❒ List of Guest Researchers

*STA Fellowship

Nationality and Name	Affiliation	Term	Research Subject
America			
Justin Schwartz	National High Magnetic Field Laboratory Florida State University	1994.3.13 to 1994.3.19	Studies on Fabrication Processes of BiSrCaCuO Superconductors
Ronald B. Goldfarb	National Institute of Standards and Technology	1993.7.6 to 1993.8.14	A Study on AC Loss Measurement Methods
Yukikazu Iwasa	Francis Bitter National Magnet Laboratory of Massachusetts Institute of Technology	1994.3.11 to 1994.3.31	Research and Development on Systems and Materials for Magnetic Refrigeration
James S. Brooks	Boston University	1993.11.9 to 1993.12.31	Electronic Structure of Organic Conductors
Australia			
A.J. D. Farmer	Commonwealth of Science and Industrial Research	1994.1.23 to 1994.1.29	Fundamental Research of Plasma Diagnostics in Free-Burning Arcs
Brazil			
Flavio Beneduce Neto	Institute for Technological Research of the State of Sao Paulo	1993.6.28 to 1993.8.13	The Technological Capacitation in Materials Project—Metallurgy Area
Joao Pedro Valls Tosetti	Institute for Technological Research of the State of Sao Paulo	1993.6.28 to 1993.8.13	Same as above
Canada			
J.S. Kirkaldy	McMaster University	1993.9.5 to 1993.9.12	Computer-Assisted Materials Design and Process Simulation
W.R. Datars	McMaster University	1994.2.24 to 1994.3.6	dHvA Effect Study of Intercalated Graphite
China			
Yao Qizhou	Institute of Metal Research Academia Sinica	1994.3.22 to 1994.3.31	Study on Mutual Research Works on BiSrCaCuO Superconductors Developments
Zeng Quan Pu	Northwest Institute for Non-ferrous Metal Research	1993.11.25 to 1993.12.18	Production and Evaluation of Particulate-Reinforced Titanium Matrix Composites
Gui-Wen Qiao	Institute of Metal Research Academia Sinica	1994.3.11 to 1994.3.26	High-Resolution Electron Microscopy of the Bi System Superconducting Ultrathin Films
Liu Jian Hong	Metal Materials Department, Harbin Institute of Technology	1994.1.12 to 1995.4.30	Microstructure and Mechanical Properties of Ti_2AlNb
Ding Ya Ping	Shanghai Nuclear Engineering Research and Design Institute	1993.11.30 to 1993.12.20	Studies of Local Corrosion Damage of Corrosion Resistant Alloys in High Temperature Water
Tian Bo Yuan	Shanghai Nuclear Engineering Research and Design Institute	1993.11.30 to 1993.12.9	Same as above

Nationality and Name	Affiliation	Term	Research Subject
Czecho			
B. Strnadel*	Technical University, Institute of Metal Science	1993.2.1 to 1994.1.31	Cyclic $\gamma \leftrightarrow \varepsilon$ Transformation Behavior and Its Effect on the Shape Memory Characteristics in Fe-Mn-Si-Cr-Ni Alloy
France			
J.J. Balette Pape*	University of Bordeaux	1992.1.9 to 1993.7.8	Deformation Mechanisms of Metal Matrix Composites
Germany			
Holger Norenberg*	Rostock University	1992.3.3 to 1993.4.20	Investigation of Arsenic Adsorption on GaAs(001) using RHEED and HRSEM
H.G. Gross*	Association of Quality Assurance in Material Welding Techniques	1993.3.22 to 1993.9.21	Investigation for Correlation between Laser Speckle Method and Mechanical Properties during Welding Cycle
India			
R. Sethumadhavan*	Bishop-Heber College	1994.2.1 to 1995.1.31	Fundamental Study on Biocompatibility of Materials
R. Chatterjee*	Indian Institute of Technology	1993.2.16 to 1994.2.15	Development of High-T_c Superconducting Tape by Vapor Deposition Technique
Korea			
Sung-Keun Lee	Department of Metallurgical Engineering Dong-A University	1994.1.5 to 1994.8.20	Fretting Fatigue of Biomaterials under Pseudo-Body Fluid
Park Jong Man	Korea Atomic Energy Research Institute	1993.10.25 to 1994.1.24	Technique of TEM and *In Situ* Observation of Radiation Damage in Metals
Kim Kyong-Jooong	Korea Research Institute of Standards and Science	1993.4.26 to 1993.6.25	The Technical Cooperation for the New Materials Evaluation Center Project
Lee Hae-Moo	Korea Research Institute of Standards and Science	1993.4.26 to 1993.10.22	Same as above
Kyung-Haeng Cho	Korea Research Institute of Standards and Science	1993.7.26 to 1993.12.16	Same as above
Seung-Seok Lee	Korea Research Institute of Standards and Science	1993.9.13 to 1993.12.7	Same as above
Philippines			
Cherry Lane P. Causing	Industrial Technology Development Institute	1993.7.12 to 1993.12.3	Japan-Asean Cooperation Program on Materials Science and Technology, Philippine Project on Atmospheric Corrosion (Metallic Coating)
Poland			
Jozsef Toth*	Institute of Nuclear Research of the Hungarian Academy of Science	1994.3.22 to 1994.9.21	The Control of Surface Atomic Layers of Solids and the Development of Surface Electron Spectroscopic Tomography
Russia			
A.P. Kuprin*	Moscow State University	1992.3.31 to 1993.9.30	Hydrogen and Its Effects on the Electric Properties of Metals and Semiconductors by using the *In Situ* Analysis in the Electron Microscope
Leopold I. Cherniavsky	Institute of Inorganic Chemistry, Russian Academy of Sciences, Siberian Branch	1994.3.21 to 1994.3.30	R&D of Superconducting Materials
Thailand			
Noppadon Suttisiri	Department of Physica, Faculty of Science, Kasetsert University	1993.10.3 to 1994.1.2	Laser Induced CVD Technique and Its Application to Manufacture of Composite Materials

Nationality and Name	Affiliation	Term	Research Subject
U.K.			
Tahir Irfan Khan*	University of Cambridge	1993.2.7 to 1994.2.6	Study Changes in Diffusion Bonding Surface Structure using RHEED after Ion Bombardment and Atom-Radical Surface Modification Techniques
Ukraine			
Nikolai T. Kartel	Institute for Sorption and Endoecology	1994.1.5 to 1994.1.31	Fundamental Research on Adsorption under Electric Potential on Metal-Doped or Electron Doped Dispersed Carbons

❒ List of Visitors

M: Meguro Site T: Tsukuba Site

Nationality and Name	Affiliation	Site	Date
Brazil			
Dr. Francisco de Souza Dantas and his party	Instituto de Pesquisas Tecnologicas do Estado de Sao Paulo	M	Apr. 1993
Prof. Wander Luiz and his party	University of Minas Gerais	T	Jul. 1993
Canada			
Prof. J.S. Kirkaldy and his party	McMaster University	M	Sep. 1993
China			
Dr. Zhou Lian	Northwest Institute for Non-Ferrous Metal Research	M	May 1993
Prof. Jiang Zhougshuo and his party	Institute of Metal Research, Academia Sinica	T	Jun. 1993
Mr. Ding Fuchang and his party	Central Iron & Steel Research Institute Ministry of Metallurgical Industry	M	Jul. 1993
Prof. Tang Xiangyun	Tsinghua University	M	Jul. 1993
Prof. Liu Zhi-Guo	Nanjing University	M, T	Aug. 1993
Prof. Shi Changxu	National Natural Science Foundation of China	M, T	Sep. 1993
Prof. Zhang Xingqian and his party	University of Science and Technology Beijing	T	Sep. 1993
Prof. Liu Ziang Huai	Shanghai Institute of Metallurgy, Academia Sinica	T	Sep. 1993
Prof. Hu Zhuangqi and his party	Institute of Metal Research, Academia Sinica	M, T	Sep. 1993
Prof. Liao Longguo	Technical Information Centre, Ministry of Metallurgical Industry	T	Sep. 1993
Prof. Yang Ying-chang	Beijing University	T	Oct. 1993
Mr. Mashi-Ning and his party	Surface Engineering Branch, China Machinery Engineering Society	M	Dec. 1993
Czech			
Dr. Josef Ćadek	Institute of Physical Metallurgy Academy of Science of the Czech Republic	M	Sep. 1993
Dr. Radovan Vaśina	Institute of Physical Metallurgy Academy of Science of the Czech Republic	M	Jan. 1994
Finland			
Mr. Markus Koskenlinna and his party	Technology Development Center of Finland	M	Nov. 1993
Formosa			
Prof. Y.W. Chen-Yang	Chung Yuan Christian University	M	Sep. 1993
France			
Prof. V.M. Nigon	Universite' Claude Bernard Lyon	T	Apr. 1993
Dr. B. Vinet	Centre d'Etude Nucleaires de Grenoble	T	Aug. 1993
Prof. Marc Aucouturier	Centre National de la Recherche Scientifipue	M, T	Nov. 1993

Nationality and Name	Affiliation	Site	Date
Germany			
Dr. Horst Vehoff	Max-Planck-Institut für Eisenforschung GmbH	M, T	Jun. 1993
Dr. Peter Neumann	Max-Planck-Institut für Eisenforschung GmbH	M	Jun. 1993
Dr. J. Linke and his party	Institute for Reactorwerkstoffe Forschungszentrum Julich	T	Oct. 1993
Prof. K.-H. Schwalbe	GKSS Research Center	M	Feb. 1994
Indonesia			
Ms. I.S. Akbar and her party	ASEAN Cooperation, Division	T	Mar. 1994
Korea			
Dr. Lee Wan Iae	Hang-Yang University	T	Feb. 1994
Netherlands			
Prof. Dr. Peter H. Kes	Leiden University	T	Jul. 1993
Pakistan			
Mr. M.S. Aslam and his party	Embassy of Pakistan	T	Jun. 1993
Russia			
Mr. I.G. Neizvestny and his party	U.S.S.R. Academy of Science Siberian Branch	T	Sep. 1993
Mr. J.I. Tychkov and his party	Ministry of the Russian Federation for Atomic Energy	T	Sep. 1993
Singapore			
Dr. Nee Lam Loh and his party	Nanyang Technological University	T	Mar. 1994
Sweden			
Prof. A. Flodstrom and his party	Royal Institute of Technology	T	Aug. 1993
Prof. F. Ingman and his party	Royal Institute of Technology	M, T	Oct. 1993
Dr. L. Bergström and his party	Institute for Surface Chemistry	M	Feb. 1994
Switzerland			
Dr. J.G. Bednorz and his party	IBM Zurich Research Laboratory	T	Aug. 1993
Dr. A. Schilling	Eidgenössische Technische Hochschule Zurich	T	Oct. 1993
Prof. Dr. Ø. Fischer and his party	University of Geneva	T	Oct. 1993
Venezuela			
Dr. J.C. Nava Paz	Shell Research Arnhem	M	Apr. 1993
U.K.			
Dr. T. James Marrow	University of Oxford	T	Jun. 1993
Dr. Brian F. Dyson	National Physical Laboratory	M	Aug. 1993
Dr. R.C. Thomson	University of Cambrige	M	Aug. 1993
Dr. C.M. Friend and his party	Cranfield Institute of Technology	M	Oct. 1993
Dr. Connie Cox	Embassy of Great Britain	T	Mar. 1994
U.S.A.			
Dr. S.L. Allen and his party	Lawrence Livermore National Laboratory	T	Apr. 1993
Dr. Gregory C. Stangle	Alfred University	M	May 1993
Prof. K. Jimmy Hsia	Illinois University	M	Jun. 1993
Mr. M.J. Mayo and his party	University of Pennsylvania	T	Jun. 1993
Dr. I. Ahmad and his party	U.S. Army Research Office-Far East	T	Sep. 1993
Prof. E.E. Hellstrom	Applied Superconductivity Center, University of Wisconsin	T	Nov. 1993

❒ Brief Introduction of STA Fellowship

The Science and Technology Agency (STA), an administrative organ of the Government of Japan, offers opportunities for promising young foreign researchers in the fields of science and technology to conduct research at Japan's national laboratories and public research corporations (excluding universities and university-affiliated institutes). The program is managed by the Research Development Corporation of Japan (JRDC), a statutory organization under the supervision of STA in cooperation with the Japan International Science and Technology Exchange Center (JISTEC).

Fellowship qualifications are as follows:

1. Possession of doctor's degree.
2. Less than 35 years of age, in principle.
3. Sufficient good health for research work and life in Japan.
4. Sufficient language ability in Japanese or English.

The tenure will be 6 months to 2 years. JRDC provides expenses for round-trip, monthly living with family, initial setting-in and travel in Japan. Research expenses willl be paid for the host institute. Further information can be obtained at:

Japan International Science and Technology Exchange Center (JISTEC)
2-20-5, Takezono
Tsukuba City, Ibaraki Pref. 305, Japan
Phone +81-298-53-8250
Fax +81-298-53-8260

Organization of NRIM

❒ Organization

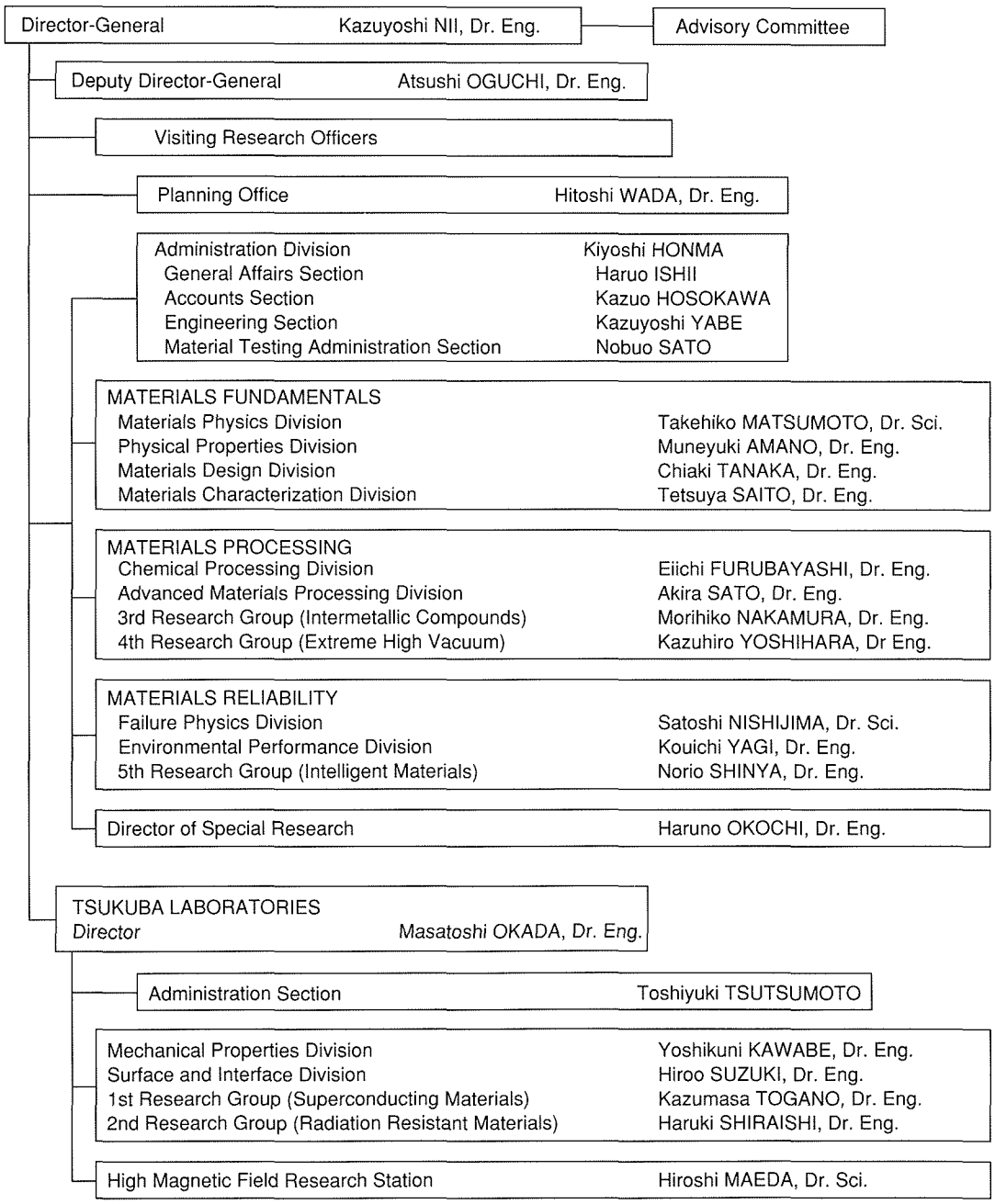

❒ Budget and Personnel in Fiscal Year of 1994

Budget	
Research and facilities	5,422
Personnel expenses	3,694
Total	9,116

unit: million yen

Personnel	
Administrative staffs	91 (9)
Researchers	331 (103)
Total	422 (112)

Number in parenthesis: Tsukuba Site

How to get to NRIM

To NRIM Meguro Site
2-3-12 Nakameguro, Meguro-ku, Tokyo 153
Phone +81-3-3719-2272, Fax +81-3-3719-2177

Narita Airport
↓ by JR Narita Express train approxmately 60 minutes
Tokyo Station
↓ by JR Yamanote Line train approximately 25 minutes
Ebisu Station
↓ by taxi approximately 5 minutes, or on foot approximately 15 minutes
NRIM

To NRIM Tsukuba Site
1-2-1 Sengen, Tsukuba-shi, Ibaraki 305
Phone +81-298-53-1000, Fax +81-298-53-1005

Narita Airport
↓ by JR Narita Express train approxmately 60 minutes
Tokyo Station
Yaesu-Minami Exit
↓ by Joban Highway Bus for Tsukuba Center approximately 70 minutes
Tsukuba Center
Bus Terminal
↓ by taxi approximately 5 minutes, or on foot approximately 15 minutes
NRIM

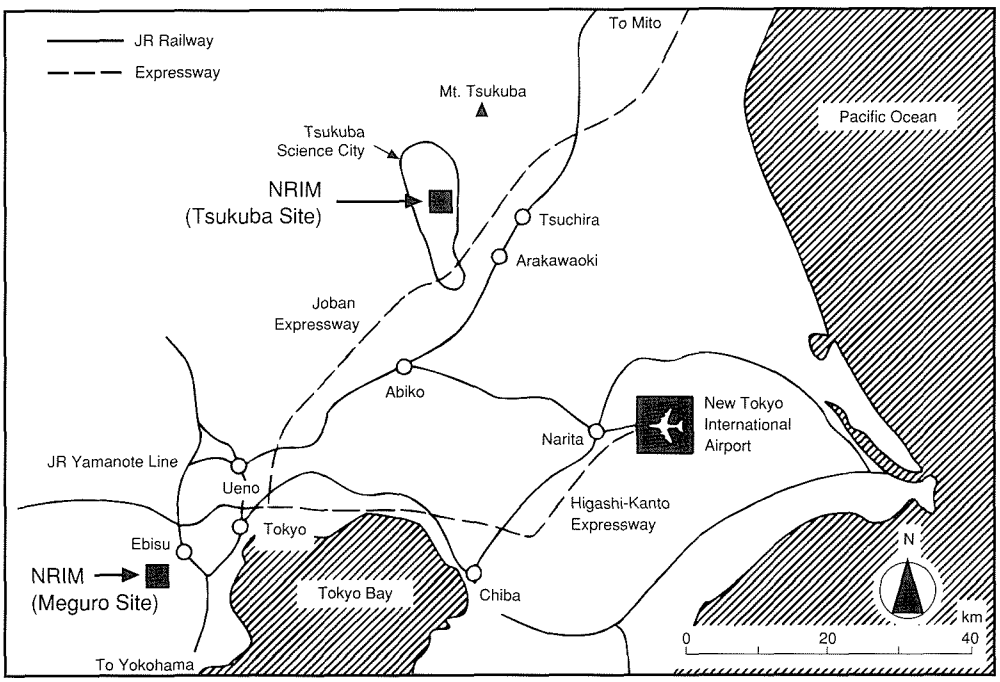

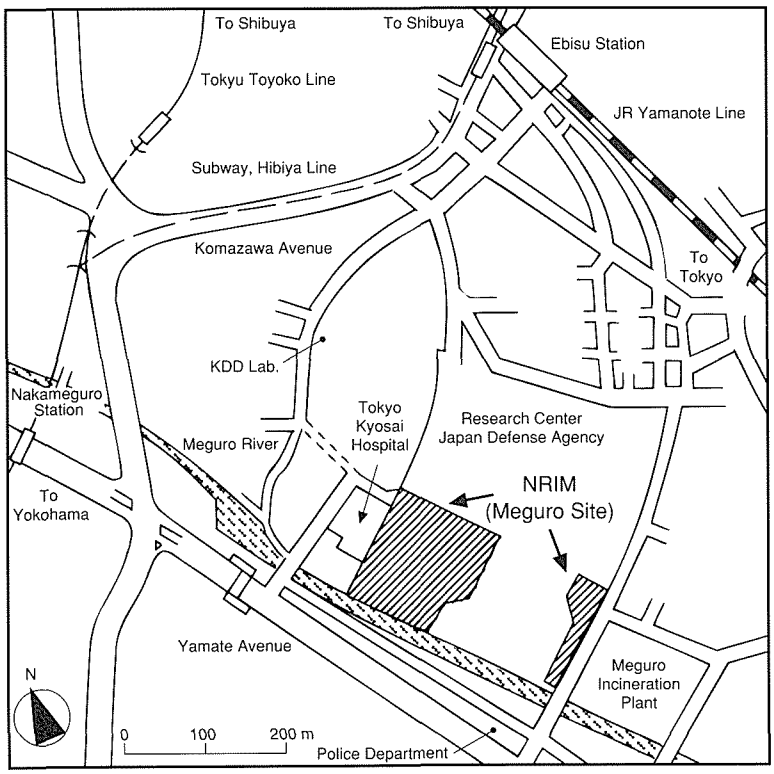

Meguro Site

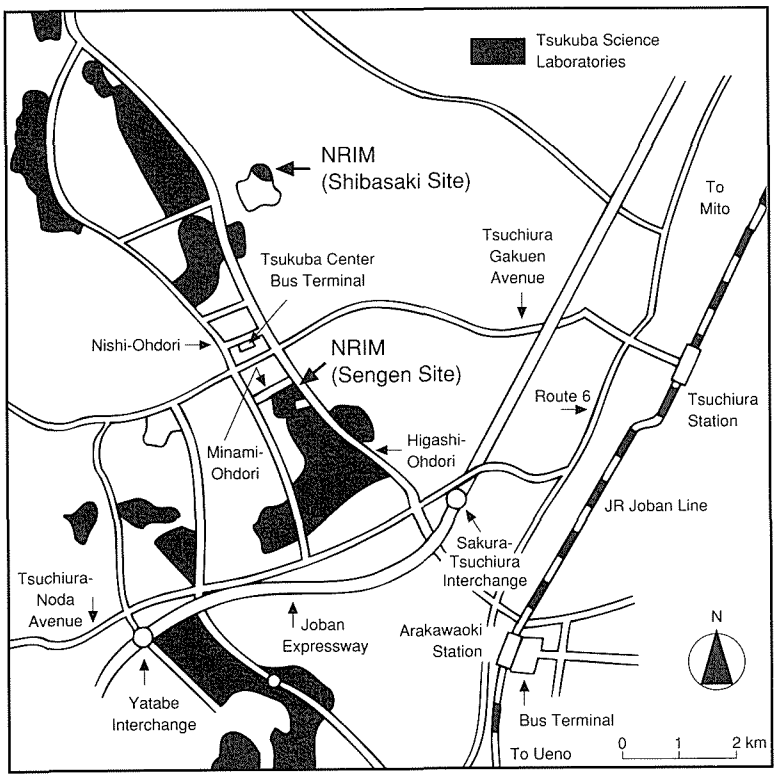

Tsukuba Site

List of Keywords

E

F

G

H

NRIM Research Activities
1994
Date of Issue: 22 December, 1994

Publisher:
Toshikazu ISHII
Planning Office
National Research Institute for Metals
1-2-1, Sengen, Tsukuba-shi, Ibaraki 305 Japan
Phone: +81-298-53-1000, Fax: +81-298-53-1005

Typeset using SGML by Uniscope Inc., Tokyo

NRIM Research Activities

1994